Ocean Engineering & Oceanography 5

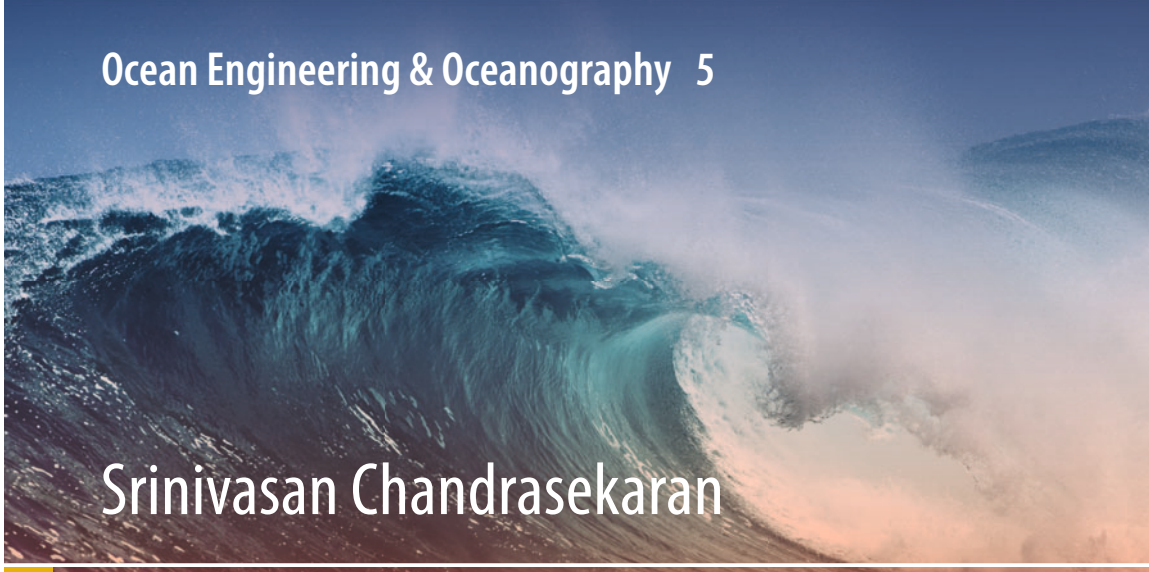

Srinivasan Chandrasekaran

Dynamic Analysis and Design of Offshore Structures

Springer

Ocean Engineering & Oceanography

Volume 5

More information about this series at http://www.springer.com/series/10524

Srinivasan Chandrasekaran

Dynamic Analysis and Design of Offshore Structures

Springer

Srinivasan Chandrasekaran
Department of Ocean Engineering
Indian Institute of Technology Madras
Chennai, Tamil Nadu
India

ISSN 2194-6396 ISSN 2194-640X (electronic)
Ocean Engineering & Oceanography
ISBN 978-81-322-2276-7 ISBN 978-81-322-2277-4 (eBook)
DOI 10.1007/978-81-322-2277-4

Library of Congress Control Number: 2015930819

Springer New Delhi Heidelberg New York Dordrecht London

Printed on acid-free paper

Springer (India) Pvt. Ltd. is part of Springer Science+Business Media (www.springer.com)

To
My parents, teachers, family members and friends

Preface

Offshore structures are unique in the field of engineering, as they pose many challenges in the development and conceptualization of design. As innovative platform geometries are envisaged to alleviate the encountered environmental loads efficiently, detailed understanding of their analysis and basic design becomes important. Structural dynamics, being an important domain of offshore engineering, require intensive teaching and guidance to illustrate the fundamental concepts, in particular as applied to ocean structures. With the vast experience of teaching this subject and guiding research, a humble attempt is made to present the basics in a closed form, which will be useful for graduate students and researchers. Chapters in this book are organized such that the reader gets an overall idea of various types of offshore plants, basic engineering requirements, fundamentals of structural dynamics and their applications to preliminary design. Numerical examples and application problems are chosen to illustrate the use of experimental, numerical and analytical studies in the design and development of new structural form for deep-water oil exploration. This book is an effort in the direction of capacity building of practicing and consulting offshore structural engineers who need to understand the basic concepts of dynamic analysis of offshore structures through a simple and straightforward approach.

Video lectures of the courses available at the following websites: (i) http://nptel.ac.in/courses/114106035; (ii) http://nptel.ac.in/courses/114106036; and (iii) http://nptel.ac.in/courses/114106037, which also substitute the classroom mode of understanding of the contents of this book.

My sincere thanks are due to my professors, colleagues and my students who have given their valuable input and feedback to develop the contents of this book. In particular, I wish to express my thanks to Mrs. Indira and Ms. Madhavi for their editorial assistance and graphic art support extended during the preparation of manuscript of the book. Author acknowledges the support extended by Centre of Continuing Education, Indian Institute of Technology Madras for publishing this book.

I also owe a lot of thanks to all the authors and publishers who have earlier attempted to publish books on structural dynamics and allied topics, based on which I developed my concepts on the said subject.

Srinivasan Chandrasekaran

Contents

Figures

Tables

Notations

ρ_a	Mass density of air
C_w	Wind pressure coefficient
θ	Phase angle
$v(t)$	Gust component
F_D	Drag force
F_L	Lift force
v_z	Wind speed at elevation of z m above MSL
V_{10}	Wind speed at 10 m above MSL
F_g	Average gust factor
L_u	Integral length scale
δ	Surface drag coefficient/logarithmic decrement
ω_p	Peak frequency
σ_z^2	Variance of $U(t)$
H	Wave height
λ	Wave length
d	Water depth
η	Wave surface elevation
k	Wave number
ω	Wave circular frequency
f	Cyclic frequency
ρ	Density of fluid
C_d	Drag coefficients
C_m	Inertia coefficients
Δx	Distance between the column members
S_0	Intensity of earthquake
ω_g	Natural frequency of the ground
ξ_g	Damping of the ground
$\bar{F}_0$	Force amplitude on the structure
$f(t)$	Excitation force
$[k]$	Stiffness

$[m]$	Mass element
$[c]$	Damping element
W	Vertical load
x_0	Initial displacements
$\dot{x}_0$	Initial velocities
ω_n	Natural frequency
A	Area
μ	Coefficient of absolute viscosity
ω_d	Damped vibration frequency
ξ	Damping ratio
C_c	Critical damping
t	Time period
p_o	Amplitude of varying load $f(t)$
a_{ij}	Flexibility influence coefficient
$\ddot{x}$	Acceleration
m^*	Generalized mass
ω^*	Generalized frequency
U/S	Upstream
D/S	Downstream
Y	Depth of immersion
CBF	Blockage factor
S	Center to center distance of the cylinder
D	Diameter of the cylinder
T	Draft
FB	Total buoyancy
a	Area of perforation
d	Water depth
g	Acceleration due to gravity
$\mathrm{H_{FX}}(\omega)$	The transfer function
$\mathrm{h_{FX(t)}}$	Impulse response function
$C_X(\tau)$	Auto-covariance
$R_X(\tau)$	Auto-correlation
$F_m(m)$	Cumulative distribution function
$\{f_m(m)\}$	Probability density function
P_f	Probability of failure
H_s	Significant wave height
T_p	Spectral peak period
u_c	Current velocity
u_w	Mean wave speed
$G(x)$	Performance function
β_{HL}	Reliability index
s_g	Stress range in each group
n_g	Number of cycles in each group
D_{RC}	Fatigue damage estimated by range counting

D_{RFC}	Rain flow counting
D_{LCC}	Level crossing counting
D_{PC}	Peak counting
D_{NB}	Narrow band approximation
n_g	Number of cycles
D	Total damage
σ	Stress
VCG	Vertical center of gravity
A_w	Water plane area
Δ	Displacement
GM_{La}	Lateral meta-centric heights
GM_{Lo}	Longitudinal meta-centric heights
I	Moment of Inertia
RAO	Response amplitude operator

About the Author

Srinivasan Chandrasekaran is a faculty member of the Department of Ocean Engineering at Indian Institute of Technology Madras, Chennai, India. He has teaching, research and industrial experience of about 23 years during which he has supervised many sponsored research projects and offshore consultancy assignments both in India and abroad. His areas of current research are dynamic analysis and design of offshore platforms, development of geometric forms of compliant offshore structures for ultra-deep water oil exploration and production, sub-sea engineering, rehabilitation and retrofitting of offshore platforms, structural health monitoring of ocean structures, seismic analysis and design of structures and risk analyses, and reliability studies of offshore and petroleum engineering plants. He has also been a visiting fellow under the invitation of Ministry of Italian University Research to University of Naples Federico II, Italy, for a period of 2 years during which he conducted research on advanced nonlinear modeling and analysis of structures under different environment loads with experimental verifications. He has published 110 research papers in international journals and refereed conferences organized by professional societies around the world. He has also authored three textbooks which are quite popular among graduate students of civil and ocean engineering. He is a member of many national and international professional bodies and delivered many invited lectures and keynote addresses in the international conferences, workshops and seminars organized in India and abroad.

Chapter 1
Introduction to Offshore Platforms

Abstract This chapter deals with the evolution of platform and various types of offshore platforms and their structural action under different environmental loads. The newly evolved structural forms and their discrete characteristics are discussed in this chapter. This chapter also gives the reader a good understanding about the structural action of different forms in the offshore. An overview of the construction stages of offshore plants and their foundation systems is presented.

Keywords Offshore structures · Bottom-supported structures · Compliant platforms · Tension leg platforms · Triceratops · Floating · Storage and regasification unit

1.1 Introduction

Offshore structures are being challenged to counteract the depletion of oil resources with the new set of discoveries. By 2010, the increase in drilling platforms induced the demand for offshore structures in deep sea. Hence, the quest on the research and development of the deep-water structures has resulted in the recent advancement and thrust in this area. Expansion of the structures from shallow to deep waters makes the accessibility difficult, and hence, the structures demand higher deck areas consisting of additional space for third-party drilling equipment. Specific challenges in Arctic regions in shallow waters that arise due to low temperature, remoteness, ice conditions, ecosystem, and safety necessitate an adaptive design of offshore platforms addressing these factors.

Development of offshore platforms depends on various factors:

- Structural geometry with a stable configuration
- Easy to fabricate, install, and decommission
- Low CAPEX
- Early start of production
- High return on investment by increased and uninterrupted production

S. Chandrasekaran, *Dynamic Analysis and Design of Offshore Structures*,
Ocean Engineering & Oceanography 5, DOI 10.1007/978-81-322-2277-4_1

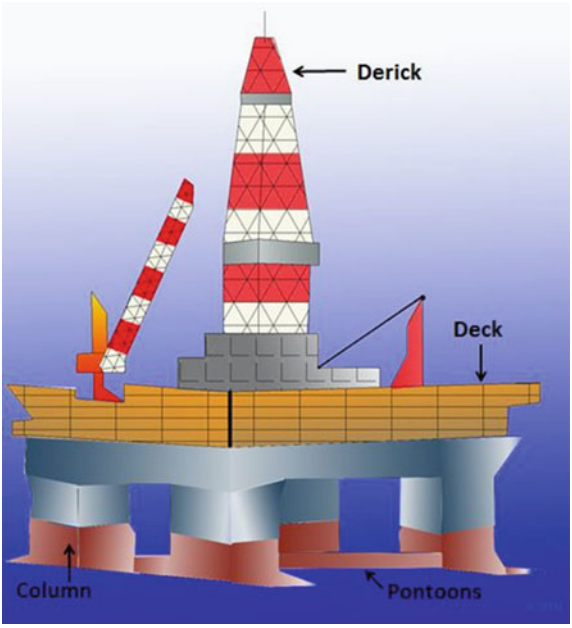

Fig. 1.1 Deep-water drilling semisubmersible with vertical riser storage

Newly generated structural forms do not have any precedence to compare and understand their behavior and complexities. It is therefore important to understand the response of the structure and then select the structure that is most suitable to the environment. This is one of the essential features of the front-end engineering design (FEED). Figure 1.1 shows a drilling semisubmersible for deep-water drilling with vertical riser storage.

1.2 Types of Offshore Platforms

Offshore platforms fall under three major categories: (i) fixed platforms; (ii) compliant platforms; and (iii) floating platforms. They are further classified as follows:

(i) *Fixed platforms*

- (a) Jacket platform
- (b) Gravity platform

(ii) *Compliant platforms*

- (a) Guyed tower
- (b) Articulated tower
- (c) Tension leg platform

(iii) *Floating platforms*

(a) Semisubmersible
(b) Floating Production Unit (FPU)
(c) Floating storage and offloading (FSO)
(d) Floating production, storage and offloading (FPSO) System
(e) Spar

1.2.1 Bottom-supported Structures

Energy is the driving force of the progress of civilization. Industrial advancements were first stoked by coal and then by oil and gas. Oil and gas are essential commodities in world trade. Oil exploration that initially started ashore has now moved to much deeper waters owing to the paucity of the resources at shallow waters (Bhattacharyya et al. 2003). Until date, there are more than 20,000 offshore platforms of various kinds installed around the world. Geologists and geophysicists search for the potential oil reserve within the ground under ocean seafloor, and engineers take the responsibility of transporting the oil from the offshore site to the shore location (Dawson 1983). There are five major areas of operation from exploration to transportation of oil: (i) exploration; (ii) exploration drilling; (iii) development drilling; (iv) production operations; and (v) transportation (Chandrasekaran and Bhattacharyya 2011; Clauss et al. 1992; Clauss and Birk 1996). Ever since the first offshore structure was constructed, more advanced design technologies emerged for building larger platforms that cater to deeper water requirements; each design is unique to the specific site (Ertas and Eskwaro-Osire 1991). A precise classification of the offshore platform is difficult because of the large variety of parameters involved, such as functional aspects, geometric form, construction, and installation methods. However, the platforms are broadly classified based on the geometric configurations, in general (Chandrasekaran 2013a, b, c). Offshore installations are constructed for varied purposes: (i) exploratory and production drilling; (ii) preparing water or gas injection into reservoir; (iii) processing oil and gas; (iv) cleaning the produced oil for disposal into sea; and (v) accommodation facilities. They are not classified on the basis of their functional use but based on their geometric (structural) *form* (Sadehi 1989, 2001, 2007; Sarpkaya and Isaacson 1981). As the platforms are aimed for greater water depths, their structural *form* changes significantly; alternatively, the same *form* cannot be used at a different water depth. It means that the geometric evolution of the platform needs to be adaptive to counteract the environmental loads at the chosen water depths (Patel 1989). Furthermore, the technological complexities faced by new offshore platforms including analysis and design, topside details, construction, and installation are not available in the open domain; they are protected and owned by the respective companies/agencies as part of their copyright. Because of such practices, knowledge on the complexities in designing the offshore plants is not available to the practicing young engineers, in particular. Hence, prior to the knowledge of FEED, it

is necessary to understand different structural *forms* of offshore structures, which are successful in the past. As it is well known that each platform is unique in many ways, learning about their structural configurations, limitations with respect to the sea states and water depth, construction complexities, decommissioning issues, and their structural action will be an important stage in the pre-FEED (Hsu 1981; Paik and Thayamballi 2007).

The present trend is to design and install offshore platforms in regions that are inaccessible and difficult to use the existing technologies (Anagnostopoulos 1982). The structural *form* of every platform is largely derived on the basis of structural innovativeness but not on the basis of the functional advantages. Revisiting the existing platforms constructed around the world will impart decent knowledge to offshore engineers (Gerwick 1986; Graff 1981a, b). Offshore platforms are classified either as bottom-supported or floating. Bottom-supported platforms can be further classified as fixed or compliant-type structures; *compliant* means flexible (mobility). Compliancy changes the dynamic behavior of such platforms. Floating structures are classified as neutrally buoyant type (e.g., semisubmersibles, FPSO, mono-column spars) and positively buoyant type (e.g., tension leg platforms). It is important to note that buoyancy plays a very important role in floating-type offshore structures, as the classifications are done based on buoyancy (Bea et al. 1999). Table 1.1 shows the list of jacket platforms constructed worldwide.

Fixed-type platforms are called template-type structures, which consist of the following:

- A jacket or a welded space frame, which is designed to facilitate pile driving and also acts as a lateral bracing for the piles
- Piles, which are permanently anchored to the seabed to resist the lateral and vertical loads that are transferred from the platform
- A superstructure consisting of the deck to support other operational activities

The jacket platform complex, shown in Fig. 1.2, consists of process, wellhead, riser, flare support, and living quarters.

Table 1.1 Offshore jacket platforms constructed worldwide

Name of the platform	Water depth (m)	Country
Cognac Fixed Platform	312	US
Pompano	393	US
Bullwinkle	412	US
Canyon Station	91	US
Amberjack Fixed Platform	314	US
Alma Fixed Platform	67	Canada
North Triumph Fixed Platform	76	Canada
South Venture Fixed Platform	23	Canada
Blacktip	50	Australia
CaNguVang	56	Vietnam
East Belumut A	61	Malaysia

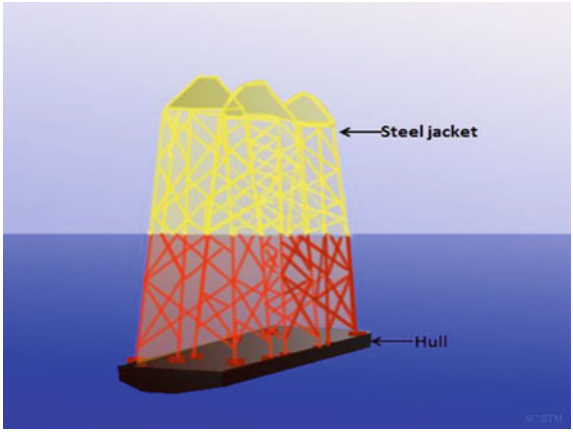

Fig. 1.2 Bullwinkle steel jacket

The advantages of offshore jacket platforms are as follows: (i) support large deck loads; (ii) possibility of being constructed in sections and transported; (iii) suitable for large field and long-term production (supports a large number of wells); (iv) piles used for foundation result in good stability; and (v) not influenced by seafloor scour. Few disadvantages are as follows: (i) cost increases exponentially with increase in water depth; (ii) high initial and maintenance costs; (iii) not reusable; and (iv) steel structural members are subjected to corrosion, causing material degradation in due course of service life.

1.2.1.1 Gravity Platform

In addition to steel jackets, concrete was also prominently used to build some offshore structures. These structures are called gravity platforms or gravity-based structures (GBS). A gravity platform relies on the weight of the structure to resist the encountered loads instead of piling (API-RP2A 1989). In regions where driving piles become difficult, structural forms are designed to lie on its own weight to resist the environmental loads. These structures have foundation elements that contribute significantly to the required weight and spread over a large area of the seafloor to prevent failure due to overturning moments caused by lateral loads. Gravity platforms are capable of supporting large topside loads during tow-out, which minimizes the hookup work during installation. Additional large storage spaces for hydrocarbons add up to their advantage. Their salient advantages include the following: (i) constructed onshore and transported; (ii) towed to the site of installation; (iii) quick installation by flooding; and (iv) use of traditional methods and labor for installation. Table 1.2 shows the list of gravity platforms constructed worldwide. These platforms are also known to be responsible for seabed scouring due to large foundations, causing severe environmental impact (Chandrasekaran 2013a).

Gravity platforms had serious limitations, namely (i) not suitable for sites of poor soil conditions, as this would lead to significant settlement of foundation; (ii) long

Table 1.2 Gravity platforms constructed worldwide (Courtesy: Pennwell Publishing Co.)

Name of the platform	Water depth (m)
Ekofisk 1	70
Beryl A	119
Brent B	140
Frigg CDP1	98
Frigg TP 1	104
Frigg MCP01	94
Brent D	142
Statfjord A	145
Dunlin A	153
Frigg TCP2	103
Ninian	136
Brent C	141
Cormorant	149
Statfjord B	145
Maureen	95.6
Stafjord C	145
Gulfaks A	133.4
GulfaksB	133.4
GulfaksC	214
Oseberg	100
Slebner	80
Oseberg North	100
Draugen	280
Heidrun	280
Troll	330

construction period which thereby delays the early start of production; and (iii) natural frequencies falling within the range of significant power of the input wave spectrum (Boaghe et al. 1998). Gravity structures are constructed with reinforced cement concrete and consist of large cellular base, surrounding several unbraced columns that extend upward from the base to support the deck and equipment above the water surface (Reddy and Arockiasamy 1991). Gravity platforms consist of production risers as well as oil supply and discharge lines, contained in one of the columns; the corresponding piping system for exchange of water is installed in another; and drilling takes place through the third column. This particular type is referred as CONDEEP (concrete deep-water) structure and was designed and constructed in Norway. During construction, base of the platform is constructed in dry-dock after which it is floated and moored in a deep harbor. The construction is then completed by slip-forming the large towers in a continuous operation until they are topped off. The structure is then ballasted, and a steel prefabricated deck is floated over the structure and attached to its top. The construction of gravity platforms obviously requires deep harbors and deep tow-out channels. The

floatation chambers are used as storage tanks, and platform stability is ensured through skirts. Steel gravity platforms exist off Nigeria, where the presence of rock close to seafloor ruled out the possibility of using piles to fix the structures to the seabed. Figure 1.3 shows the Hibernia gravity base structure. The platform is a steel gravity base structure with a weight of 112,000 ton and height of 241 m and has steel skirts for penetration into the seabed.

1.2.2 Compliant Structures

To overcome the above negative factors, one should design a structural *form,* which should attract fewer forces and remain flexible to withstand the cyclic forces. The structural *form* is improved to overcome the geometric constraints imposed by the fixed-type platforms. This is a special kind of reverse engineering, which makes offshore platforms unique. This leads to continuous improvement from one platform to the other. Hence, FEED is on a constant update as new structural forms are attempted for oil and gas exploration in deep and ultra-deep waters (Chandrasekaran 2013b). Fixed-type offshore structures became increasingly expensive and difficult to install in greater water depths. Hence, modified design concept evolved for structures in water depths beyond 500 m.

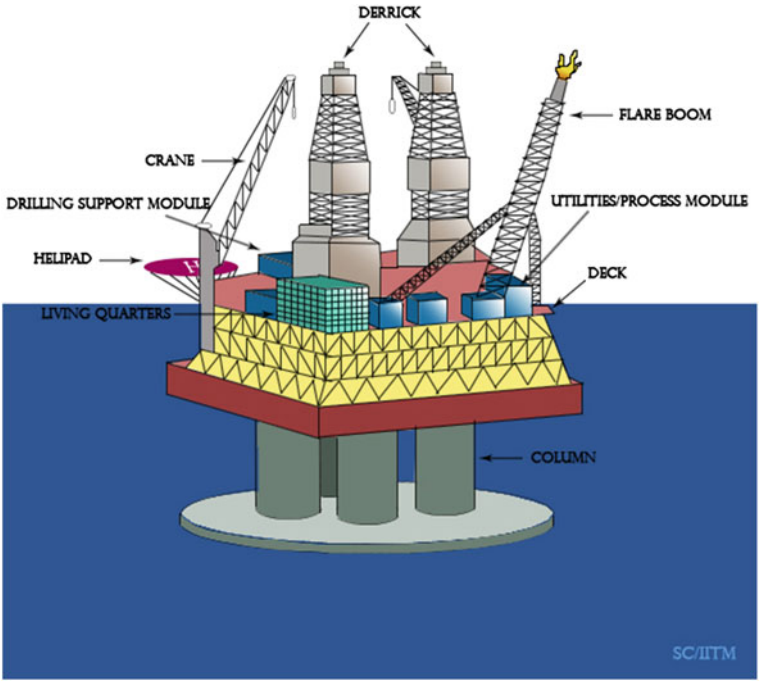

Fig. 1.3 Hibernia gravity base structure

A compliant tower is similar to that of a traditional platform, which extends from surface to the sea bottom and transparent to waves. A compliant tower is designed to remain flexible (adaptive) with the forces of waves, wind, and current. Classification under compliant structure includes those structures that extend to the ocean bottom and are anchored directly to the seafloor by piles and/or guidelines (Mather 2000). Guyed towers, articulated tower and tension leg platform (TLP) fall under this category. The structural action of complaint platforms is significantly different from that of the fixed ones, as they resist lateral loads not by their weight but by their relative movement. In fact, instead of resisting the lateral loads, the structural geometry enables the platform to move in line with the wave forces. To facilitate the production operation, they are position-restrained by cables/tethers or guy wires. By attaching the wires to the complaint tower, majority of the lateral loads are counteracted by the horizontal component of the tension in the cables; the vertical component adds to the weight and improves stability (Chakrabarti 1994; Dawson 1983).

1.2.2.1 Guyed Towers

Guyed tower is a slender structure made up of truss members that rest on the ocean floor and is held in place by a symmetric array of catenary guylines. The foundation of the tower is supported with the help of spud can arrangement, which is similar to the inverted cone placed under suction. The structural action of the guyed tower makes its innovation more interesting, which is one of the successful *form* improvements in the offshore structural design. The upper part of the guy wire is a lead cable, which acts as a stiff spring in moderate seas. The lower portion is a heavy chain, which is attached with clump weights. Under normal operating conditions, the weights will remain at the bottom, and the tower-deck motion will be nearly insignificant. However, during a severe storm, the weights on the storm-ward side will lift off the bottom, softening the guying system and permitting the tower and guying system to absorb the large wave loads. Since the guylines are attached to the tower below mean water level close to the center of applied environmental forces, large overturning moments will not be transmitted through the structure to the base. This feature has evolved in the design of the tower to be of a constant square cross section along its length, reducing the structural steel weight as compared with that of a conventional platform (Moe and Verley 1980).

Exxon in 1983 installed the first guyed tower named Lena guyed tower in the Mississippi Canyon Block in a 300 m water depth. Though the structural *form* resembles a jacket structure, it is compliant and is moored by catenary anchor lines. The tower has a natural period of 28 s in sway mode while bending, and torsion modes have a period of 3.9 and 5.7 s, respectively. The tower consists of 12 buoyancy tanks of diameter 6 m and length of about 35 m. Around 20 guylines are attached to the tower with clump weights of about 180 ton to facilitate the holding of the tower in position. The advantages of guyed towers are (i) low cost (lower than steel jacket); (ii) good stability as guylines and clump weights improve restoring force; and (iii) possible reuse. The disadvantages are as follows: (i) high

maintenance costs; (ii) applicable to small fields only; (iii) exponential increase in cost with increase in water depth; and (iv) difficult mooring. These factors motivated to further innovation in the platform geometry, which resulted in articulated towers. Figures 1.4, 1.5, 1.6, 1.7, 1.8, and 1.9 show different types of platforms that are existing in various oil fields around the world.

1.2.2.2 Articulated Towers

One of the earliest compliant structures that started in relatively shallow waters and slowly moved into deep water is the articulated tower. An articulated tower is an upright tower that is hinged at its base with a universal joint, which enables free rotation about the base. When there was a need to improve the structural *form* from fixed to compliant, researchers thought of both modes of compliancy, namely (i) rotational and (ii) translational. Enabling large translational motion could make the platform free from position-restrained, and hence, rotational compliancy was attempted. In such geometric *forms*, it is important to note that the design introduces a single-point failure deliberately, which is the universal joint (Choi and Lou 1991; Helvacioglu and Incecik 2004). The tower is ballasted near the universal joint and has a large buoyancy tank at the free surface to provide large restoring force (moment). The tower extends above the free surface and accommodates a deck and a fluid swivel. In deeper water, it is often advantageous to introduce double articulation, the second one being at a mid-depth (Nagamani and Ganapathy 2000). Provision of more articulation reduces the bending moment along the tower (Nazrul and Suhail 2003). Fatigue is an important criterion for this type of system design as the universal joints are likely to fail under fatigue loads. The advantages of

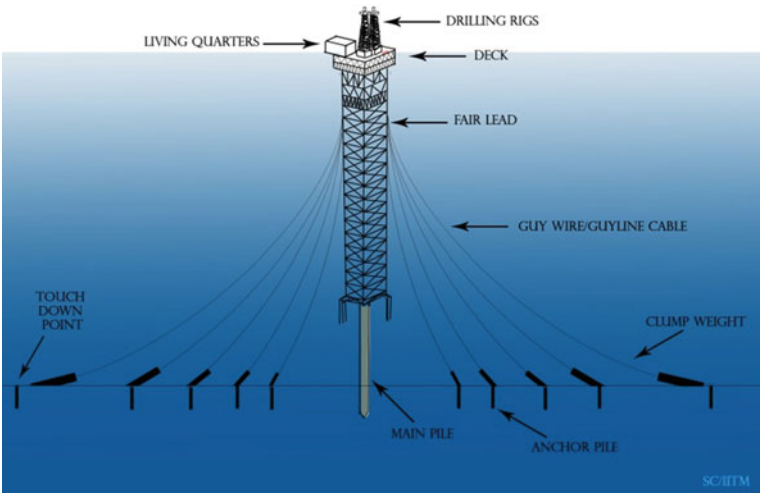

Fig. 1.4 Lena guyed tower in Mississippi Canyon Block

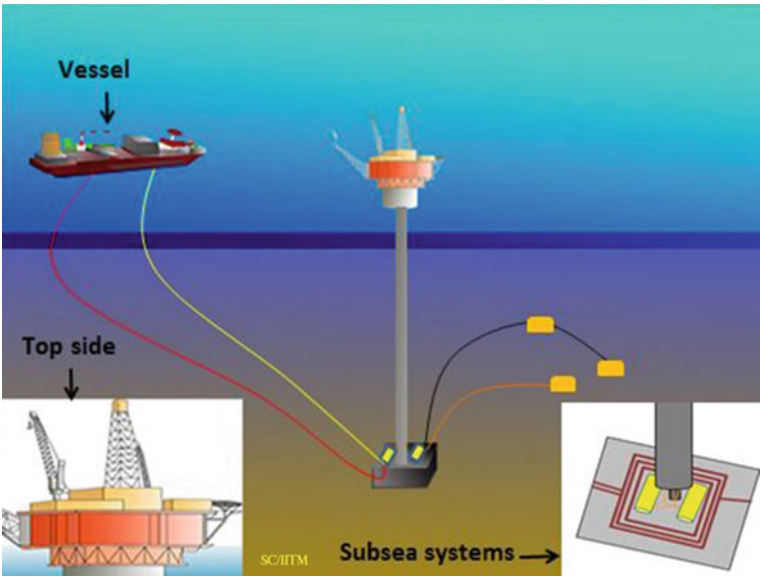

Fig. 1.5 Articulated tower

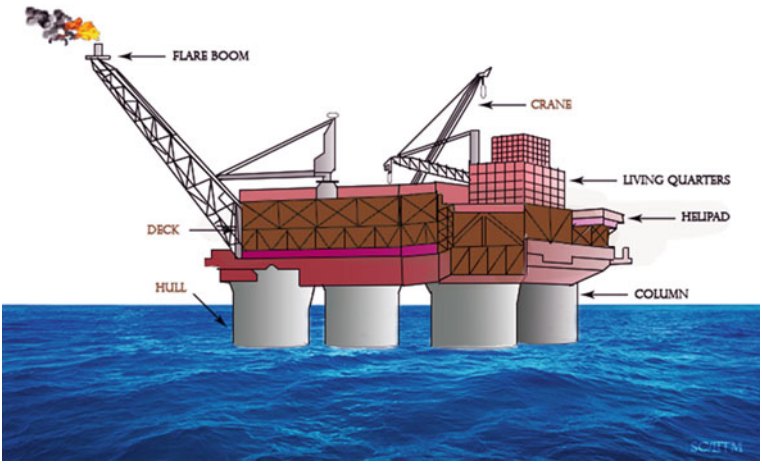

Fig. 1.6 Tension leg platform

articulated towers are as follows: (i) low cost; (ii) large restoring moments due to high center of buoyancy; and (iii) protection of risers by tower. There are few disadvantages: (i) suitable only for shallow water as the tower shows greater oscillations for increased water depth, (ii) cannot operate in bad weather; (iii) limited to small fields; and (iv) fatigue of universal joint leads to a single-point failure.

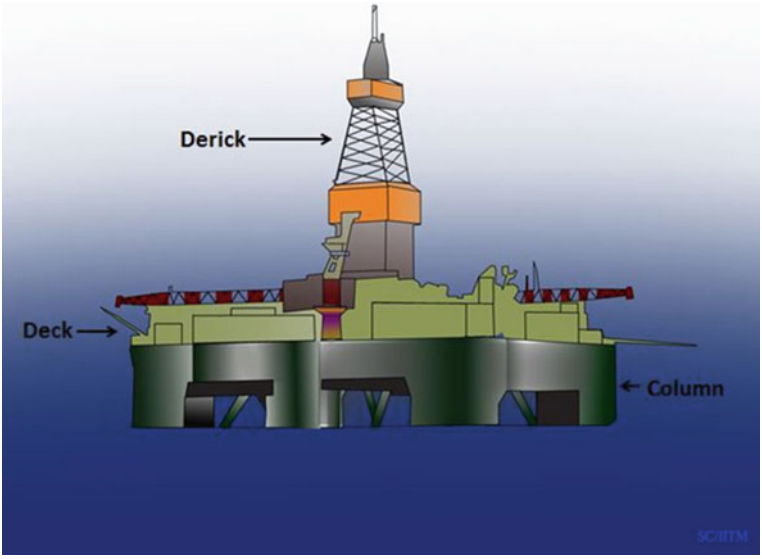

Fig. 1.7 Semisubmersible

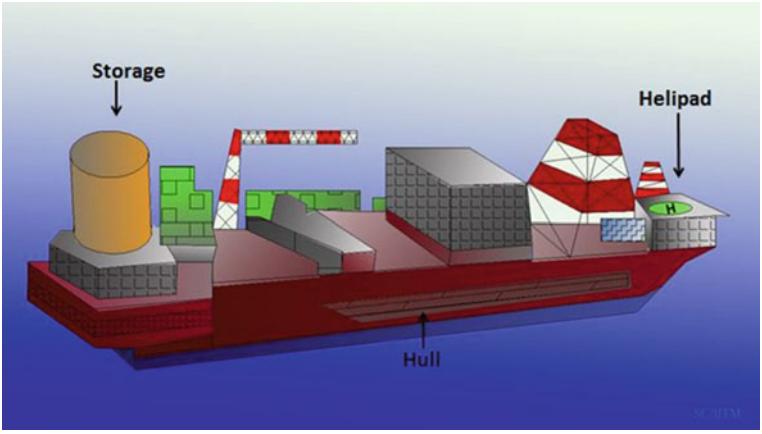

Fig. 1.8 FPSO platform

In both the above structural *forms* of complaint towers, it is seen that the structure (tower) extends through the water depth, making it expensive for deep waters. Therefore, successive structural *forms* are motivated toward the basic concept of not extending the tower to the full water depth but only to retain it near the free surface level. In such kinds of structural geometry, it is inevitable to make the platform weight dominant. To improve the installing features and decommissioning procedures, the geometry is attempted to be buoyancy dominant instead of

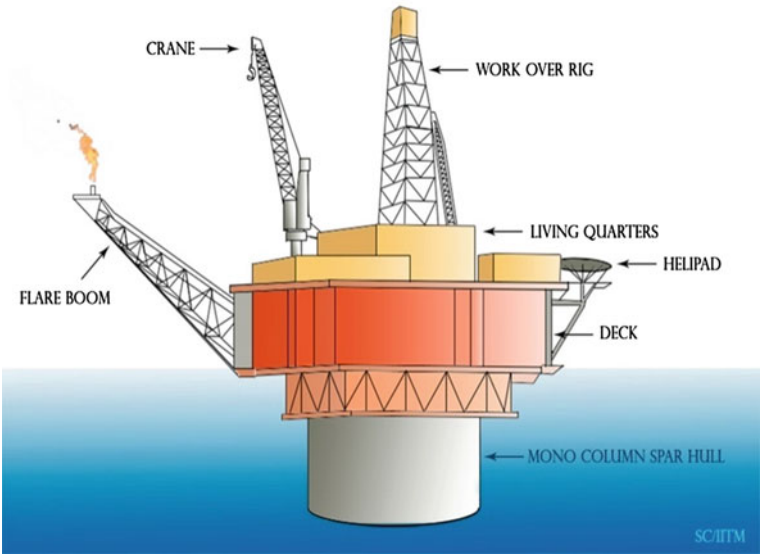

Fig. 1.9 SPAR platform

weight dominant (buoyancy force exceeds the weight by manifold). While this enabled easy fabrication and installation, it also demanded skilled labor and high expertise for installation and commissioning of such platforms. The evolved structural geometry is TLPs (Vannucci 1996; de Boom et al. 1984; Yan et al. 2009; Yoneya and Yoshida 1982; Demirbilek 1990).

1.2.2.3 Tension Leg Platform

A TLP is a vertically moored compliant platform. Taut mooring lines vertically moor the floating platform, with its excess buoyancy; they are called tendons or tethers. The structure is vertically restrained, while it is compliant in the horizontal direction, which permits surge, sway, and yaw motions. The structural action resulted in low vertical force in rough seas, which is the key design factor (Chandrasekaran and Jain 2002a, b; Rijken et al. 1991). Substantial pretension is required to prevent the tendons from falling slack even in the deepest trough, which is achieved by increasing the free-floating draft (Chandrasekaran et al. 2006b). Typical natural periods of the TLP are kept away from the range of wave excitation periods and typically for TLP resonance periods of 132 s (surge/sway) and 92 s (yaw) as well as 3.1 s (heave) and 3.5 s (pitch/roll), which are achieved through proper design (Nordgren 1987). The main challenge for the TLP designers is to keep the natural periods in heave and pitch below the range of significant wave energy, which is achieved by an improved structural *form* (Paik and Roesset 1996; Kobayashi et al. 1987; Low 2009). TLP technology preserves many of the

operational advantages of a fixed platform while reducing the cost of production in water depths up to about 1,500 m (Iwaski 1981; Haritos 1985; Chandrasekaran et al. 2004, 2007a; Chandrasekaran and Jain 2004). Its production and maintenance operations are similar to those of fixed platforms. TLPs are weight sensitive but have limitations in accommodating heavy payloads (Tabeshpour et al. 2006; Yoshida et al. 1984). Usually, a TLP is fabricated and towed to an offshore well site wherein the tendons are already installed on a prepared seabed. Then, the TLP is ballasted down so that the tendons may be attached to the TLP at its four corners. The mode of transportation of TLP allows the deck to be joined to the TLP at dockside before the hull is taken offshore (Bar-Avi 1999).

The advantages of TLPS are as follows: (i) mobile and reusable; (ii) stable as the platform has minimal vertical motion; (iii) low increase in cost with increase in water depth; (iv) deep-water capability; and (v) low maintenance cost. Few disadvantages are, namely (i) high initial cost; (ii) high subsea cost; (iii) fatigue of tension legs; (iv) difficult maintenance of subsea systems; and (v) little or no storage.

1.2.3 Floating Platform

Semisubmersibles, FPSO systems, FPUs, FSO systems, and spar platforms are grouped under this category.

1.2.3.1 Semisubmersible

Semisubmersible marine structures are well known in the oil and gas industries and belong to the category of neutrally buoyant structure. These structures are typically moveable only by towing. These semisubmersibles have a relatively low transit draft, with a large water plane area, which allows them to be floated to a stationing location. On location, it is ballasted, usually by seawater, to assume a relatively deep draft or semisubmerged condition, with a smaller water plane area, for operation. Semisubmersible platforms have the principal characteristic of remaining in a substantially stable position and have minimal motions in all the degrees of freedom due to environmental forces such as the wind, waves, and currents. The main parts of the semisubmersibles are the pontoons, columns, deck, and the mooring lines. The columns bridge the deck and the pontoons, i.e., the deck is supported by columns. Flotation of semisubmersibles is accomplished with pontoons. The pontoons provide a relatively large water plane area, as is desirable for transit. When submerged for stationing and operations, the columns connecting the pontoons to the upper deck present a lower water plane area, thereby attracting less wave loads and thus reducing the motions.

The advantages of semisubmersibles are as follows: (i) mobility with high transit speed ($\sim$ 10 kts); (ii) stable as they show minimal response to wave action; and (iii) large deck area. Few disadvantages are as follows: (i) high initial and operating costs;

(ii) limited deck load (low reserve buoyancy); (iii) structural fatigue; (iv) expensive to move large distances; (v) availability of limited dry-docking facilities; and (vi) difficult to handle mooring systems and land BOP stack and riser in rough seas.

1.2.3.2 Floating Production, Storage and Offloading (FPSO) Platform

FPSO is an acronym for floating production, storage and offloading systems. Offloading of the crude oil is usually to a shuttle tanker. Typically converted or newly built tankers are examples of custom-made designs for production and storage of hydrocarbons. These stored hydrocarbons are then transported by other vessels to terminals or deep-water ports. The design variants of FPSO are FPS and FSO. FPS is an acronym for floating production systems devoid of storage facility. Now, it is a universal term to refer to all production facilities that float rather than structurally supported by the seafloor, and typical examples include TLPs, spars, semisubmersibles, and shipshape vessels. FSO is an acronym for floating, storage and offloading system. Like the FPSO, these are typically converted or newly built tankers, and they differ from the FPSO by not incorporating the processing equipment for production; the liquids are stored for shipment to another location for processing. Offloading indicates transfer of produced hydrocarbons from an offshore facility into shuttle tankers or barges for transport to terminals or deep-water ports. An FPSO relies on subsea technology for the production of hydrocarbons and typically involves pipeline export of produced gas with shuttle tanker (offloading) transport of produced liquids. FPSOs are usually ship-shaped structures and are relatively insensitive to water depth. Mooring systems of FPSOs are classified as 'permanent mooring' or 'turret mooring.' Majority of FPSOs deployed worldwide are permanently moored, i.e., the FPSOs with their moorings and riser systems are capable of withstanding extreme storms in the field. On the other hand, disconnectable FPSOs have attracted more attention recently. They are typically turret moored. Disconnectable turret is designed for FPSO to be able to disconnect to avoid certain extreme environments.

The advantages of the FPSOs are as follows: (i) low cost; (ii) mobile and reusable; (iii) reduced lead time; (iv) quick disconnecting capability, which can be useful in iceberg-prone areas; (v) little infrastructure required; and (vi) turret mooring system enables FPS (converted ship type) to head into the wind/waves reducing their effect. Few disadvantages are as follows: (i) limited to small fields; (ii) low deck load capacity; (iii) damage to risers due to motion; (iv) poor stability in rough seas; and (v) little oil storage capabilities.

1.2.3.3 Spar Platform

A spar belongs to the category of neutrally buoyant structures and consists of a deep-draft floating caisson. This caisson is a hollow cylindrical structure similar to a very large buoy. Its four major components are hull, moorings, topsides, and risers.

The spar relies on a traditional mooring system, i.e., anchor-spread mooring or catenaries mooring system, to maintain its position. The spar design is commonly used for drilling, production, or both. The distinguishing feature of a spar is its deep-draft hull, which produces very favorable motion characteristics. The hull is constructed by using normal marine and shipyard fabrication methods, and the number of wells, surface wellhead spacing, and facilities weight dictates the size of the center well and the diameter of the hull. In the classic or full cylinder hull forms, the whole structure is divided into upper, middle, and lower sections. The upper section is compartmentalized around a flooded center well housing different types of risers, namely production riser, drilling riser, and export/import riser. This upper section provides buoyancy for the spar. The middle section is also flooded but can be configured for oil storage. The bottom section, called keel, is also compartmentalized to provide buoyancy during transport and to contain any field-installed, fixed ballast. The mooring lines are a combination of spiral strand wire and chain. Taut mooring system is possible due to small motions of the spar and has a reduced scope, defined as the ratio of length of the mooring line to water depth, and cost compared with a full catenary system. Mooring lines are anchored to the seafloor with a driven or suction pile.

The advantages of spar platforms are as follows: (i) low heave and pitch motion compared to other platforms; (ii) use of dry trees (i.e., on surface); (iii) ease of fabrication; (iv) unconditional stability as its center of gravity is always lower than the center of buoyancy, resulting in a positive GM (metacentric height); and (v) derive no stability from its mooring system and hence does not list or capsize even when completely disconnected from its mooring system. Few disadvantages include the following: (i) Installation is difficult as the hull and the topsides can only be combined offshore after the spar hull is upended; (ii) have little storage capacity which brings along the necessity of a pipeline or an additional FSO; and (iii) have no drilling facilities.

1.3 New-generation Offshore Platforms

As the availability of oil and gas reserves moves toward higher waters depths, oil and gas exploration is targeted at deep and ultra-deep waters. As the encountered environmental loads are more severe in greater water depths, the geometric *form* of offshore platforms proposed for deep and ultra-deep waters needs special attention. Apart from being cost-effective, the proposed geometric form shall also have better motion characteristics under the encountered forces arising from the rough sea. Offshore structures that are found suitable for deep and ultra-deep waters are shown in Fig. 1.10.

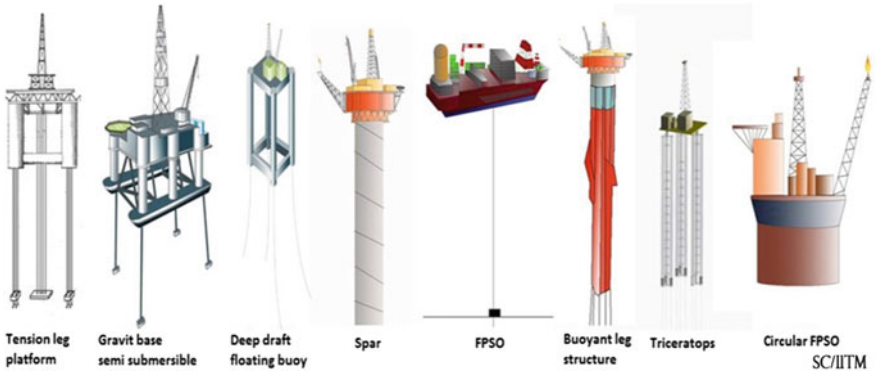

Fig. 1.10 Different types of ultra-deep-water structures

1.3.1 Buoyant Leg Structure (BLS)

Buoyant leg structures (BLSs) are tethered spars with single or group of cylindrical water-piercing hulls; these are alternative structural forms to TLPs and conventional spars. They are positively buoyant wherein the buoyancy exceeds the mass of the structure. Although being positively buoyant, positive metacentric height is maintained to ensure the desired structural stability even after the removal of tethers from the structure. This characteristic ensures high stability and deep draft, which makes the structural form relatively insensitive to increased water depth. Since the BLS is a deep-draft structure, the exposed structural part near the free surface is reduced, and the forces exerted on the structure reduce when compared with the conventional TLPs. Since the risers are inside the moon pool of the BLS, the forces exerted on the risers are also minimized, but below the keel of the BLS, some forces like wave or current act. Halkyard et al. (1991) initially proposed the concept of a tension buoyant tower, which is modified subsequently by other researchers (Robert and Capanoglu 1995; Perryman et al. 1995). The structural form of BLS is evolved by combining the advantageous features of spars and TLPs where its deep-draft hull limits the vertical motion to a significant extent (Shaver et al. 2001); BLS resembles spar due to its shape and deep-draft feature, and its response behavior is similar to that of a TLP due to its restoring system. BLS is simple to fabricate, easy to load-out, tow, and install (Capanoglu et al. 2002). Figure 1.11 shows the views of buoyant tower in the fabrication yard, while different stages of installation of BLS are shown in Fig. 1.12. Installation process of BLS is the combination of the installation procedures of spar and TLP. Since spar is a stable structure, it is installed simply by free-floating, while TLP is generally installed by achieving required pretension in tethers using the following techniques: (i) ballast; (ii) pull-down; or (iii) both pull-down and ballast methods. During the installation of BLS, the structure can be free-floated using its permanent ballast. Pretension in the tethers can be achieved by the above-mentioned procedure. In the ballast method, the

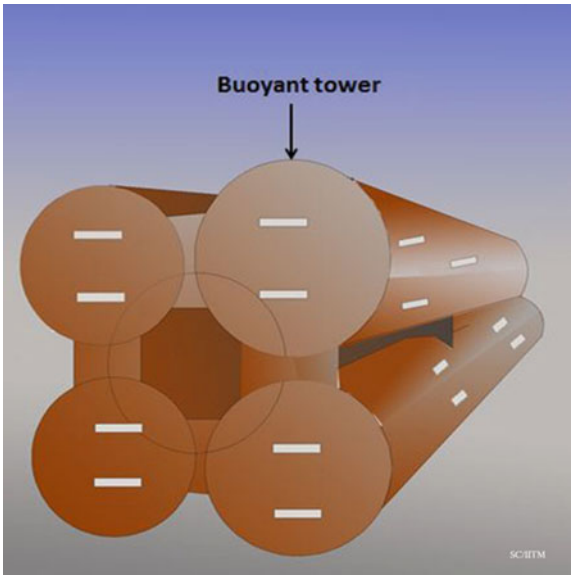

Fig. 1.11 Buoyant tower in the fabrication yard

structure is additionally ballasted until it achieves the required draft; tethers are then attached from the structure to the seafloor. Additional ballast is removed from the structure to enable pretension in the tethers. In the pull-down method, free-floating structure is pulled down until it achieves the required draft; excess buoyancy that is transferred to the tethers helps to achieve the desired pretension. Pull-down and ballast methods are the combination of the above-mentioned procedures. BLS imposes improved motion characteristics and more convenient riser systems, as they consist of simple hulls in comparison with spars or TLPs. BLS is more economic than TLPs or spars due to the reduced cost of commissioning. The first buoyant tower drilling production platform, CX-15 for Peru's Corvina offshore field, is installed in September 2012 at a water depth of more than 250 m with a production capacity of 12,200 barrels per day.

1.3.2 Triceratops

More innovative geometric forms of offshore platforms are evolved in the recent past to improve the motion characteristics of these platforms under deep and ultra-deep waters. Triceratops, Non-ship shaped FPSOs and Min Doc are few of them. The conceptual idea of a triceratops discussed in literature indicated favorable characteristics of the platform under deep and ultra-deep waters (White et al. 2005); Fig. 1.13 shows the conceptual view of the triceratops. Geometric innovativeness imposed in the design by the introduction of ball joints between the deck and BLS makes triceratops different from other new-generation offshore platforms.

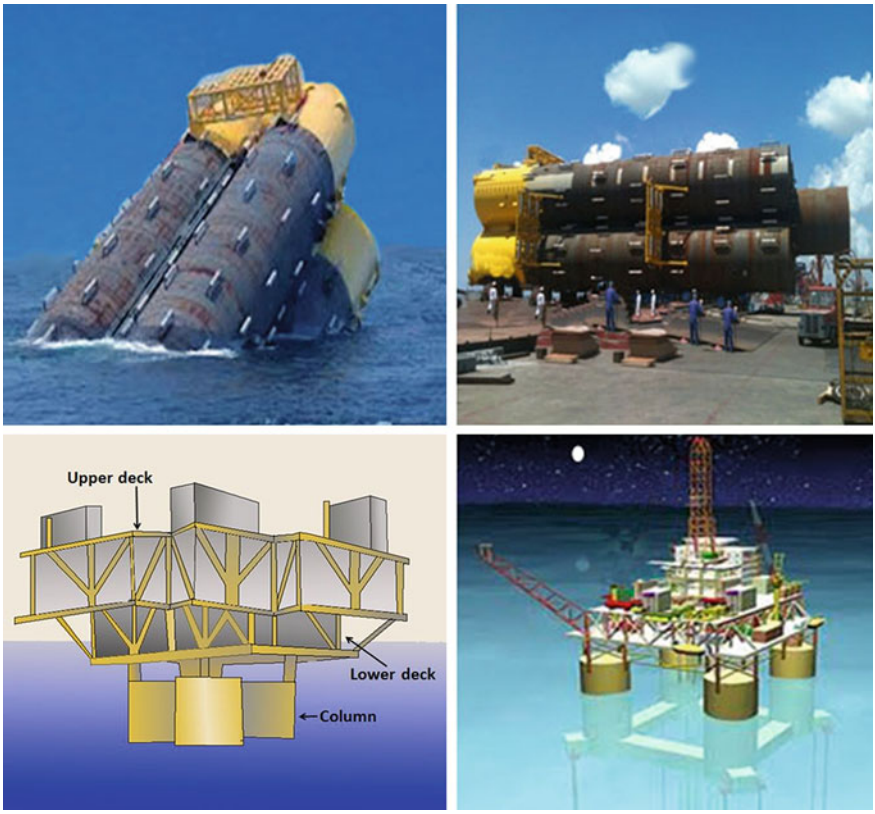

Fig. 1.12 Load out and installed structure in offshore field

Fig. 1.13 Conceptual view of triceratops

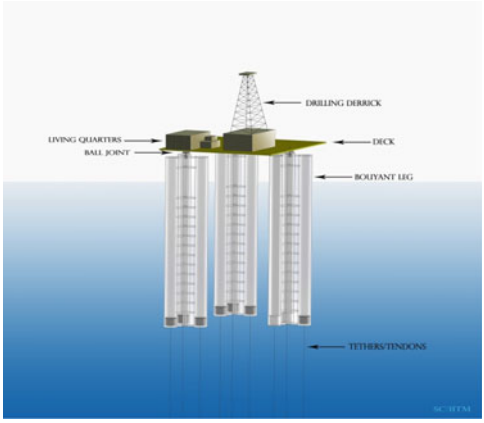

Triceratops consists of three BLS units, deck, and three ball joints between the BLS units and the deck. The restoring system is either with restraining legs or with the tether. Ball joints transfer all translations but not rotations about any axis, making the platform different from other classic types of offshore structures. The distinct motion characteristics of its structural members such as BLS and the deck provide uniqueness to its structural behavior under lateral loads. Common types of offshore platforms have rigid body motion due to the rigid connection between the members, which makes the platform to respond as a single unit. As triceratops is integrated with different structural elements, it behaves as a rigid body in all translations degrees of freedom but not in rotations about any axis due to the presence of the ball joints. Rotational responses of BLS differ from that of the deck. Studies focusing on their response behavior become interesting as the responses of BLS and the deck are dealt separately, which is not a common practice in most of the offshore platforms. In addition, the derived geometric form has few advantages: (i) reduction in forces exerted on the platform due to the decrease in the exposed part of the structure near the free surface and (ii) protection of risers from lateral forces as they are located inside the moon pool of the BLS. The presence of ball joints between the deck and BLS restrains the transfer of the rotational motion of the deck from BLS; translational motion and rotational motion of BLS under the encountered environmental loads are significantly high. However, due to the deep draft of the BLS, there is more possibility of unusual corrosion. Corrosion challenges can be overcome by few techniques such as (i) frequent inspection using corrosion testing probes; (ii) use of sacrificial anodes; (iii) anti-corrosive coatings; and (iv) use of cathodic protection. The salient advantages are, namely (i) better motion characteristics; (ii) suitable for deep waters; (iii) improved dynamics in comparison with TLPs and spars; (iv) wells within protected environment and are laterally supported; (v) simple structure; (vi) simple station keeping; (vii) easy to install and decommission (installation can be part by part or as a whole structure); (viii) reusable and relocated; (ix) simple restraining system (does not require high-strength systems such as TLPs); (x) highly stable structure; and (xii) relatively low cost.

1.3.3 Floating, Storage and Regasification Units (FSRUs)

Transportation of unprocessed crude from the drilling/exploratory platform to the onshore site involves expensive systems like transportation through pipes, large vessels, etc., which makes the oil production more expensive. In particular, the offshore platforms located offshore prove to be highly uneconomical. Key components of FSRU consist of regasification equipment that transforms LNG at −160 °C to has at high-pressure storage tanks, loading arms for receiving LNG, export manifolds, and seawater pumps that uses seawater to regasify the LNG. FSRU is the more cost-effective alternative to meet the lower demand of LNG than traditional, land-based terminals. It contains regasification unit, gas turbine with generator, air compressors, fuel pumps, firewater and foam systems, freshwater

systems, cranes, lubrication oil system, lifeboats, and helipad. The LNG is stored at −160° in double-walled insulated tanks to limit boil-off. The outer walls of the tank are made of prestressed reinforced concrete or steel to limit the temperature during storage period. Despite the high-quality insulation, a small amount of heat still penetrates the LNG tanks, causing minor evaporation. The resulting boil-off gas is captured and fed back into the LNG tank using compressor and recondensing systems. This recycling process prevents any natural gas from escaping the terminal under normal operating conditions. The LNG is subsequently extracted from the tanks, pressurized, and regasified using heat exchangers. The tanks are equipped with submerged pumps that transfer the LNG toward other high-pressure pumps. The compressed LNG (at around 80 times atmospheric pressure) is then turned back into a gaseous state in vaporizers. Once returned to its gaseous state, the natural gas is treated in a number of ways, including metering and odorizing, before it is fed into the transmission network.

The LNG is warmed using the heat from the seawater. This is done in a heat exchanger (with no contact between the gas and the seawater), resulting in a slight drop in the temperature of the seawater, which reaches 6 °C at the end of the discharge pipe, quickly becoming imperceptible once diluted. Natural gas is odorless. Although non-toxic, it is inflammable and is odorized to ensure even the slightest leak can be identified. This is done by injecting tetrahydrothiophene (THT), which is an odorant detectable in very small doses, at the terminal before the natural gas is distributed.

Gas turbine equipped at the topside of the FSRU uses multiple units of generating capacity of up to 10–12 MW. The instrument air system provides air for the plant and the instrument air in process control and maintenance. Inert gas (nitrogen) is generated on demand by a membrane package using dry, compressed air. A backup inert gas supply system consisting of compressor seals, cooling medium, expansion drums, and utility stations is also provided. The oil pump provides high-pressure oil to the engine. The fuel is pumped from the fuel tank to the primary fuel filter/water separator, which is then pressurized to 650 kPa gauge pressure by the fuel transfer pump. The pressurized fuel is passed through the secondary/tertiary fuel filter. Water supply for the fire-fighting systems is supplied by firewater pumps at a pumping rate of about 600–5,000 m^3/h at the discharge flange at a pressure of about 18 bar. A film-forming fluoroprotein (FFFP) concentrate system is provided to enhance the effectiveness of the deluge water spray that protects the separator module, which has high potential for hydrocarbon pool fires. FFFP is a natural protein foaming agent that is biodegradable and non-toxic. The freshwater maker system will utilize a reverse osmosis process to desalinate the seawater at the rate of 5 m^3/h. The saline effluent from the freshwater is directed overboard through the seawater discharge caissons, while the freshwater will be stored in a freshwater tank. Water delivered to the accommodation module is further sterilized in a UV sterilization plant before stored in a potable water header tank. The lubrication system contains an oil cooler, oil filter, gear-driven oil pump, pre-lube pump, and an oil pan that meets offshore tilt requirements. The internal lubrication system is designed to provide a constant supply of filtered, high-pressure oil. This system

meets the tilt requirements for non-emergency offshore operations. Lubrication oil should have special features in offshore requirements such as (i) water solubility; (ii) non-sheering on water surface; (iii) excellent lubrication properties; (iv) bio-degradable; and (v) non-toxic to aquatic environment.

Exercise

1. With the depletion of onshore and offshore shallow water reserves, the_____ of oil in deep waters has become a challenge to offshore industry.
2. An offshore structure has no _____ access to dry land and may be required to stay in _____ in all weather conditions.
3. _____ differs from the other fixed structures strictly by weight contained in their base structure.
4. Most floating production systems and virtually all semisubmersibles, FPSs and FPSOs, produce oil and gas from the wells on the seabed called _____.
5. _____ generally show very high displacements, which demands protection of the well casings from the environment.
6. The tension leg platform is heave restrained by _____.
7. Deep-water floating production systems are generally concentrated in _____.
8. Offshore structures are classified by two independent parameters, namely _____ and _____.
9. A mobile offshore drilling unit [MODU] configuration is largely determined by two parameters, namely_____ and _____.
10. Production units have several functions such as _____, _____, _____, _____, _____, and _____.
11. Functional requirements for offshore facilities are determined by the primary variables _____, _____, and _____.
12. Functional operation of offshore structures influences the _____ of the structure.
13. List two desirable characteristics of exploratory drilling platforms deployed in extreme sea states: _____ and _____.
14. Three of the most common forms of drilling platforms are _____, _____, and _____.
15. Drilling platforms with _____ and _____ are set on the seafloor by _____.
16. Semisubmersibles have good _____ in severe environments and stay longer in drilling modes.
17. Jack-up rigs are usually _____ during transit and are _____ from one site to the other.

18. In shallow waters, the most common type of production platform is _____.
19. Production techniques may originate from _____, and drilling may be performed with _____.
20. Storage capacity of the structure is governed by the _____ and _____.
21. Bottom-founded structure with notable exception in terms of construction material is _____.
22. Bottom-supported structures are also called as _____.
23. Fixed structure behaves as a _____ and usually resists the lateral loads encountered.
24. _____ bottom-supported structures are usually designed such that their lowest natural frequency is below the energy content of the _____.
25. _____, _____, and _____ cause the offshore structures to deflect.
26. _____ is achieved through taut moorings anchored to the seabed.
27. Floating structures have various _____.
28. _____ such as semisubmersible, spars, and drill ships are _____ unrestrained and are allowed to have _____ degrees of freedom such as _____.
29. _____ such as tension leg platform, tethered buoyant towers, or buoyant leg structures are _____ to the seabed and _____ restrained.
30. Match the following:

1. Payload of bottom-supported structure	(a) Resisted by vessel inertia and stability, mooring strength
2. Regulatory and design practices: floating structure	(b) Buoyancy
3. Environmental loads of floating structure	(c) Resisted by foundation bearing capacity
4. Construction of bottom-supported structure	(d) Resisted by strength of the structure and foundation, compliant structure inertia
5. Payload of floating structure	(e) Tubular space frame: fabrication yards
6. Installation of bottom-supported structure	(f) Plate and frame displacement hull : ship yards
7. Regulatory and design practices: bottom-supported	(g) Barge (dry) transport and launch, upend, piled foundation
8. Construction of floating structure	(h) Wet or dry transport, towing to site and attachment to preinstalled moorings
9. Installation of floating structure	(i) Oil industry practices and government petroleum regulation
10. Environmental loads of bottom-supported structure	(j) Oil industry practices, government petroleum regulation, and coast guard and international maritime regulations

31. _____ platform is typically controlled by their functional gravity loads and lateral force and overturning moments due to wind, wave, and current.
32. For floating structure, it is necessary to evaluate _____ loads due to _____.
33. _____ is a term used to define a system for keeping the facility within a specified distance at the desired location.
34. Jack-up rigs are primarily used for _____; similar to _____ with movable legs.
35. Semisubmersibles are _____ type of offshore structures, which are primarily designed for _____ and _____purposes.
36. Drill ships are primarily used for _____.
37. Tension leg platform is primarily designed for _____, which is developed from semisubmersibles that are _____ to the seafloor with tethers.
38. _____ is designed primarily for production with a composition of steel framed tubular structure attached to seabed with piles driven into seafloors.
39. _____ are typically large reinforced concrete, bottom-mounted structure which resist the lateral loads by its self-weight.
40. _____ is a structure designed for small field production, which is composed of slender truss steel structure supported by _____ foundation.

Answers

1. Exploration and production
2. Fixed access; position
3. Gravity-based structure
4. Subsea wells
5. Floating platforms
6. Vertical tendons or tethers
7. Gulf of Mexico
8. Functions and configurations
9. Variable deck payload and transit speed requirements
10. Processing, drilling, work over, accommodation, oil storage, and riser support
11. Reservoir and fluid characteristics, water depth, and ocean environment
12. Configuration
13. Limited structural motions and good station keeping
14. Drill ships, jack-up barges, and semisubmersibles
15. Buoyant legs and pontoons; ballasting
16. Motion characteristics
17. Buoyant; towed
18. Fixed piled structures or jacket structures

19. Wet or dry tress; subsea blowout preventer (BOP) or surface BOP.
20. Size of the shuttle tankers and frequency of the ships
21. Gravity-based structure
22. Fixed structure
23. Rigid body
24. Compliant; waves
25. Waves, wind, and current
26. Compliancy
27. Degrees of compliancy
28. Neutrally buoyant structures; dynamically; six; heave surge, sway, pitch, roll, and yaw
29. Positively buoyant structures; tethered; heave
30. 1(c); 2(j); 3(a); 4(e); 5(b); 6(g); 7(i); 8(f); 9(h); 10(d)
31. Fixed
32. Inertial; acceleration
33. Station keeping
34. Exploratory drilling; barge
35. Floating; exploratory and production
36. Exploratory drilling
37. Production; tethered
38. Fixed jacketed structure
39. Gravity-based structures
40. Guyed tower; spud can

Chapter 2
Environmental Forces

Abstract This chapter deals with different types of environmental loads on offshore structures. It also includes code information regarding the loads. Step-by-step method for load estimate on a cylindrical member and an example structure is detailed. The procedure for estimating wave loads is illustrated through examples. Solved numerical examples and exercise are given at the end for practice.

Keywords Wind forces · Wave forces · Aerodynamic admittance function · Current forces · Wave theories · Marine growth · Design requirements · Allowable stress method · Limit state method · Fabrication and erection loads

2.1 Introduction

Loads acting on offshore structures are classified into the following categories:

- Permanent loads or dead loads
- Operating loads or live loads
- Other environmental loads including earthquake loads
- Construction and installation loads
- Accidental loads

While the design of buildings onshore is influenced mainly by the permanent and operating loads, the design of offshore structures is dominated by environmental loads, especially waves, and the loads arising in the various stages of construction and installation. In civil engineering, earthquakes are normally regarded as accidental loads (see Eurocode 8), but in offshore engineering, they are treated as environmental loads.

Environmental loads are those caused by environmental phenomena. These include wind, waves, current, tides, earthquakes, temperature, ice, seabed movement, and marine growth. Their characteristic parameters, defining design load values, are determined in special studies on the basis of available data. According to

S. Chandrasekaran, *Dynamic Analysis and Design of Offshore Structures*,
Ocean Engineering & Oceanography 5, DOI 10.1007/978-81-322-2277-4_2

US and Norwegian regulations (or codes of practice), the mean recurrence interval for the corresponding design event must be 100 years, while according to the British rules, it should be 50 years or greater. The different loads to be considered while designing the structure are wind loads, wave load, mass, damping, ice load, seismic load, current load, dead load, live load, impact load, etc.

2.2 Wind Force

Wind forces on offshore structures are caused by complex fluid-dynamics phenomenon, which is generally difficult to calculate with high accuracy. Most widely used engineering approaches to estimate wind forces on offshore structures are based on few observations as listed below:

- When stream of air flows with constant velocity (v), it will generate force on the flat plate of area (A).
- The plate will be placed orthogonal to the flow direction.
- This force will be proportional to (Av^2).
- The proportionality constant is independent of the area, which is verified by experimental studies.

Hence, the wind force on a plate orthogonal to the wind flow direction can be determined by the net wind pressure as given below:

$$p_{\mathrm{w}} = \frac{1}{2}\rho_{\mathrm{a}} C_{\mathrm{w}} v^2 \tag{2.1}$$

where ρ_{a} is mass density of air (1.25 kg/m^3), and C_{w} is wind pressure coefficient. It is important to note that the mass density of air increases due to the water spray (splash) up to a height of 20–20 m above MSL. Hence, the total wind-induced force on the plate is given by:

$$F_{\mathrm{w}} = p_{\mathrm{w}} A \tag{2.2}$$

If the plate has an angle (θ) with respect to the wind direction, then the appropriate projected area, normal to the flow direction, should be used in the above equation. The wind pressure coefficient C_{w} is determined under controlled stationary wind flow conditions in a wind tunnel. It depends on the Reynolds number; typical values of 0.7–1.2 are used for cylindrical members. Natural wind has two components: (i) mean wind component (which is static component) and (ii) fluctuating, gust component (which is a dynamic component). The gust component is generated by the turbulence of the flow field in all the three spatial directions. For offshore locations, mean wind speed is much greater than the gust component, which means that in most of the design cases, a static analysis will suffice. The wind velocity is given by:

$$v(t) = \bar{v} + v(t) \tag{2.3}$$

where $\bar{v}\sqrt{a^2 + b^2}$ is the mean wind velocity and $v(t)$ is the gust component. The spatial dependence of the mean component is only through the vertical coordinate, while $v(t)$ is homogeneous in both space and time. Wind force in the directions parallel (drag force) and normal to the wind direction (lift force) is given by:

$$\begin{aligned} F_{\mathrm{D}} &= \frac{1}{2}\rho C_{\mathrm{D}} \bar{v}_{\mathrm{z}} A \\ F_{\mathrm{L}} &= \frac{1}{2}\rho C_{\mathrm{L}} \bar{v}_{\mathrm{z}} A \end{aligned} \tag{2.4}$$

Wind spectrum above water surface is given by 1/7th power law, which is:

$$v_z = V_{10}\left[\frac{z}{10}\right]^{\frac{1}{7}} \tag{2.5}$$

where v_z is the wind speed at elevation of z m above MSL, V_{10} is the wind speed at 10 m above MSL, and 10 m is called the reference height. Power law is purely empirical and most widely used. It is tested with the actual field measurements and found to be in good agreement. As Eq. (2.5) gives mean wind component, the gust component can be obtained by multiplying a gust factor with the sustained wind speed. Average gust factor (F_{g}) is in the range of 1.35–1.45; variation of the gust factor along the height is negligible. The sustained wind speed, which is to be used in the design, is the *one minute average wind speed*, according to the US Weather Bureau. The product of sustained wind speed and the gust factor will give the *fastest mile velocity*. 200 year sustained wind velocity of 125 miles per hour is to be used for the design of offshore structures.

Wind produces a low-frequency excitation. The fluctuating component is modeled probabilistically. Drag force on the members is caused by the encountered waves and wind. Wave forces alone acting on the member will cause inertia and drag forces, while earthquake forces cause only inertia forces on the members. Hence, vibration of the structure induced by wind and waves is different from that caused by earthquakes. For the design of members under wind loads, most of the international codes prefer quasi-static analysis. Very slender and flexible structures are wind-prone; for members under wave action, de-amplification takes place in flexible structures due to compliancy. While considering wind as a dynamic process, the following parameters are important:

- Length of the record: The record can be continuous, intermittent or a selective whose values are usually above the threshold ones. For the record to be continuous, average values of the wind velocity is lesser than that of the intermittent because of the longer length of the record when compared with the former.
- Wind spectrum: It is used as input for the structural analysis, which defines the fluctuating wind component.
- Gust component: It is approximated by the *aerodynamic admittance function*.

Aerodynamic admittance function is an intelligent way to define the cross-spectrum in the analysis, indirectly. There are two reasons for using the aerodynamic admittance function: (i) to bypass the rigorous random analysis and (ii) possibility of an accurate measurement of this function through wind-tunnel experiments. In this manner, the spatial variations of wind velocity are handled intelligently in the design. Force due to wind is given by:

$$\begin{aligned} F_{\mathrm{w}}(t) &= \frac{1}{2}\rho_{\mathrm{a}} C_{\mathrm{w}} v^2 A \\ &= \frac{1}{2}\rho_{\mathrm{a}} C_{\mathrm{w}} A[\bar{v} + v(t)]^2 \\ &= \frac{1}{2}\rho_{\mathrm{a}} C_{\mathrm{w}} A\left[\bar{v}^2 + (v(t))^2 + 2\bar{v}v(t)\right] \end{aligned} \tag{2.6}$$

by neglecting higher powers of gust component,

$$\cong \bar{F}_{\mathrm{w}} + \rho_{\mathrm{a}} C_{\mathrm{w}} A\, \bar{v} v(t)$$

In the above equation, wind force is expressed as a sum of mean component and the gust component. Wind is considered as an ergodic process; the (one-sided) power spectral density of the wind process is then related to the wind spectrum as:

$$S_{\mathrm{F}}^{+}(\omega) = [\rho_{\mathrm{a}} C_{\mathrm{w}}\, A\, \bar{v}]^2 S_{\mathrm{U}}^{+}(\omega) \tag{2.7}$$

Substituting Eq. (2.2) in Eq. (2.7) and rearranging the terms, we get:

$$S_{\mathrm{F}}^{+}(\omega) = \frac{4[\bar{F}_{\mathrm{w}}]^2}{[\bar{v}]^2}\left[\chi\left\{\frac{\omega\sqrt{A}}{2\pi\bar{v}}\right\}\right]^2 S_{\mathrm{U}}^{+}(\omega) \tag{2.8}$$

In the above equation, force and the response spectra are connected by the *aerodynamic admittance function*, which varies as below:

$$\begin{aligned} &\text{for} \quad \frac{\omega\sqrt{A}}{2\pi\bar{v}} \Rightarrow 0, \quad \chi\left\{\frac{\omega\sqrt{A}}{2\pi\bar{v}}\right\} \Rightarrow 1 \\ &\text{for} \quad \frac{\omega\sqrt{A}}{2\pi\bar{v}} \Rightarrow \infty, \quad \chi\left\{\frac{\omega\sqrt{A}}{2\pi\bar{v}}\right\} \Rightarrow 0 \end{aligned} \tag{2.9}$$

Aerodynamic admittance function is proposed through an empirical relationship by Davenport (1977):

$$\chi(x) = \left\{\frac{1}{\left[1 + (2x)^{4/3}\right]}\right\} \tag{2.10}$$

Wind spectra for the design of offshore structures are listed below with the details. For the reference height of z = 10 m, wind spectra as applied to offshore structures are expressed in terms of circular frequency as given below:

$$S_u^+(\omega) = fG_u^+(f) \tag{2.11}$$

(i) *Davenport spectrum*

$$\frac{\omega S_u^+(\omega)}{\delta \overline{U}_p^2} = \frac{4\theta^2}{\left(1+\theta^2\right)^{4/3}} \tag{2.12}$$

(ii) *Harris spectrum*

$$\frac{\omega S_u^+(\omega)}{\delta \overline{U}_p^2} = \frac{4\theta}{\left(2+\theta^2\right)^{5/6}} \tag{2.13}$$

Derivable variable θ is given by:

$$\theta = \frac{\omega L_u}{2\pi \overline{U}_{10}} = \frac{\delta L_u}{\overline{U}_{10}}, \quad 0 < \theta < \infty \tag{2.14}$$

where L_u is integral length scale (=1,200 m for Davenport and 1,800 m for Harris spectrum), δ is surface drag coefficient referred to $\bar{U}_{10}$. For offshore locations, $\delta = 0.001$. It is important to note that none of these spectrum used in the analysis of wind speed is recorded offshore; they are based on onshore records. Hence, these applications to offshore locations are questionable. They have serious problem when used for low-frequency flexible structures. Alternatively, for large floating structures, following spectra are recommended by Dyrbye and Hassen (1997):

(a) *Kaimal spectrum*

$$\frac{\omega S_u^+(\omega)}{\sigma_u^2} = \frac{6.8\,\theta}{(1+10.2\,\theta)^{5/3}} \tag{2.15}$$

where σ_u^2 is the variance of $U(t)$ at reference height of 10 m?

(b) *API (2000) spectrum*

$$\frac{\omega S_u^+(\omega)}{\sigma_u(z)^2} = \frac{\left(\omega/\omega_p\right)}{\left[1+1.5\left(\omega/\omega_p\right)\right]^{5/3}} \tag{2.16}$$

where ω_p is peak frequency and σ_z^2 is the variance of $U(t)$, which is not assumed as independent.

$$0.01 \leq \frac{\omega_p z}{\overline{U}(z)} \leq 0.1 \tag{2.17}$$

Usually, a value of 0.025 is obtained in lieu of the values computed from the above equation. Standard deviation and speed are given by:

$$\sigma_u(z) = \begin{cases} 0.15\overline{U}(z)\left(\frac{Z_s}{Z}\right)^{0.125} : Z \leq Z_s \\ 0.15\overline{U}(z)\left(\frac{Z_s}{Z}\right)^{0.275} : Z > Z_s \end{cases} \tag{2.18}$$

where Z_s is the thickness of the surface layer, which is usually taken as 20 m.

2.3 Wave Forces

Wind-generated sea surface waves shall be represented as a combination of series of regular waves. Regular waves of different magnitude and wave lengths from different directions are combined to represent the sea surface elevation. Water particle kinematics of regular waves is expressed by the sea surface elevation by various wave theories (Srinivasan and Bhattacharyya 2012). Among all the theories, Airy's wave theory is commonly used because it assumes linearity between the kinematic quantities and the wave height, which makes the wave theory simple. Airy's theory assumes a sinusoidal wave form of wave height (H), which is small in comparison with the wave length (λ) and water depth (d) as given below:

$$\begin{aligned} \eta(x,t) &= \frac{H}{2}\cos(kx - \omega t) \\ k &= \frac{2\pi}{\lambda} \\ \dot{u}(x,t) &= \frac{\omega H}{2}\frac{\cosh(ky)}{\sinh(kd)}\cos(kx - \omega t) \\ \dot{v}(x,t) &= \frac{\omega H}{2}\frac{\sinh(ky)}{\sinh(kd)}\sin(kx - \omega t) \\ \ddot{u}(x,t) &= \frac{\omega^2 H}{2}\frac{\cosh(ky)}{\sinh(kd)}\sin(kx - \omega t) \\ \ddot{v}(x,t) &= -\frac{\omega^2 H}{2}\frac{\sinh(ky)}{\sinh(kd)}\cos(kx - \omega t) \end{aligned} \tag{2.19}$$

Airy's theory is valid up to mean sea level only. However, due to the variable submergence effect, the submerged length of the members will be continuously changing. This will attract additional forces due to their variable submergence at any given time. To compute the water particle kinematics up to the actual level of submergence, stretching modifications suggested by various researchers are used.

(a) Wheeler suggested the following modification in the horizontal water particle velocity and acceleration to include the actual level of submergence of the member:

$$\begin{aligned} \dot{u}(x,t) &= \frac{\omega H}{2}\frac{\cosh\left(ky\left[\frac{d}{d+\eta}\right]\right)}{\sinh(kd)}\cos(kx-\omega t) \\ \ddot{u}(x,t) &= \frac{\omega^2 H}{2}\frac{\cosh\left(ky\left[\frac{d}{d+\eta}\right]\right)}{\sinh(kd)}\sin(kx-\omega t) \end{aligned} \tag{2.20}$$

(b) Chakrabarti suggested the modification as given below:

$$\begin{aligned} \dot{u}(x,t) &= \frac{\omega H}{2}\frac{\cosh(ky)}{\sinh(k(d+\eta))}\cos(kx-\omega t) \\ \ddot{u}(x,t) &= \frac{\omega^2 H}{2}\frac{\cosh(ky)}{\sinh(k(d+\eta))}\sin(kx-\omega t) \end{aligned} \tag{2.21}$$

The sea state, in a short term, which is typically 3 h, is assumed as zero-mean, ergodic Gaussian process. This can be defined completely by a wave spectrum. For North Sea, Johnswap spectrum is recommended. For open sea conditions, Peirson–Moskowitz (P–M) spectrum is recommended. In a long term, variation of sea state is slower than the short-term fluctuations. It is often approximated by a series of stationary, non-zero-mean Gaussian process, which is specified by the significant wave height (H_s) and peak wave period (T_p). Following are a few relevant spectra, applicable in the design of offshore platforms.

2.4 Wave Theories

Wave theories serve to calculate the particle velocities, accelerations, and the dynamic pressure as functions of the surface elevation of the waves. For long-crested regular waves, the flow can be considered two-dimensional and are characterized by parameters such as wave height (H), period (T) and water depth (d), as shown in Fig. 2.1. $k = 2\pi/L$ denotes the wave number, $\omega = 2\pi/T$ denotes the wave circular frequency, and $f = 1/T$ denotes the cyclic frequency. Different wave theories available are as follows:

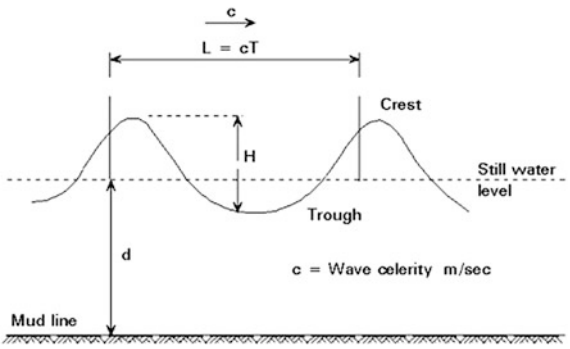

Fig. 2.1 Definition of wave parameters

- Linear or first-order or Airy theory
- Stokes fifth-order theory
- Solitary wave theory
- Cnoidal theory
- Dean's stream function theory
- Numerical theory by Chappelear

Figure 2.2 shows the chart for the selection of the most appropriate theory, based on the parameters, H, T, and d. For example, linear wave theory can be applied when $H/gT^2 < 0.01$ and $d/GT^2 > 0.05$, besides other ranges, as shown in the figure.

(a) *PM spectrum for wave loads*

$$S^+(\omega) = \frac{\alpha g^2}{\omega^5} \exp\left[-1.25\left(\frac{\omega}{\omega_0}\right)^{-4}\right] \tag{2.22}$$

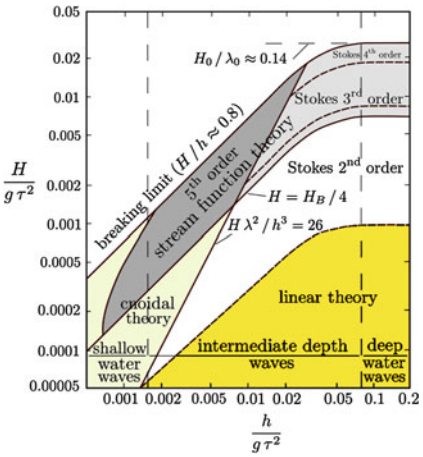

Fig. 2.2 Wave theory selection chart (Sarpakaya and Issacson 1981)

where α is Phillips constant $\cong 0.0081$.

(b) *Modified PM spectrum (2 parameters H_s, ω_0)*

$$S^+(\omega) = \frac{5}{16} H_s \frac{\omega_0^4}{\omega^5} \exp\left[-1.25\left(\frac{\omega}{\omega_0}\right)^{-4}\right] \tag{2.23}$$

(c) *International Ship Structures Congress (ISSC) spectrum (2 parameters H_s, $\bar{\omega}$)*

$$\begin{aligned} S^+(\omega) &= 0.1107 H_s \frac{\omega^{-4}}{\omega^5} \exp\left[-0.4427\left(\frac{\omega}{\bar{\omega}}\right)^{-4}\right] \\ \overline{\omega} &= \frac{M_1}{M_0} \end{aligned} \tag{2.24}$$

where M_1 and M_0 are spectral moments.

(d) *Johnswap spectrum (5 parameters $H_s, \omega_{0o}, \gamma, \tau_a, \tau_b$)*

$$S^+(\omega) = \frac{\overline{\alpha} g^2}{\omega^5} \exp\left[-1.25\left(\frac{\omega}{\omega_0}\right)^{-4}\right] \gamma^{a(\omega)} \tag{2.25}$$

where γ is the peakness parameter.

$$a(\omega) = \exp\left[-\frac{(\omega - \omega_0)^2}{2\overline{\sigma}^2 \omega_0^2}\right] \tag{2.26}$$

where $\bar{\sigma}$ is spectral width parameter and is given by:

$$\overline{\sigma}_a = 0.07, \quad \omega \leq \omega_0 \tag{2.27}$$

$$\overline{\sigma}_b = 0.09, \quad \omega > \omega_0 \tag{2.28}$$

The modified Phillips constant is given by:

$$\overline{\alpha} = 3.25 \times 10^{-3} H_s^2 \omega_0^4 [1 - 0.287 \ln(\gamma)] \tag{2.29}$$

$$\gamma = 5 \text{ for} \frac{T_p}{\sqrt{H_s}} \leq 3.6 \tag{2.30}$$

$$= \exp\left[5.75 - 1.15 \frac{T_p}{\sqrt{H_s}}\right] \text{ for } \frac{T_p}{\sqrt{H_s}} > 3.6 \tag{2.31}$$

$$H_s = 4\sqrt{m_0} \tag{2.32}$$

where γ varies from 1 to 7.

Main force components, rising from the wave loads, are grouped as follows: (i) *Froude–Krylov force*, which is caused by the pressure effects due to the undisturbed incident waves; (ii) *diffraction force*, which is caused by the pressure effects due to the presence of the structure in the fluid-flow domain; (iii) *hydrodynamic added mass and potential damping forces*, which is caused by the pressure effects due to the motion of the structural components in ideal fluid; and (iv) *viscous drag force*, which is caused by the pressure effects due to the relative velocity between the water particle and the structural component. For slender structures, *Froude–Krylov force and diffraction forces* are idealized by a single inertia term. Velocity and acceleration do not differ significantly from the values of the cylinder axis when $D/\lambda < 0.2$. When the waves act on the slender structures, the structure oscillates, which will set up waves radiating away from it. Reaction forces are then set up in the fluid, which will be proportional to the acceleration and velocity of the structure. Reaction force proportional to the acceleration of the structure will result in an added mass term, contributing to the inertia force. Reaction force proportional to the velocity results in the potential damping force. If the structure is compliant, the added mass forces associated with the relative acceleration between the fluid particles and the structures are included. Drag force is computed by replacing the water particle velocity with the relative velocity term. The total force acting normal to the axis of the member is given by:

$$\begin{aligned} q_n &= \rho\, \mathrm{d}V \cdot a_n + (C_m - 1)\rho\, \mathrm{d}V(a_n - \ddot{x}_n) + \frac{1}{2}\rho\, C_d\, \mathrm{d}A(v_n - \dot{x}_n)|v_n - \dot{x}_n| \\ &= C_m \rho \mathrm{d}V \cdot a_n - (C_m - 1)\rho \mathrm{d}V\, \ddot{x}_n + \frac{1}{2}\rho\, C_d\, \mathrm{d}A(v_n - \dot{x}_n)|v_n - \dot{x}_n| \end{aligned} \tag{2.33}$$

where ρ is density of fluid, (C_d, C_m) are the drag and inertia coefficients, (v_n, a_n) are velocity and acceleration of the water particle normal to the axis of the member, $\dot{x}, \ddot{x}$ are the velocity and acceleration of the structure, and (dA, dV) are exposed area and displaced volume of water per unit length, respectively.

The above equation has two main issues: first, the relative motion formulation is valid only if the structure motion is of large amplitude; second, the relative velocity formation of the drag produces both excitation and damping forces. In the above equation, the most critical aspect is the evaluation of the drag and inertia coefficients, which is dependent on flow conditions, Keulegan–Carpenter number, and Reynolds number. The recommended value of drag coefficient is 0.6–1.2, while that of the inertia coefficient is 1.2–2.0, as seen in the literature (APR RP 2A). As in the case of bottom-supported structures (gravity platforms), when the diameter of the member is very large, incident waves are disturbed by the presence of the structure. In such cases, viscous force becomes less significant due to the smaller values of the ratio of wave height to member diameter ($H/D \ll 1$). In such cases, the above equations cannot be applied; it is recommended that the analyzer should use numerical methods to determine the forces on the members.

Offshore structures have large plane area. Larger topside is required for accommodating the equipment layout as discussed in the previous chapter. As the

deck is supported by few column members, their spacing plays an important role in order to reduce the interference of the waves by their presence. For a large spacing of c/c distance of column members, there can be cancellation of forces. Let us consider an example of the tension leg platform (TLP). For a typical size of topside of 90 × 90 m, resting on four columns, phase angle (θ) is given by the following relationship:

$$\theta = \frac{2\pi\Delta x}{\lambda} \tag{2.34}$$

where Δx is the c/c distance between the column members (leg spacing) and λ is the wave length. For the spacing between the columns of 90 m and wave period of 10 s, the phase angle will be 1.2π, which can cause cancellation of forces on members. It is important to note that the spacing of the members is chosen in such a manner that the force cancellation effects at the dominant wave frequencies are expected to have close to the natural frequency of the platform. The forces on a submerged structure in waves appear from the pressure distribution on its surface. For a small structure, Morison equation is valid because the flow structure is complex. However, for large structures (relative to the wavelength), the flow remains essentially attached to the surface. It is therefore easier to compute this pressure field. If the computation of the scattered wave potential is waived and its effect is incorporated by a force coefficient, then this force is called the *Froude–Krylov* force. Thus, the calculation of the force is performed assuming that the structure does not distort the wave field in its vicinity. The force is computed by a pressure-area method using the incident wave pressure that is acting on the submerged surface of the structure. Then, a force coefficient is used to account for the wave diffraction.

For a few basic shapes of the structural forms, a closed form expression is obtained by the Froude–Krylov theory: (i) horizontal cylinder, (ii) horizontal half-cylinder, (iii) vertical cylinder, (iv) sphere, (v) hemisphere, and (vi) rectangular barge.

(a) Force on a horizontal cylinder is given by:

$$f_{\mathrm{H}} = r\ell \int_0^{2\pi} p \cos\theta \, \mathrm{d}\theta$$

(b) Force on a vertical cylinder:

Consider a vertical cylinder placed on the ocean bottom and extended above the still water level, as shown in Fig. 2.3:

Velocity potential is given by:

$$\varphi = \frac{gH}{2\omega} \frac{\cosh(ks)}{\cosh(kd)} \sinh(kx - \omega t) \tag{2.35}$$

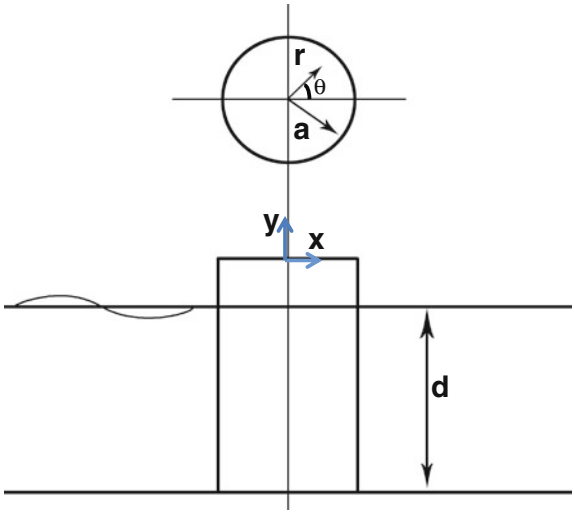

Fig. 2.3 Bottom-supported cylinder

Dynamic pressure is given by:

$$\begin{aligned} p &= \rho \frac{\partial \varphi}{\partial t} \\ &= \rho g \frac{H}{2} \frac{\cosh(ks)}{\cosh(kd)} \cos(kx - \omega t) \end{aligned} \tag{2.36}$$

Horizontal force per unit length is given by:

$$\begin{aligned} f_x &= \rho \int_0^{2\pi} \int_{-d}^{0} \frac{\partial \varphi_0}{\partial t} a \cos\theta \, \mathrm{d}\theta \, \mathrm{d}\ell \\ f_x &= \frac{\rho g a H}{2 \cosh(kd)} \int_{-d}^{0} \cosh(ks) \mathrm{d}s \int_0^{2\pi} \cos[ka \cos\theta - \omega t] \cos\theta \, \mathrm{d}\theta \end{aligned} \tag{2.37}$$

This reduces to the following form, which accounts for the diffraction effect:

$$f_x = C_{\mathrm{H}} \frac{\pi \rho g H a}{k} J_1(ka) \tanh(kd) \sin \omega t \tag{2.38}$$

The above method of computing the forces by the incident wave alone is known as Froude–Krylov theory. It does not give the correct value of the force, as the phase value is accounted for in the equation. It is due to this fact a force coefficient is used in the expression as a multiplier. For a vertical cylinder, the horizontal force coefficient is taken as 2; for small values of *ka*; the value changes as *ka* increases.

Table 2.1 Forces on members of different geometric shapes using Froude–Krylov theory

Basic shape	Horizontal force	C_H	Vertical force	C_V	K_a range
Horizontal cylinder	$C_H\rho V\dot{u}_0$	2.0	$C_V\rho V\dot{v}_0$	2.0	0–1.0
Horizontal half-cylinder	$C_H\rho V[\dot{u}_0 + C_1\omega v_0]$	2.0	$C_V\rho V[\dot{v}_0 + C_2\omega u_0]$	1.1	0–1.0
Vertical cylinder	$C_H\rho V\frac{2J_1(ka)}{ka}\frac{\sinh\left[\frac{k\ell_1}{2}\right]}{\left[\frac{k\ell_1}{2}\right]}\dot{u}_0$	2.0	–	–	–
Rectangular block	$C_H\rho V\frac{\sinh\left[\frac{k\ell_3}{2}\right]}{\left[\frac{k\ell_3}{2}\right]}\frac{\sinh\left[\frac{k\ell_1}{2}\right]}{\left[\frac{k\ell_1}{2}\right]}\dot{u}_0$	1.5	$C_V\rho V\frac{\sinh\left[\frac{k\ell_2}{2}\right]}{\left[\frac{k\ell_3}{2}\right]}\frac{\sinh\left[\frac{k\ell_1}{2}\right]}{\left[\frac{k\ell_1}{2}\right]}\dot{v}_0$	6.0	0–5.0
Hemi sphere	$C_H\rho V[\dot{u}_0 + C_3\omega v_0]$	1.5	$C_V\rho V[\dot{v}_0 + C_4\omega u_0]$	1.1	0–0.8
Sphere	$C_H\rho V\dot{u}_0$	1.5	$C_V\rho V\dot{v}_0$	1.1	0–1.75

Table 2.1 shows the equations for forces using Froude–Krylov theory for different geometric shapes of members.

Where V = submerged volume of the structure; C_H and C_V are force coefficients in the horizontal and vertical directions, respectively; subscript zero indicates that the amplitude of the water particle velocity or acceleration is computed at the center of the geometric shape; and l_1 and l_3 are the length and underwater depth of the rectangular block, respectively. The numerical values of C_1–C_4 depend on the diffraction parameter ka and are given in Table 2.2. The forces in Table 2.1 are given in terms of the water particle acceleration and velocity at the center of the structure wherever possible. The force coefficients shown are applicable over a small range of diffraction parameter. If the values of ka are much different from the range given in the table, values of the force coefficients are to be used with caution.

Table 2.2 Numerical values of C_1–C_4

ka	C_1	C_2	C_3	C_4
0.1	0.037	15.019	0.042	12.754
0.2	0.075	7.537	0.085	6.409
0.3	0.112	5.056	0.127	4.308
0.4	0.140	3.825	0.169	3.268
0.5	0.186	3.093	0.210	2.652
0.6	0.223	2.612	0.252	2.249
0.7	0.259	2.273	0.292	1.966
0.8	0.295	2.024	0.332	1.760
0.9	0.330	1.834	0.372	1.603
1.0	0.365	1.685	0.411	1.482
1.5	0.529	1.273	0.591	1.156
2.0	0.673	1.105	0.745	1.034
2.5	0.792	1.031	0.867	0.989
3.0	0.886	0.999	0.957	0.977
3.5	0.955	0.989	1.015	0.978
4.0	1.000	0.087	1.945	0.985

2.5 Current Forces

The presence of current in water produces the following distinct effects: Current velocity should be added vectorially to the horizontal water particle velocity before computing the drag force, because drag force depends on the square of the water particle velocity. Current decreases slowly with the increase in depth, but even a small magnitude of current velocity can cause significant drag force. This effect is insignificant and generally neglected. Current makes the structure itself to generate waves, which in turn creates diffraction forces. However, these values are negligible for realistic value of current acting on the normal-sized members. The presence of current is alternatively accounted by increasing the wave height to 10–15 % and neglects the presence of current per se.

2.6 Earthquake Loads

Offshore platforms which do not have stiff connection with the seabed are indirectly influenced by earthquakes; those which are bottom-supported are affected by earthquakes directly. Compliant structures that are position-restrained by tethers will be subjected to dynamic tether tension variations under the presence of earthquake forces. This will give rise to the dynamic tether tension variations, which in turn shall affect the response of the platform under lateral loads. Earthquakes give rise to the horizontal and vertical motions for a typical duration of 15–30 s. Earthquake acceleration exhibits random characteristics due to (i) the nature of the mechanism causing earthquakes; (ii) wave propagation; (iii) reflection; and (iv) deflection. Effects of earthquake forces give rise to horizontal and vertical motions with durations of 15–30 s. Earthquake loads exhibit random characteristics due to the nature of the mechanism causing earthquake, wave propagation, reflection, and deflection. Earthquakes can result in inertia forces due to the acceleration and damping forces due to the motion of the water particles.

In case of the analysis of compliant structures like TLPs, earthquake forces are handled in an indirect manner. Water waves generated due to the ground motion are neglected. Stiffness of TLP tether is modeled as axial tension members; slackening of tethers is neglected. The dynamic tether tension variation, caused by the horizontal motion of the earthquakes, is used to update the stiffness matrix of the TLP using the following equation (Chandrasekaran and Gaurav 2008):

$$\Delta T = \frac{AE}{\ell}\left[x(t) - x_g(t)\right] \tag{2.39}$$

where $x(t)$ is the instantaneous response vector of TLP and $x_g(t)$ is the ground displacement vector, which is given by:

$$x_g(t) = \begin{Bmatrix} x_{1g}(t) \\ 0 \\ x_{3g}(t) \\ 0 \\ 0 \\ 0 \end{Bmatrix} \tag{2.40}$$

where x_{1g} and x_{3g} are the horizontal and vertical ground displacements, respectively. Ground motions can be generated using Kanai-Tajimi ground acceleration spectrum (K-T spectrum), which is given by:

$$\begin{aligned} S_{\ddot{x}_g \ddot{x}_g}(\omega) &= \left[\frac{\omega_g^4 + 4\xi_g^2 \omega_g^2 \omega^2}{\left(\omega_g^2 - \omega^2\right)^2 + 4\xi_g^2 \omega_g^2 \omega^2} \right] S_0 \\ S_0 &= \frac{2\xi_g \sigma_g^2}{\pi \omega_g (1 + 4\xi_g^2)} \end{aligned} \tag{2.41}$$

where S_0 is the intensity of earthquake, ω_g is the natural frequency of the ground, ξ_g is the damping of the ground, and σ_g^2 is the variance of the ground acceleration. These are the three parameters on which K-T spectrum depends on, which need to be chosen for any analytical studies on TLP under seismic action. The above three parameters should be estimated from the representative earthquake records by established estimation processes (Chandrasekaran et al. 2006). For example, an earthquake occurred in GoM, approximately at 250 miles WSW of Anna Maria, Florida on September 10, 2006 at 14:56:07 (coordinated universal time). The signal was epicentered 26.34N, 86.57W. Incidentally, MARS TLP was operating in the Mississippi Canyon Block, which is also located in GoM. The three parameters S_0, ω_g, and ξ_g are chosen such that the real earthquake is simulated for analysis purposes (Chandrasekaran and Gaurav 2008). Studies showed that the dynamic tether tension variations caused by the earthquake forces are in the order of about 65 % more than that of the normal values. Even structures with rigid degrees of freedom like heave are excited, which may result in the loss of functionality of the platform.

2.7 Ice and Snow Loads

Ice loads are dominant in offshore structures in the Arctic regions. Prediction of ice loads is associated with a significant degree of uncertainty, as there are various ice conditions that exist in the service life of an offshore platform. They are level ice, broken ice, ice ridges, and icebergs. Offshore structures show different types of

failure under ice loads, namely creep, cracking, buckling, spalling, and crushing. Ice loads exhibit random variations in both space and time. They are classified into: (i) total or global loads and (ii) local loads or pressure. Global loads affect the overall motion and stability of the platform, while local loads affect the members at connections. In the level ice condition, frequency of interaction between the structure and ice is important; number of interactions per unit time is important to quantify the ice loads on offshore platforms. Total ice force can result in a periodic loading and can cause dynamic amplification in flexible/slender structures. Current codes include equations for the extreme static ice loads, which depend on the geometric shape of the structure. Studies show that ice loads in a conical structure are lesser than that of the cylindrical structure (Sanderson 1988). This is because a well-designed cone shape can change the ice-failure mode from crushing to bending. Estimating (predicting) ice forces on offshore platforms has a lot of uncertainties. Ice forces often control the design of the platform in operational conditions, in particular. The design ice loads use varying factors for level ice, first-year ridge ice, and multi-year ridge ice; the factored values are 2, 5, and 7, respectively.

There are four approaches for addressing ice forces on offshore platforms: (a) experimental studies on scaled models; (b) numerical studies; (c) field studies; and (d) data mining. Experimental studies use scaling laws to determine the ice loads and ice–structure interaction. This method claims many advantages due to the capability of testing many types of structural shapes in large testing facilities. However, such tests are expensive apart from a strong disagreement of the model ice not being accurately scaled as of the sea ice. As the ice failure is dependent on the geometric shape significantly, ice-failure behavior cannot be accurately studied. This may result in overprediction of ice loads. Numerical modeling uses high-end software to model ice forces for different interaction scenarios, which makes it very cost-effective and instructive. However, limited validation of results with that of the experiments is reported in the literature. The more practical way to estimate ice loads is from data mining. Previous platforms can be visited to determine the ice loads through field measurements. This will give a real picture of the ice loads. In the frequency domain approach, excitation caused by ice loads is modeled as sinusoidal pseudo-excitation, and the response is characterized by the transfer function. Ice force spectrum on a narrow conical structure is given by:

$$S^{+}(f) = \frac{A\bar{F}_0^2 \bar{T}^{(-\delta)}}{f^{\gamma}} \exp\left[-\frac{B}{\bar{T}^{(\alpha)} f^{\beta}}\right] \tag{2.42}$$

where A (=10) and B (=5.47) are constants; $\bar{F}_0$ is the force amplitude on the structure; $\bar{T} = L_b/v$ is the period of ice; L_b is ice-breaking length, which is typically 4–10 times of thickness of ice; v is the velocity; and $\alpha, \beta, \gamma, \delta$ are constants whose values are typically 0.64, 0.64, 3.5, and 2.5, respectively. Force amplitude on the structure is given by:

$$\bar{F}_0 = C\,\sigma_f h^2 \left(\frac{D}{L_c}\right)^{0.34} \tag{2.43}$$

where C is the constant; σ_f is bending strength of ice (0.7 MPa); h is the ice thickness; D is the diameter of the ice cone, and L_c is the characteristic length of ice, which is given by the following equation:

$$L_c = \left[\frac{Eh^3}{12g\rho_w}\right]^{0.25} \tag{2.44}$$

where E is Young's modulus of ice (=0.5 GPa) and ρ_w is density of water.

2.8 Marine Growth

Marine growth or biofouling is the ubiquitous attachments of soft and hard bio-particles on the surface of a submerged structure. It ranges from seaweeds to hard shelled barnacles. Its growth on the surface of the structure increases its diameter and affects its roughness. Its main effect is to increase the wave forces on the members by increasing not only exposed areas and volumes, but also the drag coefficient due to higher surface roughness. In addition, it increases the unit mass of the member, resulting in higher gravity loads and in lower member frequencies. Depending upon the geographic location, the thickness of marine growth can reach 0.3 m or more. It is accounted for in the design through appropriate increases in the diameters and masses of the submerged members.

2.9 Mass

Mass is contributed by the structural mass and hydrodynamic added mass of the structure. For a slender structure, mass of the displaced volume of the structure will be significant and should be considered in the analysis. Added mass depends on the submerged volume of the platform, which also varies with respect to period of vibration. This is due to the variation in buoyancy, which in turn changes the tether tension variation that affects the natural frequency of motion. Based on the equipment layout plan and the chosen structural form, one can compute the mass of the platform readily. It is also important to establish the fact that a desired proportion between center of buoyancy and center of mass is maintained to ensure stability under free-floating conditions. This is important to enable smooth construction process in case of floating.

2.10 Damping

For steel offshore structures, structural damping is usually considered to vary from 0.2 to 0.5 % of that of the critical damping (Adams and Baltrop 1991). For concrete structures, it can be of the order 0.5–1.5 %. Hydrodynamic damping originates from the radiation damping and viscous damping effects. Radiation damping is determined using potential theory. It exhibits a strong dependence on frequency and submergence effects. Literature shows that the drag damping is lower for structures with large diameter column members ($\sim$0.1 %). Damping ratio for offshore structures (wet structures), including the effects of added mass, can be expressed as a ratio of that of the dry structures, as given below:

$$\xi_{\text{wet}} = \xi_{\text{wet}} \frac{\left(m^*_{\text{dry}}\right)\left(\omega^*_{\text{dry}}\right)}{\left(m^*_{\text{wet}}\right)\left(\omega^*_{\text{wet}}\right)} \tag{2.45}$$

where m^* and ω^* are generalized mass and frequency, respectively (Naess and Moan 2013). Literature shows that the total damping ratio is about 2 % for the first three modes of bottom-supported structures.

2.11 Dead Load

Dead load is the weight of the overall platform in air, which includes piling, superstructure, jacket, stiffeners, piping, conductors, corrosion anodes, deck, railing, grout, and other appurtenances. Dead load excludes the following: weight of the drilling equipment placed on the platform including the derrick, draw works, mud pumps, mud tanks, etc.; weight of production or treatment equipment located on the platform including separators, compressors, piping manifolds, and storage tanks; weight of drilling supplies that cause variable loads during drilling such as drilling mud, water, fuel, casing, etc.; weight of treatment supplies employed during production such as fluid in the separator, storage in the tanks; drilling load, which is approximate combination of derrick load, pipe storage, rotary table load, etc.

2.12 Live Load

Live loads are acting in addition to the equipment loads. They include load caused by impacts of vessels and boats on the platform. Dynamic amplification factor is applied to such loads to compute the enhanced live loads. Live loads are generally designated as factor times of the applied static load. These factors are assigned by the designer depending on the type of platform. Table 2.3 gives the live load factors that are used in the platform design.

Table 2.3 Typical live load values used in platform design (Graff 1995)

Description	Uniform load on decks (kN/m^2)	Concentrated load on deck (kN/m^2)	Concentrated load on beams
Walkway, stair	4.79	4.38	4.45 kN/m^2
Areas >40 m^2	3.11		
Areas for light use	11.9	10.95	267 kN

Table 2.4 Impact factor for live loads

Structural item	Load direction	
	Horizontal	Vertical
Rated load in craned	20 %	100 %
Drilling hook loads	–	–
Supports of light machinery	–	20 %
Supports of rotating machinery	50 %	50 %
Boat landings	890 kN	890 kN

2.13 Impact Load

For structural components which experience impact under live loads, the stipulated live loads in Table 2.3 should be increased by an impact factor, as given in Table 2.4. Deck floor loads can be taken as 11.95 kN/m^2 in the drilling rig area, 71.85 kN/m^2 in the derrick area, and 47.9 kN/m^2 for pipe racks, power plants, and living and accommodation areas.

2.14 General Design Requirements

Design methodology of offshore platforms differs with different types of offshore structures. For example, vertical deformation will be lesser in case of bottom-supported structures such as jacket platform and GBS. Such platforms are highly rigid and tend to attract more forces. Hence, the design criteria should be to limit the stresses in the members. Displacement of the members under the applied loads will be insignificant. On the contrary, compliant structures are more flexible, as they all displaced more under wave action. They also create more disturbances in the waves. Hence, the design criteria will be to control displacement instead of limiting the stresses in the members. Orientation of the platform is another important aspect in the design. Preferred orientation is that members are oriented to have less projected area to the encountered wave direction. This induces lesser response on the members. Predominant wave direction for the chosen site is made available to the designer based on which the platform orientation is decided (Chandrasekaran and Bhattacharyya 2012). Following are the list of data required for the design of offshore structures:

- Land topographical survey of sufficient area covering the chosen site for platform installation
- Hydrographical survey of the proposed location (hydrographic charts are used for this purpose)
- Information regarding silting at the site
- Wind rose diagram showing information on wind velocities, duration, predominant direction round the year
- Cyclonic tracking data showing details of the past cyclonic storm such as wind velocities, direction, peak velocity period, etc., are indicated.
- Oceanographic data including general tide data, tide table, wave data, local current, seabed characteristics, temperature, rainfall, and humidity
- Seismicity level and values of acceleration
- Structural data of existing similar structures, preferably in the close vicinity
- Soil investigation report

2.15 Steel Structures

The analysis of an offshore structure is an extensive task, embracing consideration of the different stages, i.e., execution, installation, and in-service stages, during its life. Many disciplines such as structural, geotechnical, naval architecture, and metallurgy are involved. The analytical models used in offshore engineering are in some respects similar to those adopted for other types of steel structures. Only the salient features of offshore models are presented here. The same model is used throughout the analysis with only minor adjustments to suit the specific conditions, e.g., at supports in particular, relating to each analysis. Stick models (beam elements assembled in frames) are used extensively for tubular structures (jackets, bridges, and flare booms) and lattice trusses (modules and decks). Each member is (normally) rigidly fixed at its ends to other elements in the model. If more accuracy is required, particularly for the assessment of natural vibration modes, local flexibility of the connections may be represented by a joint stiffness matrix. In addition to its geometrical and material properties, each member is characterized by hydrodynamic coefficients, e.g., relating to drag, inertia, and marine growth, to allow wave forces to be automatically generated. Integrated decks and hulls of floating platforms, involving large bulkheads, are described by plate elements. The characteristics assumed for the plate elements depend on the principal state of stress to which they are subjected. Membrane stresses are taken when the element is subjected merely to axial load and shear. Plate stresses are adopted when bending and lateral pressure is to be taken into account. After developing a preliminary model for analysis, member stresses are checked for preliminary sizing under different environmental loads.

The verification of an element consists of comparing its characteristic resistance(s) to a design force or stress. It includes (i) a strength check where the characteristic resistance is related to the yield strength of the element and (ii) a stability check for

Table 2.5 Coefficient for resistance to stresses

Condition	Axial	Strong axis bending	Weak axis bending
Normal	0.60	0.66	0.75
Extreme	0.80	0.88	1.00

elements in compression where the characteristic resistance relates to the buckling limit of the element. An element (member or plate) is checked at typical sections (at least both ends and midspan) against resistance and buckling. This verification also includes the effect of water pressure for deepwater structures. Tubular joints are checked against punching under various load patterns. These checks may indicate the need for local reinforcement of the chord using over-thickness or internal ring-stiffeners. Elements should also be verified against fatigue, corrosion, temperature, or durability wherever relevant.

2.16 Allowable Stress Method

This method is presently specified by American codes (API, AISC). The loads remain unfactored, and a unique coefficient is applied to the characteristic resistance to obtain an allowable stress as shown in Table 2.5.

'Normal' and 'extreme,' respectively, represent the most severe conditions under which (a) the plant is to operate without shutdown and (b) the platform is to endure over its lifetime.

2.17 Limit State Method

This method is enforced by European and Norwegian authorities and has now been adopted by American Petroleum Institute (API) as it offers a more uniform reliability. Partial factors are applied to the loads and to the characteristic resistance of the element as given in Table 2.6. They reflect the amount of confidence placed in

Table 2.6 Load factors

Limit state	Load categories				
	P	L	D	E	A
ULS (normal)	1.3	1.3	1.0	0.7	0.0
ULS (extreme)	1.0	1.0	1.0	1.3	0.0
FLS	0.0	0.0	0.0	1.0	0.0
PLS (accidental)	1.0	1.0	1.0	1.0	1.0
PLS (post-damage)	1.0	1.0	1.0	1.0	0.0
SLS	1.0	1.0	1.0	1.0	0.0

the design value of each parameter and the degree of risk accepted under a limit state as discussed below:

- Ultimate limit state (ULS), which corresponds to an ultimate event considering the structural resistance with appropriate reserve.
- Fatigue limit state (FLS), which relates to the possibility of failure under cyclic loading.
- Progressive collapses limit state (PLS), which reflects the ability of the structure to resist collapse under accidental or abnormal conditions.
- Service limit state (SLS), which corresponds to the criteria for normal use or durability (often specified by the plant operator).

where the following explanations are applicable:

P represents permanent loads (structural weight, dry equipment, ballast, and hydrostatic pressure)
L represents live loads (storage, personnel, and liquid)
D represents deformations (out-of-level supports and subsidence)
E represents environmental loads (wave, current, wind, and earthquake)
A represents accidental load (dropped object, ship impact, blast, and fire). The material partial factors for steel are normally taken equal to 1.15 for ULS and 1.00 for PLS and SLS design. Guidance for classifying typical conditions into typical limit states is given in Table 2.7.

The analysis of the offshore platform is an iterative process, which requires progressive adjustment of the member sizes with respect to the forces they transmit, until a safe and economical design is achieved. It is therefore of utmost importance to start the main analysis from a model which is close to the final optimized one. The simple rules given below provide an easy way of selecting realistic sizes for the main elements of offshore structures in moderate water depth (up to 80 m) where dynamic effects are negligible.

Jacket Pile Sizes

- Calculate the vertical resultant (dead weight, live loads, and buoyancy), the overall shear, and the overturning moment (environmental forces) at the mudline.
- Assuming that the jacket behaves as a rigid body, derive the maximum axial and shear force at the top of the pile.
- Select a pile diameter in accordance with the expected leg diameter and the capacity of pile-driving equipment.
- Derive the penetration from the shaft friction and tip bearing diagrams.
- Assuming an equivalent soil subgrade modulus and full fixity at the base of the jacket, calculate the maximum moment in the pile and derive its wall thickness.

Table 2.7 Conditions specified for various limit states

Conditions	Loadings				Design criterion
	P/L	E	D	A	
Construction	P				ULS, TSLS
Load-out	P	Reduced wind	Support displacement		ULS
Transport	P	Transport wind and wave			ULS
Tow-out (accidental)	P			Flooded compartment	PLS
Launch	P				ULS
Lifting	P				ULS
In-place (normal)	P + L	Wind, wave and snow	Actual		ULS, SLS
In-place (extreme)	P + L	Wind and 100 year wave	Actual		ULS, SLS
In-place (exceptional)	P + L	Wind and 10,000 year wave	Actual		PLS
Earthquake	P + L	10^{-2} quake			ULS
Rare earthquake	P + L	10^{-4} quake			PLS
Explosion	P + L			Blast	PLS
Fire	P + L			Fire	PLS
Dropped object	P + L			Drill collar	PLS
Boat collision	P + L			Boat impact	PLS
Damaged structure	P + reduced L	Reduced wave and wind			PLS

Deck Leg Sizes

- Adapt the diameter of the leg to that of the pile.
- Determine the effective length from the degree of fixity of the leg into the deck (depending upon the height of the cellar deck).
- Calculate the moment caused by wind loads on topsides and derive the appropriate thickness.

Jacket Bracings

- Select the diameter in order to obtain a span/diameter ratio between 30 and 40.
- Calculate the axial force in the brace from the overall shear and the local bending caused by the wave assuming partial or total end restraint.
- Derive the thickness such that the diameter/thickness ratio lies between 20 and 70 and eliminate any hydrostatic buckle tendency.

Deck Framing

- Select spacing between stiffeners (typically 500–800 mm).
- Derive the plate thickness from formulae accounting for local plastification under the wheel footprint of the design forklift truck.
- Determine by straight beam formulae the sizes of the main girders under 'blanket' live loads and/or the respective weight of the heaviest equipment.

The static in-place analysis is the basic and generally the simplest of all analyses. The structure is modeled as it stands during its operational life and subjected to pseudo-static loads. This analysis is always carried at the very early stage of the project, often from a simplified model, to size the main elements of the structure. The main model should account for eccentricities and local reinforcements at the joints. For example, a typical model for North Sea jacket may feature over 800 nodes and 4,000 members. The contribution of appurtenances, such as risers, J-tubes, caissons, conductors, boat-fenders, etc., to the overall stiffness of the structure is normally neglected. They are therefore analyzed separately and their reactions applied as loads at the interfaces with the main structure. Since their behavior is nonlinear, foundations are often analyzed separately from the structural model. They are represented by an equivalent load-dependent secant stiffness matrix; coefficients are determined by an iterative process where the forces and displacements at the common boundaries of structural and foundation models are equated. This matrix may need to be adjusted to the mean reaction corresponding to each loading condition. The static in-place analysis is performed under different conditions where the loads are approximated by their pseudo-static equivalent. The basic loads relevant to a given condition are multiplied by the appropriate load factors and combined to produce the most severe effect in each individual element of the structure. A dynamic analysis is normally mandatory for every offshore structure, but can be restricted to the main modes in the case of stiff structures.

2.18 Fabrication and Installation Loads

These loads are temporary and arise during fabrication and installation of the platform or its components. During fabrication, various structural components generate lifting forces, while in the installation, phase forces are generated during platform load-out, transportation to the site, launching and upending, as well as during lifts related to installation. According to the Det Norske Veritas (DNV) rules, the return period for computing design environmental conditions for installation and fabrication loads is three times as that of the duration of the corresponding phase. API-RP2A, on the other hand, leaves this design return period up to the owner, while the BS6235 rules recommend a minimum recurrence interval of 10 years for the design environmental loads associated with transportation of the structure to the offshore site.

2.19 Lifting Force

Lifting forces are functions of the weight of the structural component being lifted, the number and location of lifting eyes used for the lift, the angle between each sling and the vertical axis, and the conditions under which the lift is performed, as shown in Fig. 2.4. All members and connections of a lifted component must be designed for the forces resulting from static equilibrium of the lifted weight and the sling tensions. Moreover, API-RP2A recommends that in order to compensate for any side movements, lifting eyes and the connections to the supporting structural members should be designed for the combined action of the static sling load and a horizontal force equal to 5 % this load, applied perpendicular to the padeye at the center of the pinhole. All these design forces are applied as static loads if the lifts are performed in the fabrication yard. If, however, the lifting derrick or the structure

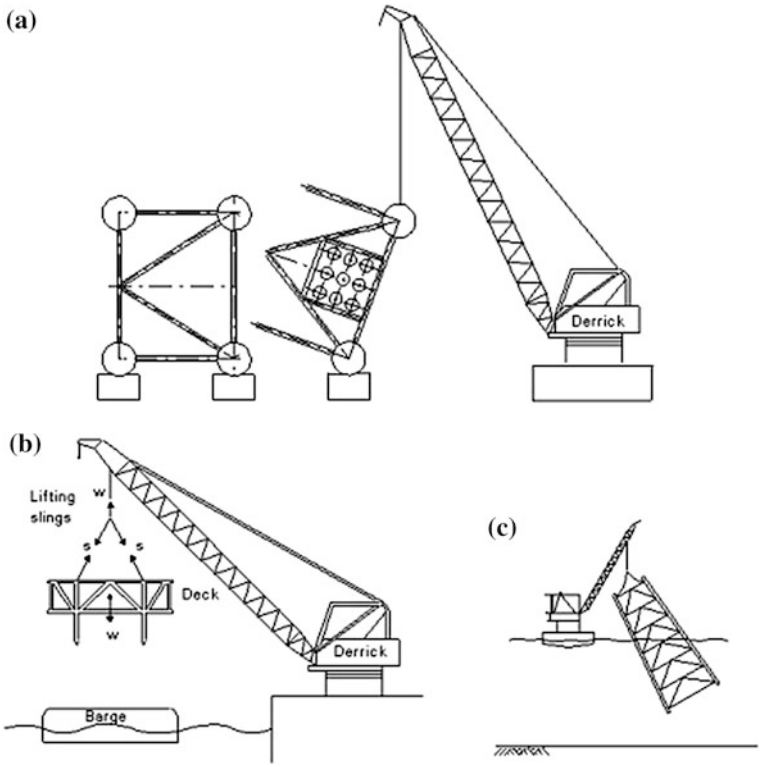

Fig. 2.4 Lifts under different conditions. **a** Derrick and structure on land. **b** Derrick on land, structure on floating barge. **c** Derrick and structure in the sea

to be lifted is on a floating vessel, then dynamic load factors should be applied to the static lifting forces. A factor of 2 is applied for members and connections and 1.35 for all other secondary members. For load-out at sheltered locations, the corresponding minimum load factors for the two groups of structural components are 1.5 and 1.15, respectively.

2.20 Load-Out Force

These are forces generated when the jacket is loaded from the fabrication yard onto the barge. If the load-out is carried out by direct lift, then, unless the lifting arrangement is different from that to be used for installation, lifting forces need not be computed. This is because lifting in the open sea creates a more severe loading condition, which requires higher dynamic load factors. If load-out is done by skidding the structure onto the barge, a number of static loading conditions must be considered, with the jacket supported on its side. Such loading conditions arise from the different positions of the jacket during the load-out phases as shown in Fig. 2.5. Since movement of the jacket is slow, all loading conditions can be taken as static.

Typical values of friction coefficients for the calculation of skidding forces are as follows: (i) steel on steel without lubrication (0.25); (ii) steel on steel with lubrication (0.15); (iii) steel on Teflon (0.10); and (iv) Teflon on Teflon (0.08). A typical ballast and displacement values are indicated in the figure.

2.21 Transportation Forces

These forces are generated when platform components (jacket, deck) are transported offshore on barges or self-floating. They depend upon the weight, geometry, and support conditions of the structure (by barge or by buoyancy) and also on the environmental conditions (waves, winds, and currents) that are encountered during transportation. The types of motion that a floating structure may experience are shown schematically in Fig. 2.6.

In order to minimize the associated risks and secure safe transport from the fabrication yard to the platform site, it is important to plan the operation carefully by considering the following (API-RP2A):

- Previous experience along the tow route
- Exposure time and reliability of predicted ‘weather windows’
- Accessibility of safe havens
- Seasonal weather system
- Appropriate return period for determining design wind, wave, and current conditions, taking into account the characteristics of the tow such as size, structure, sensitivity, and cost.

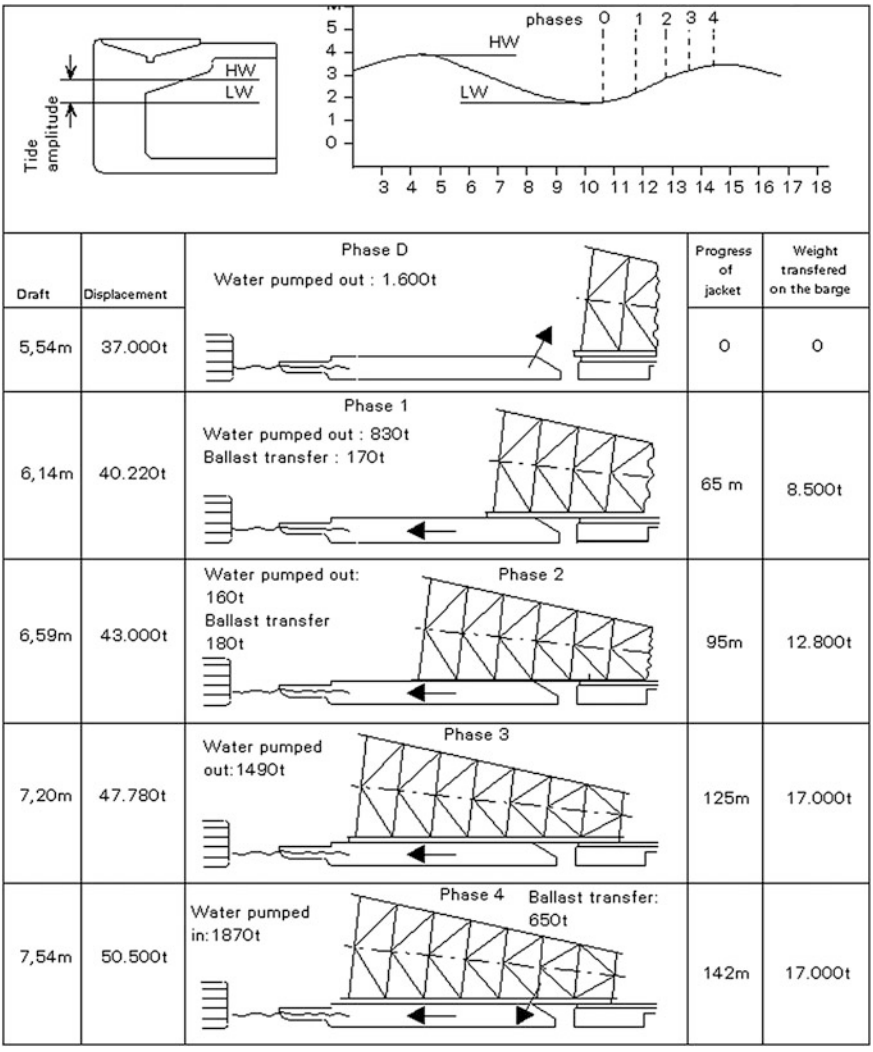

Fig. 2.5 Different phases of jacket load-out by skidding

The motion of the tow, i.e., the structure and supporting barge, generates transportation forces. They are determined from the design winds, waves, and currents. If the structure is self-floating, the loads are calculated directly. According to API-RP2A, towing analyses must be based on the results of model basin tests or appropriate analytical methods and must consider wind and wave directions parallel, perpendicular, and at 45° to the tow axis. Inertial loads shall be computed from a rigid body analysis of the tow by combining roll and pitch with heave motions, when the size of the tow, magnitude of the sea state, and experience make

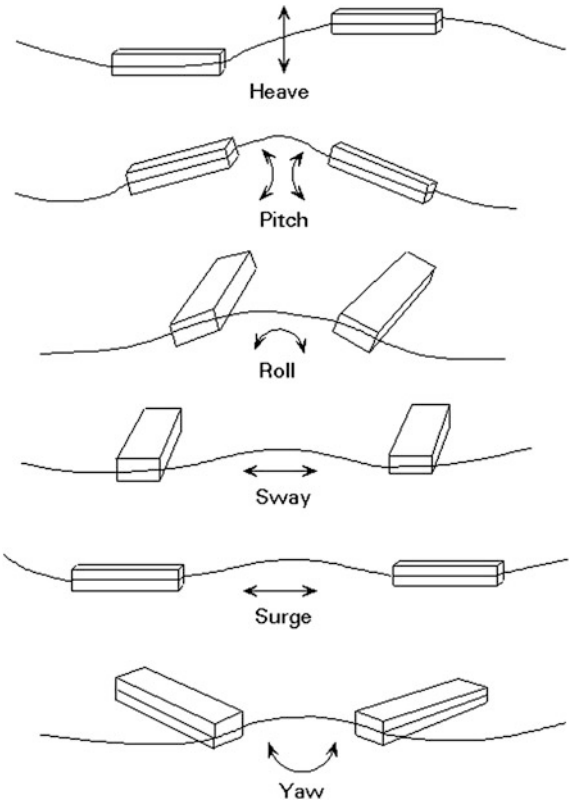

Fig. 2.6 Motion of floating objects during installation

such assumptions reasonable. For open sea conditions, typical values are 20° (for single amplitude roll motion) and 10° for single amplitude pitch motion. The period of roll or pitch is taken as 10 s, while heave acceleration is taken as 0.2 g. When transporting a large jacket by barge, stability against capsizing is a primary design consideration because of the high center of gravity of the jacket. Moreover, the relative stiffness of jacket and barge may need to be taken into account together with the wave slamming forces that could result during a heavy roll motion of the tow, as shown in Fig. 2.7. Structural analyses are carried out for designing the tie-down braces and the jacket members affected by the induced loads.

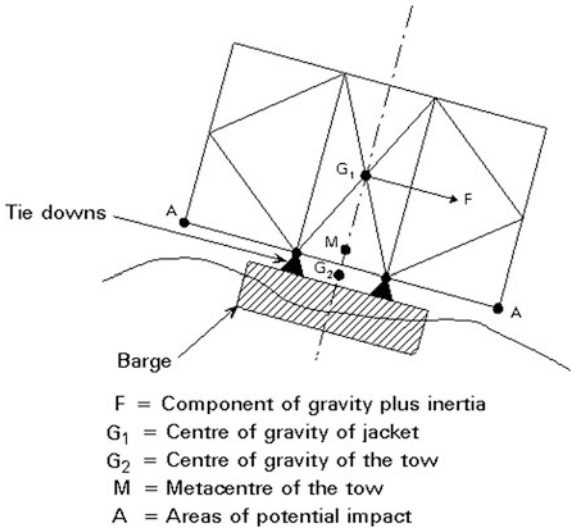

Fig. 2.7 View of launch barge and jacket undergoing motion

2.22 Launching and Upending Force

These forces are generated during the launch of a jacket from the barge into the sea and during the subsequent upending into its proper vertical position to rest on the seabed. A schematic view of the five stages the operation can be seen in Fig. 2.8.

Five stages in a launch-upending operation are as follows: (i) jacket slides along the skid beams; (ii) jacket rotates on the rocker arms; (iii) jacket rotates and slides simultaneously; (iv) detaches completely and comes to its floating equilibrium position; and (v) jacket is upended by a combination of controlled flooding and simultaneous lifting by a derrick barge. Both the static and dynamic loads for each

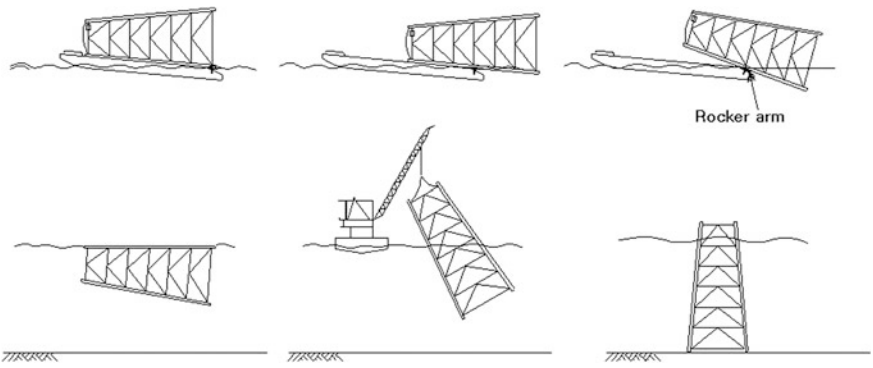

Fig. 2.8 Launching and upending

stage of the above under the action of wind, waves, and current need to be included in the analysis.

To start the launch, the barge must be ballasted to an appropriate draft and trim angle and subsequently the jacket must be pulled toward the stern by a winch. Sliding of the jacket starts as soon as the downward force (gravity component and winch pull) exceeds the friction force. As the jacket slides, its weight is supported on the two legs that are part of the launch trusses. The support length keeps decreasing and reaches a minimum, equal to the length of the rocker beams, when rotation starts. It is generally at this instant that the most severe launching forces develop as reactions to the weight of the jacket. During the last two stages, variable hydrostatic forces arise, which have to be considered at all members affected. Buoyancy calculations are required for every stage of the operation to ensure fully controlled, stable motion. Computer programs are available to perform the stress analyses required for launching and upending and also to portray the whole operation graphically.

2.23 Accidental Load

According to the DNV rules, accidental loads are ill-defined with respect to intensity and frequency, which may occur as a result of an accident or exceptional circumstances. Examples of accidental loads are loads due to collision with vessels, fire or explosion, dropped objects, and unintended flooding of buoyancy tanks. Special measures are normally taken to reduce the risk from accidental loads. For example, protection of wellheads or other critical equipment from a dropped object can be provided by specially designed, impact resistant covers. An accidental load can be disregarded if its annual probability of occurrence is less than 10^{-4}. This number is the estimate of order of magnitude and is extremely difficult to compute.

Exercise

1. The design stages of various offshore platform are _____, _____, and _____.
2. The data collected during the FEED stage will be further verified to make sure the _____ and _____ of such data for further use.
3. Loads on offshore structures are _____ and _____.
4. Gravity loads are arising from _____ and _____either permanent or temporary.
5. Seismic loads are arising from derived type _____.
6. Gravity loads are _____, _____, _____, _____, and _____.

7. Environmental loads are _____, _____, _____, _____, _____, and _____.
8. The fluid loads are weight of fluid on the platform during _____.
9. The wind speed at 10 m above _____ is normally provided (V_0).
10. Wind speed obtained shall be _____ to the height above for the calculation of wind speed.
11. The wind speed may be classified as _____ and _____.
12. _____ are measured in an average less than 1 min in duration.
13. Wind loads shall be calculated as per _____ guidelines.
14. Wind-driven waves are a major source of _____on offshore platforms.
15. Sustained wind speeds measured for _____ duration shall be used to compute global platform wind loads and gust wind which is measured for _____ duration shall be used to compute the wind loads to design individual members.
16. The wind pressure can be calculated as f_w = _____.
17. The total force on the platform can be calculated as F_x = _____.
18.

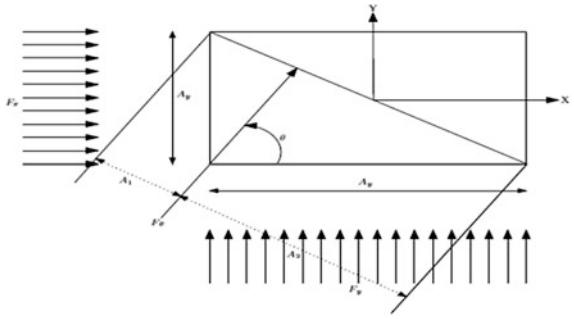

Calculate wind load on oblique directions F_θ =

19. In_____, a discrete set of design waves (maximum) and associated periods will be selected to generate loads on the structure.
20. In the spectral method, an energy spectrum of the sea state for the location will be taken and a _____ for the response will be generated.
21. Transfer function will be used to compute the _____ in the structural members.
22. Sea-state energy spectra available for use are _____, _____, and _____.
23. Tides may be classified as_____, _____, and _____.
24. Combination of astronomical tide, wind tide, and pressure differential tide are called _____.
25. The forces exerted by waves are most dominant in governing the jacket structures design especially the_____.

26. The wave loads exerted on the jacket is applied laterally on all members, and it generates _____ on the structure.
27. Period of wind-generated waves in the open sea can be in the order of _____.
28. Waves are called _____ and contain most part of _____.
29. Relationship between significant wave height (H_s) and the maximum wave height (H_{max}) is _____.
30. Match the design wave height for various regions is tabulated below:

I. Bay of Bengal	(a) 11 m for 1 year and 24 m for 100 years
II. Gulf of Mexico	(b) 6 m for 1 year and 12 m for 100 years
III. South China Sea	(c) 5 m for 1 year and 12 m for 100 years
IV. Arabian Sea	(d) 14 m for 1 year and 22 m for 100 years
V. Gulf of Thailand	(e) 12 m for 1 year and 24 m for 100 years
VI. Persian Gulf	(f) 8 m for 1 year and 18 m for 100 years
VII. North Sea	(g) 8 m for 1 year and 18 m for 100 years

31. Draw the current profile of wave-driven currents and tidal currents.
32. Name some standard spectrum available in the literature.
33. Ocean currents are classified into few types based on their nature they are _____, _____, and _____.
34. Write down the expression for current variation along the depth and explain the terms involved in it.
35. Marine growth is an important part in increasing the loads on _____.
36. Growth of marine algae increases the _____ and _____which in turn increase the wave or current loading.
37. The thickness of marine growth generally _____ with depth from the mean sea level, and it is maximum in the _____.
38. Splash Zone is a region where the water levels _____ between low to high.
39. Write down the expression for Morison equation and explain the terms appropriately.
40. Algebraic sum of wave and current loads is different from calculation of load by adding the horizontal water particle velocity with the current velocity and computing the loads. This is because of _____.
41. Interaction between the wave and current modifies the _____.
42. Name some wave theories.
43. API-RP2A recommends to use a chart for such selection based on _____ and _____.
44. The reserve buoyancy is defined as buoyancy in _____.

45. The buoyancy force can be calculated using _____method and _____ method.
46. Sketch a jacket structure and mark the MSL, LAT, and HAT in the jacket structure.
47. Write down the empirical equation to estimate the force F_{ice}.
48. Platforms located in the vicinity of the river mouth will be subjected to _____.
49. Write down the empirical equation to estimate the force F_{mud}.
50. Scour is removal of seafloor soils caused by _____ and _____.
51. Explain the force regime.
52. P-M spectral method describes the fully developed sea determined by _____ parameter that is _____.
53. In P-M spectrum, fetch and duration are considered _____.
54. _____spectrum is on basis of the assumption that the spectrum is narrow banded, and individual wave height and wave period follow Rayleigh distribution.
55. ISSC spectrum suggested modification in form of the _____.
56. _____ proposed modification in the P-M spectrum in terms of _____ and _____.
57. Write down the expression for Morison equation for force per unit length experienced by the structure due to its motion through the water.
58. Site-dependent databases are being developed to characterize the time varying fluid induced loads of _____, _____, and _____.
59. Explain the linear wave theory with the neat sketch and write the expression for velocity potential.
60. List the assumptions based on which the Morison equation is derived.

Answers

1. front end engineering design (FEED) or concept selection; basic design; detailed design
2. authenticity and reliability
3. gravity loads and environmental loads
4. dead weight of structure and facilities
5. gravity loads
6. structural dead loads; facility dead loads; fluid loads; live loads; and drilling loads
7. wind loads; wave loads; current loads; buoyancy loads; ice loads; and mud loads
8. operation

9. lowest astronomical tide (LAT)
10. extrapolated
11. gust and sustained wind velocity
12. Gusts
13. API-RP2A
14. environmental forces
15. 10 min average; 3 s
16. 1/2 ($\rho g V^2$)
17. $F_\theta F_x f_w A_x C_s$
18. $F_x\cos(\theta) + F_y\sin(\theta)$
19. design wave method
20. transfer function
21. stresses
22. PM spectra, Johnswap spectra, and ISSC spectra
23. astronomical tide, wind tide, and pressure differential tide
24. storm surge
25. foundation piles
26. overturning moment
27. 2–20 s
28. gravity waves and wave energy
29. H_{max} = 1:86 H_s
30. I (f/g); II (e); III (a); IV (f/g); V (b); VI (c); VII (d)
31.

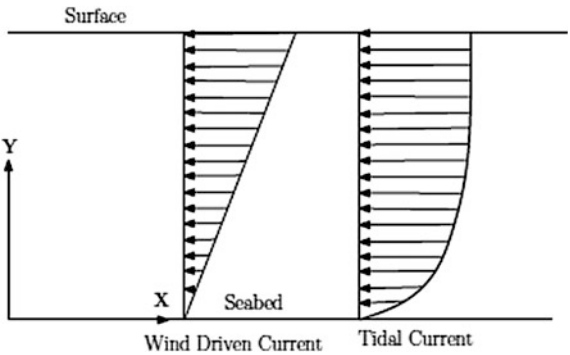

32. PM spectra; Johnswap spectra; and ISSC spectra
33. tidal current, wind-driven current, and current generated due to ocean circulation
34. $V_T = V_0\left(\frac{y}{h}\right)^{1/7}$ V_T is the tidal current at any height from seabed, V_0 is the tidal current at the surface, y is the distance measure in meter from seabed, and h is the water depth
35. offshore structures
36. diameter and roughness of members

37. decrease and splash zone
38. fluctuate
39. Morison equation $F_T = F_D + F_I = \left(\frac{1}{2}C_D\rho_w DV|V| + \frac{\pi}{4}D^2C_M\rho_w a\right)$ where F_T is the total force, ρ_w is the density of water, C_D and C_M are the drag and inertia coefficients, respectively, D is the diameter of the member including marine growth, V is the velocity, and a is the acceleration
40. nonlinear term in the drag equation
41. wave parameters and wave field
42. linear/Airy wave theory; Stokes wave theory (up to 5th order approximations); stream function wave theory (up to 22nd order approximations); cnoidal wave theory
43. d/gT^2 and H/gT^2
44. excess of its weight
45. marine method and rational method
46.

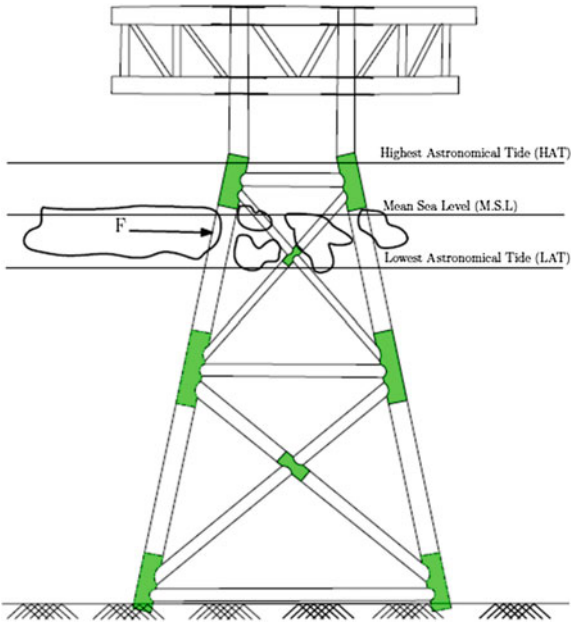

47. $f_{ice} = C\,f\,A$ where f_{ice} crushing strength of ice varies between 1.5 and 3.5 MPa; C_{ice} = ice force coefficient varies between 0.3 and 0.7; and A area struck by ice (diameter of member x ice sheet thickness)
48. mud load
49. Mud loads can be calculated using $F_{mud} = C_{mud}\,\tau\,D$ where C_{mud} = force coefficient varies from 7 to 9; τ = shear strength of soil 5–10 kPa; and D = Diameter of pile or member
50. currents and waves
51. 1. $D/L > 1$ condition approximate to pure reflection; $D/L > 0.2$ diffraction is increasingly important; $D/L < 0.2$ diffraction is negligible; $D/L_0 > 0.2$ inertia; $D/L_0 < 0.2$ drag dominant where D is the diameter of the structure; L is the wave length; and L_0 is the deepwater wavelength
52. one; wind speed
53. infinite
54. Bretschneider
55. Bretschneider spectrum
56. International Towing Tank Conference (ITTC); significant wave height and zero crossing frequency
57. $$f = m\ddot{x} + C_A\rho\frac{\pi}{4}D^2\ddot{x} + \frac{1}{2}C_D\rho D|\dot{x}|\dot{x}$$
58. wind, wave, and current
59. **Linear Wave Theory**

Airy wave theory is considered in the calculation of wave kinematics. Consider a progressive wave with water surface elevation depicted by cosine curve,

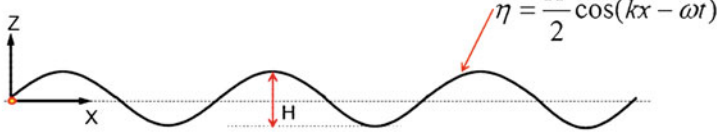

and the corresponding velocity potential is given by:

$$\phi = -\frac{H}{2}\frac{\omega}{k}\frac{\cosh k(h+z)}{\sinh kh}\sin(kx - \omega t)$$

60. Assumptions are as follows:

- Flow is assumed to be not disturbed by the presence of the structure.
- Force calculation is empirical calibrated by experimental results.
- Suitable coefficients need to be used depending on the shape of the body or structure.
- Validity range shall be checked before use and generally suitable for most jacket type structures where $D/L \ll 0.2$ where D is the diameter of the structural member and L is the wave length.

Chapter 3
Introduction to Structural Dynamics

Abstract This chapter deals with introduction to structural dynamics and its application to offshore structures. Basics of single degree of freedom are discussed to highlight the conventional mathematical model of single degree of freedom. Free vibration analysis and forced vibration analysis are discussed with focus on few important dynamic characteristics of the single-degree-of-freedom and multi-degrees-of-freedom models. Solved numerical examples of determining natural frequencies and mode shapes of different mathematical model of single-degree-of-freedom and multi-degrees-of-freedom systems are included.

Keywords Single-degree-of-freedom · Multi-degrees-of-freedom · Un-damped free vibration · Forced vibration · Structural damping · Half power method · Influence coefficient method · Dunkerley's method · Stodla method · Mode superposition · Mode truncation · Static correction

3.1 Introduction

For understanding the advantages of the offshore structural forms and action, it is necessary to convert the structure into simple basic mathematical models for dynamic analysis. However, it is important to note that complexities arising from the mechanical and process equipment that forms a major part of topside activity of offshore structures pose serious limitation to such idealized mathematical models considered for dynamic analysis. Dynamic loads are defined as time-varying loads whose magnitude, direction of application, or position vary continuously with time. As repose to these applied loads, response of the structure also varies with respect to time. Basic approaches to evaluate the response of structures to such dynamic loads are (i) deterministic and (ii) non-deterministic. In *deterministic approach*, in which the time history of the loading is fully known with the highly varying and irregular load magnitude, loading can be classified as prescribed dynamic loading. In *non-deterministic approach*, in which the time history of the loading is not

S. Chandrasekaran, *Dynamic Analysis and Design of Offshore Structures*,
Ocean Engineering & Oceanography 5, DOI 10.1007/978-81-322-2277-4_3

completely known but can be defined in statistical sense, the loading is termed as random dynamic loading. Deterministic analyses lead to displacement time history corresponding to the given (completely known) load time history. Other aspects such as stress, strain, and internal forces are derived from the established displacement patterns. In case of non-deterministic analyses, results obtained will provide statistical information of the displacement pattern under the action of a statistically defined loading (random loads). Other aspects such as stress, strain, and internal forces such as bending moment and shear shall be computed directly by similar independent non-deterministic analyses rather than from deriving them from the displacement results as in the earlier case.

Essential characteristics of dynamic loading are their time-varying nature and presence of inertia force. Inertia force is the force, which resists acceleration, which is the most essential characteristic of dynamic analysis as they represent a significant portion of the total load. As the applied load is time-varying, dynamic analysis is never a single solution like static analysis and the response is then evaluated.

3.2 Fundamentals of Structural Dynamics

All bodies having mass and elasticity are capable of vibration. Mass is an inherent property of a body, and elasticity causes relative motion of the parts. Due to an external force, the body gets vibrated, and the internal inherent forces in the form of elastic energy are developed, and this tries to bring back the structure to its original position. At equilibrium, the total energy is converted to kinetic energy, and then, the body continues to move in the opposite direction. Then, kinetic energy is converted into strain or elastic energy due to which the body returns to its equilibrium position. By this way, the vibratory motion is repeated indefinitely with the exchange of energy. Thus, any motion, which repeats itself after an interval of time, is called *vibration.* The major factors that cause vibration are the unbalanced centrifugal force in the system, elastic property of the system, and external excitation.

Before getting into the subject, it is necessary to understand some terminologies. A motion, which repeats itself after an equal interval of time, is called *periodic motion.* The time taken to complete one cycle is called the *time period*, and the number of cycles per unit time is called *frequency*. *Free vibrations* are the vibrations which are caused due to initial displacement with the absence of an external force, and their frequency is called *natural frequency*. The mode, which has the lowest natural frequency, is called the *fundamental mode of vibration.* When the frequency of the external vibration matches with the natural frequency of a vibrating body, the amplitude of vibration becomes excessively large, and this is known as resonance. *Degree of freedom* is defined as the number of independent displacement components of a structural system that are necessary at any given time to represent the effect of all significant inertia forces present in the system. Systems, which have infinite number of degrees of freedom, are called *continuous systems*, and systems with finite number of degrees of freedom are called *discrete* or *lumped systems.*

3.3 Mathematical Model of Structural System

Idealization of offshore structures to simple mathematical models in dynamic analysis is the most essential key point in the analysis. Generally, the analysis is carried out by not considering the serious limitations and complexities arising from the topside equipment (and their dynamic loads). More accurate analysis, incorporating the required details of dynamic response behavior of machineries (under static condition and under operation), shall be carried out to understand the platform behavior in more detail; this is beyond the scope of this chapter. Structural idealizations originate from defining the degrees of freedom for the idealized mathematical model. The inertia forces are mass proportional, and an approximate method of understanding degree of freedom shall be oriented toward the number of locations where the mass is said to be concentrated. Figure 3.1 shows an idealized mathematical model of single-degree-of-freedom (SDOF) system. As the mass is said to be lumped at one point and it is contained to move in only direction (marked by an arrow direction), the shown model is an idealized case of SDOF system. Basic and essential characteristics of the SDOF system are, namely (i) mass element (m) representing the inertial characteristics of the system; (ii) spring element represented by stiffness (k) that identifies the presence of elastic restoring force and potential energy of the system; (iii) damping element (c) or dashpot representing frictional characteristics of energy loss or dissipation of energy in the system; and (iv) an excitation force ($f(t)$) representing the external force acting on the system. Energy is stored by the mass in the form of kinetic energy $\left(\frac{1}{2}m\dot{x}^2\right)$ and by the spring in the form of potential energy $\left(\frac{1}{2}kx^2\right)$. Dissipation energy will always act in the opposite direction.

In the idealized SDOF system, it is not necessary that all the four parameters need to be present. The most important are the mass element and spring element; inertial force is characterized by mass element, which is one of the most important features of dynamic analysis, and restoration to the mean position of the vibrating mass under any given external/internal action of forces is characterized by spring element. A system can be termed as un-damped system if damping element is not present, and if the system is not excited by external force, it is called as free vibration. As the system is constrained so that it can vibrate only in one direction, it is termed as SDOF model.

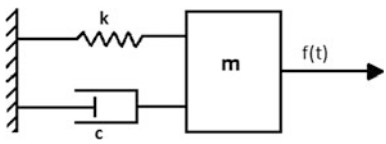

Fig. 3.1 Single-degree-of-freedom model

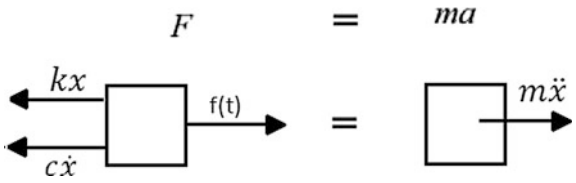

Fig. 3.2 Free body diagram of single-degree-of-freedom model

3.4 Single-Degree-of-Freedom Model

The simplest vibratory system is described by a single mass connected to a spring (and possibly a dashpot). The mass is allowed to displace only along the direction of spring elongation. Restoration will be attained by the spring force of stiffness (k) applied opposite to that of the external force. Figure 3.2 shows the free body diagram of the single degree of freedom under external force $f(t)$. Forces acting on the body under the free state are, namely (i) external force $f(t)$ acting to the right as shown; (ii) internal restoration force offered by the spring acting in the direction opposite to that of the applied external force; and (iii) damping force offered by the dashpot acting in the direction opposite to that of the external force. Equilibrium of these set of forces can be arrived by employing Newton's second law of motion. Using appropriate sign conventions for the force directions and by equating the net force to the inertial force, we get a second-order, non-homogeneous ordinary differential equation as given below:

$$m\ddot{x} + c\dot{x} + kx = f(t) \tag{3.1}$$

with the initial conditions as $x(t = 0) = x_0$ and $\dot{x}(t = 0) = \dot{x}_0$, the above equation can be solved.

3.5 Equation of Motion

Equations of motion are equations that describe the behavior of a physical system in terms of its motion as a function of time. The equation of motion can be obtained by employing the following methods:

- Simple harmonic motion method
- Newton's method
- Energy method
- Rayleigh's method
- D'Alembert's method

Consider the spring–mass system of simple pendulum, which is constrained to move in the rectilinear manner along the axis of the spring. Springs of stiffness k,

which is fixed at one end, carry a mass m at its free end. The body is displaced from its equilibrium position vertically downward. The equilibrium position is called static equilibrium. In equilibrium position, the gravitational pull W is balanced by the force in the spring such that $mg = W = k\delta$.

3.5.1 Simple Harmonic Motion Method (SHM Method)

The equation of motion using the SHM method involves three important considerations: (i) Acceleration will be always proportional to its displacement or the particle/body measured along the path; (ii) the body will always be directed toward the equilibrium position (fixed point); and (iii) direction is opposite always toward its motion.

$$\ddot{x} \propto -(x)$$

$$\ddot{x} = -kx,$$

where k is the proportionality constant.

$$\ddot{x} + kx = 0$$

3.5.2 Newton's Law

The equation of motion using the Newton's law of motion is derived by equating the forces.

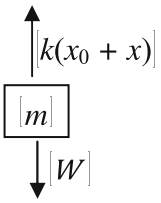

$$W - k(x_0 + x) = m\ddot{x}$$

$$W = k\,(x_0)$$

$$m\ddot{x} + k(x) = 0$$

3.5.3 Energy Method

In a conservative system, the total sum of the energy is constant. In the vibratory system, the energy is partly potential and partly constant. The kinetic energy is a function of the velocity, and the potential energy is a function of displacement.

$$\text{K.E.} = \frac{1}{2}m\dot{x}^2$$

$$\text{P.E.} = \frac{1}{2}kx^2$$

$$\frac{\mathrm{d}}{\mathrm{d}t}\left(\frac{1}{2}m\dot{x}^2 + \frac{1}{2}kx^2\right) = 0$$

$$\dot{x}[m\ddot{x} + kx] = 0$$

$$m\ddot{x} + kx = 0$$

3.5.4 Rayleigh's Method

It is assumed that maximum kinetic energy at the mean position is equal to the maximum potential energy at the extreme position. If the motion is assumed to be simple harmonic, then

$$x = A\sin\omega_n t$$

where x = displacement of the body from mean position to the extreme position.

$$\dot{x} = \omega_n A\cos\omega_n t$$

Maximum velocity at mean position

$$\dot{x} = A\omega_n$$

So, maximum kinetic energy at the mean position = $\frac{1}{2}m\dot{x}^2 = \frac{1}{2}m\omega_n^2 A^2$

Maximum kinetic energy at the extreme position = $\frac{1}{2}kA^2$

$$\frac{1}{2}m\omega_n^2 A^2 = \frac{1}{2}kA^2$$

$$\omega_n = \sqrt{\frac{k}{m}}$$

These methods are widely used for the determination of the natural frequency of the system.

3.5.5 D'Alembert's Principle

D'Alembert's principle states that if the resultant force acting on the body along with the inertia force is zero, then the body will remain in the equilibrium. In this approach, the dynamic problem is converted into a static problem. This methodology cannot be applied to the multi-degree problem without proper understanding of the constraints.

$$F + F_i = 0$$

where F is the resultant force acting on the system and F_i is the inertial force.

It is to be mentioned that the inertial force and the accelerating force are equal in magnitude but opposing in direction. The inertial force is an external force acting on the body. Mathematically, the equation of motion for the spring–mass system in vertical position can be written as

$$m\ddot{x} + kx = 0$$

3.6 Un-damped Free Vibration

In the absence of external force $f(t)$, the vibratory motion set in the body shall be termed as free vibration. One may wonder how the body will vibrate in the absence of any external force; it is the initial displacement given to the body makes it to vibrate. Vibratory motion will be set also due to the presence of elastic restoring force (kx) that continuously attempts to bring the vibrating mass to original position. Such vibration induced by the initial displacement and not by the external force is termed as free vibration. The whole action of restoration may also be influenced by the presence of dashpot in the system. As explained earlier, there is no necessity of the presence of dashpot in an idealized mathematical model of SDOF system. In the absence of such damping force, the induced vibration is called un-damped vibration. In the present case of un-damped free vibration, there is no loss of energy due to friction or resistance to this motion in any other form. In simple terms, if there is no external force applied on the system making $f(t) = 0$, and therefore, the system will experience free vibration. Motion of the system will be established by an initial disturbance (i.e., initial conditions). Furthermore, if there is no resistance or damping in the system making $C = 0$, the oscillatory motion will continue forever with a constant amplitude. Such a system is shown in Fig. 3.3.

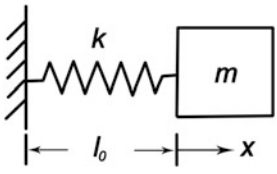

Fig. 3.3 Un-damped free vibration of single-degree-of-freedom model

Based on the free body diagram explained earlier, equation of motion for un-damped free system can be written as follows:

$$m\ddot{x} + kx = 0 \tag{3.2}$$

Dividing by mass throughout, we get the following form:

$$\ddot{x} + \frac{k}{m} = 0$$
$$\ddot{x} + \omega^2 = 0$$

where

$$\omega^2 = \frac{k}{m}$$

For the second-order differential equation as shown above, auxiliary equation is given as follows:

$$D^2 + \omega^2 = 0$$
$$D = \pm i\omega$$

Complimentary function is given as follows:

$$x(t) = C_1 \cos \omega t + C_2 \sin \omega t \tag{3.3}$$

Using the initial condition as explained earlier, the above equation reduces to the following form:

$$x(t) = x_0 \cos \omega t + \frac{\dot{x}_0}{\omega} \sin \omega t \tag{3.4}$$

where x_0 and $\dot{x}_0$ are initial displacements and velocities, respectively, and ω_n is the natural frequency of the said vibrating motion. It can be easily seen that the natural frequency is dependent on the mass of the system and spring constant or restoring force coefficient of the system; it is independent of the said initial displacement given to preset the vibrating motion to the body.

3.7 Damped Free Vibration

While discussing the above case of free vibration of SDOF model, one may wonder about the duration of such vibration being setup by the given initial displacement. The duration of such vibration is hypothetically infinite, as no external (or) internal agency is responsible to control such induced vibration. But in practice, one can

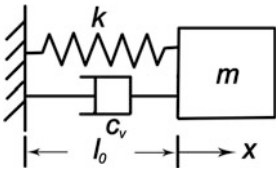

Fig. 3.4 Damped free vibration of single-degree-of-freedom model

notice that such vibrations do not extend for infinite time duration; the reason is that some external agency is responsible to stop such vibration. Hence, it is now necessary to update our existing mathematical model to include this factor in the analysis. In case of any external force being responsible for controlling the vibration, air will offer resistance to such motion. In case of offshore structures, waves contribute significantly toward this action, and hence, damping should be included in the revised model. However, one may still consider the analysis under the absence of any external force $f(t)$. Hence, free vibration (no external force) of a SDOF system with damping is shown in Fig. 3.4. Damping force is commonly considered proportional to the magnitude of velocity of motion of the body, which shall be applied in the direction opposite to the direction of external force $f(t)$. This is termed as viscous damping. Alternatively, resistance to vibratory motion may also arise from friction between the following surfaces: (i) the plane on which the body is moving and (ii) the plane of the body itself that is in motion. Such forces arising purely from frictional resistance are termed as coulomb damping. In this case, damping force depends on the coefficient of friction between the two surfaces and remains independent of the velocity of motion of the body. It is customary practice to assume viscous damping in dynamic analysis of offshore structures. Damping that produces a damping force proportional to the mass's velocity is commonly referred to as 'viscous damping,' and is denoted graphically by a dashpot. Reasons for not considering coulomb damping are explained in the later part through a numerical example.

Damping is the resistance offered by a body to the motion of a vibratory system. The resistance may be applied by a liquid or solid internally or externally. If the value of the damping is small in the mechanical system, then it will have very less influence on natural frequency. The main advantage of providing damping in mechanical systems is just to control the amplitude of vibration so that the failure occurring because of resonance may be avoided.

3.7.1 Viscous Damping

When the system is allowed to vibrate in a viscous medium, the damping is called viscous. Viscosity is the property of the fluid by virtue of which it offers a resistance to the motion of one layer over the adjacent one. When two plates are separated by fluid film of thickness t and the upper plate is allowed to move parallel to the fixed

plate with a velocity $\dot{x}$, then the net force F required for maintaining the velocity $\dot{x}$ of the plate is expressed as

$$F = \frac{\mu A}{t}\dot{x}$$

where A is the area of plate, t is thickness of the fluid film, and μ is the coefficient of absolute viscosity of the film. The force can also be written as follows:

$$F = c\dot{x}$$
$$c = \frac{\mu A}{t}$$

where c is viscous damping coefficient.

3.7.2 Coulomb Damping

Coulomb damping results from the sliding of two dry surfaces. Displacement of a system in coulomb damping is shown in Fig. 3.5. Damping force is equal to the product of the normal force and the coefficient of friction μ and is assumed to be independent of the velocity once the motion is initiated. Because the sign of the damping force is always opposite to that of the velocity, the differential equation of motion for each sign is valid only for half-cycle intervals.

To determine the decay of amplitude, we resort to the work–energy principle of equating the work done to the change in kinetic energy. By choosing a half-cycle starting at the extreme position with velocity equal to zero and the amplitude equal to X_1, the change in the kinetic energy is zero and the work done on m is also zero.

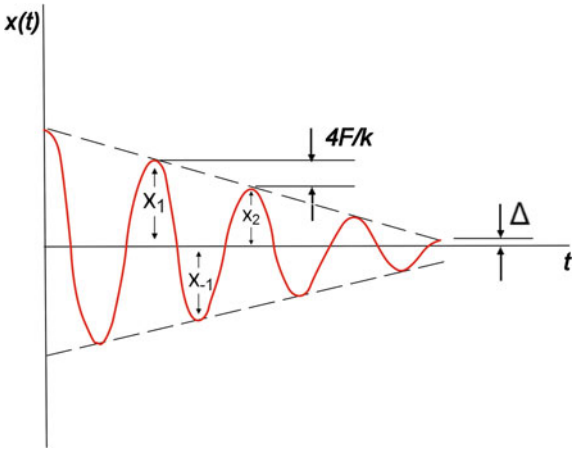

Fig. 3.5 Displacement of a system in coulomb damping

$$\frac{1}{2}k\left(X_1^2 - X_{-1}^2\right) - F_d(X_1 + X_{-1}) = 0$$

or

$$\frac{1}{2}k(X_1 + X_{-1}) = F_d$$

where X_{-1} is the amplitude after the half-cycle as shown in Fig. 3.5. By repeating this procedure for the next half-cycle, a further decrease in amplitude of $2F_d/k$ will be found, so that the decay in amplitude per cycle is a constant and is given as follows:

$$X_1 - X_2 = \frac{4F_d}{k}$$

The motion will cease when the amplitude becomes less than Δ; at this position, spring force is insufficient to overcome the static friction force, which is generally greater than the kinetic friction force. It can also be shown that the frequency of oscillation is the same as that of the un-damped system. Amplitude of the coulomb damping system decays linearly with time. For damped free vibration of SDOF system, equation of motion is given as follows:

$$m\ddot{x} + c\dot{x} + kx = 0 \tag{3.5}$$

This is a second-order, homogeneous, ordinary differential equation (ODE). If all parameters (mass, spring stiffness, and viscous damping) are constants, then the equation becomes linear with constant coefficients that can be solved by a simple characteristic equation method. The characteristic equation for this problem is given as follows:

$$ms^2 + cs + k = 0 \tag{3.6}$$

This determines two independent roots that fall into one of the following three cases:

1. If $c^2 - 4mk < 0$, the system is termed under-damped. The roots of the characteristic equation are complex conjugates, corresponding to oscillatory motion with an exponential decay in amplitude.
2. If $c^2 - 4mk = 0$, the system is termed critically damped. The roots of the characteristic equation are repeated, corresponding to simple decaying motion with at most one overshoot of the system's resting position.
3. If $c^2 - 4mk > 0$, the system is termed over-damped. The roots of the characteristic equation are purely real and distinct, corresponding to simple exponentially decaying motion.

To simplify the solutions coming up, we define the critical damping C_c, the damping ratio ξ, and the damped vibration frequency ω_d as follows:

$$C_c = 2m\sqrt{k/m} = 2m\omega_n$$
$$\xi = c/C_c$$
$$\omega_d = \sqrt{1-\xi^2}\omega_n$$

where ω_d is termed damped vibration frequency. This will be the same as the natural frequency for an un-damped system. Solution in time domain is discussed below for each of the three cases.

3.7.3 Under-damped Systems

When $c^2 - 4mk < 0$ (equivalent to $\xi < 1$ or $c < C_c$), the characteristic equation has a pair of complex conjugate roots. The displacement solution for this kind of system is given as follows:

$$x(t) = \mathrm{e}^{-\xi\omega_n t}[A\cos(\omega_d t) + B\sin(\omega_d t)] \tag{3.7}$$

With the initial conditions as $x(t = 0) = x(0)$ and $\dot{x}(t = 0) = \dot{x}$, Eq. (3.7) becomes

$$x(t) = \mathrm{e}^{-\xi\omega_n t}\left[x_0\cos(\omega_d t) + \frac{\dot{x}_0 + \xi\omega_n x_0}{\omega_d}\sin(\omega_d t)\right] \tag{3.8}$$

The displacement plot of an under-damped system is shown in Fig. 3.6.

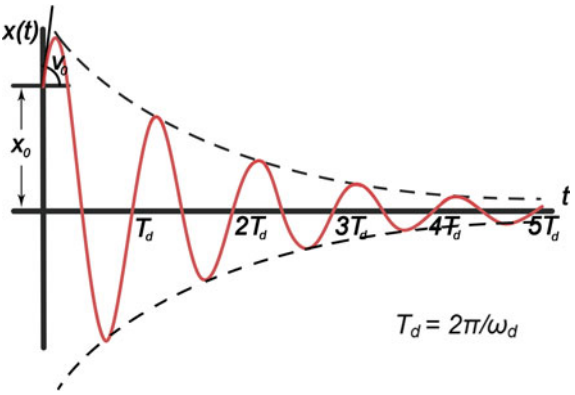

Fig. 3.6 Response of under-damped system

The damping ratio ξ can be experimentally determined from the free response by the logarithmic decrement method. To illustrate this approach, note from Eq. (3.8) that the period of damped oscillations is given as follows:

$$T = \frac{2\pi}{\omega_d}$$

Evaluate Eq. (3.8) at $t = 0$ and $t = \frac{2\pi}{\omega_d}$

$$\text{At } t = 0, \quad x(t) = x_1 = x_0 \tag{3.9}$$

$$\text{At } t = \frac{2\pi}{\omega_d}, \quad x(t) = x_2 = \mathrm{e}^{-\xi\omega_n \frac{2\pi}{\omega_d}} x_0 \tag{3.10}$$

x_1 and x_2 are the two consecutive positive peaks of the response. Dividing Eq. (3.9) by (3.10), we get the following form:

$$\begin{aligned} \frac{x_1}{x_2} &= \mathrm{e}^{-\xi\omega_n \frac{2\pi}{\omega_d}} = \mathrm{e}^{\frac{2\pi\xi}{\sqrt{1-\xi^2}}} \\ \ln\frac{x_1}{x_2} &= \frac{2\pi\xi}{\sqrt{1-\xi^2}} \end{aligned} \tag{3.11}$$

Equation (3.11) is called logarithmic decrement and is denoted by δ.

$$\delta = \ln\frac{x_1}{x_2} = \frac{2\pi\xi}{\sqrt{1-\xi^2}} \tag{3.12}$$

Logarithmic decrement is also given by the following relationship:

$$\delta = \frac{1}{n}\ln\frac{x}{x_n} \tag{3.13}$$

where x is the amplitude at particular maxima and x_n represents the amplitude after further n cycles.

3.7.4 Critically Damped Systems

When $c^2 - 4mk = 0$ (equivalent to $\xi = 1$ or $c = C_c$), the characteristic equation has repeated real roots. Displacement time history is given as follows:

$$x(t) = (A + Bt)\mathrm{e}^{-\omega_n t} \tag{3.14}$$

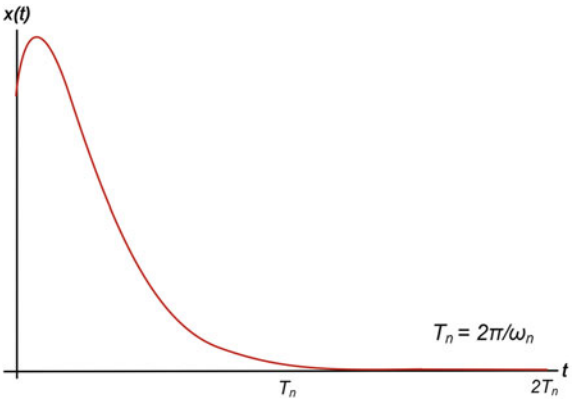

Fig. 3.7 Response of critically damped system

Using the given initial conditions, equation reduces to the following form:

$$x(t) = \mathrm{e}^{-\omega_n t}[x_0 + (\dot{x}_0 + \omega_n x_0)t] \tag{3.15}$$

The critical damping factor C_c can be interpreted as the minimum damping that result in non-periodic motion (i.e., simple decay). Displacement plot of a critically damped system with positive initial displacement and velocity is shown in Fig. 3.7.

3.7.5 Over-damped Systems

When $c^2 - 4mk > 0$ (equivalent to $\xi > 1$ or $c > C_c$), the characteristic equation has two distinct real roots. Displacement time history is given as follows:

$$x(t) = A\mathrm{e}^{\left[-\xi+\sqrt{\xi^2-1}\right]\omega_n t} + B\mathrm{e}^{\left[-\xi-\sqrt{\xi^2-1}\right]\omega_n t} \tag{3.16}$$

Using the given initial conditions, equation reduces to the following form:

$$\begin{aligned} x(t) = {} & \frac{x_0\omega_n\left[\xi + \sqrt{\xi^2-1}+\right] + \dot{x}_0}{2\omega_n\sqrt{\xi^2-1}}\mathrm{e}^{\left[-\xi+\sqrt{\xi^2-1}\right]\omega_n t} \\ & + \frac{-x_0\omega_n\left[\xi - \sqrt{\xi^2-1}+\right] - \dot{x}_0}{2\omega_n\sqrt{\xi^2-1}}\mathrm{e}^{\left[-\xi-\sqrt{\xi^2-1}\right]\omega_n t} \end{aligned} \tag{3.17}$$

The displacement plot of an over-damped system is shown in Fig. 3.8.

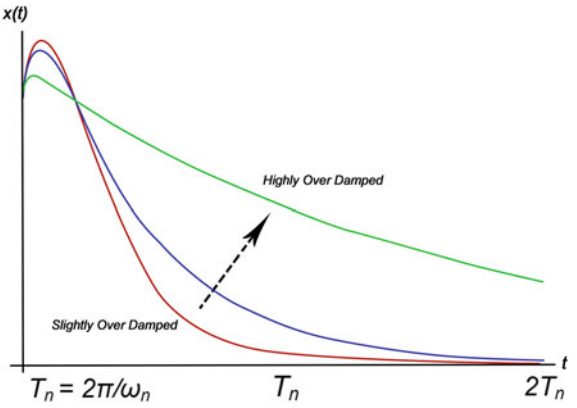

Fig. 3.8 Response of over-damped system

The motion of an over-damped system is non-periodic, regardless of the initial conditions; larger the damping, longer the time to decay from an initial disturbance. If the system is heavily damped $\xi \gg 1$, the displacement solution takes the approximate form as given below:

$$x(t) \approx x_0 + \frac{\dot{x}_0}{2\xi\omega_n}\left(1 - e^{-2\xi\omega_n t}\right) \tag{3.18}$$

3.7.6 Half Power Method

This is used to calculate the damping from the response of the amplitude as shown in Fig. 3.9. The first step is to locate the peak amplitude. Corresponding frequencies are noted as f_1 and f_2.

$$\frac{x_{st}}{\sqrt{\left(1-\beta^2\right)^2 + 2\beta\zeta}} = \frac{x_{st}}{\sqrt{2\zeta}} = \frac{1}{\sqrt{2}}\left(\frac{x_{st}}{2\zeta}\right)$$

Solving we get $\beta_1 = 1 - \zeta - \zeta^2$; $\beta_2 = 1 + \zeta - \zeta^2$. Simplifying and neglecting higher powers, we get $\zeta = \frac{\beta_2 - \beta_1}{2}$;

$$\zeta = \frac{1}{2}\left(\frac{\omega_2 - \omega_1}{\omega_n}\right) = \frac{1}{2}\left(\frac{f_2 - f_1}{f_n}\right)$$

The value of the ζ depends upon the quality of the graph. The area representing the energy should represent 50 % of the area of the spectrum. This is used only for forced function. This is not related to degrees of freedom.

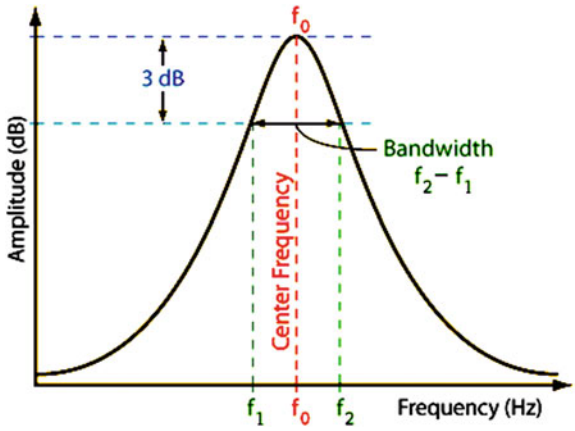

Fig. 3.9 Half power bandwidth method

3.8 Forced Vibration

In the presence of external force $f(t)$, the resulting vibration is termed as force vibration. Such vibrations can be either un-damped or damped as the case may be considered in the analysis. Examples of forced excitation include wave action on the offshore platform that is inherently and always present in the system. Equation of motion for forced vibration is given as follows:

$$m\ddot{x} + c\dot{x} + kx = f(t) \tag{3.19}$$

Figure 3.10 shows damped SDOF system in the presence of external force $f(t)$. Subjecting the system to a harmonically varying load $f(t)$ amplitude p_o and circular frequency ω, equation of motion is given as follows:

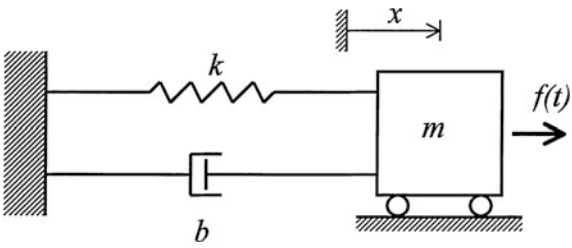

Fig. 3.10 Damped single degree of freedom under external excitation

$$m\ddot{x} + c\dot{x} + kx = f(t) = p_o \sin \omega t \tag{3.20}$$

Response of the single degree of freedom is further analyzed for two cases: (i) un-damped and (ii) damped.

3.8.1 Un-damped Forced Vibration

Equation of motion is further modified as given below:

$$m\ddot{x} + kx = f(t) = p_o \sin \omega t \tag{3.21}$$

Complete solution of the above equation contains two parts, namely (i) complementary solution and (ii) particular integral. Complementary solution to the equation is given as follows:

$$x_c(t) = A \cos \omega t + B \sin \omega t \tag{3.22}$$

Particular solution depends on the form of dynamic loading. In case of harmonic excitation as considered in the present argument, it is simple to assume that the resulting response shall also be harmonic and in phase with the loading. Particular solution for the assumed conditions is given as follows:

$$x_p(t) = C \sin \omega t \tag{3.23}$$

in which the amplitude C is to be evaluated. Substituting Eq. (3.23) in Eq. (3.21), we get the following:

$$-m\omega^2 C \sin \omega t + kC \sin \omega t = p_o \sin \omega t$$

Dividing throughout by $(k \sin \omega t)$ (which is nonzero in general) and $k/m = \omega^2$, we get the following form:

$$C = \frac{p_o}{k} \frac{1}{1 - \beta^2} \tag{3.24}$$

where β is defined as the ratio of frequency of the applied load to natural frequency of the system and is given by the following relationship:

$$\beta = \frac{\omega}{\omega_n}$$

Complete solution to the equation of motion is the sum of complementary solution and particular integral as given below:

$$\begin{aligned} x(t) &= x_c(t) + x_p(t) \\ x(t) &= A\cos\omega t + B\sin\omega t + \frac{p_o}{k}\frac{1}{[1-\beta^2]}\sin\omega t \end{aligned} \tag{3.25}$$

In the above equation, constants A and B depend on the initial conditions. For the system at rest $\{x(0) = \dot{x}(0) = 0\}$, it can be seen that

$$A = 0 \quad \text{and} \quad B = \frac{p_o}{k}\frac{\beta}{[1-\beta^2]}$$

Substituting these in Eq. (3.25), we get the following:

$$x(t) = \frac{p_o}{k}\frac{1}{[1-\beta^2]}(\sin\omega t - \beta\sin\omega_n t) \tag{3.26}$$

where $p_o/k = x_{\text{st}}$ is termed as static displacement that is caused by the applied external load p_o and $1/(1-\beta^2)$ is the magnification factor (MF) representing the amplification effect of the harmonically applied loading. Equation (3.26) contains two distinct terms:

(i) $\sin\omega t$ term represents the response component at frequency of the applied loading which is called steady-state response
(ii) $\beta\sin\omega_n t$ represents the response component at natural frequency of vibration and is termed as transient response. This depends on the initial conditions assigned to the body and shall vanish eventually. It is interesting to note that this term will not vanish in case of hypothetical un-damped system.

Therefore, in dynamic analysis, one is more interested in the steady-state response.

3.8.2 Damped Forced Vibration

Considering equation of motion including viscous damping, Eq. (3.20) is modified by dividing it by m and noting that $c/m = 2\xi\omega n$; modified form is given as below:

$$\ddot{x}(t) + 2\xi\omega n\dot{x}(t) + \omega^2 x(t) = \frac{p_0}{m}\sin\omega t \tag{3.27}$$

Complementary solution is given as follows:

$$x_c(t) = [A\cos\omega_d t + B\sin\omega_d t]\exp(-\xi\omega_n t) \tag{3.28}$$

Particular solution is of the following form:

$$x_p(t) = G1\cos\omega t + G2\sin\omega t \tag{3.29}$$

Equation (3.29) contains both the harmonic terms that are essential, as the response of a damped system shall not be in phase with the loading. Substituting in Eq. (3.27) and rearranging the terms, we get the following form:

$$\begin{aligned}&\left[G1\omega^2 + G2\omega(2\xi\omega_n) + G1\omega_n^2\right]\cos\omega t\\ &\quad + \left[-G2\omega^2 - G1\omega(2\xi\omega_n) + G2\omega^2 - \frac{p_0}{m}\right]\sin\omega t = 0\end{aligned} \tag{3.30}$$

In order to satisfy this equation for all values of t, it is necessary that each of the two square bracket quantities equal zero; thus, it reduces to the form as given below:

$$\begin{aligned}G1(1-\beta^2) + G2(2\xi\beta) &= 0\\ G2(1-\beta^2) - G1(2\xi\beta) &= p_o/k\end{aligned} \tag{3.31}$$

where β is the frequency ratio. Solving these two equations simultaneously, we get the following:

$$\begin{aligned}G1 &= \frac{p_o}{k}\left[\frac{-2\xi\beta}{(1-\beta^2)^2 + (2\xi\beta)^2}\right]\\ G2 &= \frac{p_o}{k}\left[\frac{1-\beta^2}{(1-\beta^2)^2 + (2\xi\beta)^2}\right]\end{aligned} \tag{3.32}$$

Substituting the values and combining the results of complimentary solution, Eq. (3.28) reduces the following form:

$$\begin{aligned}x(t) &= [A\cos\omega_d t + B\sin\omega_d t]\exp(-\xi\omega t)\\ &\quad + \frac{p_o}{k}\left[\frac{1}{(1-\beta^2)^2 + (2\xi\beta)^2}\right][(1-\beta^2)\sin\omega t - (2\xi\beta)\cos\omega t]\end{aligned} \tag{3.33}$$

First term on the right-hand side of Eq. (3.33) represents transient response which damps out in accordance with $\exp(-\xi\omega_n t)$; second term represents the steady-state harmonic response, which will continue indefinitely. The constants A and B can be evaluated for any given initial conditions, $x(0)$ and $\dot{x}(0)$. As explained earlier, transient response will not be of primary inters, and therefore, evaluation of constants $A\&B$ is not discussed further.

3.9 Steady-State Response

Steady-state response of equation of motion for a damped forced vibration, as presented in Eq. (3.33), is given below:

$$x_p(t) = \frac{p_o}{k}\left[\frac{1}{(1-\beta^2)^2 + (2\xi\beta)^2}\right]\left[(1-\beta^2)\sin\omega t - (2\xi\beta)\cos\omega t\right] \tag{3.34}$$

This displacement can be interpreted easily by plotting two corresponding rotating vectors in the complex plane as shown in Fig. 3.11. Components along the real axis are identical to the terms of the above equation. Real component of the resultant vector gives the steady-state response in the following form:

$$x_p(t) = \rho\sin(\omega t - \theta) \tag{3.35}$$

Amplitude of the response is given as below:

$$\rho = \frac{p_o}{k}\left[\left(1-\beta^2\right)^2 + (2\xi\beta)^2\right]^{-1/2} \tag{3.36}$$

Phase angle by which the response lags behind the applied loading is given as follows:

$$\theta = \tan^{-1}\left[\frac{2\xi\beta}{1-\beta^2}\right] \tag{3.37}$$

where $0 < \theta < 180^\circ$ is the range. Ratio of the resultant harmonic response amplitude to the static displacement is termed as dynamic magnification factor and is given as follows:

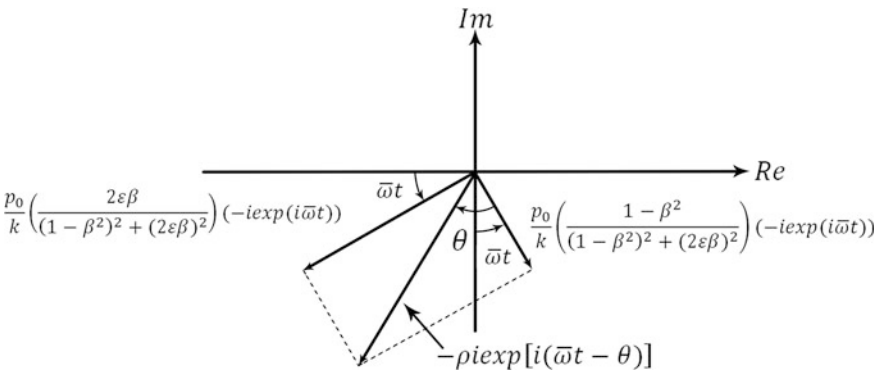

Fig. 3.11 Steady-state response of damped single-degree-of-freedom system

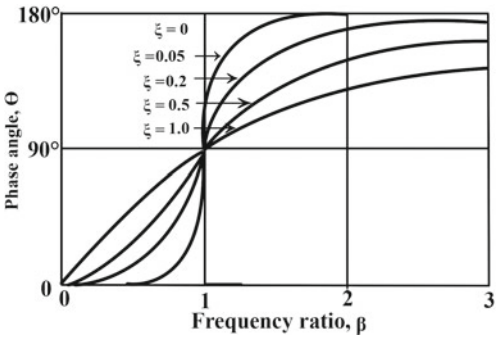

Fig. 3.12 Variation of frequency ratio with phase angle for damped vibration

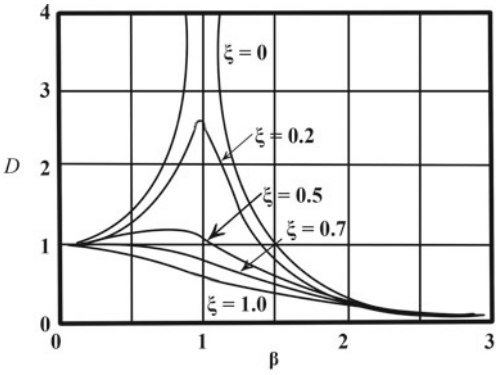

Fig. 3.13 Variation of dynamic magnification factor with frequency ratio for damped vibration

$$D = \frac{\rho}{p_o/k}\left[\left(1-\beta^2\right)^2+(2\xi\beta)^2\right]^{-1/2} \tag{3.38}$$

Figure 3.12 shows the variation of frequency ration with phase angle for different values of damping ratios. Figure 3.13 shows the variation of dynamic magnification factor with frequency ratio for different damping ratios.

3.10 Two-Degrees-of-Freedom Model

Systems that require two independent coordinates to specify their position during vibration are termed as two-degrees-of-freedom systems. In general, a system requiring n number of independent coordinates/parameters to specify its position is called a system with n degrees of freedom. Two-degrees-of-freedom system is therefore a specific case of a multi-degrees-of-freedom system. Number of degrees of freedom generally equals the number of discrete masses of the system, but this is not always true. Figure 3.14 shows two different forms of two-degrees-of-freedom

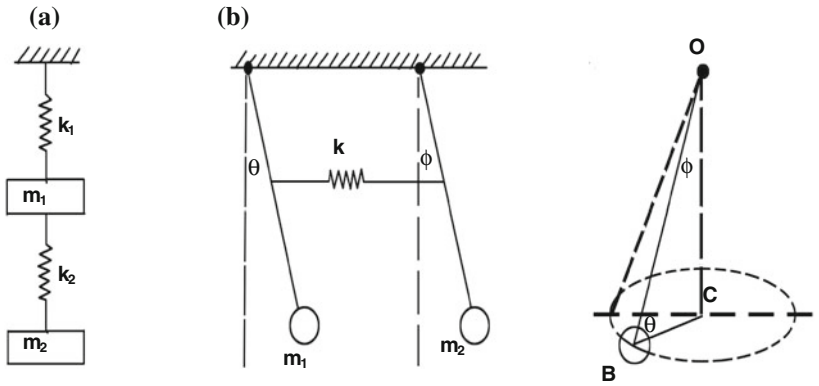

Fig. 3.14 Two-degrees-of-freedom system models. **a** Mass and stiffness in series; **b** two pendulums connected with a bar of stiffness k

models. Two masses connected by spring in series with stiffness k_1 and k_2 require two independent coordinates, namely x_1 and x_2; the second system of two pendulums connected by a rod of known stiffness, k, has two independent coordinates, namely θ and Φ, respectively.

3.11 Un-damped Free Vibrations and Principal Modes of Vibration

As a general rule, two-degrees-of-freedom system shall have two natural frequencies. Under certain condition, it is possible for both the masses to vibrate at any of these natural frequencies; this shall induce a definite relationship between the amplitudes of the two displacement coordinates. This resulting configuration is referred as principal mode of vibration; it is therefore easy to realize that a two-degrees-of-freedom model shall have two principal modes of vibrations. Under normal mode of vibration, both the masses pass through their respective mean equilibrium position simultaneously and reach their extreme position simultaneously as well. In case of forced harmonic excitation, resultant vibration of the masses takes place at the excitation frequency. Figure 3.15 shows a spring–mass un-damped system with two degrees of freedom, x_1 and x_2, respectively. Masses are constrained to move only in the vertical direction; masses m_1 and m_2 have displacements x_1 and x_1, respectively, and are measured from their respective static equilibrium positions. Free body diagram of the system under the action of forces is also shown in Fig. 3.15.

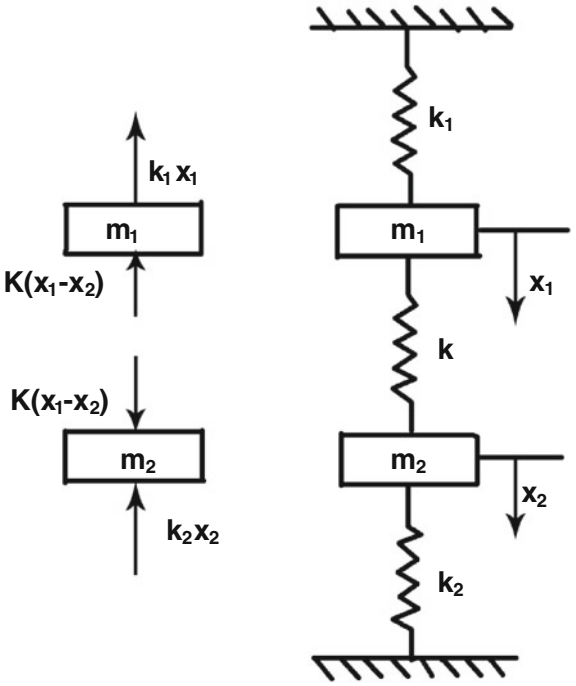

Fig. 3.15 Spring–mass un-damped two-degrees-of-freedom system

Equations of motion can be obtained by applying Newton's second law of motion. Let the displacements and forces are measured positive when acting downward. Applying Newton's law to the free body diagrams of the two masses m_1 and m_2, we get the following:

$$m_1\ddot{x}_1 = -k_1x_1 - k(x_1 - x_2) \tag{3.39}$$

$$m_2\ddot{x}_2 = k(x_1 - x_2) - k_2x_2 \tag{3.40}$$

Rearranging and rewriting the above equations, we get the following:

$$m_1\ddot{x}_1 + (k + k_1)x_1 - kx_2 = 0 \tag{3.41}$$

$$m_2\ddot{x}_2 + (k + k_2)x_2 - kx_1 = 0 \tag{3.42}$$

Considering that both the masses are vibrating at the same natural frequency ω but with different amplitudes, solution of displacements is assumed as below:

$$x_1 = X_1 \sin \omega t \tag{3.43}$$

$$x_2 = X_2 \sin \omega t \tag{3.44}$$

Substituting for x_1 and x_2, Eqs. (3.41) and (3.42) are rewritten as follows:

$$-m_1X_1\omega^2 \sin \omega t + (k + k_1)x_1 \sin \omega t - kx_2 \sin \omega t = 0 \tag{3.45}$$

$$-m_2X_2\omega^2 \sin \omega t + (k + k_2)x_2 \sin \omega t - kx_1 \sin \omega t = 0 \tag{3.46}$$

Rearranging the terms in above equations, we get the following:

$$\left\{\left(k + k_1 - m_1\omega^2\right)X_1 - kX_2\right\} \sin \omega t = 0 \tag{3.47}$$

$$\left\{-kX_1 + \left(k + k_2 - m_2\omega^2\right)X_2\right\} \sin \omega t = 0 \tag{3.48}$$

As assumed solutions involve $\sin \omega t$, the term $\sin \omega t$ cannot be equal to zero all the times. Therefore, Eqs. (3.47) and (3.48) simplify to the following:

$$\left(k + k_1 - m_1\omega^2\right)X_1 - kX_2 = 0 \tag{3.49}$$

$$-kX_1 + \left(k + k_2 - m_2\omega^2\right)X_2 = 0 \tag{3.50}$$

The above equations are homogeneous linear algebraic equations in X_1 and X_2. By carefully examining both the equations, it can be seen that two equations are connected through spring constant k, in the absence of which these equations will become independent. The spring k is therefore called a coupling spring. By employing Cramer's rule, these equations can be solved.

$$X_1 = \frac{\begin{vmatrix} 0 & -k \\ 0 & k + k_2 - m_2\omega^2 \end{vmatrix}}{\Delta\omega} \tag{3.51}$$

$$X_2 = \frac{\begin{vmatrix} k + k_1 - m_1\omega^2 & 0 \\ -k & 0 \end{vmatrix}}{\Delta\omega} \tag{3.52}$$

For solution other than the trivial one of $x_1 = x_2 = 0$, a necessary condition is given as follows:

$$\Delta\omega = \begin{vmatrix} (k + k_1 - m_1\omega^2) & -k \\ -k & (k + k_2 - m_2\omega^2) \end{vmatrix} = 0 \tag{3.53}$$

The above equation is termed as characteristic equation from which the values of ω are established. Simplifying and rearranging, we get the following:

$$m_1m_2\omega^4 - [(k + k_1)m_2 + (k + k_2)m_1]\omega^2 + (k + k_1)(k + k_2) - k^2 = 0 \tag{3.54}$$

Dividing by $m_1 m_2$, the above equation reduces to the following form:

$$\omega^4 - \left(\frac{k+k_1}{m_1} + \frac{k+k_2}{m_2}\right)\omega^2 + \frac{kk_1 + kk_2 + k_1k_2}{m_1 m_2} = 0 \tag{3.55}$$

The above equation is a quadratic equation in ω^2 and can be solved for ω. Alternatively, another approach can be used to obtain the mode shapes of vibration. Mode shapes are the deflected profile of the vibrating masses indicating the relative position of the masses at any specific frequency at which mode shape is plotted. Hence, for every frequency of vibration, there exists a pre-defined pattern of displaced position of the masses, which is termed as mode shape. Mode shape is a graphical display of the relative amplitudes of two coordinates and their phase–angle relationship. Apart from indicating the relative position of masses at any particular frequency of vibration, mode shapes also indicate the qualitative measure of the design of the system. For example, if the mode shape corresponding to the fundamental frequency shows torsion, the system can be stated as unstable; in such cases, revision in the design is sought. Equations (3.49) and (3.50) can be rewritten as follows:

$$\frac{X_1}{X_2} = \frac{k}{k + k_1 - m_1\omega^2} \tag{3.56}$$

$$\frac{X_1}{X_2} = \frac{k + k_2 - m_2\omega^2}{k} \tag{3.57}$$

Equating both, we get the following:

$$\frac{k}{k + k_1 - m_1\omega^2} = \frac{k + k_2 - m_2\omega^2}{k} \tag{3.58}$$

$$m_1 m_2 \omega^4 - [(k+k_1)m_2 + (k+k_2)m_1]\omega^2 + (k+k_1)(k+k_2) - k^2 = 0 \tag{3.59}$$

The roots of the above quadratic equation may be written as follows:

$$\omega^2 = \frac{1}{2}\left[\left(\frac{k+k_1}{m_1} + \frac{k+k_2}{m_2}\right) \pm \sqrt{\left(\frac{k+k_1}{m_1} + \frac{k+k_2}{m_2}\right)^2 - 4\frac{kk_1 + kk_2 + k_1k_2}{m_1 m_2}}\right] \tag{3.60}$$

This can be further simplified as follows:

$$\omega^2 = \frac{1}{2}\left[\left(\frac{k+k_1}{m_1} + \frac{k+k_2}{m_2}\right) \pm \sqrt{\left(\frac{k+k_1}{m_1} - \frac{k+k_2}{m_2}\right)^2 + 4\frac{k^2}{m_1 m_2}}\right] \tag{3.61}$$

It can be seen that roots of the above equation shall yield positive real values of ω. In the simplified form, above equation can be written as given below:

$$\omega^2 = \frac{1}{2}\left(A \pm \sqrt{A^2 - 4B}\right) \tag{3.62}$$

Two finite positive values of the above equation, say for example, be denoted as ω_1^2 and ω_2^2. Out of the four values, namely $(\pm\omega_1, \pm\omega_2)$, use of negative sign will simply change the signs of the arbitrary constants X_1 and X_2; it does not affect the solution. Lesser value of the above frequency is called fundamental frequency (or first harmonic frequency). The general solution can be expressed as given below:

$$x_1 = X_{11} \sin \omega_1 t + X_{12} \sin \omega_2 t \tag{3.63}$$

$$x_2 = X_{21} \sin \omega_1 t + X_{22} \sin \omega_2 t \tag{3.64}$$

where X_{11}, X_{12}, X_{21} and X_{22} are the arbitrary constants which can be determined by initial conditions. It is seen that mode shapes corresponding to each frequency indicate the relative position of mass at that corresponding frequency; it is therefore obvious that position of masses may not be the same. However, all masses can be made to vibrate at a specific frequency such that all the masses will pass their equilibrium position simultaneously and will reach their maximum displacements. Such a pattern of mode of vibration is called the principal mode of vibration. Fundamental mode of vibration is called first mode, and the next successive mode is called second mode and so on. When the system vibrates in the first mode of vibration (i.e., when $\omega = \omega_1$), amplitude ratio in Eqs. (3.56) and (3.57) becomes

$$\frac{X_{11}}{X_{21}} = \frac{k}{k + k_1 - m_1\omega_1^2} = \frac{k + k_2 - m_2\omega_1^2}{k} = \frac{1}{\mu_1} \tag{3.65}$$

$$\frac{X_{12}}{X_{22}} = \frac{k}{k + k_1 - m_1\omega_2^2} = \frac{k + k_2 - m_2\omega_2^2}{k} = \frac{1}{\mu_2} \tag{3.66}$$

Constants μ_1 and μ_2 represent amplitude ratios to frequencies ω_1 and ω_2, respectively. Combining the above two expressions, we get the following:

$$k\mu_{1,2} = k + k_1 - m\omega_{1,2}^2 \tag{3.67}$$

Substituting for $\omega_{1,2}^2$, we get the following:

$$k\mu_{1,2} = \frac{m_1}{2}\left[\left(\frac{k + k_1}{m_1} - \frac{k + k_2}{m_2}\right) \pm \sqrt{\left(\frac{k + k_1}{m_1} - \frac{k + k_2}{m_2}\right)^2 + 4\frac{k^2}{m_1 m_2}}\right] \tag{3.68}$$

Since the quantity under the radical sign is greater than the quantity outside, the sign of the quantity under the radical sign decides the sign of expression on the right. Hence, μ_1 and μ_2 are of opposite signs. For any one of the amplitudes (X_1 or X_2) in the ratio (X_1/X_2) is assumed to be unity, then the corresponding mode is called as normal mode of vibration.

3.12 Multi-degrees-of-Freedom

All the concepts introduced in the single and two degrees of freedom can be extended to multi-degrees-of-freedom systems. Equations of motion of a multi-degrees-of-freedom can be derived using Newton's second law of motion as described earlier. However, it is advantageous and necessary to know few more additional methods of writing equations of motion for multi-degrees-of-freedom. For a multi-degrees-of-freedom system with n degrees, there exist n natural frequencies, each associated with the corresponding mode shape. The method of determining these natural frequencies from the characteristic equation is also applicable to such systems. However, increase in the number of degrees of freedom will make the characteristic equation more complex. Thanks to the property of orthogonality that is exhibited by mode shapes of multi-degrees-of-freedom system, analysis of such system is simplified.

3.13 Equation of Motion for Multi-degrees-of-Freedom System

Consider an un-damped system shown in Fig. 3.16 having n degrees of freedom. Differential equation for each mass can be written separately using Newton's second law. If $x_1, x_2, x_3, \ldots x_n$ are the displacements from the equilibrium position of the respective masses at any instant, then

$$\begin{aligned} m_1\ddot{x}_1 &= -k_1x_1 - k_2(x_1 - x_2) \\ m_2\ddot{x}_2 &= k_2(x_1 - x_2) - k_3(x_2 - x_3) \\ m_3\ddot{x}_3 &= k_3(x_2 - x_3) - k_4(x_3 - x_4) \\ &\ldots \\ m_n\ddot{x}_n &= k_n(x_{n-1} - x_n) \end{aligned} \tag{3.69}$$

These equations can be arranged in the following forms.

$$\begin{aligned} &m_1\ddot{x}_1 + k_1x_1 + k_2(x_1 - x_2) = 0 \\ &m_2\ddot{x}_2 - k_2(x_1 - x_2) + k_3(x_2 - x_3) = 0 \\ &m_3\ddot{x}_3 - k_3(x_2 - x_3) + k_4(x_3 - x_4) = 0 \\ &\ldots \\ &m_n\ddot{x}_n - k_n(x_{n-1} - x_n) = 0 \end{aligned} \tag{3.70}$$

The above equation is the required equation of motion, which can also be written in the matrix form as given below:

$$\begin{bmatrix} m_1 & 0 & 0 & \ldots & 0 \\ 0 & m_1 & 0 & \ldots & 0 \\ 0 & 0 & m_1 & \ldots & 0 \\ \ldots & \ldots & \ldots & \ldots & \ldots \\ 0 & 0 & 0 & \ldots & m_1 \end{bmatrix} \begin{Bmatrix} \ddot{x}_1 \\ \ddot{x}_2 \\ \ddot{x}_3 \\ \ldots \\ \ddot{x}_n \end{Bmatrix} + \begin{bmatrix} (k_1 + k_2) & 0 & 0 & \ldots & 0 \\ 0 & (k_2 + k_3) & 0 & \ldots & 0 \\ 0 & 0 & (k_3 + k_4) & \ldots & 0 \\ \ldots & \ldots & \ldots & \ldots & \ldots \\ 0 & 0 & 0 & \ldots & k_n \end{bmatrix} \begin{Bmatrix} x_1 \\ x_2 \\ x_3 \\ \ldots \\ x_n \end{Bmatrix} = \begin{Bmatrix} 0 \\ 0 \\ 0 \\ \ldots \\ 0 \end{Bmatrix} \tag{3.71}$$

$$[M]\{\ddot{x}\} + [K]\{x\} = \{0\} \tag{3.72}$$

where $[M]$ is a square matrix of nth order having only diagonal elements in this case; $[K]$ is a symmetric square stiffness matrix of order n, and $\{x\}$ is a column matrix of n elements corresponding to the dynamic displacements of the respective n masses. Equation (3.72) is similar to that of the equation of motion of a single degree of freedom except that $[M]$ and $[K]$ are a matrix of nth order where n is the degree of freedom.

3.14 Influence Coefficients

Equations of motion of a multi-degrees-of-freedom system can also be written in terms of influence coefficients that are extensively used in structural dynamics. For a linear spring, the force necessary to cause a unit elongation is called the spring constant. In more complex systems, we can express the relation between the displacement at a point and the forces acting at various other points of the system by means of influence coefficients. There are two types of influence coefficients, namely (i) flexibility influence coefficients and (ii) stiffness influence coefficients. To illustrate the concept of an influence coefficient, let us consider the multi-degrees-of-freedom spring–mass system shown in Fig. 3.16.

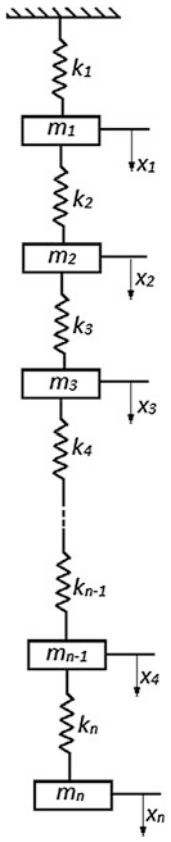

Fig. 3.16 Un-damped multi-degrees-of-freedom model

Let the system be acted on by just one force F_j and let the displacement at point i (i.e., mass m_i) due to F_j be x_{ij}. The flexibility influence coefficient, denoted by a_{ij}, is defined as the deflection at point i due to a unit load at point j. Since the deflection increases proportionately with the load for a linear system, we have the following relationship:

$$x_{ij} = a_{ij}F_j \tag{3.72}$$

If several forces $F_j (j = 1, 2, \ldots, n)$ act at different points of the system, then the total deflection at any point i can be found by summing up the contributions of all force F_j. This is given as below:

$$x_i = \sum_{j=1}^{n} x_{ij} = \sum_{j=1}^{n} a_{ij}F_j \quad i = 1, 2, \ldots, n \tag{3.73}$$

Equation (3.73) can be expressed in matrix form as follows:

$$\bar{x} = [a]\overline{F} \tag{3.74}$$

where $\bar{x}$ and $\overline{F}$ are displacement and force vectors, and $[a]$ is the flexibility matrix and is given as follows:

$$[a] = \begin{bmatrix} a_{11} & a_{12} & - & a_{1n} \\ a_{21} & a_{22} & - & a_{2n} \\ - & - & - & - \\ a_{n1} & a_{n2} & - & a_{nn} \end{bmatrix} \tag{3.75}$$

The stiffness influence coefficient, denoted by k_{ij}, is defined as the force at point i due to a unit displacement at point j when all the points other than the point j are restrained. Total force at point i, which is F_i, can be obtained by summing up the forces due to all such displacements $x_j (j = 1, 2, \ldots, n)$ and is given as follows:

$$F_i = \sum_{j=1}^{n} k_{ij}x_j \qquad i = 1, 2, \ldots, n \tag{3.76}$$

Equation (3.76) can be stated in matrix form as given below:

$$\overline{F} = [k]\bar{x} \tag{3.77}$$

where $[k]$ is the stiffness matrix and is given as follows:

$$[k] = \begin{bmatrix} k_{11} & k_{12} & - & k_{1n} \\ k_{21} & k_{22} & - & k_{2n} \\ - & - & - & - \\ k_{n1} & k_{n2} & - & k_{nn} \end{bmatrix} \tag{3.78}$$

By comparing Eqs. (3.74) and (3.77), following relationship can be deduced:

$$\bar{x} = [a]\overline{F} = [a][k]\bar{x} \tag{3.79}$$

It can be further seen that the following relationship also holds good.

$$[a][k] = [I] \tag{3.80}$$

where $[I]$ denotes the unit matrix. Equation (3.80) is equivalent to the following statement:

$$[k] = [a]^{-1} \quad \text{and} \quad [a] = [k]^{-1} \tag{3.81}$$

That is, the stiffness and flexibility influence coefficient matrices are inverse of one another. Further, more interesting observations can be made as listed below:

- Since deflection at point i due to a unit load at point j is the same as the deflection at point j due to a unit load at point i for a linear system (Maxwell's reciprocal theorem), we shall conclude that $a_{ij} = a_{ji}$ and $k_{ij} = k_{ji}$.
- Flexibility and stiffness influence coefficients can be calculated from the principles of basic structural mechanics.
- Influence coefficient matrix shall always be a square, symmetric matrix with positive leading diagonal elements.

3.15 Eigenvalue Problem

Let us now consider a multi-degrees-of-freedom system shown in Fig. 3.16. Differential equations of motion for the system are given as below:

$$\begin{aligned}
&[m_1\ddot{x}_1 + (k_1 + k_2)x_1] - k_2x_2 = 0\\
&-k_2x_1 + [m_2\ddot{x}_2 + (k_2 + k_3)x_2] - k_3x_3 = 0\\
&-k_3x_2 + [m_3\ddot{x}_3 + (k_3 + k_4)x_3] - k_4x_4 = 0\\
&\cdots\\
&-k_nx_{n-1} + (m_n\ddot{x}_n + k_nx_n) = 0
\end{aligned} \tag{3.82}$$

For the principal mode of vibration, let us assume the solution as follows:

$$\begin{aligned}
x_1 &= X_1 \sin \omega t\\
x_2 &= X_2 \sin \omega t\\
x_3 &= X_3 \sin \omega t\\
&\cdots\\
x_n &= X_n \sin \omega t
\end{aligned} \tag{3.83}$$

Substituting Eq. (3.83) in Eq. (3.82) and canceling out the common terms, we get the following:

$$\begin{aligned}
&[(k_1 + k_2) - m_1\omega^2]X_1 - k_2X_2 = 0 \\
&-k_2X_1 + [(k_2 + k_3) - m_2\omega^2]X_2 - k_3X_3 = 0 \\
&-k_3X_2 + [(k_3 + k_4) - m_3\omega^2]X_3 - k_4X_4 = 0 \\
&\ldots \\
&-k_nX_{n-1} + (k_n - m_n\omega^2)X_n = 0
\end{aligned} \tag{3.84}$$

For the above equations, solution other than $X_1 = X_2 = X_3 = X_n = 0$ is possible only when the determinant composed of the coefficients of X's vanishes; this condition is expressed mathematically as below:

$$\begin{vmatrix}
[(k_1 + k_2) - m_1\omega^2] & -k_2 & - & 0 & 0 \\
-k_2 & [(k_2 + k_3) - m_2\omega^2] & -k_3 & 0 & 0 \\
0 & -k_3 & - & 0 & 0 \\
- & - & - & - & - \\
- & - & - & -k_n & (k_n - m_n\omega^2)
\end{vmatrix} = 0 \tag{3.85}$$

Solution to the above equation yields n values of ω^2 corresponding to n natural frequencies. Mode shapes can be obtained from Eq. (3.84).

3.16 Dynamic Matrix Method

Equation of motion of multi-degrees-of-freedom can be written in the matrix form as shown below:

$$[M]\{\ddot{x}\} + [K]\{x\} = \{0\} \tag{3.86}$$

Pre-multiplying the above equation with $[M]$ − 1, we get the following:

$$[I]\{\ddot{x}\} + [D]\{x\} = \{0\} \tag{3.87}$$

where $[D] = [M]$ − $1K]$ is termed as dynamic matrix.

For free body vibrations, assuming displacement vector as a harmonic motion of frequency ω, we get the following:

$$\{x\} = \{X\}\sin\omega t \tag{3.88}$$

$$\{\ddot{x}\} = -\omega^2\{x\} = \lambda\{x\} = -\lambda\{X\}\sin\omega t \tag{3.89}$$

where $\lambda = \omega^2$ is the eigenvalue and $\{X\}$ is the column giving the amplitudes of respective masses, i.e., eigenvectors. In other words, λ and {X} are natural frequencies and the corresponding mode shapes, respectively. Equation (3.87) reduces to the form:

$$\begin{aligned} -\lambda[I]\{X\} + [D]\{X\} &= \{0\} \\ [[D] - X[I]]\{X\} &= \{0\} \end{aligned} \tag{3.90}$$

The determinant formed from the above equation is given below:

$$[[D] - A[I]] = 0 \tag{3.91}$$

The above equation is the frequency equation and gives n values of λ (for n degrees of freedom). Further by substitution, mode shapes can be obtained.

3.17 Dunkerley's Method

Dunkerley (1894) proposed an approximate method of determining fundamental frequency of vibrating system. It is known as lower bound method as Dunkerley's frequency will always be lower. For a multi-degrees-of-freedom system, following relationship is as proposed below (Dunkerley 1894):

$$\frac{1}{\omega_n^2} = \frac{1}{\omega_1^2} + \frac{1}{\omega_2^2} + \frac{1}{\omega_3^2} + \cdots + \frac{1}{\omega_s^2} \tag{3.92}$$

where ω_n is the fundamental natural frequency of the system: $\omega_1, \omega_2, \omega_3 \ldots$ are the natural frequencies of the system with each mass acting separately at its point of application in the absence of other masses. This method shall be applicable only for discrete systems.

3.18 Matrix Iteration Method

This is one of the most commonly used methods among iterative methods for determining eigenvalues (natural frequencies) and eigenvectors (mode shapes). With the use of flexibility matrix [A] in the differential equations, this method is used when only the lowest eigenvalue and eigenvector of multi-degrees-of-freedom system are desired. The advantage of this method is that the iterative process results in the principle mode of vibration of the system and the corresponding natural frequency simultaneously. Equation of motion in terms of flexibility matrix is written as follows:

$$[A][M][\ddot{x}] + \{x\} = \{0\} \tag{3.93}$$

Substituting $\{x\} = \{X\} \sin \omega t$, we get the following:

$$\{X\} = \omega^2[A][M]\{x\} \tag{3.94}$$

The above equation is rewritten as follows:

$$\{X\} = \omega^2[B]\{X\} \tag{3.95}$$

$$[B] = [A][M]$$

Equation (3.95) is of the form:

$$\begin{Bmatrix} X_1 \\ X_2 \\ \dots \\ X_n \end{Bmatrix} = \omega^2 \begin{bmatrix} b_{11} & b_{12} & \dots & b_{1n} \\ b_{21} & b_{22} & \dots & b_{2n} \\ \dots & \dots & \dots & \dots \\ b_{n1} & b_{n1} & \dots & b_{nn} \end{bmatrix} \begin{Bmatrix} X_1 \\ X_2 \\ \dots \\ X_n \end{Bmatrix} \tag{3.96}$$

Iterative process is started by assuming a set of displacements for the right column of Eq. (3.96) and then expanding the right-hand side which results in a column of numbers. This is then normalized and compared with the new obtained value of the displacement vector. The procedure is repeated until the new set of displacements converges with that of the previous step of iteration. The iteration process with the use of Eq. (3.96) converges to the lowest value of $(1/\omega^2)$ so that the fundamental mode of vibration is obtained. For next higher modes and natural frequencies, orthogonality principle is applied to obtain a modified matrix that is free from the lower modes.

3.19 Stodola's Method

This method is a quickly converging iterative process used for calculating the fundamental natural frequency of un-damped free vibrations for multi-degrees-of-freedom systems. The procedure is to assume a reasonable deflection pattern for the given multi-degrees-of-freedom model. This may be taken same as that of the static deflection curve as in Rayleigh's method. Determine inertia loading for the assumed deflection in terms of ω^2. For the system subjected to the inertia load, determine corresponding (new) deflection pattern; this shall also be in terms of ω^2. If the assumed deflection pattern of step 1 converges with that of the derived ones of step 3, then equate the two expressions of step 1 and step 3 which shall give the value of ω^2. If the deflection patterns do not match, then the derived deflection pattern obtained in step 3 is used as starting point for the next iteration. This process is repeated until the derived deflection pattern converges with the previous set of values. The method is independent of the amplitudes of initially assumed values of displacement pattern, and the convergence is very fast.

3.20 Mode Superposition Method

For multi-degrees-of-freedom system, equation of motion is given as follows:

$$[M]\{\ddot{x}\} + [C]\{\dot{x}\} + [K]\{x\} = \{F(t)\} \tag{3.97}$$

Any arbitrary vector $\{x\}$ in a non-dimensional space can be represented as a linear combination of the mode shapes. Thus,

$$x = \sum_{r=1}^{N} q_r(t)\{\varphi^{(r)}\} = \Phi q \tag{3.98}$$

where Φ is the modal matrix with each of its column representing mode shape and $\{q\}$ is the vector of modal coordinates related to the system coordinates. Now, the following operations are performed:

$$\begin{aligned} &[M]\{\ddot{x}\} + [C]\{\dot{x}\} + [K]\{x\} = \{F(t)\} \\ &\text{pre-multiplying by } \Phi^T \\ &\Phi^T M\Phi\ddot{q} + \Phi^T C\Phi\dot{q} + \Phi^T K\Phi q = \Phi^T F \end{aligned} \tag{3.99}$$

Since mode shape Φ is orthogonal with respect to $[M]$ and $[K]$, matrix triple products involving $[M]$ and $[K]$ will yield diagonal matrices.

$$\begin{aligned} \{\varphi^{(r)}\}^T M\{\varphi^{(r)}\} &= m_r^* \\ \{\varphi^{(r)}\}^T C\{\varphi^{(r)}\} &= c_r^* \\ \{\varphi^{(r)}\}^T K\{\varphi^{(r)}\} &= k_r^* \\ \{\varphi^{(r)}\}^T F &= f_r^* \end{aligned} \tag{3.100}$$

where m_r^* represents modal mass for mode r, c_r^* represents coefficient of viscous damping in rth mode, k_r^* represents modal stiffness for rth mode, and f_r^* represents modal force in rth mode, respectively. If mode shapes are mass-orthogonalized, then the modal parameters reduce to the following:

$$\begin{aligned} m_r^* &= 1.0 \\ c_r^* &= 2\xi_r\omega_r \\ k_r^* &= \omega_r^2 \end{aligned} \tag{3.101}$$

Modal participation factor for rth mode is given as follows:

$$\Gamma_r = \frac{\{\varphi^r\}^T Mr}{\{\varphi^r\}^T M\{\varphi^r\}} \tag{3.102}$$

3.21 Mode Truncation

In a multi-degrees-of-freedom system, it is not necessary to include all modes to get rational estimate of the total response; higher modes can be truncated. Response vector $\{x\}$ can be written as follows:

$$x = \sum_{r=1}^{\hat{N}} q_r(t)\{\varphi^{(r)}\} \tag{3.103}$$

where $\hat{N} \ll N$.

The number of modes to be included depends on (i) all modes having frequency value lower than the highest frequency of the excitation force and (ii) at least 90 % of the total mass of the structural system.

3.21.1 Static Correction for Higher Mode Response

Let us consider modal contribution to the total response as the sum of two parts as shown below:

$$x = \sum_{r=1}^{\hat{N}} \{\varphi^{(r)}\} q_r(t) + \sum_{S=\hat{N}+1}^{N} \{\varphi^{(S)}\} q_s(t) \tag{3.104}$$

where the second term of the modal summation represents the error term due to the truncation of the modal summation. Now,

$$\begin{aligned} &M_s\ddot{q}_s(t) + C_s\dot{q}_s(t) + K_s q_s(t) = f_s \\ &q_s(t) = \frac{f_s}{K_s} - \frac{\ddot{q}_s(t)}{\omega_s^2} - \frac{2\xi_s\dot{q}_s(t)}{\omega_s} \end{aligned} \tag{3.105}$$

The first term in the above equation represents the response in sth mode if the load is applied statically. The other two terms represent the dynamic correction to the static response in the sth mode. It is also seen that the inertia term is inversely proportional to the square of the natural frequency and the damping term is inversely proportional to the natural frequency. Hence, in higher modes, contribution for the dynamic response terms becomes insignificant in comparison with

that of the static response. Hence, the response in higher modes can be approximated only from the static response. Now, the modal forces are given as follows:

$$\begin{aligned} f_s &= \{\varphi^{(s)}\}^T f \\ x &= \sum_{r=1}^{\hat{N}} \{\varphi^{(r)}\} q_r(t) + \sum_{S=\hat{N}+1}^{N} \frac{1}{K_S} \{\varphi^{(S)}\}\{\varphi^{(s)}\}^T f \\ &= \sum_{r=1}^{\hat{N}} \{\varphi^{(r)}\} q_r(t) + \sum_{S=\hat{N}+1}^{N} F_S f \end{aligned} \tag{3.106}$$

where F_S represents the contribution of the sth mode toward the flexibility matrix f of the system. It is important to note that the response of higher modes can be approximated by considering the static response only; still it is necessary to compute all the mode shapes in order to compute the contribution of higher modes to the structural flexibility.

$$\sum_{S=\hat{N}+1}^{N} \frac{1}{K_S} \{\varphi^{(S)}\}\{\varphi^{(s)}\}^T = K^{-1} - \sum_{r=1}^{\hat{N}} \frac{1}{K_r} \{\varphi^{(r)}\}\{\varphi^{(r)}\}^T = K^{-1} - \sum_{r=1}^{\hat{N}} F_r \tag{3.107}$$

The above equation shows that the higher mode contribution to the structural flexibility is computed by subtracting the contribution of the lower modes from the total structural flexibility matrix. Hence, the total response is given as follows:

$$x = \sum_{r=1}^{\hat{N}} \{\varphi^{(r)}\} q_r(t) + \left[K^{-1} - \sum_{r=1}^{\hat{N}} F_r \right] f \tag{3.108}$$

The second term in the above equation is called *static correction* to account for the higher mode response. It is also called *missing mass correction*.

3.22 Rayleigh–Ritz Method—Analytical Approach

In the coordinate system, total energy at any instant of time during the vibration remains constant. We know that the total energy is the sum of potential energy (PE) and kinetic energy (KE). When the mass reaches the maximum, the potential energy is maximum and the kinetic energy becomes zero. When mass crosses the

equilibrium position, potential energy becomes zero and the kinetic energy becomes maximum. Considering this, the following equation is valid:

$$\begin{aligned}(\text{PE})\max &= (\text{KE})\max \\ \frac{1}{2}M\int_0^l y^2 \mathrm{d}x\omega^2 &= \frac{1}{2}\int_0^l EI\left(\frac{\mathrm{d}^2 y}{\mathrm{d}x^2}\right)^2 \mathrm{d}x \\ -\omega^2 &= \frac{1/2\int_0^l EI\left(\frac{\mathrm{d}^2 y}{\mathrm{d}x^2}\right)^2 \mathrm{d}x}{\frac{1}{2}M\int_0^l y^2 \mathrm{d}x} = \frac{U}{T}\end{aligned} \tag{3.109}$$

where ω be the frequency and m be the mass/unit volume

Procedure suggested by Rayleigh is as follows:

1. Any shape resembling the fundamental mode shape can be assumed; boundary conditions should be satisfied.
2. By trial and error method, try many functions to get the lowest value of the frequency from Eq. (3.109).
3. Profile or the shape function assumed should correspond to fundamental mode and should satisfy the kinematics boundary condition.

In Ritz method, it is suggested that the shape function y is assumed such that it is linear combination of different function with unknown parameters. For example:

$$\text{let } y = a\varphi_1(x) + b\varphi_2(x) + c\varphi_3(x) + \cdots \tag{3.110}$$

The necessary condition is that Eq. (3.110) must completely satisfy all the BC.

For, (PE)max = (KE)max;

$$\omega^2 = N \tag{3.111}$$

$$\text{that is } N = \frac{U}{T}; \quad \text{where } U = \text{PE};\ T = \text{KE} \tag{3.112}$$

Partially differentiating with respect to a:

$$\frac{\partial N}{\partial a} = \frac{T\left(\partial u/\partial a\right) - u\left(\partial T/\partial a\right)}{T^2} = 0 \tag{3.113}$$

$$T\left(\partial u/\partial a\right) - u\left(\partial T/\partial a\right) = 0 \tag{3.114}$$

$$\partial u/\partial b - \frac{U}{T}\partial T/\partial b = 0 \tag{3.115}$$

$$\partial u/\partial c - \frac{U}{T}\partial T/\partial c = 0 \tag{3.116}$$

$$\partial u/\partial d - \frac{U}{T}\partial T/\partial d = 0 \tag{3.117}$$

The above homogeneous equations lead to eigenvalue problem. Also, we know that $N = \frac{U}{T} = \omega^2$.

Hence, Eq. (3.117) becomes

$$\partial u/\partial d - \omega^2\left(\partial T/\partial d\right) = 0 \tag{3.118}$$

$$504EI - 6\omega^2 m.$$

Example 1

For a cantilever beam with uniformly distributed mass, determine the natural frequency. Take length of the beam as 1 m.

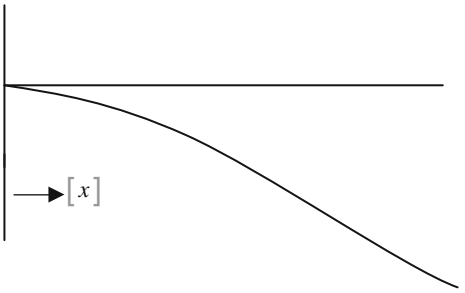

Step 1: *Boundary condition* At $x = 0$; $y = 0$; which is satisfied; At $x = 0$; $\frac{dy}{dx} = 0$; which is also satisfied

$$U = \text{PE} = 1/2\int_0^l EI\left(\frac{d^2y}{dx^2}\right)^2 dx$$

$$\frac{dy}{dx} = 2ax + 3bx^2$$

$$\frac{d^2y}{dx^2} = 2a + 6bx$$

Step 2:

$$U = \text{PE} = {}^1\!/_2 \int_0^l EI(2a + 6bx)^2$$

$$U = \frac{EI}{2} \int 4a^2 l + 12b^2 l^3 + 12abl^2$$

$$\text{For unit length, } U = \frac{EI}{2} \int 4a^2 + 12b^2 + 12ab$$

Step 3:

$$T = \frac{1}{2} m \int_0^l y^2 \mathrm{d}x;$$

$$T = \frac{1}{2} m \int_0^l \left(ax^2 + bx^3\right)^2 \mathrm{d}x;$$

$$T = \frac{1}{2} m \left(\frac{a^2 l^5}{5} + \frac{b^2 l^7}{7} + \frac{2abl^6}{6}\right);$$

$$\text{For unit length, } T = \frac{1}{2} m \left(\frac{a^2}{5} + \frac{b^2}{7} + \frac{2ab}{6}\right)$$

Step 4:

$$\begin{aligned} &\frac{\partial u}{\partial a} - \omega^2 \frac{\partial T}{\partial a} = 0 \\ &\frac{\partial u}{\partial a} = \frac{EI}{2}(8a + 12b) \\ &\frac{\partial T}{\partial a} = \frac{m}{2}\left(\frac{2a}{5} + \frac{b}{3}\right) \\ &\frac{EI}{2}(8a + 12b) - \omega^2 \frac{m}{2}\left(\frac{2a}{5} + \frac{b}{3}\right) = 0 \end{aligned} \tag{3.119}$$

Step 5:

$$\begin{aligned} &\frac{\partial u}{\partial b} = \frac{EI}{2}(24a + 12b) \\ &\frac{\partial T}{\partial a} = \frac{m}{2}\left(\frac{2b}{7} + \frac{a}{3}\right) \\ &\frac{EI}{2}(24a + 12b) - \omega^2 \frac{m}{2}\left(\frac{2b}{7} + \frac{a}{3}\right) = 0 \end{aligned} \tag{3.120}$$

$$
\begin{aligned}
&15EI(8a+12b)-\omega^2 m(6a+5b)=0\\
&21EI(12a+24b)-\omega^2 m(7a+6b)=0\\
&\left(120EI-6\omega^2 m\right)a+\left(180EI-5\omega^2 m\right)b=0\\
&\left(252EI-7\omega^2 m\right)a+\left(504EI-6\omega^2 m\right)b=0\\
&\begin{bmatrix}120EI-6\omega^2 m & 180EI-5\omega^2 m\\ 252EI-7\omega^2 m & 504EI-6\omega^2 m\end{bmatrix}\begin{Bmatrix}a\\ b\end{Bmatrix}=\{0\}
\end{aligned}
\tag{3.121}
$$

It is in the form of $[A]\{X\}=0$. The above equation can be solved to obtain the natural frequency.

Example 2

As a simple supported beam of length L, total mass m also carries a concentrated mass m at the center. Find its ω_n lowest of its transverse vibration.

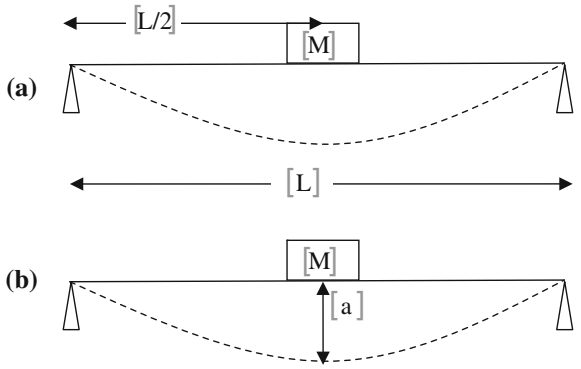

(a) y = vertical deflection due to loads

$$\text{Let } U=\frac{EI}{2}\int_0^l\left(\frac{\mathrm{d}^2y}{\mathrm{d}x^2}\right)^2\mathrm{d}x$$

$$y=a\sin\left(\frac{\pi x}{\ell}\right)$$

Boundary condition

$$\text{at } x=0;\quad y=0;$$
$$\text{at } x=\ell;\quad y=0;$$

at $x=\ell/2$; $y=a$; which is all satisfied.

$$\frac{\mathrm{d}y}{\mathrm{d}x} = \left(\frac{\pi}{\ell}\right) a \cos\left(\frac{\pi x}{\ell}\right)$$

$$\frac{\mathrm{d}y}{\mathrm{d}x} = -\left(\frac{\pi}{\ell}\right)^2 a \sin\left(\frac{\pi x}{\ell}\right)$$

$$U = \frac{EI}{2} \int_0^l \left[\left(\frac{\pi}{\ell}\right)^2 a \sin\left(\frac{\pi x}{\ell}\right)\right]^2 \mathrm{d}x$$

$$= \frac{EI}{2} \int_0^l \left(\frac{\pi^2}{\ell^2}\right)^2 a^2 \sin^2\left(\frac{\pi x}{\ell}\right) \mathrm{d}x$$

$$\text{let} \frac{\pi x}{\ell} = \theta; \quad \cos 2\theta = 1 - 2\sin^2\theta;$$

$$\sin^2\theta = \frac{1}{2}\left[\frac{1-\cos 2\theta}{2}\right] = \frac{1}{2}\left[1 - \cos\left(\frac{2\pi x}{\ell}\right)\right] = \frac{1}{2}\int_0^l \left[1 - \cos\left(\frac{2\pi x}{\ell}\right)\right] \mathrm{d}x$$

$$U = \frac{EI}{2}\left(\frac{\pi^4}{\ell^4}\right) a^2 \frac{1}{2} \int_0^l \left[1 - \cos\left(\frac{2\pi x}{\ell}\right)\right] \mathrm{d}x$$

$$U = \frac{EI}{2}\left(\frac{\pi}{\ell}\right)^4 \ell a^2$$

(a) Kinetic energy due to moment
Deflection at middle = a
Let the displacement $x = a\cos\omega t$; velocity = $-a\omega \sin\omega t$; max velocity = $|-a\omega|$
KE due to concentrated mass $M = \frac{1}{2}MV^2 = \frac{1}{2}M(a^2\omega^2)$

(b) Due to mass of the beam m

$$T = \frac{1}{2}\left(\frac{m}{\ell}\right) \int_0^\ell y^2 \mathrm{d}x = \frac{1}{2}\left(\frac{m}{\ell}\right)\omega^2 \int_0^\ell y^2 \mathrm{d}x$$

$$= \frac{1}{2}\left(\frac{m}{\ell}\right)\omega^2 \left(\frac{a^2}{2}\right) \int_0^\ell 1 - \cos\left(\frac{2\pi x}{\ell}\right) \mathrm{d}x$$

$$T = \frac{m\omega^2 a^2}{4}$$

where m is the total mass of the entire beam.

$$\text{Total KE} = \frac{1}{2}Ma^2\omega^2 + \frac{1}{4}M\left(\omega^2 a^2\right) = \frac{1}{2}\omega^2 a^2\left(M + \frac{M}{2}\right)$$

$$(\text{KE})\max = (\text{PE})\max$$

$$\omega^2 = \frac{EI\left(\ell/2\right)\left(\pi/\ell\right)^4}{\left(M + \frac{M}{4}\right)}$$

Comparison by Dunkerley's Method

(a) Deflects due to central load, M

$$y_{11} = \frac{48EI}{M\ell^3}$$

(b) Deflects due to total load,

$$y_{22} = \frac{48EI}{m\ell^3}$$

$$\left(\frac{1}{\omega^2}\right) = \frac{M\ell^3}{48EI} + \frac{m\ell^3}{\pi^4 EI}$$

$$\omega^2 = \frac{EI\left(\pi/\ell\right)^4 \ell/2}{\left(1.013M + \frac{M}{2}\right)}$$

Exercise

1. All bodies possess _____ and _____ which results in vibration of the body.
2. At equilibrium, whole of elastic energy is converted into _____ and the body continues to move in opposite direction because of it.
3. Whole of the kinetic energy is converted into _____ due to which the body again returns to the equilibrium position.
4. Any motion which repeats itself after an interval of time is called _____.
5. A motion that repeats itself after equal interval of time is called _____.

6. Number of cycles per unit time is called _____.
7. Maximum displacement of a vibrating body from the equilibrium position is called _____.
8. When system vibrates without any external force, it is called _____.
9. Natural frequency is expressed in _____ (units).
10. Minimum number of _____ required to specify the motion of system at any instant is known as _____.
11. Degree of freedom may vary between _____.
12. _____ beam is an example for infinite degrees of freedom.
13. Motion of simple pendulum is an example for _____.
14. Resistance offered to the motion of the vibrating body is called _____.
15. When there is phase difference in the system, the vibrating motion can be expressed as _____ (*Hint*: equation of response).
16. When the frequency of external excitation is equal to natural frequency of the vibrating body, then the system is in _____ and amplitude of vibration becomes extensively _____.
17. Mechanical system consists of _____, _____, and _____.
18. Continuous system is also called _____.
19. In a vibrating system, there is an exchange of energy from _____.
20. Energy is stored by mass in the form _____ and spring in the form of _____.
21. Sketch the basic vibratory system with SDOF.
22. In the vibratory system, if the amount of external excitation is known in magnitude, it is called _____.
23. If system vibrates indefinitely and the amplitude decays because of _____ and vanishes continuously, such kind of vibration is called _____.
24. _____ occurs as a result of interference between two waves of slightly different frequencies moving along the same straight line in the same direction.
25. If springs with stiffness k_1 and k_2 are connected in parallel, their effective stiffness is equal to _____.
26. 'Mass develops an inertia force proportional to its acceleration and opposite in direction.' This is stated by _____.

27. The tension leg platform is heave restrained by _____.
28. Match the design wave height for various regions is tabulated below:

I. Bay of Bengal	(a) 11 m for 1 yr and 24 m for 100 yrs
II. Gulf of Mexico	(b) 6 m for 1 yr and 12 m for 100 yr
III. South China Sea	(c) 5 m for 1 yr and 12 m for 100 yrs
IV. Arabian Sea	(d) 14 m for 1 yr and 22 m for 100 yrs
V. Gulf of Thailand	(e) 12 m for 1 yr and 24 m for 100 yrs
VI. Persian Gulf	(f) 8 m for on 1 yr and 18 m for 100 yrs
VII. North Sea	(g) 8 m for 1 yr and 18 m for 100 yrs

29. Growth of marine algae increases the _____ and _____which in turn increase the wave or current loading.
30. In P-M spectrum fetch and duration are considered _____.
31. Algebraic sum of wave and current loads is different from calculation of load by adding the horizontal water particle velocity with the current velocity and computing the loads. This is because of _____.
32. Seismic loads are arising from derived type _____.

Answers

1. Mass; restoring capacity (elasticity)
2. Kinetic energy
3. Elastic or strain energy
4. Vibration or oscillation
5. Periodic motion
6. Frequency
7. Amplitude
8. Free vibration
9. rad/s or hertz
10. Independent coordinates; degrees of freedom
11. Zero to infinity
12. Cantilever
13. Simple harmonic motion
14. Damping (friction)
15. $x = A \sin(\omega t + \varphi)$
16. Resonance; large

17. Mass, stiffness and damping
18. Distributed systems
19. One form to another (PE to KE or vice versa)
20. Kinetic energy = $1/2\, m\dot{x}^2$; Potential energy = 1/2 kx^2
21. 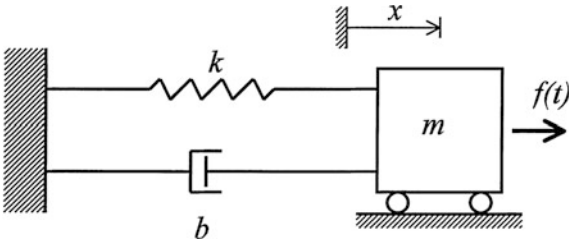

22. Deterministic vibration
23. Damping; transient vibration
24. Beating phenomenon
25. $k_{\text{eff}} = k_1 + k_2$
26. D'Alembert's Principle
27. Vertical tendons or tethers
28. I (f/g); II (e); III (a); IV (f/g); V (b); VI (c); VII (d)
29. Diameter and roughness of members
30. Infinite
31. Nonlinear term in the drag equation
32. Gravity loads

Solved Numerical Examples

33. Determine the natural frequency of the mass m placed at one end of the cantilever beam of negligible mass. (*Hint*: deflection = $Wl^3/3EI$)

    Deflection = $WL^3/3EI$; stiffness = load/deflection; $k = 3EI/L^3$; $\omega = \sqrt{\frac{k}{m}} = \sqrt{\frac{3EI}{L^3 m}}$ rad/s or $\frac{1}{2\pi}\sqrt{\frac{3EI}{L^3 m}}$ Hz
34. Determine the natural frequency of the mass m placed at the middle of the fixed beam of length (L m) negligible mass. (*Hint*: deflection = $Wl^3/192EI$)

    Deflection = $WL^3/3EI$; stiffness = load/deflection; $k = 3EI/L^3$; $\omega = \sqrt{\frac{k}{m}} = \sqrt{\frac{3EI}{L^3 m}}$ rad/s or $\frac{1}{2\pi}\sqrt{\frac{3EI}{L^3 m}}$ Hz

35. List the types of damped system and sketch the responses neatly.

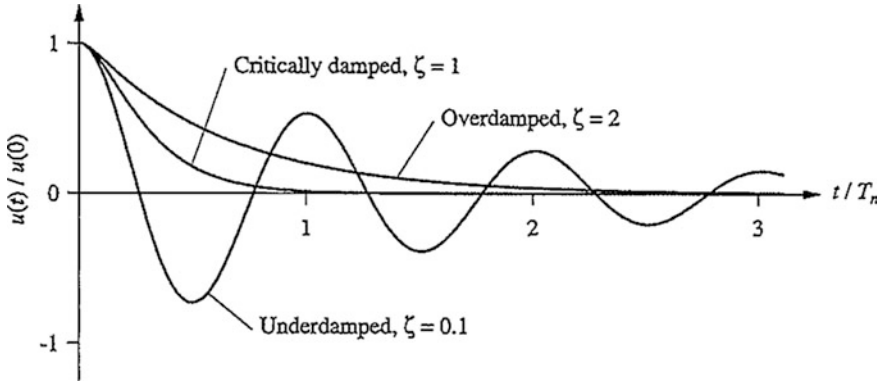

36. Unknown mass m is attached to the one end of the spring of stiffness k having the natural frequency of 12 Hz. When 1 kg mass is attached with the m and the natural frequency of the system is lowered by 25 %, determine the value of unknown mass m and stiffness k.
Let

$$f1 = 12\text{ Hz} = \frac{1}{2\pi}\sqrt{\frac{k}{m}}\text{ Hz}; f2 = 12 \times (75/100) = \frac{1}{2\pi}\sqrt{\frac{k}{m+1}}\text{ Hz};$$

$$f1/f2 = 12/9 = \left(\sqrt{\frac{k}{m}}\right) \Big/ \left(\sqrt{\frac{k}{m+1}}\right) = (1.333)2 = \frac{\frac{k}{m}}{\frac{k}{m+1}} = \frac{m+1}{m};$$

$$m = 1.2857\,\text{kg}$$

$$12 = \frac{1}{2\pi}\sqrt{\frac{k}{m}};\ 12 \times 2\pi = \sqrt{\frac{k}{m}}; 5{,}684.89 = \frac{k}{m};$$

$$k = 7{,}276.6592\,\text{N/m}$$

37. Cylinder of diameter D and mass m floats vertically in a liquid of mass density ρ. It is made to oscillate by giving some initial displacement. Find the period of oscillation. What will be the frequency if salty liquid of specific gravity 1.2 is used?
Let us assume x is the displacement of the cylinder

$$\text{Restoring force} = (\rho A x)g;$$

According to Newton's law, $mx + \ddot{\rho} Axg = 0$

$$\omega_n = \sqrt{\frac{\rho Ag}{m}}; \quad T = \frac{2\pi}{\omega} = \frac{2\pi}{\sqrt{\frac{\rho Ag}{m}}} \text{ s}$$

if salt water ρ = 1.2; $\omega_n = \sqrt{\frac{1.2\rho Ag}{m}}$ rad/s where $A = \frac{\pi}{4} d^2$

38. Find the natural frequency of the system

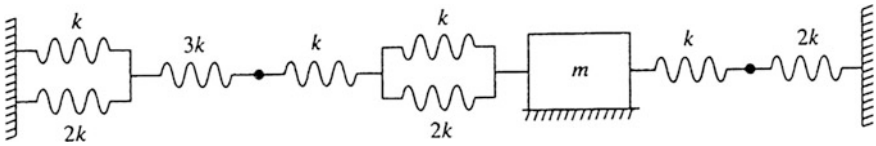

Take m = 20 kg; k = 1,000 N/m

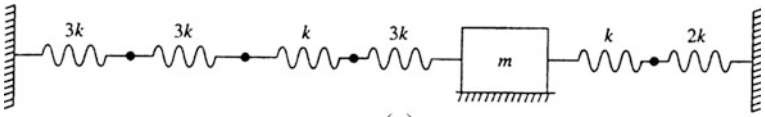

(a)

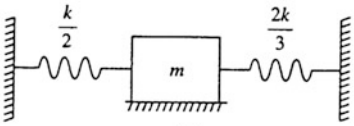

(b)

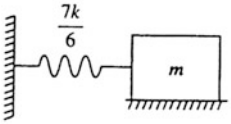

(c)

$$\omega = \sqrt{\frac{k}{m}} = \sqrt{\frac{7 \times 1{,}000}{6 \times 20}} = 7.637 \text{ rad/s}$$

39. Find the natural frequency of the system

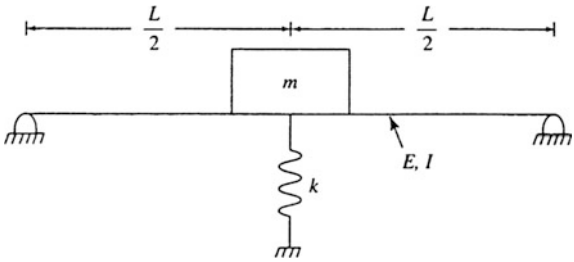

Take $E = 210 \times 10^9$ N/m^2; $I = 1.5 \times 10^{-5}$ m^4; $k = 1{,}500$ N/m; $L = 3$ m
(*Hint*: displacement $x = \frac{PL^3}{48EI}$)
Displacement $x = \frac{PL^3}{48EI}$; Take $E = 210 \times 10^9$ N/m^2; $I = 1.5 \times 10^{-5}$ m^4; $k = 1{,}500$ N/m; $m = 100$ kg

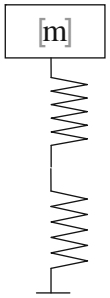

$$k = \frac{48E\,I}{3}$$

$$k = k$$

$$K_{\text{eff}} = \frac{48EI}{L^3} + k$$

$$K_{\text{eff}} = \left(\frac{48 \times 210 \times 10^9 \times 1.5 \times 10^{-5}}{10^3}\right) + 1{,}500 = 152.7 \times 10^3 \text{ N/m};$$

$$\omega = \sqrt{\frac{k}{m}} = \sqrt{\frac{152.7 \times 10^3}{100}} = 39.0768 \text{ rad/s}$$

40. Find the natural frequency of the system

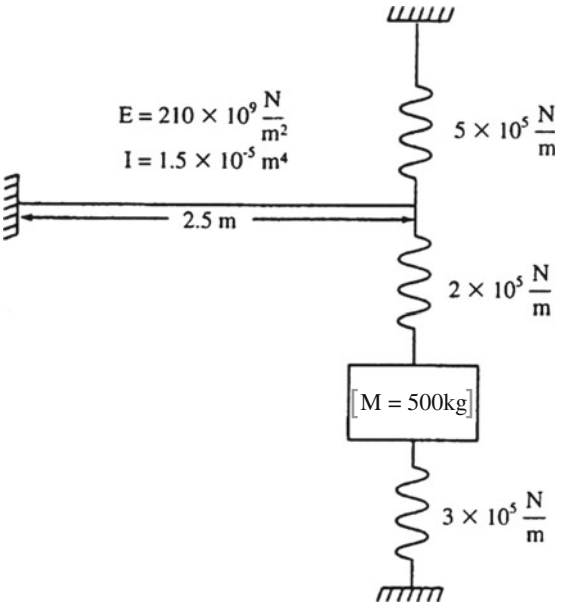

$$k \text{ beam} = \frac{3EI}{L^3} = \frac{3 \times 210 \times 10^9 \times 1.5 \times 10^{-5}}{2.5^3} = 6.05 \times 10^5 \text{ N/m};$$

$$K_{\text{eff}} = \left(\frac{1}{\frac{1}{(6.05 \times 10^5 + 5 \times 10^5)} + \frac{1}{2 \times 10^5}} \right) + 3 \times 10^5 = 4.693 \times 10^5 \text{ N/m};$$

$$\omega = \sqrt{\frac{k}{m}} = \sqrt{\frac{4.693 \times 10^5}{500}} = 30.6366 \text{ rad/s}$$

41. Sketch the simple SDOF mathematical model and explain the components of it.

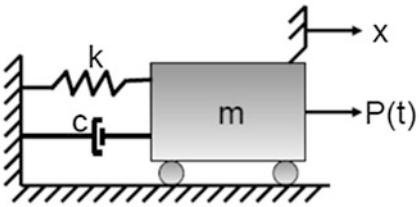

Mass element ,m - representing the mass and inertial characteristic of the structure

Spring element ,k - representing the elastic restoring force and potential energy capacity of the structure.

Dashpot, c - representing the frictional characteristics and energy losses of the structure

Excitation force, P(t) - represents the external force acting on structure.

42. Draw the mathematical model of the system

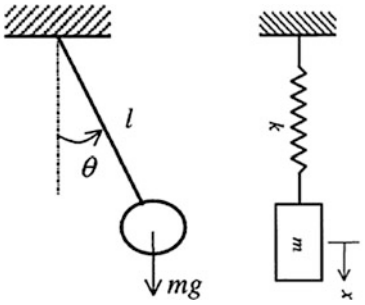

43. Draw the Free body diagram of the system

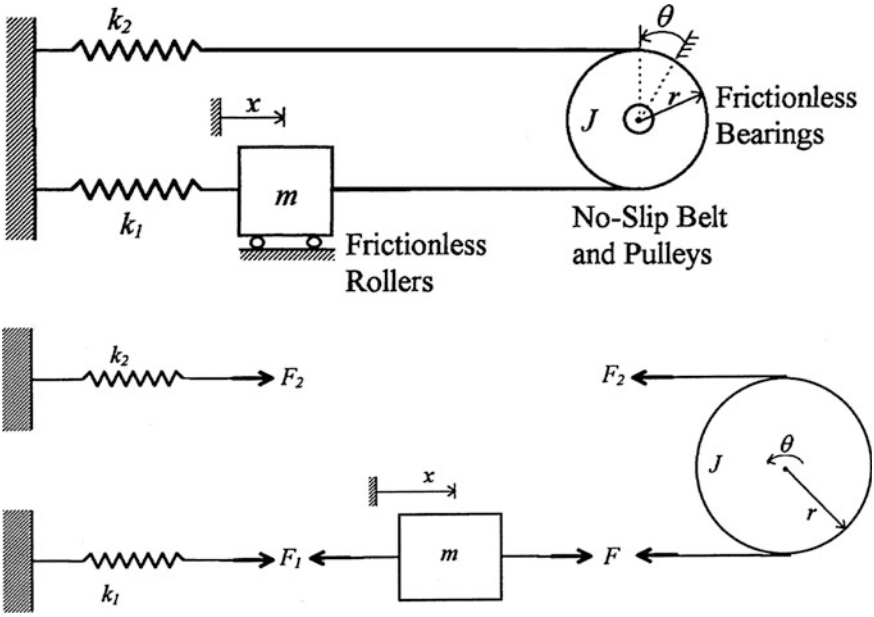

44. Sketch the periodic loading and non-periodic loading

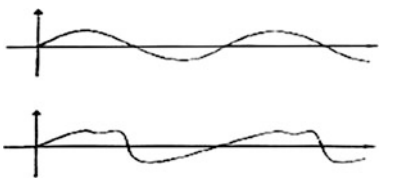

45. Write the equation of motion for the system given below:

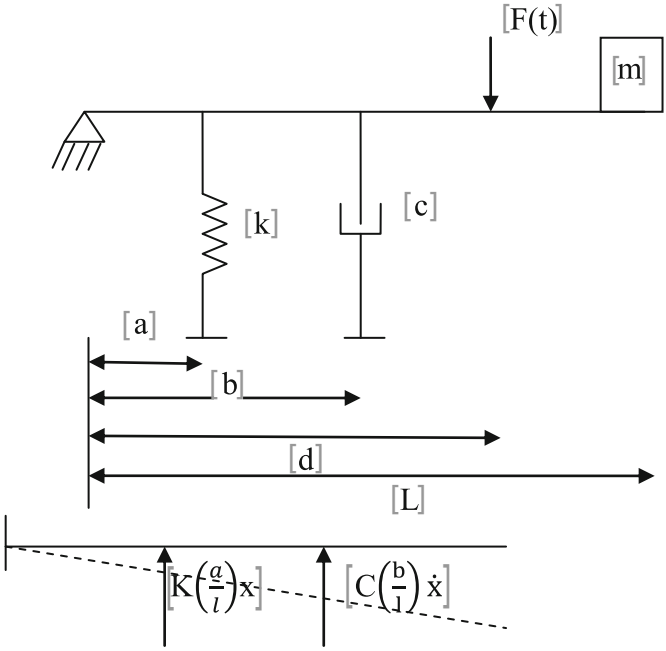

$$m\ddot{x} + c\left(\frac{b}{l}\right)^2 \dot{x} + \left(\frac{a}{l}\right)^2 x = \frac{d}{L}P(t)$$

46. A damper offers resistance 0.05 N at constant velocity 0.04 m/s. The damper is used with stiffness of 9 N/m. Determine the damping ratio and frequency of the system when the mass of the system is 0.10 kg.

Damping force $F = C\dot{x}$

$\dot{x} = 0.04$ m/s,

$F = 0.05$ N

$C = F/\dot{x} = 0.05/0.04 = 1.25$ N s/m

$C_c = 2\sqrt{km} = 2\sqrt{9 \times 0.1} = 1.897$ N s/m

$$\xi = \frac{C}{C_c} = \frac{1.25}{1.897} = 0.658$$

The system is under-damped. The frequency of damped vibration is given as follows:

$$\omega = \sqrt{\frac{k}{m}} = \sqrt{\frac{9}{0.1}} = 9.487\,\text{rad/s}$$
$$\omega_d = \omega\sqrt{1-\xi^2} = 9.487\sqrt{1-0.658^2} = 5.379\,\text{rad/s}$$

47. A vibrating system is defined by the following parameters: M = 3 kg, k = 100 N/m, and C = 3 N s/m. Determine (a) the damping factor, (b) the natural frequency of damped vibration, (c) logarithmic decrement, (d) the ratio of two consecutive amplitudes, and (e) the number of cycles after which the original amplitude is reduced to 20 %.
Critical damping is given as follows:

$$C_c = 2\sqrt{km} = 2\sqrt{100\times 3} = 34.64\,\text{N s/m}$$
$$\xi = \frac{C}{C_c} = \frac{3}{34.64} = 0.086$$
$$\omega = \sqrt{\frac{k}{m}} = \sqrt{\frac{100}{3}} = 5.773\,\text{rad/s}$$
$$\omega_d = \omega\sqrt{1-\xi^2} = 5.773\sqrt{1-0.086^2} = 5.730\,\text{rad/s}$$
$$\delta = \frac{2\pi\xi}{\sqrt{1-\xi^2}} = \frac{2\pi(0.086)}{\sqrt{1-0.086^2}} = 0.5424$$

The ratio of two consecutive amplitudes is given as follows:

$$e^{\delta} = \frac{x_n}{x_{n+1}}$$
$$\frac{x_n}{x_{n+1}} = e^{0.5424} = 1.72$$
$$\delta = \frac{1}{n}\ln\left[\frac{x_n}{x_{n+1}}\right]$$
$$n = 2.96\,\text{cycles}$$

The amplitude of the response will decay by 20 % in about 3 cycles.

48. A mass of 7 kg is kept on two slabs of isolators placed one over the other. One of the isolators is synthetic rubber with stiffness of 5 kN/m and damping coefficient of 100 N s/m; second isolator is fibrous felt of 10 kN/m and damping coefficient of 400 N s/m. If the assembly is vibrated in the vertical direction actuating the series of isolators, determine the damped and un-damped natural frequencies of the system.

Isolators are connected in series, and hence, equivalent stiffness and damping coefficients can be readily determined.

$$\frac{1}{k_e} = \frac{1}{5{,}000} + \frac{1}{10{,}000}$$
$$k_e = 3{,}333.33\,\text{kN/m}$$
$$C_e = \frac{1}{100} + \frac{1}{400} = 80\,\text{N s/m}$$
$$\omega_n = \sqrt{\frac{k_e}{m}} = 21.822\,\text{rad/s}$$
$$\xi = \frac{C_e}{2\sqrt{k_e m}} = \frac{80}{2\sqrt{(3{,}333.33 \times 7)}} = 0.26$$
$$\omega_d = \omega_n\sqrt{1-\xi^2} = 21.822\sqrt{(1-0.26^2)} = 21.07\,\text{rad/s}$$

49. A vibrating system having mass 1 kg is suspended by a spring of stiffness 1,000 N/m, and it is put to harmonic excitation of 10 N. Assuming viscous damping determine the following: (i) resonant frequency; (ii) amplitude at resonance; (iii) frequency corresponding to the peak amplitude; and (iv) damped frequency. Take C = 40 N s/m.

(a) Frequency at resonance

$$\omega = \omega_\text{n} = \sqrt{(k/m)} = \sqrt{(1000/1)} = 31.62\ \text{rad/s}$$

Damping factor ξ is given by:

$$\xi = c/2m\,\omega_n = 40/(2 \times 2 \times 31.62) = 0.632$$

(b) Amplitude at resonance

$$x_\text{resonance} = \frac{F}{C\omega_n} = \frac{10}{40 \times 31.62} = 7.91\,\text{mm}$$

(c) Frequency corresponding to the peak amplitude is given as follows:

$$\omega_\text{peak} = \omega_n\sqrt{1-2\xi^2} = 31.628 \times \sqrt{1-(2 \times 0.632^2)} = 14.185\,\text{rad/s}$$

(d) Damped frequency is given as follows:

$$\omega_d = \sqrt{(1-\xi^2)}\omega_n = 31.62 \times \sqrt{(1-0.632^2)}$$
$$= 24.5\,\text{rad/s}$$

50. A body of mass 70 kg is suspended from a spring which deflects 2 cm under the load. It is subjected to damping whose value is tuned to be 0.23 times of the value that required for critical damping. Find the natural frequency of the un-damped and damped vibrations and ratio of successive amplitudes for damped vibrations. If the body is subjected to a periodic disturbing force of 700 N and of frequency equal to 0.78 the natural un-damped frequency, find the amplitude of forced vibrations and the phase difference with respect to the disturbing force.

Spring stiffness k = force/deflection $= (70 \times 9.81)/(2 \times 10^{-2}) = 34,335$ N/m

$$\xi = C/C_c = 0.23$$

Un-damped natural frequency is given as follows:

$$\omega_n = \sqrt{\frac{k}{m}} = \sqrt{\frac{(34.335 \times 10^3)}{70}} = 22.15 \text{ rad/s}$$

Damped natural frequency is given as follows:

$$\begin{aligned}\omega_d &= \sqrt{(1-\xi^2)}\omega_n \\ &= 22.15 \times \sqrt{(1-0.23^2)} = 21.57 \text{ rad/s}\end{aligned}$$

Logarithmic decrement is given as follows:

$$\begin{aligned}\delta &= 2\pi\xi/\sqrt{(1-\xi^2)} \\ &= 2\pi \times 0.23/\sqrt{(1-0.23^2)} = 1.48\end{aligned}$$

Ratio of successive amplitudes is given as follows:

$$\frac{A_1}{A_2} = e^{\delta} = e^{1.48} = 4.39$$

The relation is valid. Hence,

$$A/(F/k) = \frac{1}{\sqrt{(1-\beta^2)^2 + (2 \times \xi \times \beta)^2}}$$

Given that F = 700 N, k = 34.335 × 10^3 N/m, β = 0.78

$$A = \frac{\frac{700}{34,335}}{\sqrt{(1-0.78^2)^2 + (2 \times 0.23 \times 0.78)^2}} = 0.038 \text{ m}$$

Phase difference is given by:

$$\tan\theta = \frac{2 \times \xi \times \beta}{1 - \beta^2} = \frac{2 \times 0.23 \times 0.78}{1 - 0.78^2} = 0.916$$

$$\theta = 42^0 29'$$

51. Determine the effect of mass suspended on the spring–mass system shown below:

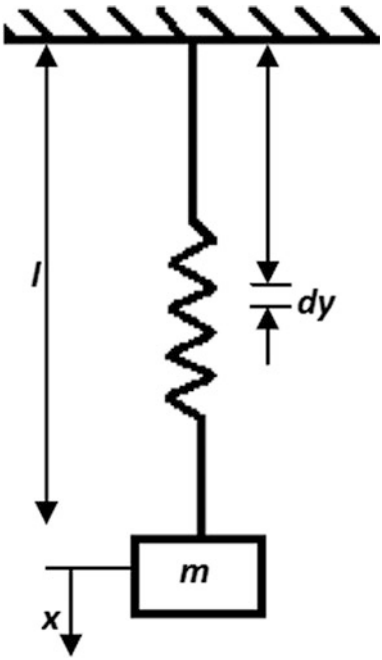

Let x and $\dot{x}$ be the displacement and velocity of mass. Velocity of spring element at a distance y from the fixed end may be written as $\frac{\dot{x}y}{l}$ where ℓ is the total length of spring. Kinetic energy of spring element dy is given as follows:

$$\frac{1}{2}(\rho \mathrm{d}y)\left(\frac{\dot{x}y}{l}\right)^2$$

where ρ is the mass of spring per unit length. Total kinetic energy of the system is then given as follows:

$$\text{KE} = \frac{1}{2}m\dot{x}^2 + \int_0^l \frac{1}{2}(\rho \mathrm{d}y)\left(\frac{\dot{x}y}{l}\right)^2$$
$$= \frac{1}{2}m\dot{x}^2 + \frac{1}{2}\rho\dot{x}^2\frac{l}{3} = \frac{1}{2}m\dot{x}^2 + \frac{1}{6}m_s\dot{x}^2$$

where mass of spring is $m_s = \rho$l
Potential energy of the system = $\frac{1}{2}kx^2$
Total energy of the system = K.E + P.E

$$\frac{1}{2}m\dot{x}^2 + \frac{1}{2}m_s\frac{\dot{x}^2}{3} + \frac{1}{2}kx^2 = \text{constant}$$

Differentiating the above equation w.r.t. time

$$m\ddot{x} + \frac{m_s\ddot{x}}{3} + kx = 0$$

$$\left(m + \frac{m_s}{3}\right)\ddot{x} + kx = 0$$

$$\omega_n = \sqrt{\frac{k}{m + \frac{m_s}{3}}}\ \text{rad/s}$$

52. Circular cylinder of mass 4 kg and radius 15 cm is connected to a spring of stiffness 4,000 N/m as shown in the below figure. It is free to roll on horizontal rough surface without slipping. Determine the natural frequency.

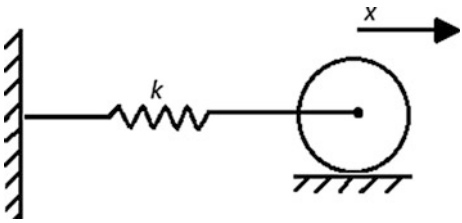

Total energy of the system

$$\begin{aligned}
\mathrm{T} &= \text{K.E. due to translator motion} + \text{K.E. due to rotary motion} + \text{P.E. of spring} \\
&= \frac{1}{2}m\dot{x}^2 + \frac{1}{2}I\dot{\theta}^2 + \frac{1}{2}kx^2 \\
&= \frac{1}{2}mr^2\dot{\theta}^2 + \frac{1}{2}\cdot\frac{1}{2}mr^2\dot{\theta}^2 + \frac{1}{2}kr^2\theta^2 (\text{since } x = r\theta) \\
\mathrm{T} &= \frac{3}{4}m^2r^2\dot{\theta}^2 + \frac{1}{2}kr^2\theta^2 = \text{constant}
\end{aligned}$$

Differentiating with respect to time, we get the following:

$$0 = \frac{3}{4}\cdot 2mr^2\dot{\theta}\ddot{\theta} + kr^2\dot{\theta}\theta = 0$$

$$\frac{3}{2}mr^2\ddot{\theta} + kr^2\theta = 0$$

$$\omega_n = \sqrt{\frac{kr^2}{(3/2)mr^2}} = \sqrt{\frac{2k}{3m}}\,\text{rad/s}$$

53. In a two-degrees-of-freedom system shown in the below figure, let $m_1 = m_2 = m$ and $k_1 = k_2 = k$. Determine both the natural frequencies of vibration and their amplitude ratios.

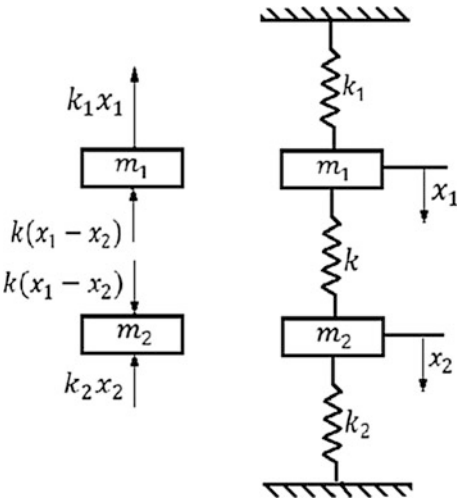

Equations of motion of the system can be written using Newton's law
From the free body diagrams shown above, following equations can be written as follows:

$$m_1\ddot{x}_1 = -k_1x_1 - k(x_1 - x_2)$$
$$m_2\ddot{x}_2 = k_1(x_1 - x_2) - k_2x_2$$

Rearranging in matrix form,

$$\begin{bmatrix} m_1 & 0 \\ 0 & m_2 \end{bmatrix} \begin{Bmatrix} \ddot{x}_1 \\ \ddot{x}_2 \end{Bmatrix} + \begin{bmatrix} k_1 + k & -k \\ -k & k + k_2 \end{bmatrix} \begin{Bmatrix} x_1 \\ x_2 \end{Bmatrix} = \begin{Bmatrix} 0 \\ 0 \end{Bmatrix}$$

Solving the above equation using the classical eigensolver and substituting $m_1 = m_2 = m$ and $k_1 = k_2 = k$, we get the following:

$$\omega^2 = \frac{1}{2}\left[\frac{4k}{m} \pm \sqrt{0 + \frac{4k^2}{m^2}}\right] = \frac{3k}{m}, \frac{k}{m}$$

Therefore, the natural frequencies are

$$\omega_{1,2} = \sqrt{\frac{3k}{m}}, \sqrt{\frac{k}{m}}$$

For the first principle mode of vibration, for $\omega = \sqrt{\frac{3k}{m}}$, we get

$$\left(\frac{X_1}{X_2}\right)_1 = \frac{1}{k}\left[k + k - m\left(\frac{3k}{m}\right)\right] = -1$$

Also, for the second mode of vibration $\omega = \sqrt{\frac{k}{m}}$, we get

$$\left(\frac{X_1}{X_2}\right)_1 = \frac{1}{k}\left[k + k - m\left(\frac{k}{m}\right)\right] = +1$$

Thus, the two amplitude ratios are +1 and −1.

54. For the system shown in the below figure, find out the natural frequencies of vibration and principal modes of vibration.

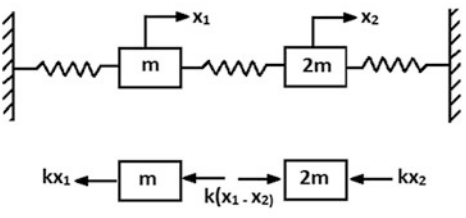

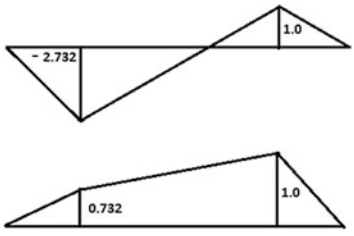

Let the displacement of the two masses be x_1 and x_2 from mean equilibrium positions. Assuming $x_1 > x_2$, for the free body diagrams shown, the differential equations of motion as obtained by applying Newton's law are given as follows:

$$m\ddot{x}_1 = -k(x_1 - x_2) - kx_1$$
$$2m\ddot{x}_2 = k(x_1 - x_2) - kx_2$$

Let the assumed solutions be $x_1 = A\sin\omega t$ and $x_2 = B\sin\omega t$
Substituting for x_1 and x_2 and their derivatives in the differential equations of motion, we have

$$\left(2k - m\omega^2\right)A - kB = 0$$
$$-kA + \left(2k - 2m\omega^2\right)B = 0$$

The amplitude ratios from above two equations are as follows:

$$\frac{A}{B} = \frac{k}{2k - m\omega^2} = \frac{2k - 2m\omega^2}{k}$$

or

$$\left(2k - 2m\omega^2\right)\left(2k - m\omega^2\right) = k^2$$

Simplifying further, the quadratic equation in ω^2 is as follows:

$$\omega^4 - \left(\frac{3k}{m}\right)\omega^2 + \left(\frac{3k^2}{2m^2}\right) = 0$$

The roots of quadratic equation are as follows:

$$\omega^2 = \left(\frac{3 \pm \sqrt{3}}{2}\right)\frac{k}{m}$$

Therefore, $\omega_1^2 = 2.366k/m$ and $\omega_2^2 = 0.634k/m$
So

$$\omega_1 = \sqrt{2.366k/m} \quad \text{and} \quad \omega_2 = \sqrt{0.634k/m}$$

To obtain the first principal mode of vibration, substitute $\omega^2 = 2.366\,k/m$ in the expression for amplitude ratio. We get the following:

$$\left(\frac{A}{B}\right)_1 = \frac{2k - (2m)(2.366)(k/m)}{k} = \frac{2k - 4.732k}{k} = -2.732$$

The second principal mode of vibration is obtained by substituting $\omega^2 = 0.634k/m$

$$\left(\frac{A}{B}\right)_2 = \frac{2k - (2m)(0.634)(k/m)}{k} = \frac{0.732k}{k} = 0.732$$

Mode shapes are shown in the figure.

55. One type of seismograph, a device that records earthquakes, can be modeled as shown in the below figure. Determine (a) the differential equations of motion, and (b) the frequency equation and the natural frequencies.

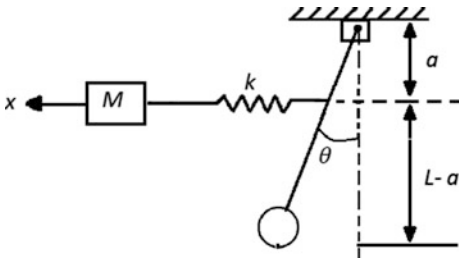

The figure shows the model of the seismograph in displaced position. Let the displacement of the mass M be x and that of the oscillating pendulum be θ from static equilibrium position. Let us assume θ to be small. Applying Newton's law to the free body diagram of the mass, we have

$$M\ddot{x} = -k(x - a\theta)$$

Similarly, applying Newton's law to free body diagram of the pendulum by taking moments of inertia about the pivot O, we get the following:

$$I_0\ddot{\theta} = -mgL\theta + ka(x - a\theta)$$

Neglecting the mass moment of inertia of the bob about its own center of gravity, we get

$$I = mL^2$$

For obtaining solutions to the differential equations of motion, let us assume that

$$x = A\sin\omega t \text{ and } \theta = \mathrm{B}\sin\omega t$$
$$(k - M\omega^2)A - kaB = 0$$
$$-kaA + (mgL + ka^2 - I_0\omega^2)B = 0$$

Amplitude ratios are given as follows:

$$\frac{A}{B} = \frac{ka}{k - M\omega^2} = \frac{mgL + ka^2 - mL^2\omega^2}{ka}$$

This leads to the quadratic equation in ω^2 as given below:

$$(\omega^2)^2 - \left[\frac{k}{M} + \frac{mgL + ka^2}{mL^2}\right]\omega^2 + \frac{kg}{ML} = 0$$

$$\omega_{1,2}^2 = \frac{1}{2}\left[\frac{k}{M} + \frac{mgL + ka^2}{mL^2}\right] \pm \frac{1}{2}\sqrt{\left[\frac{k}{M} + \frac{mgL + ka^2}{mL^2}\right]^2 - 4\frac{kg}{ML}}$$

56. Find the flexibility influence coefficients of the system shown below:

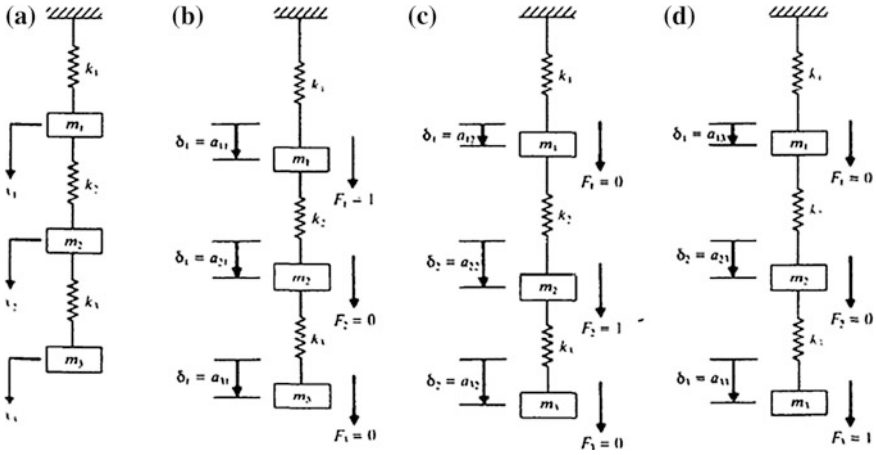

Let $x_1, x_2, \ldots$ and x_n denote the displacements of the masses $m_1, m_2, \ldots$ and m_n, respectively. The flexibility influence coefficients of the system can be determined in terms of the spring stiffness k_1, k_2, and k_n, as follows. If we apply a unit force at mass m_1, and no force at the other masses ($F1 = 1$, $F2 = 0$, $F3 = 0$), as shown in Figure (b), the deflection of the mass, m_1, is equal to δ_1, = 1/k_1, = a_{11}. Since the other two masses m_2, and m_3 move undergo rigid body translation by the same amount of deflection δ_1, we have, by definition:

$$a_{21} = a_{31} = \delta 1 = \frac{1}{k_1}$$

Next, we apply a unit force at mass m_2 and no force at masses m_1 and m_3. As shown in Figure (c), since the two springs k_1 and k_2 offer resistance, the deflection of mass is given as follows:

$$\delta_2 = \frac{1}{k_{eq}} = \frac{1}{k_1} + \frac{1}{k_2} = \frac{k_1 + k_2}{k_1 k_2} = a_{22}$$

The mass m_3 undergoes the same displacement δ_2 (rigid body translation), while the mass m_1 moves through a smaller distance given by $\delta_1 = 1/k_1$. Hence

$$a_{32} = \delta_2 = \frac{k_1 + k_2}{k_1 k_2} \quad \text{and} \quad a_{12} = \delta_1 = \frac{1}{k_1}$$

Finally, when we apply a unit force to mass m_3 and no force to masses m_1 and m_2, as shown in Figure (d), the displacement of mass m_3 is given as follows:

$$\delta_3 = \frac{1}{k_1} + \frac{1}{k_2} + \frac{1}{k_3} = \frac{k_1 + k_2 + k_3}{k_1 k_2 k_3} = a_{33}$$

While the displacements of masses m_2 and m_1 are given by

$$\delta_2 = \frac{1}{k_1} + \frac{1}{k_2} = \frac{k_1 + k_2}{k_1 k_2} = a_{23}$$

and

$$a_{13} = \delta_1 = \frac{1}{k_1}$$

According to Maxwell's reciprocity theorem, we have

$$a_{ij} = a_{ji}$$

Thus, the flexibility matrix of the system is given as follows:

$$[a] = \begin{bmatrix} \frac{1}{k_1} & \frac{1}{k_1} & \frac{1}{k_1} \\ \frac{1}{k_1} & (\frac{1}{k_1} + \frac{1}{k_2}) & (\frac{1}{k_1} + \frac{1}{2}) \\ \frac{1}{k_1} & (\frac{1}{k_1} + \frac{1}{k_2}) & (\frac{1}{k_1} + \frac{1}{k_2} + \frac{1}{k_3}) \end{bmatrix}$$

The stiffness matrix of the system can be found from the relation $[k] = [a] - 1$ or can be derived by using the definition of k_{ij}.

$$[k] = \begin{bmatrix} (k_1 + k_2) & -k_2 & 0 \\ -k_2 & (k_2 + k_3) & -k_3 \\ 0 & -k_3 & k_3 \end{bmatrix}$$

57. Determine the natural frequency coefficient of the spring–mass system shown below by Dunkerley's method?

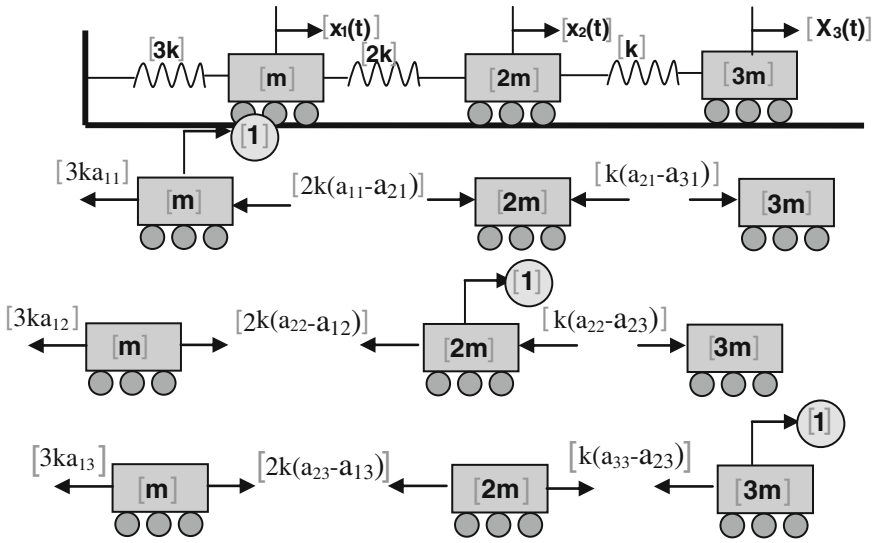

$$a_{11} = a_{12} = a_{13} = 1/3k$$
$$a_{21} = a_{31} = 1/3k$$
$$a_{22} = 1/3k + 1/2k = 5/6k$$
$$a_{22} = a_{32} = a_{23}$$
$$a_{33} = 1/3k + 1/2k + 1/k = 11/6k$$

Influence coefficient matrix is given as follows:

$$\begin{bmatrix} a_{11} & a_{12} & a_{13} \\ a_{21} & a_{22} & a_{23} \\ a_{31} & a_{32} & a_{33} \end{bmatrix}$$

as compared with the Dunkerley's matrix $1/m \begin{bmatrix} 1/\omega_1^2 & \dots & \dots \\ \dots & 1/\omega_2^2 & \dots \\ \dots & \dots & 1/\omega_3^2 \end{bmatrix}$

Dunkerley's frequency is given as follows:

$$1/\omega^2 = 1/\omega_1^2 + 1/\omega_2^2 + 1/\omega_3^2$$

On substituting, we get the following:

$$1/\omega^2 = 3m/k$$
$$\omega = 0.333\sqrt{k/m}$$

58. Determine the natural frequencies and modes shapes of the system shown in the above figure by matrix iteration method? The influence coefficients are given below:

$$a_{11} = a_{12} = a_{13} = a_{21} = a_{31} = \frac{1}{2k}$$
$$a_{22} = a_{23} = a_{32} = \frac{3}{2k}$$
$$a_{33} = \frac{5}{2k}$$

The equations for the above system in terms of influence coefficients can be written as follows:

$$x_1 = 2ma_{11}x_1\omega^2 + 2ma_{12}x_2\omega^2 + 2ma_{13}x_3\omega^2$$
$$x_2 = 2ma_{21}x_1\omega^2 + 2ma_{22}x_2\omega^2 + 2ma_{23}x_3\omega^2$$
$$x_3 = 2ma_{31}x_1\omega^2 + 2ma_{32}x_2\omega^2 + 2ma_{33}x_3\omega^2$$

The equation can be written in matrix form as

$$\begin{Bmatrix} x_1 \\ x_2 \\ x_3 \end{Bmatrix} = m\omega^2 \begin{bmatrix} 2a_{11} & 2a_{12} & 2a_{13} \\ 2a_{21} & 2a_{22} & 2a_{23} \\ 2a_{31} & 2a_{32} & 2a_{33} \end{bmatrix} \begin{Bmatrix} x_1 \\ x_2 \\ x_3 \end{Bmatrix}$$
$$= m\omega^2 \begin{bmatrix} \frac{1}{k} & \frac{1}{k} & \frac{1}{2k} \\ \frac{1}{k} & \frac{3}{k} & \frac{3}{2k} \\ \frac{1}{k} & \frac{3}{k} & \frac{5}{2k} \end{bmatrix} \begin{Bmatrix} x_1 \\ x_2 \\ x_3 \end{Bmatrix}$$
$$\begin{Bmatrix} x_1 \\ x_2 \\ x_3 \end{Bmatrix} = \frac{m\omega^2}{k} \begin{bmatrix} 1 & 1 & 1/2 \\ 1 & 3 & 3/2 \\ 1 & 3 & 5/2 \end{bmatrix} \begin{Bmatrix} x_1 \\ x_2 \\ x_3 \end{Bmatrix}$$

First iteration

Let us assume $\begin{Bmatrix} x_1 \\ x_2 \\ x_3 \end{Bmatrix} = \begin{Bmatrix} 1 \\ 1 \\ 1 \end{Bmatrix}$

$$\begin{Bmatrix} 1 \\ 1 \\ 1 \end{Bmatrix} = \frac{m\omega^2}{k} \begin{bmatrix} 1 & 1 & 1/2 \\ 1 & 3 & 3/2 \\ 1 & 3 & 5/2 \end{bmatrix} = 2.5 \frac{m\omega^2}{k} \begin{Bmatrix} 1 \\ 2.2 \\ 2.6 \end{Bmatrix}$$

Second iteration

$$\begin{Bmatrix} 1 \\ 2.2 \\ 2.6 \end{Bmatrix} = \frac{m\omega^2}{k} \begin{bmatrix} 1 & 1 & 1/2 \\ 1 & 3 & 3/2 \\ 1 & 3 & 5/2 \end{bmatrix} \begin{Bmatrix} 1 \\ 2.2 \\ 2.6 \end{Bmatrix} = 4.5 \frac{m\omega^2}{k} \begin{Bmatrix} 1 \\ 2.555 \\ 3.133 \end{Bmatrix}$$

Third iteration

$$\begin{Bmatrix} 1 \\ 2.555 \\ 3.133 \end{Bmatrix} = \frac{m\omega^2}{k} \begin{bmatrix} 1 & 1 & 1/2 \\ 1 & 3 & 3/2 \\ 1 & 3 & 5/2 \end{bmatrix} \begin{Bmatrix} 1 \\ 2.555 \\ 3.133 \end{Bmatrix} = 5.12 \frac{m\omega^2}{k} \begin{Bmatrix} 1 \\ 2.61 \\ 3.22 \end{Bmatrix}$$

Fourth iteration

$$\begin{Bmatrix} 1 \\ 2.61 \\ 3.22 \end{Bmatrix} = \frac{m\omega^2}{k} \begin{bmatrix} 1 & 1 & 1/2 \\ 1 & 3 & 3/2 \\ 1 & 3 & 5/2 \end{bmatrix} \begin{Bmatrix} 1 \\ 2.61 \\ 3.22 \end{Bmatrix} = 5.22 \frac{m\omega^2}{k} \begin{Bmatrix} 1 \\ 2.61 \\ 3.23 \end{Bmatrix}$$

So

$$1 = 5.22 \frac{m\omega^2}{k}, \quad \omega^2 = \frac{1}{5.22} \frac{k}{m}$$

Thus $\omega_1 = 0.437 \sqrt{\frac{k}{m}}$.

To find the second principle mode, the orthogonality relation is used as

$$\begin{Bmatrix} x_1 \\ x_2 \\ x_3 \end{Bmatrix} = \frac{m\omega^2}{k} \begin{bmatrix} 1 & 1 & 1/2 \\ 1 & 3 & 3/2 \\ 1 & 3 & 5/2 \end{bmatrix} \begin{bmatrix} 0 & \frac{-m_2}{m_1}\left(\frac{x_2}{x_1}\right) & \frac{-m_3}{m_1}\left(\frac{x_3}{x_1}\right) \\ 0 & 1 & 0 \\ 0 & 0 & 1 \end{bmatrix} \begin{Bmatrix} x_1 \\ x_2 \\ x_3 \end{Bmatrix}$$

$$= \frac{m\omega^2}{k} \begin{bmatrix} 1 & 1 & 1/2 \\ 1 & 3 & 3/2 \\ 1 & 3 & 5/2 \end{bmatrix} \begin{bmatrix} 0 & -\left(\frac{2.61}{1}\right) & -\frac{1}{2}(3.23) \\ 0 & 1 & 0 \\ 0 & 0 & 1 \end{bmatrix} \begin{Bmatrix} x_1 \\ x_2 \\ x_3 \end{Bmatrix}$$

$$= \frac{m\omega^2}{k} \begin{bmatrix} 0 & -1.61 & -1.11 \\ 0 & 0.39 & -0.11 \\ 0 & 0.39 & 1.89 \end{bmatrix} \begin{Bmatrix} x_1 \\ x_2 \\ x_3 \end{Bmatrix}$$

First iteration

Let us say $\begin{Bmatrix} x_1 \\ x_2 \\ x_3 \end{Bmatrix} = \begin{Bmatrix} 1 \\ 0 \\ -1 \end{Bmatrix}$

$$\begin{Bmatrix} 1 \\ 0 \\ -1 \end{Bmatrix} = \frac{m\omega^2}{k} \begin{bmatrix} 0 & -1.61 & -1.11 \\ 0 & 0.39 & -0.11 \\ 0 & 0.39 & 1.89 \end{bmatrix} \begin{Bmatrix} 1 \\ 0 \\ -1 \end{Bmatrix} = 0.11 \frac{m\omega^2}{k} \begin{Bmatrix} 10.9 \\ 1 \\ -17.18 \end{Bmatrix}$$

Second iteration

$$\begin{Bmatrix} 10.9 \\ 1 \\ -17.18 \end{Bmatrix} = \frac{m\omega^2}{k} \begin{bmatrix} 0 & -1.61 & -1.11 \\ 0 & 0.39 & -0.11 \\ 0 & 0.39 & 1.89 \end{bmatrix} \begin{Bmatrix} 10.9 \\ 1 \\ -17.18 \end{Bmatrix} = 2.28 \frac{m\omega^2}{k} \begin{Bmatrix} 7.65 \\ 1 \\ -14 \end{Bmatrix}$$

Third iteration

$$\begin{Bmatrix} 7.65 \\ 1 \\ -14 \end{Bmatrix} = \frac{m\omega^2}{k} \begin{bmatrix} 0 & -1.61 & -1.11 \\ 0 & 0.39 & -0.11 \\ 0 & 0.39 & 1.89 \end{bmatrix} \begin{Bmatrix} 7.65 \\ 1 \\ -14 \end{Bmatrix} = 1.93 \frac{m\omega^2}{k} \begin{Bmatrix} 7.2 \\ 1 \\ -13.5 \end{Bmatrix}$$

Fourth iteration

$$\begin{Bmatrix} 7.2 \\ 1 \\ -13.5 \end{Bmatrix} = \frac{m\omega^2}{k} \begin{bmatrix} 0 & -1.61 & -1.11 \\ 0 & 0.39 & -0.11 \\ 0 & 0.39 & 1.89 \end{bmatrix} \begin{Bmatrix} 7.2 \\ 1 \\ -13.5 \end{Bmatrix} = 1.875 \frac{m\omega^2}{k} \begin{Bmatrix} 7.13 \\ 1 \\ -13.4 \end{Bmatrix}$$

Fifth iteration

$$\begin{Bmatrix} 7.13 \\ 1 \\ -13.4 \end{Bmatrix} = \frac{m\omega^2}{k} \begin{bmatrix} 0 & -1.61 & -1.11 \\ 0 & 0.39 & -0.11 \\ 0 & 0.39 & 1.89 \end{bmatrix} \begin{Bmatrix} 7.13 \\ 1 \\ -13.4 \end{Bmatrix} = 1.864 \frac{m\omega^2}{k} \begin{Bmatrix} 7.11 \\ 1 \\ -13.37 \end{Bmatrix}$$

So

$$1 = 1.864\frac{m\omega^2}{k}$$
$$\omega_2 = 0.73\sqrt{k/m}\,\text{rad/s}$$

Similarly using orthogonality relation, we can find ω_3 which is found to be $\omega_3 = 1.41\sqrt{k/m}$

59. Determine fundamental frequency of the system using Stodola's method.

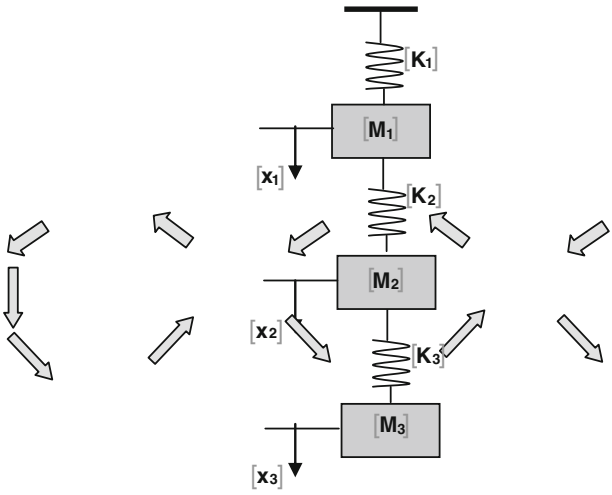

Force is necessary to cause deflection in the elastic system. In case of free vibration, only imaginary force responsible for causing deflection is the inertia force. Let Mr be the mass and Δr be the maximum deflection of the mass. ω be the vibrating frequency. Maximum inertia force is $m\ddot{x} = mr\omega 2\Delta r$

Let us assume that $m_1 = m_2 = m_3 = m$ and $k_1 = k_2 = k_3 = k$.

Description	k_1	m_1	k_2	m_2	k_3	m_3
Assumed deflection		1		1		1
Inertia force		$m_1\omega^2(1)$		$m_2\omega^2(1)$		$m_3\omega^2(1)$
Spring force	$3m\omega^2$		$2m\omega^2$		$m\omega^2$	
Spring deflection	$3m\omega^2/k_1 = 3m\omega^2/k$		$2m\omega^2/k_2 = 2m\omega^2/k$		$m\omega^2/k_3 = m\omega^2/k$	
Calculated deflection (m ω^2/k)		3		5		6
		1		1.67		2
Assumed deflection		1		1.67		2
Inertia force		$m\omega^2$		$1.67m\omega^2$		$2m\omega^2$
Spring force	$4.67m\omega^2$		$3.67m\omega^2$		$2m\omega^2$	
Spring deflection	$4.67m\omega^2/k$		$3.67m\omega^2/k$		$2m\omega^2/k$	
Calculated deflection ($m\omega^2/k$)		4.67		8.34		10.34
		1		1.79		2.21
Assumed deflection		1		1.79		2.21
Inertia force		$m\omega^2$		$1.79m\omega^2$		$2.21m\omega^2$
Spring force	$5m\omega^2$		$4m\omega^2$		$2.21m\omega^2$	
Spring deflection	$5m\omega^2/k$		$4m\omega^2/k$		$2.21m\omega^2/k$	
Calculated deflection ($m\omega^2/k$)		5		9		11.21
Converged values		1		1.80		2.24

$(1.0 + 1.8 + 2.24) = (5 + 9+11.21)m\omega^2/k$. Therefore, fundamental frequency is given as follows:

$$\omega = \sqrt{\frac{k}{m}}\sqrt{\frac{(1+1.8+2.24)}{(5+9+11.21)}} = 0.447\sqrt{\frac{k}{m}}\text{rad/s}.$$

Corresponding mode shape is given by the following vector: $\begin{Bmatrix} 1 \\ 1.8 \\ 2.24 \end{Bmatrix}$

60. For coulomb damping system with mass m = 200 kg, k = 1,500 N/m, and μk = 0.1 and calculate the decay per cycle. Take g = 9.81 m/s^2.
The decay per cycle is $4\frac{f_d}{k} = \frac{4\mu_k mg}{k} = \frac{4\times 0.1\times 200\times 9.81}{1{,}500} = 0.5232$ m.

61. Consider the harmonic oscillator described by $m\ddot{x} + \omega_n^2 x = 0$. Let m = 20 kg and k = 1,800 N/m and calculate the response $x(t)$ for initial condition $x_0 = x(0) = 0.1$ m, $\dot{v}_0 = \dot{x}(0) = 0.2$ m/s.

    The natural frequency of the oscillator is $\omega_{\mathrm{n}} = \sqrt{\frac{k}{m}} = \sqrt{\frac{1{,}800}{20}} = 9.487\,\mathrm{rad/s}$

    Amplitude is $\sqrt{x_0^2 + \left(\frac{v_o}{\omega_n}\right)^2} = \sqrt{0.1^2 + \left(\frac{0.2}{9.487}\right)^2} = 0.1022\,\mathrm{m}$

    The phase angle is $\varphi = \tan^{-1}\left(\frac{v_o}{x_o\omega_n}\right) = \tan^{-1}\left(\frac{0.2}{0.1\times 9.487}\right) = 11.9045\,\mathrm{rad}$

    $x(t) = \mathrm{A}\cos(\omega t - \varphi) = 0.1022\cos(9.487t - 11.9045)\mathrm{m}$

62. It was observed that vibration amplitude of a damped SDOF system has fallen by 50 % after five complete cycles. Assume that the system is viscous damped and calculate the damping factor ζ. Let the no of cycles be 5 nos.

$$M = 5;\ \delta = \frac{1}{m}\ln\left(\frac{x_n}{x_{m+n}}\right) = \frac{1}{5}\ln\left(\frac{x_n}{0.5x_n}\right) = 0.1386$$

    Considering the maximum $\zeta = \frac{\delta}{2\pi} = \frac{0.1386}{2\pi} = 0.0221 = 2.2064\,\%$

63. Define damping ratio.

$$\text{Damping ratio} = \zeta = \frac{\text{damping constant}}{\text{damping constant for crtically damped system}} = \frac{C}{C_{cr}}$$

64. For SDOF system, m = 4 kg, k = 1.6 × 103 N m^{-1}, and the two cases of damping: (a) c_1 = 80 N m^{-1} s^{-1}; (b) c_2 = 320 N m^{-1} s^{-1}. Calculate the damping ratio for the two cases.

$$\omega_n = \sqrt{\frac{k}{m}} = \sqrt{\frac{1.6\times 10^3}{4}} = 20\ \text{rad/s};$$
$$\zeta_1 = \frac{C_1}{C_{cr}} = \frac{80}{2\times 4\times 20} = 0.5;$$
$$\zeta_2 = \frac{C_2}{C_{cr}} = \frac{320}{2\times 4\times 20} = 2$$

65. A 200-kg machine is placed at the end of 1.8-m-long steel cantilever beam. The machine is observed to vibrate with natural frequency of 21 Hz. What is the moment of inertia of the beam's cross section about its neutral axis.

$$\omega_n = 21\ \mathrm{Hz} = \left(21\frac{\text{cycles}}{\mathrm{s}}\right)\left(2\pi\frac{\mathrm{rad}}{\text{cycle}}\right) = 131.9469\,\mathrm{rad/s};$$
$$\mathrm{k_{equ}} = m\omega^2 = (200\,\mathrm{kg}\times(131.9\,\mathrm{rad/s})^2) = 3.4820\times 10^6\,\mathrm{N/m};\ \mathrm{k_{equ}} = 3\,\mathrm{EI/L3};$$

$I = (k_{equ} \times L3)/(3E)$; $I = (3.4820 \times 10^6\ \text{N/m} \times 1.8^3\ \text{m}^3)/(3 \times 210 \times 10^9\ \text{N/m}^2)$
$= 3.2215 \times 10^{-5}\ \text{m}^4$.

66. A 60-kg drum of the diameter 40 cm containing the waste material of mass density 1,100 kg/m^3 is being hoisted by a 30-mm-diameter steel ($E = 210 \times 10^9$ N/m^2) cable. When the drum is to be hoisted 10 m, the system natural frequency is measured as 40 Hz. Determine the volume of the drum. (*Hint*: $K_{equ} = AE/L$).

$$K_{equ} = \frac{AE}{L} = \frac{(\pi \times 0.015^2\ \text{m}^2)(210 \times 10^9\ \text{N/m}^2)}{10\ \text{m}} = 1.4844 \times 10^7\ \text{N/m};$$

$$\omega_n = \sqrt{\frac{k_{equ}}{m}};\ \left[\left(40\ \frac{\text{cycles}}{\text{s}}\right)\left(2\pi \frac{\text{rad}}{\text{s}}\right)\right]^2 = \frac{1.4844 \times 10^7}{M};\ M = 235.0018\ \text{kg};$$

$Mw = M - M_d = 235.0018 - 60 = 175.0018$ kg;
Volume of the drum = Mass/Mass density = 175.0018 kg/1,100 kg/m^3 = 0.1591 m^3

67. For what value of m will resonance occur for the system shown below:

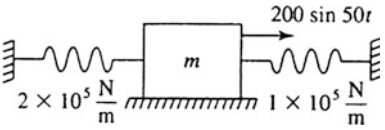

Springs are in parallel as the block is fixed and the equivalent stiffness of 3×10^5 N/m. Resonance occurs when excitation frequency 50 rad/s is equal to natural frequency. $50\ \text{rad/s} = \omega_n = \sqrt{\frac{k_{equ}}{m}};\ m = \frac{k_{equ}}{\omega_n^2} = \frac{3 \times 10^5\ \text{N/m}}{(50\ \text{rad/s})^2} = 120\ \text{kg}.$

68. A 35-kg electric motor that operates at 60 Hz is mounted on the elastic foundation of stiffness 3×10^6 N/m. The phase difference between the excitation and steady-state response is 21°. What is the damping ratio of system?

$$\omega_n = \sqrt{\frac{k}{m}} = \sqrt{\frac{3 \times 10^6 \text{N/m}}{35\ \text{kg}}} = 292.77\ \text{rad/s};$$

$$\beta = \frac{\omega}{\omega_n} = \left[\frac{(60\ \text{cycles/s})(2\pi\ \text{rad/cycle})}{292.77\ \text{rad/s}}\right] = 1.2877;$$

$$\tan\theta = \frac{2\zeta\beta}{1-\beta^2};\ \tan(180-21) = \frac{2 \times \zeta \times 1.2877}{1 - 1.2877^2};\ \zeta = 0.0982 = 9.8154\,\%$$

69. Evaluate the frequency and mode shape for the MDOF system using influence coefficient method. Use Dunkerley's method to evaluate natural frequency of the system.

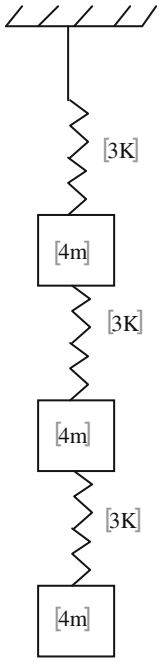

$$[\alpha] = \frac{1}{3k}\begin{bmatrix} 1 & 1 & 1 \\ 1 & 2 & 2 \\ 1 & 2 & 3 \end{bmatrix}$$

ω Dunkerley

$$\frac{1}{\omega^2} = 4m\left(\frac{1}{3k}\right) + 4m\left(\frac{2}{3k}\right) + 4m\left(\frac{3}{3k}\right) = \frac{24m}{3k}$$

$$\omega^2 = \frac{3k}{24m}$$

$$\omega = 0.354\sqrt{\frac{k}{m}}\text{rad/s}$$

Influence coefficient method

$$\begin{Bmatrix} x_1 \\ x_2 \\ x_3 \end{Bmatrix} = \frac{m\omega^2}{3k} \begin{bmatrix} 4 & 4 & 4 \\ 4 & 8 & 8 \\ 4 & 8 & 12 \end{bmatrix} \begin{Bmatrix} x_1 \\ x_2 \\ x_3 \end{Bmatrix}$$

Assuming $\begin{Bmatrix} x_1 \\ x_2 \\ x_3 \end{Bmatrix} = \begin{Bmatrix} 1 \\ 2 \\ 3 \end{Bmatrix}$;

$$\begin{Bmatrix} x_1 \\ x_2 \\ x_3 \end{Bmatrix} = \frac{24m\omega^2}{3k} \begin{bmatrix} 4 & 4 & 4 \\ 4 & 8 & 8 \\ 4 & 8 & 12 \end{bmatrix} \begin{Bmatrix} 1 \\ 1.83 \\ 2.33 \end{Bmatrix}$$

$$\begin{Bmatrix} x_1 \\ x_2 \\ x_3 \end{Bmatrix} = \frac{20.64m\omega^2}{3k} \begin{bmatrix} 4 & 4 & 4 \\ 4 & 8 & 8 \\ 4 & 8 & 12 \end{bmatrix} \begin{Bmatrix} 1 \\ 1.81 \\ 2.26 \end{Bmatrix}$$

$$\begin{Bmatrix} x_1 \\ x_2 \\ x_3 \end{Bmatrix} = \frac{20.28m\omega^2}{3k} \begin{bmatrix} 4 & 4 & 4 \\ 4 & 8 & 8 \\ 4 & 8 & 12 \end{bmatrix} \begin{Bmatrix} 1 \\ 1.80 \\ 2.25 \end{Bmatrix}$$

$$\begin{Bmatrix} x_1 \\ x_2 \\ x_3 \end{Bmatrix} = \frac{20.20m\omega^2}{3k} \begin{bmatrix} 4 & 4 & 4 \\ 4 & 8 & 8 \\ 4 & 8 & 12 \end{bmatrix} \begin{Bmatrix} 1 \\ 1.80 \\ 2.25 \end{Bmatrix}$$

$$\frac{20.20m\omega^2}{3k} = 1$$

$$\omega^2 = \frac{3k}{20.20m}$$

$$\omega = 0.385\sqrt{\frac{k}{m}}\,\text{rad/s}$$

70. Evaluate the frequency and mode shape for the MDOF system using influence coefficient method. Use Dunkerley's method to evaluate natural frequency of the system.

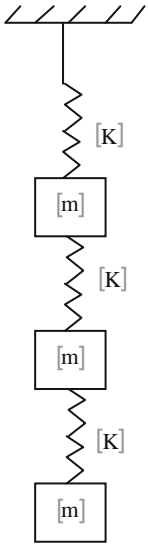

$$[\alpha] = \frac{1}{k}\begin{bmatrix} 1 & 1 & 1 \\ 1 & 2 & 2 \\ 1 & 2 & 3 \end{bmatrix}$$

ω Dunkerley

$$\frac{1}{\omega^2} = m\left(\frac{1}{k}\right) + m\left(\frac{2}{k}\right) + m\left(\frac{3}{k}\right) = \frac{6m}{k}$$

$$\omega^2 = \frac{k}{6m}$$

$$\omega = 0.408\sqrt{\frac{k}{m}}\ \text{rad/s}$$

Influence coefficient method

$$\begin{Bmatrix} x_1 \\ x_2 \\ x_3 \end{Bmatrix} = \frac{m\omega^2}{k} \begin{bmatrix} 1 & 1 & 1 \\ 1 & 2 & 2 \\ 1 & 2 & 3 \end{bmatrix} \begin{Bmatrix} x_1 \\ x_2 \\ x_3 \end{Bmatrix}$$

Assuming $\begin{Bmatrix} x_1 \\ x_2 \\ x_3 \end{Bmatrix} = \begin{Bmatrix} 1 \\ 2 \\ 3 \end{Bmatrix}$;

$$\begin{Bmatrix} x_1 \\ x_2 \\ x_3 \end{Bmatrix} = \frac{6m\omega^2}{k} \begin{bmatrix} 1 & 1 & 1 \\ 1 & 2 & 2 \\ 1 & 2 & 3 \end{bmatrix} \begin{Bmatrix} 1 \\ 1.83 \\ 2.33 \end{Bmatrix}$$

$$\begin{Bmatrix} x_1 \\ x_2 \\ x_3 \end{Bmatrix} = \frac{5.16m\omega^2}{k} \begin{bmatrix} 1 & 1 & 1 \\ 1 & 2 & 2 \\ 1 & 2 & 3 \end{bmatrix} \begin{Bmatrix} 1 \\ 1.81 \\ 2.26 \end{Bmatrix}$$

$$\begin{Bmatrix} x_1 \\ x_2 \\ x_3 \end{Bmatrix} = \frac{5.07m\omega^2}{k} \begin{bmatrix} 1 & 1 & 1 \\ 1 & 2 & 2 \\ 1 & 2 & 3 \end{bmatrix} \begin{Bmatrix} 1 \\ 1.81 \\ 2.25 \end{Bmatrix}$$

$$\begin{Bmatrix} x_1 \\ x_2 \\ x_3 \end{Bmatrix} = \frac{5.05m\omega^2}{k} \begin{bmatrix} 1 & 1 & 1 \\ 1 & 2 & 2 \\ 1 & 2 & 3 \end{bmatrix} \begin{Bmatrix} 1 \\ 1.80 \\ 2.25 \end{Bmatrix}$$

$$\frac{5.05m\omega^2}{k} = 1$$

$$\omega^2 = \frac{k}{5.05m}$$

$$\omega = 0.445\sqrt{\frac{k}{m}}\,\text{rad/s}$$

71. Evaluate the fundamental frequency and mode shape for the MDOF system using Dunkerley's method, influence coefficient method, Stodola's method, and Rayleigh–Ritz method.

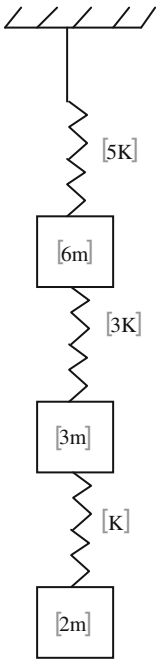

Dunkerley's Method

$$[\alpha] = \frac{1}{15k}\begin{bmatrix} 3 & 3 & 3 \\ 3 & 8 & 8 \\ 3 & 8 & 23 \end{bmatrix}$$

ω Dunkerley

$$\frac{1}{\omega^2} = 6m\left(\frac{13}{15k}\right) + 3m\left(\frac{8}{15k}\right) + 2m\left(\frac{23}{15k}\right) = \frac{88m}{15k}$$

$$\omega^2 = \frac{15k}{88m}$$

$$\omega = 0.41\sqrt{\frac{k}{m}}\text{rad/s}$$

Influence Coefficient Method

$$\begin{Bmatrix} x_1 \\ x_2 \\ x_3 \end{Bmatrix} = \frac{m\omega^2}{15k}\begin{bmatrix} 18 & 9 & 6 \\ 18 & 24 & 16 \\ 18 & 24 & 16 \end{bmatrix}\begin{Bmatrix} x_1 \\ x_2 \\ x_3 \end{Bmatrix}$$

Assuming $\begin{Bmatrix} x_1 \\ x_2 \\ x_3 \end{Bmatrix} = \begin{Bmatrix} 1 \\ 2 \\ 3 \end{Bmatrix}$;

$$\begin{Bmatrix} x_1 \\ x_2 \\ x_3 \end{Bmatrix} = \frac{54m\omega^2}{15k} \begin{bmatrix} 18 & 9 & 6 \\ 18 & 24 & 16 \\ 18 & 24 & 16 \end{bmatrix} \begin{Bmatrix} 1 \\ 2.11 \\ 3.78 \end{Bmatrix}$$

$$\begin{Bmatrix} x_1 \\ x_2 \\ x_3 \end{Bmatrix} = \frac{59.67m\omega^2}{15k} \begin{bmatrix} 18 & 9 & 6 \\ 18 & 24 & 16 \\ 18 & 24 & 16 \end{bmatrix} \begin{Bmatrix} 1 \\ 2.16 \\ 4.06 \end{Bmatrix}$$

$$\begin{Bmatrix} x_1 \\ x_2 \\ x_3 \end{Bmatrix} = \frac{61.80m\omega^2}{15k} \begin{bmatrix} 18 & 9 & 6 \\ 18 & 24 & 16 \\ 18 & 24 & 16 \end{bmatrix} \begin{Bmatrix} 1 \\ 2.18 \\ 4.15 \end{Bmatrix}$$

$$\begin{Bmatrix} x_1 \\ x_2 \\ x_3 \end{Bmatrix} = \frac{62.52m\omega^2}{15k} \begin{bmatrix} 18 & 9 & 6 \\ 18 & 24 & 16 \\ 18 & 24 & 16 \end{bmatrix} \begin{Bmatrix} 1 \\ 2.19 \\ 4.18 \end{Bmatrix}$$

$$\begin{Bmatrix} x_1 \\ x_2 \\ x_3 \end{Bmatrix} = \frac{62.79m\omega^2}{15k} \begin{bmatrix} 18 & 9 & 6 \\ 18 & 24 & 16 \\ 18 & 24 & 16 \end{bmatrix} \begin{Bmatrix} 1 \\ 2.19 \\ 4.19 \end{Bmatrix}$$

$$\begin{Bmatrix} x_1 \\ x_2 \\ x_3 \end{Bmatrix} = \frac{62.85m\omega^2}{15k} \begin{bmatrix} 18 & 9 & 6 \\ 18 & 24 & 16 \\ 18 & 24 & 16 \end{bmatrix} \begin{Bmatrix} 1 \\ 2.19 \\ 4.19 \end{Bmatrix}$$

$$\frac{62.85m\omega^2}{15k} = 1$$

$$\omega^2 = \frac{15k}{62.85m}$$

$$\omega = 0.49\sqrt{\frac{k}{m}}\text{rad/s}$$

Stodola's Method

Description	k_1 = 5k	$m_1 = 6m$	$k_2 = 3k$	$m_2 = 3m$	$k_3 = k$	$m_3 = 2m$
Assumed deflection		1		2		4
Inertia force		$m\omega^2(6)$		$m\omega^2(6)$		$m\omega^2(8)$
Spring force	$20m\omega^2$		$14m\omega^2$		$8m\omega^2$	
Spring deflection	$4m\omega^2/k$		$4.67m\omega^2/k$		$8m\omega^2/k$	
Calculated deflection ($m\omega^2/k$)		4		8.67		16.67
		1		2.17		4.17
Assumed deflection		1		2.17		4.17
Inertia force		$6m\omega^2$		$6.51m\omega^2$		$8.34m\omega^2$
Spring force	$20.85m\omega^2$		$14.85m\omega^2$		$8.34m\omega^2$	
Spring deflection	$4.17m\omega^2/k$		$4.95m\omega^2/k$		$8.34m\omega^2/k$	
Calculated deflection ($m\omega^2/k$)		4.17		9.12		17.47
		1		2.19		4.19
Assumed deflection		1		2.19		4.19
Inertia force		$6m\omega^2$		$6.57m\omega^2$		$8.38m\omega^2$
Spring force	$20.95m\omega^2$		$14.95m\omega^2$		$8.38m\omega^2$	
Spring deflection	$4.19m\omega^2/k$		$4.98m\omega^2/k$		$8.38m\omega^2/k$	
Calculated deflection($m\omega^2/k$)		4.19		9.17		17.55
Converged values		1		2.19		4.19

$$(1 + 2.19 + 4.19) = (4.19\omega 2 + 9.17\omega 2 + 17.55\omega 2)m/k$$

$$\omega^2 = \frac{7.38k}{30.91m}$$

$$\omega = 0.49\sqrt{\frac{k}{m}}\text{rad/s}$$

Rayleigh–Ritz Method

(1)	(2)	(3)	(4)	(5)	(6) = (3) × (5)	(7) = (1) × $(5)^2$
m	$\varphi r'$	FI $= m\varphi r'$		$\varphi r''/X_1$	FI × $\varphi r''$	m × $\varphi r''$
$6m$ $3m$ $2m$	1 2 4	$6m \times 1 = 6m$ $3m \times 2 = 6m$ $2m \times 4 = 8m$	$X_2 = \frac{4m}{k} + \left(\frac{6m+8m}{3k}\right) = \frac{8.67m}{k}$ $X_3 = \frac{8.67m}{k} + \left(\frac{8m}{k}\right) = \frac{16.67m}{k}$	1 2.17 4.17	$\frac{6m}{k}$ $\frac{13.02m}{k}$ $\frac{33.36m}{k}$ $\Sigma = \frac{52.38m}{k}$	$6 \times (1)2 = 6$ $3 \times (2.17)$ $2 = 14.13$ $2 \times (4.17)$ $2 = 34.78$ $\Sigma = 54.91$
$6m$ $3m$ $2m$	1 2.17 4.17	$6m \times 1 = 6m$ $3m \times 2 = 6.51m$ $2m \times 4 = 8.34m$	$X_1 = \left(\frac{6m+6.51m+8.34m}{5k}\right) = \frac{4.17m}{k}$ $X_2 = \frac{4.17m}{k} + \left(\frac{6.51m+8.34m}{3k}\right) = \frac{9.12m}{k}$ $X_3 = \frac{9.12m}{k} + \left(\frac{8.34m}{k}\right) = \frac{17.46m}{k}$	1 2.19 4.19	$\frac{6m}{k}$ $\frac{14.26m}{k}$ $\frac{34.94m}{k}$ $\Sigma = \frac{45.46m}{k}$	$6 \times (1)2 = 6$ $3 \times (2.19)$ $2 = 14.39$ $2 \times (4.19)$ $2 = 35.11$ $\Sigma = 55.5$
$6m$ $3m$ $2m$	1 2.19 4.19	$6m \times 1 = 6m$ $3m \times 2 = 6.57m$ $2m \times 4 = 8.38m$	$X_1 = \left(\frac{6m+6.57m+8.38m}{5k}\right) = \frac{4.19m}{k}$ $X_2 = \frac{4.19m}{k} + \left(\frac{6.57m+8.34m}{3k}\right) = \frac{9.17m}{k}$ $X_3 = \frac{9.17m}{k} + \left(\frac{8.38m}{k}\right) = \frac{17.55m}{k}$	1 2.19 4.19	$\frac{6m}{k}$ $\frac{14.39m}{k}$ $\frac{35.11m}{k}$ $\Sigma = \frac{55.5m}{k}$	$6 \times (1)2 = 6$ $3 \times (2.19)$ $2 = 14.39$ $2 \times (4.19)$ $2 = 35.11$ $\Sigma = 55.5$

72. Evaluate the fundamental frequency and mode shape for the MDOF system using Stodola's method.

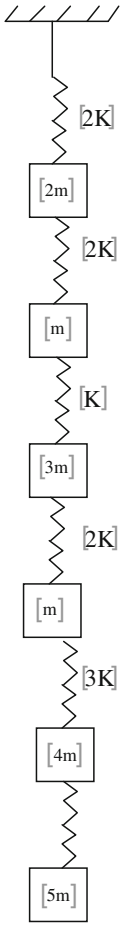

Description	k_1	m_1	k_2	m_2	k_3	m_3	k_4	m_4	k_5	M_5
	$2k$	$2m$	$2k$	m	k	$3m$	$2k$	$4m$	$3k$	$5m$
Assumed deflection		1		2		3		4		5
Inertia force ($m\omega^2$)		2		2		9		16		25
Spring force ($m\omega^2$)	54		52		50		41		25	
Spring deflection ($m\omega^2/k$)	27		26		50		20.5		8.33	
Calculated deflection ($m\omega^2/k$)		27		53		103		123.5		131.83
		1		1.96		3.81		4.57		4.88
Assumed deflection		1		1.96		3.81		4.57		4.88
Inertia force ($m\omega^2$)		2		1.96		11.43		18.28		24.4
Spring force ($m\omega^2$)	58.07		56.07		54.11		42.68		24.4	
Spring deflection ($m\omega^2/k$)	29.04		28.04		54.11		21.34		8.13	
Calculated deflection ($m\omega^2/k$)		29.04		57.08		111.19		132.53		140.66
		1		1.97		3.83		4.56		4.84
Assumed deflection		1		1.97		3.83		4.56		4.84
Inertia force ($m\omega^2$)		2		1.96		11.49		18.24		24.2
Spring force ($m\omega^2$)	57.9		55.9		53.93		42.44		24.2	
Spring deflection ($m\omega^2/k$)	28.95		27.95		53.93		21.22		8.07	
Calculated deflection ($m\omega^2/k$)		28.95		56.9		110.83		132.05		140.12
Converged values		1		1.97		3.83		4.56		4.84

$$(1 + 1.97 + 3.83 + 4.56 + 4.84) = (28.95 + 56.9 + 110.83 + 1320.05 + 140.12)\omega^2 m/k$$

$$\omega^2 = \frac{16.2k}{468.85m}$$

$$\omega = 0.19\sqrt{\frac{k}{m}}\text{rad/s}$$

73. Obtain all mode shapes and corresponding frequency of the system shown below:

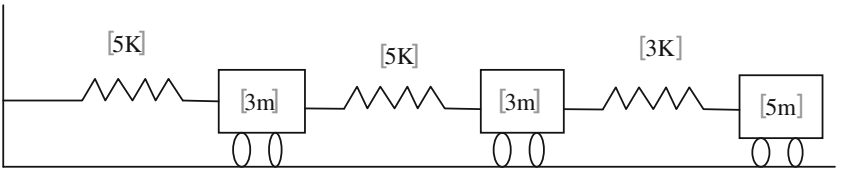

$$[\alpha] = \frac{1}{15k}\begin{bmatrix} 3 & 3 & 3 \\ 3 & 6 & 6 \\ 3 & 6 & 11 \end{bmatrix}$$

Influence coefficient method

$$\begin{Bmatrix} x_1 \\ x_2 \\ x_3 \end{Bmatrix} = \frac{m\omega^2}{15k}\begin{bmatrix} 9 & 9 & 15 \\ 9 & 18 & 30 \\ 3 & 18 & 55 \end{bmatrix}\begin{Bmatrix} x_1 \\ x_2 \\ x_3 \end{Bmatrix}$$

Assuming $\begin{Bmatrix} x_1 \\ x_2 \\ x_3 \end{Bmatrix} = \begin{Bmatrix} 1 \\ 2 \\ 3 \end{Bmatrix}$;

$$\begin{Bmatrix} x_1 \\ x_2 \\ x_3 \end{Bmatrix} = \frac{72m\omega^2}{15k}\begin{bmatrix} 9 & 9 & 15 \\ 9 & 18 & 30 \\ 3 & 18 & 55 \end{bmatrix}\begin{Bmatrix} 1 \\ 1.88 \\ 2.92 \end{Bmatrix}$$

$$\begin{Bmatrix} x_1 \\ x_2 \\ x_3 \end{Bmatrix} = \frac{69.72m\omega^2}{15k}\begin{bmatrix} 9 & 9 & 15 \\ 9 & 18 & 30 \\ 3 & 18 & 55 \end{bmatrix}\begin{Bmatrix} 1 \\ 1.87 \\ 2.92 \end{Bmatrix}$$

$$\begin{Bmatrix} x_1 \\ x_2 \\ x_3 \end{Bmatrix} = \frac{69.63m\omega^2}{15k}\begin{bmatrix} 9 & 9 & 15 \\ 9 & 18 & 30 \\ 3 & 18 & 55 \end{bmatrix}\begin{Bmatrix} 1 \\ 1.87 \\ 2.92 \end{Bmatrix}$$

$$\frac{69.63m\omega^2}{15k} = 1$$

$$\omega^2 = \frac{15k}{69.63m}$$

$$\omega = 0.22\sqrt{\frac{k}{m}}\text{rad/s}$$

II Mode shape

$$\begin{Bmatrix} A_1 \\ B_1 \\ C_1 \end{Bmatrix} = \begin{Bmatrix} 1 \\ 1.87 \\ 2.92 \end{Bmatrix}$$

$$m_1A_1A_2 + m_2B_1B_2 + m_3C_1C_2 = 0$$

$$3mA_2 + 5.61mB_2 + 14.6mC_2 = 0$$

$$A_2 = -1.87B_2 - 4.87C_2$$

$$\begin{Bmatrix} A_2 \\ B_2 \\ C_2 \end{Bmatrix} = \begin{bmatrix} 0 & -1.87 & -4.87 \\ 0 & 1 & 0 \\ 0 & 0 & 1 \end{bmatrix} \begin{Bmatrix} A_2 \\ B_2 \\ C_2 \end{Bmatrix}$$

$$\begin{Bmatrix} x_1 \\ x_2 \\ x_3 \end{Bmatrix} = \frac{m\omega^2}{15k} \begin{bmatrix} 9 & 9 & 15 \\ 9 & 18 & 30 \\ 3 & 18 & 55 \end{bmatrix} \begin{bmatrix} 0 & -1.87 & -4.87 \\ 0 & 1 & 0 \\ 0 & 0 & 1 \end{bmatrix} \begin{Bmatrix} A_2 \\ B_2 \\ C_2 \end{Bmatrix}$$

$$\begin{Bmatrix} x_1 \\ x_2 \\ x_3 \end{Bmatrix} = \frac{m\omega^2}{15k} \begin{bmatrix} 0 & -7.83 & -28.83 \\ 0 & 1.17 & -13.83 \\ 0 & 1.17 & 11.17 \end{bmatrix} \begin{Bmatrix} x_1 \\ x_2 \\ x_3 \end{Bmatrix}$$

Assuming $\begin{Bmatrix} x_1 \\ x_2 \\ x_3 \end{Bmatrix} = \begin{Bmatrix} 1 \\ -1 \\ 1 \end{Bmatrix}$

$$\begin{Bmatrix} x_1 \\ x_2 \\ x_3 \end{Bmatrix} = \frac{m\omega^2}{15k} \begin{bmatrix} 0 & -7.83 & -28.83 \\ 0 & 1.17 & -13.83 \\ 0 & 1.17 & 11.17 \end{bmatrix} \begin{Bmatrix} 1 \\ -1 \\ 1 \end{Bmatrix}$$

$$\begin{Bmatrix} x_1 \\ x_2 \\ x_3 \end{Bmatrix} = \frac{-21m\omega^2}{15k} \begin{bmatrix} 0 & -7.83 & -28.83 \\ 0 & 1.17 & -13.83 \\ 0 & 1.17 & 11.17 \end{bmatrix} \begin{Bmatrix} 1 \\ 0.71 \\ -0.48 \end{Bmatrix}$$

$$\begin{Bmatrix} x_1 \\ x_2 \\ x_3 \end{Bmatrix} = \frac{8.28m\omega^2}{15k} \begin{bmatrix} 0 & -7.83 & -28.83 \\ 0 & 1.17 & -13.83 \\ 0 & 1.17 & 11.17 \end{bmatrix} \begin{Bmatrix} 1 \\ 0.90 \\ -0.55 \end{Bmatrix}$$

$$\begin{Bmatrix} x_1 \\ x_2 \\ x_3 \end{Bmatrix} = \frac{8.81m\omega^2}{15k} \begin{bmatrix} 0 & -7.83 & -28.83 \\ 0 & 1.17 & -13.83 \\ 0 & 1.17 & 11.17 \end{bmatrix} \begin{Bmatrix} 1 \\ 0.98 \\ -0.58 \end{Bmatrix}$$

$$\begin{Bmatrix} x_1 \\ x_2 \\ x_3 \end{Bmatrix} = \frac{9.05m\omega^2}{15k} \begin{bmatrix} 0 & -7.83 & -28.83 \\ 0 & 1.17 & -13.83 \\ 0 & 1.17 & 11.17 \end{bmatrix} \begin{Bmatrix} 1 \\ 1.01 \\ -0.59 \end{Bmatrix}$$

$$\begin{Bmatrix} x_1 \\ x_2 \\ x_3 \end{Bmatrix} = \frac{9.10m\omega^2}{15k} \begin{bmatrix} 0 & -7.83 & -28.83 \\ 0 & 1.17 & -13.83 \\ 0 & 1.17 & 11.17 \end{bmatrix} \begin{Bmatrix} 1 \\ 1.03 \\ -0.59 \end{Bmatrix}$$

$$\begin{Bmatrix} x_1 \\ x_2 \\ x_3 \end{Bmatrix} = \frac{8.94m\omega^2}{15k} \begin{bmatrix} 0 & -7.83 & -28.83 \\ 0 & 1.17 & -13.83 \\ 0 & 1.17 & 11.17 \end{bmatrix} \begin{Bmatrix} 1 \\ 1.05 \\ -0.60 \end{Bmatrix}$$

$$\begin{Bmatrix} x_1 \\ x_2 \\ x_3 \end{Bmatrix} = \frac{9.08m\omega^2}{15k} \begin{bmatrix} 0 & -7.83 & -28.83 \\ 0 & 1.17 & -13.83 \\ 0 & 1.17 & 11.17 \end{bmatrix} \begin{Bmatrix} 1 \\ 1.05 \\ -0.59 \end{Bmatrix}$$

$$\frac{9.08m\omega^2}{15k} = 1$$

$$\omega^2 = \frac{15k}{9.08m}$$

$$\omega = 1.29\sqrt{\frac{k}{m}}\,\text{rad/s}$$

III Mode shape

$$\begin{Bmatrix} A_1 \\ B_1 \\ C_1 \end{Bmatrix} = \begin{Bmatrix} 1 \\ 1.87 \\ 2.92 \end{Bmatrix} \begin{Bmatrix} A_2 \\ B_2 \\ C_2 \end{Bmatrix} = \begin{Bmatrix} 1 \\ 1.05 \\ -0.59 \end{Bmatrix}$$

$$m_1A_1A_3 + m_2B_1B_3 + m_3C_1C_3 = 0$$
$$m_1A_2A_3 + m_2B_2B_3 + m_3C_2C_3 = 0$$
$$3mA_3 + 5.61B_3 + 14.6C_3 = 0$$
$$3mA_3 + 3.15mB_3 + 3mC_3 = 0$$

$$A_3 = -1.87B_3 - 4.87C_3; \quad B_3 = 7.16C_3; \quad C_3 = C_3$$

$$\begin{Bmatrix} A_3 \\ B_3 \\ C_3 \end{Bmatrix} = \begin{bmatrix} 0 & 0 & 45.04 \\ 0 & 0 & 7.16 \\ 0 & 0 & 1 \end{bmatrix} \begin{Bmatrix} A_3 \\ B_3 \\ C_3 \end{Bmatrix}$$

$$\begin{Bmatrix} x_1 \\ x_2 \\ x_3 \end{Bmatrix} = \frac{m\omega^2}{15k} \begin{bmatrix} 0 & -7.83 & -28.83 \\ 0 & 1.17 & -13.83 \\ 0 & 1.17 & 11.17 \end{bmatrix} \begin{bmatrix} 0 & 0 & 45.04 \\ 0 & 0 & 7.16 \\ 0 & 0 & 1 \end{bmatrix} \begin{Bmatrix} A_3 \\ B_3 \\ C_3 \end{Bmatrix}$$

$$\begin{Bmatrix} x_1 \\ x_2 \\ x_3 \end{Bmatrix} = \frac{m\omega^2}{15k} \begin{bmatrix} 0 & 0 & -84.89 \\ 0 & 0 & -5.45 \\ 0 & 0 & 19.55 \end{bmatrix} \begin{Bmatrix} x_1 \\ x_2 \\ x_3 \end{Bmatrix}$$

Assuming $\begin{Bmatrix} x_1 \\ x_2 \\ x_3 \end{Bmatrix} = \begin{Bmatrix} 1 \\ -1 \\ 1 \end{Bmatrix}$

$$\begin{Bmatrix} x_1 \\ x_2 \\ x_3 \end{Bmatrix} = \frac{84.89m\omega^2}{15k} \begin{bmatrix} 0 & 0 & -84.89 \\ 0 & 0 & -5.45 \\ 0 & 0 & 19.55 \end{bmatrix} \begin{Bmatrix} -1 \\ -1.06 \\ 0.23 \end{Bmatrix}$$

$$\begin{Bmatrix} x_1 \\ x_2 \\ x_3 \end{Bmatrix} = \frac{19.52m\omega^2}{15k} \begin{bmatrix} 0 & 0 & -84.89 \\ 0 & 0 & -5.45 \\ 0 & 0 & 19.55 \end{bmatrix} \begin{Bmatrix} -1 \\ -1.06 \\ 0.23 \end{Bmatrix}$$

$$\frac{19.52m\omega^2}{15k} = 1$$

$$\omega^2 = \frac{15k}{19.52m}$$

$$\omega = 0.88\sqrt{\frac{k}{m}}\text{rad/s}$$

$$\varphi = \begin{bmatrix} 1 & 1 & -1 \\ 1.87 & 1.05 & -0.06 \\ 2.92 & -0.6 & 0.23 \end{bmatrix}$$

$$\omega_n^{(1)} = 0.46\sqrt{\frac{k}{m}}\text{rad/s}; \quad \omega_n^{(2)} = 1.29\sqrt{\frac{k}{m}}\text{rad/s};$$

$$\omega_n^{(3)} = 0.88\sqrt{\frac{k}{m}}\text{rad/s}$$

Exercise on Numericals

1. Using the spring–mass system as an example, show that loss of potential energy of the mass due to displacement from the static equilibrium position will always be canceled by the work done by the equilibrium forces of the spring.
2. Ratio of (k/m) of a spring–mass system is given as 4.0. If the mass is deflected by 2 cm downward, measured for its equilibrium position and given an upward velocity of 8 cm/s, determine its amplitude and maximum acceleration.

3. Derive an expression to obtain damping ratio using half power band width method.
4. The following data are given for a vibrating system with viscous damping. Mass = 5 kg; k = 40 N/m; and C = 0.10 N/m s. Find logarithmic decrement and ratio of any two successive amplitudes.
5. Draw the resonance response of a un-damped system and write the inferences.
6. Show that in a damped system, amplitude of maximum displacement is bounded, even at resonance. What do you understand by this statement? Illustrate your answer with an appropriate figure.
7. Show that the log decrement is also given by the equation: $\delta = \frac{1}{n}\ln\left(\frac{x_0}{x_n}\right)$ where x_n represents amplitude after n cycles have elapsed. Plot also the curve showing the number of cycles elapsed against ξ for the amplitude to diminish by 50 %.
8. In coulomb damping model, show that decay in the amplitude per cycle is constant.
9. A spring–mass system is excited by a force of F_0 sin (ωt). At resonance, amplitude is measured as 0.58 cm. At 0.8 resonant frequency, amplitude measured is 0.46 cm. Determine the damping ratio ξ of the system.
10. In a damped system, damping limits the resonance response amplitude. Plot the number of cycles of the load versus resonance response and show that few cycles of excitations are required to reach the nearly full response amplitude.
11. Starting with the matrix equation, $K\phi_s = \omega_s^2 M\phi_s$, pre-multiply first with KM^{-1}, and using orthogonality relation $\phi_r^T M\phi_s = 0$, show that $\phi_r^T KM^{-1}K\phi_s = 0$. Repeat this to show that $\phi_r^T[KM^{-1}]^h K\phi_s = 0$ for h = 1, 2, 3, 4, … n, where n is number of degrees of freedom.
12. Determine the influence coefficient matrix for the multi-degrees-of-freedom system shown in the below figure:

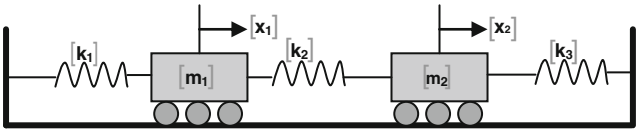

13. Determine the fundamental frequency of the system whose [M] and influence coefficient matrix δ are given as below:

$$M = \begin{bmatrix} 60 & 0 & 0 \\ 0 & 100 & 0 \\ 0 & 0 & 80 \end{bmatrix}, \; [\delta] = \begin{bmatrix} 6 & 5 & 3 \\ 5 & 7 & 4 \\ 3 & 4 & 6 \end{bmatrix}$$

14. What do you understand by mode shapes? Give its physical interpretation.
15. Why fundamental frequency is of great importance in structural dynamics?
16. A continuous structure has _____ number of degrees of freedom.
17. In structural dynamics, mass element represents _____ characteristics of the structure and _____ represents elastic restoring force.
18. A sketch of the body, isolated from all other bodies, in which all forces external to the body are shown is called _____.
19. An alternate approach which states that the system may be set in a state of dynamic equilibrium is called _____.
20. Degree of freedom of a system is the number of independent coordinates necessary to describe its position. True or false. If false, rewrite the correct statement.
21. It is observed experimentally that amplitude of free vibration of certain structure modeled as single degree of freedom decreases from 1 to 0.4 in 10 cycles. What is the % of critical damping?
22. The simplest form of periodic motion is _____.
23. What are the essential characteristics of a dynamic loading?
24. It is not always possible to obtain rigorous mathematical solutions for engineering problems. Should you agree to this statement, then which provides a reasonable link between the real physical system and mathematically feasible solution?
25. It is not always of freedom, damping element represents only dissipation of energy. Such pure elements do not exist in physical world this statement, then which provides a ra mathematical model.
26. Do both the figures shown below represent mathematical models that are dynamically equivalent? Explain your answer briefly.

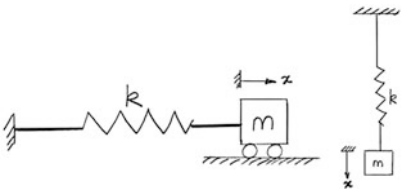

27. In a SDOF model, spring is considered a linear spring. In other words, force–displacement properties of the system are taken as linear. Is it a hypothetical situation compared to the real dynamic behavior of structures? Explain.
28. Find time period of the structure shown in the below figure. Cross section of the column is circular of 50 mm diameter, made of steel. Take E_{st} as 2 × 105 N/mm^2, mass as 100 kg, length of the column as 2 m.

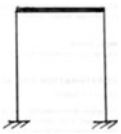

29. A cantilever beam is shown in figure below has a lumped mass of 10 kg at its tip. Length of the beam is 1.5 m and stiffness of springs attached to the mass is 100 N/m. For initial displacement of 25 mm and initial velocity of 0.5 m/s, find the displacement and velocity of the system after 1 s. Take E_{st} as 2 × 105 N/mm^2. Neglect the self-weight of the beam. Beam is made of a steel flat of size 6 mm × 100 mm.

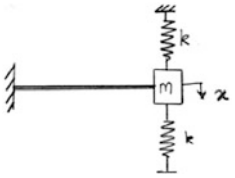

30. A vibrating system having mass of 4.5 kg and stiffness of 3,500 N/m is viscously damped so that ratio of two consecutive peaks is reduced from 1.0 to 0.85. Determine natural frequency, logarithmic decrement, damping ratio, damping coefficient, and damped natural frequency.
31. What is the difference between vibration and oscillation?
32. What is negative damping? Explain it with an example.
33. Evaluate the frequency and mode shape for the MDOF system using influence coefficient method. Use Dunkerley's method to evaluate natural frequency of the system.

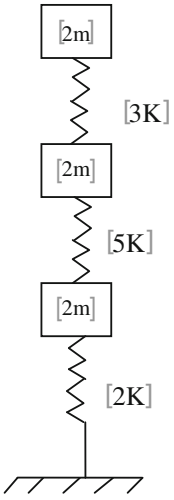

[m = 3500 kg; K = 1500 kN/m]

34. Evaluate the frequency and mode shape for the MDOF system using influence coefficient method. Use Dunkerley's method to evaluate natural frequency of the system.

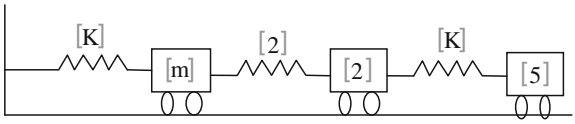

m = 35 kN; K= 1000 kN/m

35. Evaluate the frequency and mode shape for the MDOF system using influence coefficient method. Use Dunkerley's method to evaluate natural frequency of the system.

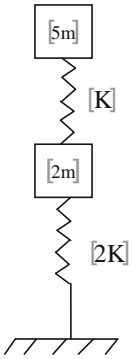

36. Evaluate the fundamental frequency and mode shape for the MDOF system using Rayleigh–Ritz method and compare the frequency with Dunkerley's method.

37.

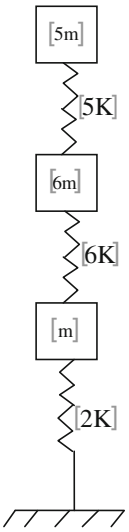

38. Evaluate the fundamental frequency and mode shape for the MDOF system using Stodola's method.

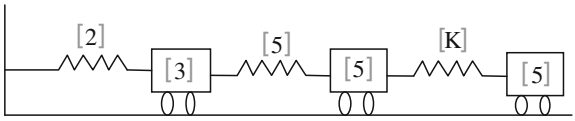

Chapter 4
Damping in Offshore Structures

Abstract This chapter deals with the methods of estimating damping in offshore structures. Different types of damping models, their comparison, and suitability to offshore structures are discussed in detail. Example problems are solved, and estimation of damping using different models is explained.

Keywords Structural damping · Viscous damping · Coulomb damping · Rayleigh damping · Caughey damping

4.1 Introduction

Under ideal conditions of no damping, if the system is set to vibration, it will be excited indefinitely at constant amplitude at its natural frequency. But in real time, any system set to vibration comes to rest, necessarily after passage of time; damping offered by the presence of air may be one of the reasons. As such, un-damped systems are hypothetical, since damping is inherently present in the atmosphere. Further, ocean structures are under the influence of waves and current, which offers significant amount of damping to the structural system that is set in vibration. The basic types of damping are, namely (i) coulomb damping and (ii) viscous damping. Coulomb damping results from sliding of two surfaces; it is also called dry damping or friction damping. The damping force is the product of the normal force and the coefficient of friction between the body surface and the plane of motion. Note that the damping force in this case is independent of velocity of motion of the body which is under vibration. In case of viscous damping, the damping force accounts for the viscosity of the system. The presence of fluid medium around the body significantly influences the damping force acting on the body. Damping force will be proportional to the magnitude of the velocity and has the unit of N/(m s). Viscous damping seems to be more relevant to offshore structural systems due to the inherent presence of liquid medium around the body.

S. Chandrasekaran, *Dynamic Analysis and Design of Offshore Structures*,
Ocean Engineering & Oceanography 5, DOI 10.1007/978-81-322-2277-4_4

The frictional forces are not conservative, as they cannot be derived from a potential function that is based on the displacement (response) of the vibrating system. However, these forces are highly responsible for dissipation of energy or conversion of energy from one form to the other. This results in reduction in response to the structural system. The energy consumed by the friction forces is converted into heat energy and dissipated by conduction, by convection to the fluid surrounding the structure and by radiation.

The frictional forces in a system may arise due to any one of the following physical processes (Wilson 1984). There can be friction among the materials, leading to internal viscous damping. This is highly practical due to the use of modern materials such as composites in offshore structures. At the connections or joints, due to the presence of materials of different composition, bimetallic coupling can result in friction forces. There can also be friction between two structural components, leading to structural damping. There can be friction between the structural members and fluid surrounding them, leading to external viscous damping. Lastly, there can be friction between the structural members at their supports which are in contact with them. This leads to coulomb damping. However, it is very difficult to quantify these damping forces in a given system, as the causes for such forces are diverse.

Structural damping is usually considered to be 0.2–0.5 % of that of the critical damping for steel platforms (Adams and Baltrop 1991). For concrete, this can be of the order of 0.5–1.5 %. Hydrodynamic damping originates from the waves surrounding the offshore structures. They are found in two common forms, namely (i) radiation damping and (ii) viscous damping. Radiation damping is determined by potential theory. It exhibits a strong dependence on frequency and submergence effects. Literature shows that the drag damping is lower for a larger diameter vertical column members in offshore structures; this is of the order 0.1 %. Damping ratio of the marine structure, including the effect of added mass can be expressed as the ratio of the dry structure, as given below:

$$\xi_{\text{wet}} = \xi_{\text{dry}} \left[\frac{m^*_{\text{dry}} \omega^*_{\text{dry}}}{m^*_{\text{wet}} \omega^*_{\text{wet}}} \right] \tag{4.1}$$

where m^* and ω^* are generalized mass and frequency, respectively (Naess and Moan 2013). Literature also shows that the total damping ratio is about 2 % for the first three modes for gravity platforms.

Classical damping is an approximate idealization if similar damping is distributed throughout the structure. However, in offshore structures, uniform distribution of damping throughout the structure is not applicable due to many reasons: (i) variation in material properties of members at connections, (ii) use of composites for variety of members, and (iii) deck and the substructure shall be even isolated so that the large displacements of the deck under wind forces do not influence the

substructure and that of the effects caused by waves do not influence the deck motion, etc. Three damping models are popular for offshore structures, namely (i) Rayleigh damping, (ii) Caughey damping, and (iii) modal damping. These are explained below with examples.

4.2 Damping Models: Rayleigh Damping

Consider a mass proportional or a stiffness proportional damping as given below:

$$C = a_0 M \tag{4.2}$$

$$C = a_1 K \tag{4.3}$$

where a_0 and a_1 are constants having units as s^{-1} and s, respectively. In both the cases, C is diagonal by virtue of modal orthogonality properties; hence, these are classical damping matrices. Physically, they represent damping models as shown in Fig. 4.1.

In case of mass proportional damping, damping can be negligibly small due to air damping, but in offshore structures, this can be significantly high. In case of stiffness proportional damping, dissipation of energy depends upon the relative displacement between the successive mass points. Keeping [C] as proportional to modal damping ratios, for the system with mass proportional damping, the damping ratio will be given by

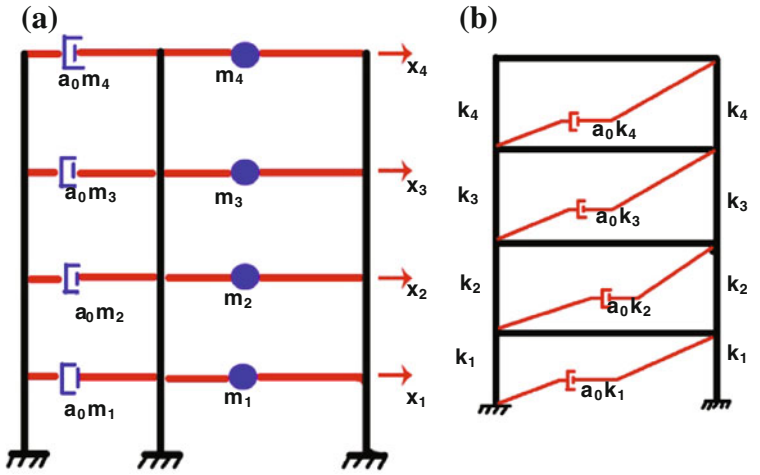

Fig. 4.1 Damping models **a** mass proportional damping **b** stiffness proportional damping

$$\begin{aligned} C_n &= a_0 M_n \\ \xi_n &= \frac{C_c}{2M_n\omega_n} = \frac{a_0 M_n}{2M_n\omega_n} \\ \xi_n &= \frac{a_0}{2}\frac{1}{\omega_n} \end{aligned} \tag{4.4}$$

The damping ratio is inversely proportional to the natural frequency. Hence, a_0 can be settled to obtain a specified value of the damping ratio in nay mode, as given below:

$$a_0 = 2\xi_i\omega_i \tag{4.5}$$

With a_0 determined, damping matrix $[C]$ is known from Eq. (4.4). Similarly, for stiffness proportional damping, we get the following relationships:

$$\begin{aligned} C_n &= a_1 K_n \\ \xi_n &= \frac{C_c}{2M_n\omega_n} = \frac{a_1\omega_n^2 M_n}{2M_n\omega_n} \\ \xi_n &= \frac{a_1}{2}\omega_n \end{aligned} \tag{4.6}$$

$$a_1 = \frac{2\xi_j}{\omega_j} \tag{4.7}$$

With a_1 determined from the above equation, damping matrix $[C]$ can be computed from Eq. (4.6). It is seen that both the damping models, being either mass proportional or stiffness proportional, are not validating the actual behavior of the offshore structures, experimentally. Hence to be consistent with the experimental observations, Rayleigh damping is proposed for offshore structures. The damping matrix will be proportional to both mass and stiffness as given below:

$$C = a_0 M + a_1 K \tag{4.8}$$

Damping ratio for *n*th mode of such a system is given by

$$\xi_n = \frac{a_0}{2}\frac{1}{\omega_n} + \frac{a_1}{2}\omega_n \tag{4.9}$$

Coefficients, a_0 and a_1, can be determined for a specific damping ratio (ξ_i, ξ_j) for *i*th and *j*th modes, respectively. For the Fig. 4.2, one can pick up the damping ratio in such a manner that it is same for both the chosen frequencies (ω_i, ω_j).

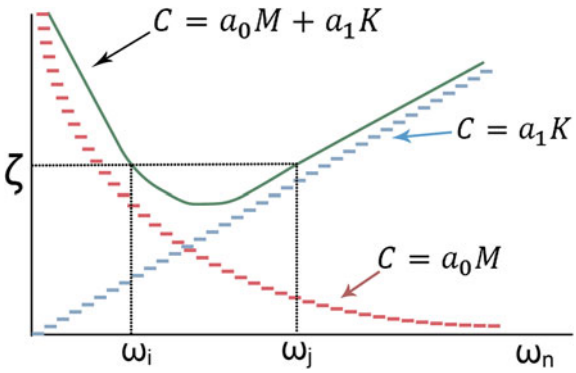

Fig. 4.2 Rayleigh damping

$$\begin{aligned}
\xi_n &= \frac{a_0}{2}\frac{1}{\omega_n} + \frac{a_1}{2}\omega_n \\
\xi_i &= \frac{a_0}{2}\frac{1}{\omega_i} \\
\xi_j &= \frac{a_1}{2}\omega_j \\
\begin{Bmatrix} \xi_i \\ \xi_j \end{Bmatrix} &= \frac{1}{2}\begin{bmatrix} \frac{1}{\omega_i} & \omega_i \\ \frac{1}{\omega_j} & \omega_j \end{bmatrix}\begin{Bmatrix} a_0 \\ a_1 \end{Bmatrix}
\end{aligned} \tag{4.10}$$

For $\xi_i, \xi_j = \xi$, then

$$\begin{aligned}
\begin{Bmatrix} a_0 \\ a_1 \end{Bmatrix} &= \frac{2\,\omega_i\omega_j}{\omega_j^2 - \omega_i^2}\begin{bmatrix} \omega_j & -\omega_i \\ -\frac{1}{\omega_j} & \frac{1}{\omega_i} \end{bmatrix}\begin{Bmatrix} \xi_i \\ \xi_j \end{Bmatrix} \\
a_0 &= 2\xi\,\frac{\omega_i\omega_j}{\omega_i + \omega_j} \\
a_1 &= \frac{2\xi}{\omega_i + \omega_j}
\end{aligned} \tag{4.11}$$

Knowing the constants a_0 and a_1, damping matrix $[C]$ can be estimated using Eq. (4.8). Few critical observations in applying this procedure are as follows: (i) Modes (i, j) with specified damping ratios need to be chosen; and (ii) one must select reasonable value of damping ratios for all the modes. For example, if one wants to include third mode in the analysis with roughly the same damping ratio in all the modes (which is desired), then one should select the third frequency such that this condition is satisfied. Hence, truncation of modes, in such cases, is also governed by the appropriate (nearly equal) damping ratios to the chosen frequencies.

4.2.1 Example Problem

Let us consider the spring-mass system shown in Fig. 4.3. Let m be 3,500 kg and k be 1,500 kN/m. Taking damping ratio for first two modes as 5 %, compute the damping ratio for the third mode.

Solution

Please note that for classical damping, it is essential that the damping in all the modes included in the analysis should be equal. Should we need to include the third mode also in the analysis, then it is essential to check whether the third mode has damping equivalent to that of the first two modes. By this way, it also necessitates the truncation of higher modes in the dynamic analysis.

By following any standard procedure explained in the previous chapters, one can readily determine all the frequencies and their corresponding mode shapes. The computed values are given below:

$$\left[\omega_1 = 0.57\sqrt{\left[\frac{k}{m}\right]} \quad 01.414\sqrt{\left[\frac{k}{m}\right]} \quad 2.163\sqrt{\left[\frac{k}{m}\right]}\right]$$

After substituting for the values of mass and stiffness, we get the following: $[\omega] = [11.8$ rad/s 29.27 rad/s 44.778 rad/s $]$. The corresponding mode shapes are as given below:

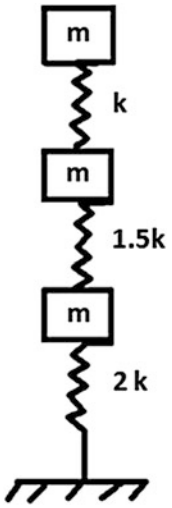

Fig. 4.3 Example problem 4.2.1

$$[\Phi] = \begin{bmatrix} 1 & 1 & 1 \\ 0.68 & -1 & -3.68 \\ 0.32 & 1 & 4.68 \end{bmatrix}$$

$$[M] = 3{,}500 \begin{bmatrix} 1 & 0 & 0 \\ 0 & 1 & 0 \\ 0 & 0 & 1 \end{bmatrix}$$

$$[K] = 1{,}500 \times 10^3 \begin{bmatrix} 1 & -1 & 0 \\ -1 & 2.5 & -1.5 \\ 0 & -1.5 & 3.5 \end{bmatrix}$$

$$a_0 = 2\left[\frac{\omega_1 \omega_2}{\omega_1 + \omega_2}\right](0.05) = 2\left[\frac{11.8 \times 29.27}{(11.8 + 29.27)}\right](0.05) = 0.841$$

$$a_1 = \frac{2\xi}{\omega_1 + \omega_2} = \frac{2 \times 0.05}{(11.8 + 29.27)} = 0.0024$$

$$[C] = a_0 M + a_1$$

$$[C] = (0.841 \times 3{,}500) \begin{bmatrix} 1 & 0 & 0 \\ 0 & 1 & 0 \\ 0 & 0 & 1 \end{bmatrix} + 0.0024 \times 1{,}500 \times 10^3 \begin{bmatrix} 1 & -1 & 0 \\ -1 & 2.5 & -1.5 \\ 0 & -1.5 & 3.5 \end{bmatrix}$$

$$= \begin{bmatrix} 6543.5 & -3600 & 0 \\ -3600 & 11943.5 & -5400 \\ 0 & -5400 & 15543.5 \end{bmatrix} \text{Ns/m}$$

To find the damping ratio in the third mode:

$$\xi_n = \frac{a_0}{2}\frac{1}{\omega_n} + \frac{a_1}{2}\omega_n$$

$$\xi_3 = \frac{a_0}{2}\frac{1}{\omega_3} + \frac{a_1}{2}\omega_3$$

$$\xi_3 = \frac{0.841}{2}\left[\frac{1}{44.778}\right] + \frac{0.0024}{2} \times 44.778 = 6.31\ \%$$

As the damping ratios in all the modes are almost equal, all the three modes shall be considered for the analysis.

4.3 Caughey Damping

If you wish to specify the damping ratios in more than two modes, then consider the general for of the classified damping. Let the natural frequencies and mode shapes satisfy the following relationship:

$$K\varphi_r = \omega_r^2 M\varphi_r \tag{4.12}$$

Pre-multiplying Eq. (4.12) on both sides, we get the following:

$$\varphi_n^T[KM^{-1}K]\varphi_r = \omega_r^2\varphi_n^T[KM^{-1}MK]\varphi_r = 0 \quad \text{for } n \neq r \text{ due to orthogonality} \tag{4.13}$$

Further, pre-multiplying Eq. (4.12) on both sides, we get the following:

$$\begin{aligned}\varphi_n^T[(KM^{-1})^2K]\varphi_r &= \omega_r^2\varphi_n^T[KM^{-1}KM^{-1}M]\varphi_r \\ &= \omega_r^2[KM^{-1}K]\varphi_r = 0 \quad \text{for } n \neq r\end{aligned} \tag{4.14}$$

By repeated application of this procedure, a family of orthogonality relations can be obtained. This can be expressed in a compact form, as given below:

$$\begin{aligned}\varphi_n^T\, C_\ell\, \varphi_r &= 0 \quad \text{for } n \neq r \\ C_\ell &= [KM^{-1}]^\ell K \quad \text{for } \ell = 0, 1, 2, \ldots\infty\end{aligned} \tag{4.15}$$

Now, pre-multiplying and rewriting the above equation as follows:

$$\begin{aligned}C_\ell &= M^{-1}M\,[K\,M^{-1}]^\ell\, K \quad \text{for } \ell = 0, 1, 2, 3, \ldots\infty \\ &= M[M^{-1}K]\,[M^{-1}K]\ldots K \\ &= M\,[M^{-1}K]^\ell \quad \text{for } \ell = 0, 1, 2, 3\ldots\infty\end{aligned} \tag{4.16}$$

Alternatively, pre-multiplying Eq. (4.12) we get the following:

$$\varphi_n^T M\,K^{-1}K\,\varphi_r = \omega_r^2\,\varphi_n^T[M\,K^{-1}]M\,\varphi_r \tag{4.17}$$

By following the same procedure as discussed above, we get the following:

$$C_\ell = M\,[M^{-1}K]^\ell \quad \text{for } \ell = -1, -2, -3, \ldots-\infty \tag{4.18}$$

Combining Eqs. (4.16) and (4.18), we get the following:

$$C_\ell = M\sum_{\ell=-\infty}^{\infty} a_\ell\,[M^{-1}K]^\ell \tag{4.19}$$

It can be shown that in the above equation, N terms in the infinite series will be independent. This shall lead to a general form of a classical damping matrix, which is given by

$$C_\ell = M \sum_{\ell=0}^{N-1} a_\ell \left[M^{-1}K\right]^\ell \tag{4.20}$$

where N is the number of degrees of freedom and a_l are constants. First three terms in the series are given by

$$\begin{aligned} a_0 M \left[M^{-1}K\right]^0 &= a_0 M \\ a_1 M \left[M^{-1}K\right]^1 &= a_1 K \\ a_2 M \left[M^{-1}K\right]^2 &= a_2 KM^{-1}K \end{aligned} \tag{4.21}$$

It can be seen that the first two terms in the series are same as the Rayleigh damping. Suppose, if one wishes to specify the damping ratios for J modes of the N degrees-of-freedom system, then J terms need to be included in the Caughey series. They could be any J of the N terms of Eq. (4.20). Typically, first J terms included will be

$$C = M \sum_{\ell=0}^{J-1} a_\ell \left[M^{-1}K\right]^\ell \tag{4.22}$$

For nth mode, generalized damping is given by

$$\begin{aligned} C_n &= \varphi_n^T C \varphi_n = \sum_{\ell=0}^{N-1} \varphi_n^T C_\ell \varphi_n \\ C_\ell &= M[M^{-1}K]^\ell \\ \text{For } \ell = 0 &: \varphi_n^T C_0 \varphi_n = \varphi_n^T (a_0 M)\varphi_n = a_0 M_n \\ \text{For } \ell = 1 &: \varphi_n^T C_1 \varphi_n = \varphi_n^T (a_1 K)\varphi_n = a_1 \omega_n^2 M_n \\ \text{For } \ell = 2 &: \varphi_n^T C_2 \varphi_n = \varphi_n^T (a_2 KM^{-1}K)\varphi_n \\ &= a_2 \omega_n^2 \varphi_n^T K \varphi_n = a_2 \omega_n^2 \left(\omega_n^2 M_n\right) = a_2 \omega_n^4 M_n \end{aligned} \tag{4.23}$$

Hence, we get the following:

$$C_n = \sum_{\ell=0}^{N-1} a_\ell \omega_n^{(2\ell-1)} M_n \tag{4.24}$$

Damping ratio is given by:

$$\xi_n = \frac{C_n}{2M_n\omega_n}$$
$$\xi_n = \frac{1}{2}\sum_{\ell=0}^{N-1} a_\ell \omega_n^{(2\ell-1)} \tag{4.25}$$

Coefficients, a_l can be determined from the damping ratios specified in any J modes, by solving J algebraic equations of Eq. (4.25), for unknowns of $a = 0, 1, \ldots, J - 1$. With a_1 determined, damping matrix $[C_n]$ is known from Eq. (4.24) and the damping ratios are given by Eq. (4.25).

4.3.1 Critical Problems Associated with Caughey Damping

- The algebraic equations of Eq. (4.25) are numerically ill-conditioned because the coefficients $(\omega_n^{-1}, \omega_n, \omega_n^3, \ldots$ can differ by orders of high magnitude.
- If more than two terms are included in the Caughey series, $[C]$ becomes a full matrix, although $[K]$ is banded and lumped mass matrix is diagonal. This will increase the computational cost for analyzing large systems.

Hence, Rayleigh damping is preferred and assumed in most of the practical cases.

4.3.2 Example Problem

Let us consider the spring-mass system shown in Fig. 4.4. Let m be 3,500 kg and k be 1,500 kN/m. Evaluate classical damping matrix for all the three modes for damping ratio of 5 %.

Solution

By following any standard procedure explained in the previous chapters, one can readily determine all the frequencies and their corresponding mode shapes.

The computed values are given below.

$$\left[\omega_1 = 0.57\sqrt{\left[\frac{k}{m}\right]} \quad 01.414\sqrt{\left[\frac{k}{m}\right]} \quad 2.163\sqrt{\left[\frac{k}{m}\right]}\right]$$

After substituting for the values of mass and stiffness, we get the following:

$$[\omega] = [11.8 \text{ rad/s } 29.27 \text{ rad/s } 44.778 \text{ rad/s }].$$

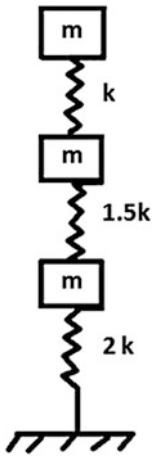

Fig. 4.4 Example problem 4.3.2

The corresponding mode shapes are as given below:

$$[\Phi] = \begin{bmatrix} 1 & 1 & 1 \\ 0.68 & -1 & -3.68 \\ 0.32 & 1 & 4.68 \end{bmatrix}$$

Caughey series for 3 degrees of freedom is given by

$$C = a_0 M + a_1 K + a_2 K M^{-1} K$$

$$\xi_n = \frac{1}{2} \sum_{\ell=0}^{2} a_\ell \omega_n^{(2\ell-1)}$$

$$\xi_n = \frac{a_0}{2}\left(\frac{1}{\omega_n}\right) + \frac{a_1 \omega_n}{2} + \frac{a_2 \omega_n^3}{2}$$

$$2\xi_n = \frac{a_0}{\omega_n} + a_1 \omega_n + a_2 \omega_n^3$$

$$2\begin{Bmatrix} 0.05 \\ 0.05 \\ 0.05 \end{Bmatrix} = \begin{bmatrix} 1/11.48 & 11.8 & 11.8^3 \\ 1/29.27 & 29.27 & 29.27^3 \\ 1/44.778 & 44.78 & 44.778^3 \end{bmatrix} \begin{Bmatrix} a_0 \\ a_1 \\ a_2 \end{Bmatrix}$$

Determine a_0, a_1, and a_2 and then obtain $[C]$ using Eq. (4.24).

4.4 Classical Damping Matrix by Damping Matrix Superpositioning

We know that the damping matrixis given by the following equation:

$$\begin{aligned} \varphi^T c \varphi &= C \\ C_n &= \xi_n (2 M_n \omega_n) \\ c &= \left(\varphi^T\right)^{-1} C \varphi^{-1} \end{aligned} \tag{4.26}$$

Determining $[C_n]$ using the above equation is inefficient because it requires inversion of two matrices of order N. Hence alternatively, using the orthogonality principle, we get the following:

$$\varphi^T m \, \varphi = M$$

It can be shown that

$$\begin{aligned} \varphi^{-1} &= M^{-1} \varphi^T m \\ \left(\varphi^T\right)^{-1} &= m \varphi M^{-1} \end{aligned} \tag{4.27}$$

From the Eq. (4.27), the required inverse matrices can be readily obtained because M is a diagonal matrix of generalized modal mass M_n; hence, M^{-1} is easily computed as all the diagonal elements are $(1/M^n)$. Further, $[K]$ is a symmetric matrix and this property can be advantageous to perform the required operation. Substituting Eq. (4.27) in Eq. (4.26), we get the following:

$$c = [m \varphi M^{-1}] C [M^{-1} \varphi^T m] \tag{4.28}$$

Since $[M]$ and $[C]$ are diagonal matrices, Eq. (4.28) can be rewritten as follows:

$$c = m \left[\sum_{n=1}^{N} \frac{2 \xi_n \omega_n}{M_n} \varphi_n \varphi_n^T \right] m \tag{4.29}$$

nth term in the above summation is the contribution of the nth mode to the damping matrix $[C]$, with its damping ratio ξ_n. If this term in not included, then $[C]$ will imply zero damping ratio in the nth mode.

4.4.1 Critical Issues

- It is practical to include any first J modes even though N degrees of freedom exist.
- Lack of damping in modes $(J + 1)$ to N does not create any numerical problems in an unconditionally stable time-stepping procedure is chosen to integrate the equation of motion.

4.4.2 Example Problem

Let us consider the spring-mass system shown in Fig. 4.5. Let m be 3,500 kg and k be 1,500 kN/m. Determine damping matrix by superimposing the damping matrices for first two modes, each with 5 % damping ratio.

Solution

By following any standard procedure explained in the previous chapters, one can readily determine all the frequencies and their corresponding mode shapes.

The computed values are given below.

$$\left[\omega_1 = 0.57\sqrt{\left[\frac{k}{m}\right]} \quad 01.414\sqrt{\left[\frac{k}{m}\right]} \quad 2.163\sqrt{\left[\frac{k}{m}\right]}\right]$$

After substituting for the values of mass and stiffness, we get the following:

$$[\omega] = [11.8 \text{ rad/s } 29.27 \text{ rad/s } 44.778 \text{ rad/s }].$$

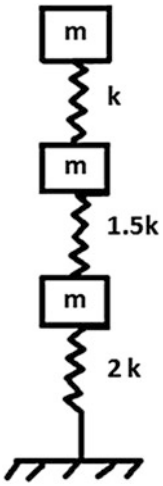

Fig. 4.5 Example problem 4.4.2

The corresponding mode shapes are as given below:

$$[\Phi] = \begin{bmatrix} 1 & 1 & 1 \\ 0.68 & -1 & -3.68 \\ 0.32 & 1 & 4.68 \end{bmatrix}$$

The damping matrix is given by Eq. (4.29). Individual term of the matrix is now determined as below:

$$\begin{aligned} c_1 &= \frac{2(0.05)(11.8)}{1.0} m\varphi_1\varphi_1^T m \\ &= \frac{2(0.05)(11.8)}{1.0}(3{,}500)\begin{bmatrix} 1 & 0 & 0 \\ 0 & 1 & 0 \\ 0 & 0 & 1 \end{bmatrix}\begin{Bmatrix} 1 \\ 0.68 \\ 0.32 \end{Bmatrix}[1 \quad 0.68 \quad 0.32](3{,}500)\begin{bmatrix} 1 & 0 & 0 \\ 0 & 1 & 0 \\ 0 & 0 & 1 \end{bmatrix} \\ c_1 &= 10^6 \begin{bmatrix} 14.46 & 9.83 & 4.63 \\ 9.83 & 6.68 & 3.15 \\ 4.63 & 3.15 & 1.48 \end{bmatrix} \end{aligned} \tag{4.30}$$

Similarly, for the second mode, we get the following:

$$\begin{aligned} c_1 &= \frac{2(0.05)(29.27)}{1.0} m\varphi_2\varphi_2^T m \\ &= \frac{2(0.05)(29.27)}{1.0}(3{,}500)\begin{bmatrix} 1 & 0 & 0 \\ 0 & 1 & 0 \\ 0 & 0 & 1 \end{bmatrix}\begin{Bmatrix} 1 \\ -1 \\ 0-1 \end{Bmatrix}[1 \quad -1 \quad -1](3{,}500)\begin{bmatrix} 1 & 0 & 0 \\ 0 & 1 & 0 \\ 0 & 0 & 1 \end{bmatrix} \\ c_1 &= 35.86 \times 10^6 \begin{bmatrix} 1 & -1 & -1 \\ -1 & 1 & 1 \\ -1 & 1 & 1 \end{bmatrix} \end{aligned} \tag{4.31}$$

Now, the total damping matrix, after superpositioning two modes, is given by

$$\begin{aligned} C &= C_1 + C_2 \\ [C] &= 10^6 \begin{bmatrix} 50.32 & -26.03 & -31.23 \\ -26.03 & 42.54 & 39.01 \\ -31.23 & 39.01 & 37.34 \end{bmatrix} \end{aligned} \tag{4.32}$$

Please note that the [C], as computed from the above method, implies that there is no damping in the third mode, as only first two modes are considered.

4.5 Evaluation of Damping from Experimental Results

Free vibration experiment is carried out to determine the natural frequency and damping coefficient of the setup. Establishing the natural frequency and damping of the system is one of the important steps in the experiments and will help to determine the dynamic characteristics of the system. For heave free vibration, a weight approximately 7 kg is placed carefully at CG location of the TLP model. The weight is removed quickly, and the resulting motions are recorded using accelerometers. A typical time history curve of the free vibration in heave direction is shown in Fig. 4.6. A small nudge is given to the TLP model in the surge direction, and the resulting motion is recorded. A time history plot of the free vibration in terms of surge acceleration is shown in Fig. 4.7. The black line in the figure is a 17-point moving average that depicts the variation of the surge acceleration without the high-frequency motions, making the overall surge variation and specifically the time period easier to identify.

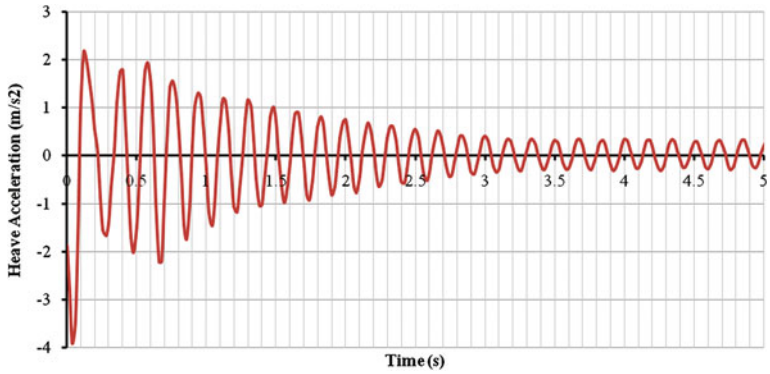

Fig. 4.6 Free vibration experiment—heave acceleration of model with perforated column

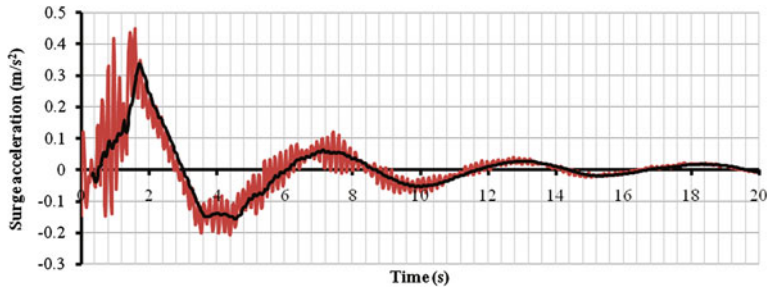

Fig. 4.7 Free vibration experiment—surge acceleration of model with perforated column

Table 4.1 Results of free vibration experiment

Description	TLP without perforated column	TLP with perforated column
Heave damped time period	0.17	0.18
Surge damped time period	4.68	5.61
Heave damping coefficient	0.014	0.02
Surge damping coefficient	0.148	0.251

Based on the results of free vibration tests carried out on the scaled model, natural period and damping coefficient in heave and surge mode are obtained from the time series shown in the above figures. Logarithmic decrement method is used to determine the damping coefficient. Results obtained are shown in Table 4.1 for the TLP with and without perforated columns. TLP with perforated columns shows higher damping coefficient and higher time period in comparison with that without perforated columns.

Exercise

1. What are the basic types of damping?
2. Explain Coulomb damping?
3. Explain viscous damping?
4. Structural Damping for steel is in the range of _____ and for that of concrete is _____.
5. Rayleigh damping can be mathematically represented as _____.
6. _____ is proposed for offshore structures.
7. If more than _____ are included in the Caughey series, [*C*] becomes a full matrix.
8. Free vibration experiment is carried out to determine the _____ and _____ of the setup.
9. _____ method is used to determine the damping coefficient.
10. TLP with perforated columns shows _____ and _____in comparison to that without perforated columns.

Answers

1. The basic types of damping are as follows: (i) coulomb damping and (ii) viscous damping
2. Coulomb damping results from sliding of two surfaces; it is also called dry damping or friction damping. The damping force is the product of the normal

force and the coefficient of friction between the body surface and the plane of motion. Note that the damping force in this case is independent of velocity of motion of the body which is under vibration.

3. Viscous damping, the damping force accounts for the viscosity of the system. The presence of fluid medium around the body significantly influences the damping force acting on the body. Damping force will be proportional to the magnitude of the velocity and has the unit of N/(m s). Viscous damping seems to be more relevant to offshore structural systems due to the inherent presence of liquid medium around the body.
4. 0.2–0.5 % and 0.5–1.5 %.
5. $C = a_0 M + a_1 K$
6. Rayleigh damping
7. Two terms.
8. Natural frequency and damping coefficient
9. Logarithmic decrement
10. Higher damping coefficient and higher time period

Chapter 5
Hydrodynamic Response of Perforated Offshore Members

Abstract This chapter deals with hydrodynamic response of perforated cylinders under regular waves through computational fluid dynamics (CFD). The chapter deals with a brief introduction of fluid–structure interaction (FSI) and wave–structure interaction. Variations in water particle kinematics along the depth when encountered by perforated members are discussed in detail as they find a lot of recent applications in the retrofitting and rehabilitation of offshore structural members.

Keywords Hydrodynamic response · Experimental studies · Perforated cylinders · Wave–structure interaction · Water particle kinematics · Retrofitting · Rehabilitation · Offshore structures · Tension leg platforms

5.1 Fluid–Structure Interaction

Fluid–structure interaction (FSI) plays an important role for structures placed in the path of flowing fluid. The presence of structure alters fluid flow field in its vicinity. Degree of compliance offered by the structure adds further complexity due to the reaction it offers to the excited force. Even though structures remain flexible (e.g., TLP) in certain degrees of freedom, dynamics becomes important. It is not their deformation capacity that is looked upon in this context. FSI becomes more important when the flow is steady flow, may be in the form of current or a vertical shear. But in real sea state, structures experience large oscillating forces in the flow direction. When structures are placed in the flowing fluid, the flow pattern is altered. Restraints are developed in the fluid medium to maintain the position of the structure. Forces acting on the structures in fluid medium shall be classified as drag (acting in-line with the direction of flow) and lift (transverse to the direction of flow). Further, drag force can be classified as higher and smaller frequency components. These components will be functions of the geometry of the structure and flow conditions. Lift forces contain oscillatory components with multiple

S. Chandrasekaran, *Dynamic Analysis and Design of Offshore Structures*,
Ocean Engineering & Oceanography 5, DOI 10.1007/978-81-322-2277-4_5

Table 5.1 Flow regimes in uniform flow

Flow region	Re range	Flow condition	Forces on cylinder
Laminar	0–40	No separation of flow	Drag forces occurring in the direction of flow
Subcritical	40–5E05	Broken stream lines	Lift forces depend on Strouhal number
			Steady drag force + smaller oscillating drag forces at double the frequency of lift force
Supercritical	5E05–7E05	III-defined vortices	Drag forces decrease rapidly
			Lift and drag forces will be seen at higher frequencies
Transcritical	>7E05	Vortices will be persistent	Similar to subcritical range
		Turbulent flow due to randomness in fluid viscosity	

frequencies. On the downstream side, flow will return to its unaltered condition. This is due to fluid viscosity and damping. The region of altered flow directly behind the structure is called *wake region*. In the wake regions, there will be one-to-one relationship between the extent of wake region and restraint loads. This implies that in the wake region, frequency content is determinant and is same as that of the restraint loads, which enables the determination of FSI in a closed form.

The data shown in Table 5.1 represent the case for cylinder whose axis is normal to the flow direction. Flow is without turbulence and boundary effects.

5.2 Vertical Cylinders in Uniform Flow

Vertical cylinders experience loading from the flowing fluid, and the FSI will be defined by Reynolds number for cylinders that are infinitely long, smooth, and fixed. Cylinder roughness and fluid turbulence reduce boundary value on either side of supercritical region. If the length of the cylinder is finite, this will introduce 3D aspect to the flow. Ends of cylinder will affect drag and lift coefficients; they are also dependent on the location of the cylinder. Vortex shedding pattern will also be affected (Table 5.2).

5.3 Flow in Deep Waters

In deep waters, flow is not uniform with depth and results in positive shear. Velocity will be greater than that near the surface. When vertical cylinder is in shear flow condition, 3D flow regime will occur. Under positive shear, wake region

Table 5.2 Reduced velocity range

Flow region	Reduced velocity	Vortex shedding	Types of vibration caused
I	1.7–2.3	Symmetric shedding	In-line oscillation only
II	2.8–3.2	Alternate shedding of vortices	Predominantly in-line vibrations
			Some transverse vibrations are also seen
III	4.5–8.0	Alternate shedding of vortices	Predominantly transverse vibration
			In-line vibrations are seen at frequency twice as that of the transverse vibration
			This is called *figure eight motion*

Source Humphries and Walker (1987)

experiences vertical upward flow. Variation in stagnation pressure causes downward flow along the length. The flow is *sheared* from upstream to downstream. There is downward flow on the U/S side and upward flow on the D/S side, as shown in Fig. 5.1.

The shear flow effect reduces the pressure coefficient at the top of the cylinder and increases the coefficient at the bottom. The pressure coefficient also changes with the strength of shear. In uniform flow, vertical cylinder will show vortices at the same frequency over its entire length, whereas in shear flow, frequency changes continuously.

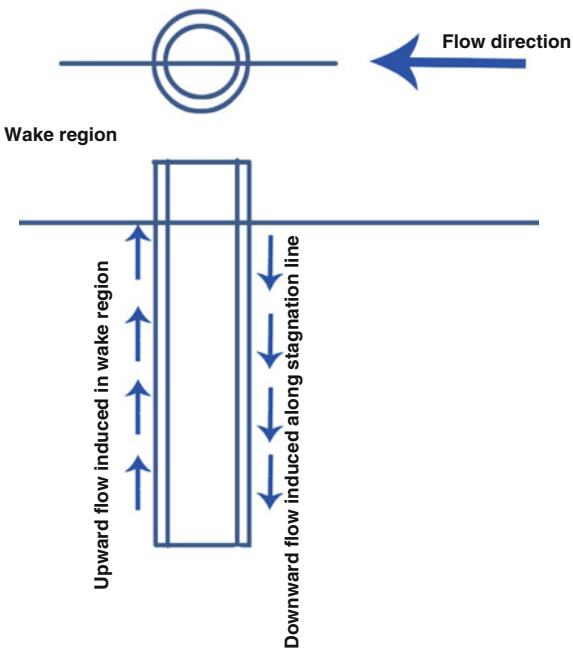

Fig. 5.1 Flow in deep waters

5.4 Horizontal Cylinder in Uniform Flow

Examples of horizontal cylinders are subsea pipelines, members of floating break waters, pontoons, etc. These members will be influenced by current and waves. Under uniform flow field, horizontal cylinder will generate waves near upper boundary (free surface). Wave resistance depends upon Froude number.

$$\text{Froude number } F_r = U_2/(2gy_1)$$

Y_1 is the depth of immersion, measured from the axis of the cylinder to free surface. When $Y_1 \gg$ radius, maximum wave resistance will occur, and minimum will occur when $F_r < 0.375$. Boundary effects and end effects of the cylinder introduce 3D effect in the flow past the cylinder of finite length. The major difference between horizontal and vertical cylinder is the appearance of lift force. When horizontal cylinder is located near boundary, flow will become unsymmetrical. Lift force will become a function of cylinder diameter and distance to the boundary. Horizontal cylinders will also be subjected to flow-induced vibrations.

5.5 Horizontal Cylinder in Shear Flow

Under shear flow, velocity variation across the face of the structure will be significant. Ratio of turbulence to velocity variation across horizontal cylinder is higher than that of a vertical cylinder. For increase in shear parameter, Strouhal number increases because of increase in vortex shedding frequency. With a fixed horizontal cylinder, load at a given velocity for a positive shear is more than that of uniform flow. At free surface, vertical load in both positive and negative shear increases significantly in comparison with uniform flow. Dynamic vertical loads on the cylinder at mid-depth under positive and negative shear contain higher energy at high frequencies. Near the surface, there is significant reduction. Horizontal cylinder at free surface suppresses eddy shedding and wake formation. Steady component of vertical load increases significantly for horizontal cylinder at free surface.

5.6 Blockage Factor

Closely spaced members, connected in different orientations, cause distortion in the fluid field around them. For closely spaced members, the structure becomes dense. For dense structures, flow field slows down as it travels through the structure. This causes blockage effect and complicates the actual velocity field around the structure. Load on the structure increases due to this blockage. Drag force is summed for each member in the dense structure. In case of group of vertical cylinders present in the flow field, blockage factor CBF = 0.25 S/D (for $0 < S/D < 4.0$) = 1.0 for $S/D = 4.0$, where S is c/c distance of the cylinder and D is diameter.

5.7 Wave–Structure Interaction (WSI)

When waves past cylinder, it causes oscillating in-line force on the cylinder. In addition, free surface also changes in case of a submerged cylinder. Large structures placed in wave field alter incident waves in its vicinity. If the dimension of the structure is large compared to the wave length, flow remains attached to the structure. When waves pass a cylinder, it causes oscillating in-line force on the cylinder. In addition, free surface also changes in case of a submerged cylinder. Several procedures can be used to explain the potential function generated in the vicinity, knowing the incident wave potential. Flow around the structure is assumed to remain attached. Separation is neglected and the fluid is assumed to be incompressible and irrotational, and structure is assumed to be rigid. Wave amplitude is assumed to be small. Fluid flow in the neighborhood is described by velocity potential. Velocity potential under linear theory is given by:

$$\Phi = \varphi \, \mathrm{e}^{(-i\omega t)} \tag{5.1}$$

where φ is spatial part of total velocity potential and ω is incident wave frequency. Total potential is the sum of potential of incident wave component and potential of scattered wave component. Scattered wave component is normally represented by continuous distribution of waves. It is assumed as superposition of numerous waves. Boundary value problem, defined in terms of Laplace partial differential equations, is transformed into original partial differential equations, in potential theory. Boundary condition includes ocean floor, free surface, submerged surface of the structure, and radiation condition, as flow approaches infinity.

5.8 Perforated Cylinders

5.8.1 Wave Forces on Perforated Members

Several analytical studies are reported in the literature highlighting the wave forces on porous bodies. Wang and Ren (1994) are one of the earliest to study wave interaction with a concentric surface-piercing porous outer cylinder protecting an impermeable inner cylinder. Free-surface elevation, net hydrodynamic forces, and wave-induced overturning moments on both cylinders are examined. Based on the analytical investigations carried out, it is seen that inner cylinder experienced more forces from long-period waves in comparison with that from short-period waves with decrease in annular spacing between the outer perforated cylinder and inner cylinder. Results showed that the existence of exterior porous cylinder reduces hydrodynamic force on the inner cylinder. Cylindrical breakwater is porous in the vicinity of the free surface and impermeable at some distance below the free surface; significant reduction is reported in wave field and hydrodynamic forces experienced by the inner cylinder (William and Li 1998). Interaction of waves with arrays of bottom-mounted,

surface-piercing circular cylinders is investigated through numerical studies (Williams and Li 2000). It is shown that the porosity of the structure results in a significant reduction in both the hydrodynamic loads experienced by the cylinders and the associated wave run-up. William et al. (2000) investigated the interaction of waves and free-floating circular cylinder with porous side walls. The porous region is bounded on top and bottom by impermeable end caps, which resulted in an enclosed fluid region within the structure. It is found that the permeability, size, and location of the porous region have a significant influence on the horizontal component of the hydrodynamic excitation and reaction loads, while their influence on the vertical components is relatively minor. Neelamani et al. (2002) carried out experimental investigations of seawater intake structure consisting of a perforated square caisson encircling a vertical suction through physical model studies. They found that the ratio of force on perforated caisson to the force on caisson with 10 % porosity is reduced to a maximum of 60 % with increase in the porosity of the caisson from 1.6 to 16.9 %. This ratio is found to increase with the increase in relative wave height and decrease with increase in relative width. Neelamani and Muni (2002) examined wave forces on a vertical cylinder protected by vertical and inclined perforated barriers; numerical studies showed that there is a significant reduction in forces on the vertical cylinder due to perforated barriers.

Song and Tao (2007) studied 3D short-crested wave interaction with a concentric porous cylindrical structure. It is recommended that porous effect should be chosen lesser than 2 in order to provide meaningful protection to the interior cylinder from the wave impact. Vijayalakshmi et al. (2008) carried out experimental investigations on perforated circular cylinder encircling an impermeable cylinder at a constant water depth for regular and random waves. Porosity of the outer cylinder is varied from 4.54 to 19.15 % to study its influence on variations in wave forces in the vicinity of the chosen twin-cylinder system. Numerical method is developed on the basis of the application of boundary integral equation on a porous body with appropriate boundary conditions; porosity is modeled using the resistance coefficient and added mass coefficient for regular waves. It is seen that the resistance coefficient increased with the increase in porosity and wave height except for a porosity of 4.54 %; added mass coefficient is almost negligible. Based on the experimental results, porosity of 10–15 % is recommended to have significant effect on force reduction. Sankarbabu et al. (2007) investigated the influence of hydrodynamic wave forces on a group of cylinders, wave run-up, and free-surface elevation in their vicinity. Results showed that the forces on inner cylinders are reduced in the presence of an outer porous cylinder when compared to that of the direct wave impact. Sankarbabu et al. (2007) investigated the hydrodynamic performance of a dual cylindrical caisson breakwater (DCBW) that is formed by a row of caissons; these caissons consist of porous outer cylinder circumscribing an impermeable inner cylinder. Based on the analytical studies carried out, it is seen that an optimum ratio of radius of inner cylinder to the outer exists as 0.5 for a satisfactory hydrodynamic performance of the DCBW; it shows improved stability and wave transformation in its vicinity. Further, they concluded that the influence of porosity on the variation of forces, run-up on the caissons, and the surface elevation

in the vicinity of the DCBW are found to be significant up to a value of 1.0; any further increase in this value results in lesser variation of the above parameters. Zhao et al. (2009) studied the interaction of waves and a porous cylinder with an inner horizontal porous plate; effects of porosity and position of the inner plate are investigated. It is shown that increase in porosity reduces wave exciting forces and efficiency of wave dissipation; inner plate eliminates the sloshing mode in surge and pitch degrees of freedom. The arrangement is recommended for effective wave energy dissipation when located at still water surface.

5.8.2 Wave Forces on Offshore Structures with Perforated Members

Ker and Lee (2002) examined the coupling problems associated with wave–structure interaction (WSI) of linear waves and porous tension leg platform (TLP), analytically. They found that the drag force in the porous body changes the response behavior of TLP significantly; at resonance frequencies, this change is significant. They also found that for long-period waves, porous TLP remains relatively transparent and is similar to that of an impermeable one, while it dissipates most of the wave energy for short-period waves. Zhong and Wang (2006) carried out analytical studies on solitary waves interacting with surface-piercing concentric porous cylinders. It was found that the hydrodynamic forces on inner cylinder increase and that of the exterior cylinder decrease with the decrease in the annular spacing. Forces on a single porous cylinder are reduced significantly in comparison with that of an impermeable cylinder of the same diameter. Further, it is also shown that for larger porosity of the outer cylinder, larger hydrodynamic forces are encountered on the inner cylinder and lesser on the outer cylinder. Existence of exterior porous cylinder reduces hydrodynamic force on the interior cylinder. Vijayalakshmi et al. (2007) verified this fact through experimental investigations by measuring wave forces and run-up on the twin, concentric perforated cylinders; results are compared with those predicted by the boundary integral method and found satisfactory. Porous effects on thin permeable plates are well quantified by Li et al. (2006); predicted values of porous effects of reflection and transmission coefficients that are estimated using analytical model are validated with experimental results. Jayalekshmi et al. (2010) investigated the dynamic response of a TLP under random waves and the effect of riser dynamics on platform behavior; an in-house finite element code is developed by the authors to perform the analysis. A random sea state is generated using the PM spectrum. Water particle kinematics is calculated using Airy's linear wave theory, and the load is evaluated using the relative form of the Morrison equation; variable submergence and current forces are also taken into account.

Adrezin et al. (1996) carried out dynamic analysis of complaint offshore structures and reiterated the fact that coupled motion analysis induces significant response in all active degrees of freedom of TLP under linear waves. Kim et al. (2007) discussed various nonlinearities associated with the analysis of TLPs under

regular waves; the effect of these nonlinearities on the dynamic response and various strategies to solve the equation of motion for the fully coupled dynamic analysis are discussed in detail (Chakrabarti 1984, 1987, 1994). Zeng et al. (2007) conducted parametric studies of TLPs with large amplitude motion. Dynamic response predicted by linear and nonlinear models are compared; they showed that the nonlinear responses of TLP, considering the effects induced by large amplitude motions, differ from that of the linear model, significantly. Two different approaches for response calculations are compared with wave approach angle as one of the primary factors in the parametric study. Kurian et al. (2008) conducted parametric studies on TLPs under random waves. Authors used PM spectrum, Airy wave theory, relative form of Morrison equation, and Newmark-Beta time integration scheme to obtain the response in time domain. Mass, damping and stiffness matrices that are required to calculate the response are derived from the literature (Chandrasekaran and Jain 2002; Chandrasekaran et al. 2004). Although coefficients used in the process of determining response are on the basis of recommendations made by other authors, both numerical and experimental investigations carried out by the authors are considered valid due to a close comparison of the same. Studies are also carried out by researchers to illustrate the influence of wave approach angle on the response of TLP in regular sea (Chandrasekaran et al. 2007; Kim et al. 2007). Numerical studies carried out on triangular TLP under a variety of wave approach angles showed that nonlinear Stokes's fifth-order wave theory is well suited for deep-sea structures such as TLPs to estimate dynamic response. Significance of other nonlinearities caused by change in tether tension and variable submergence effect is on the dynamic response of TLPs are also highlighted in the studies. Experimental studies carried out on the response analysis of TLPs showed the scale effect on the response quantities; variations between the analytical and experimental results are attributed to the boundary effect on the scaled model during experiments (Joseph et al. 2004).

5.8.3 Critical Review

A detailed review of the literature on wave interaction on porous cylinders is presented. Influence of porous region on the forces experienced by inner cylinder in the presence of perforated outer cover is highlighted. Both experimental and analytical studies carried out by various researchers show a common agreement of significant force reduction on the inner cylinder with perforated outer cover. Several studies highlighting the dynamic response of offshore TLPs under regular and random waves are also discussed; various nonlinearities associated with the response behavior of TLPs under waves are presented. Few experimental investigations carried out on dynamic response of TLP with perforated members are also discussed. It is seen from the above review that experimental investigations on dynamic response of TLPs with perforated outer cover are scarce in the literature; hence, the current research study justifies the defined objectives.

5.9 Experimental Investigations on Perforated Cylinders

Perforated cylindrical structures reduce WSI and scouring problems considerably. Existence of exterior porous cylinder reduces the hydrodynamic forces on inner cylinder caused by the direct wave impact. It is seen from the literature that for reduced annular spacing, long waves impose larger forces on the inner cylinder than the short waves. Based on the experimental investigations carried out, researchers recommended porosity of about 10–15 % beyond no appreciable reduction in hydrodynamic response is seen. Preliminary experimental investigations are carried out to study the hydrodynamic response of perforated cylinders in regular waves. Variations of forces due to regular waves in a cylinder, with and without perforated cover, are measured. Experimental setup for the study is shown in Fig. 5.2. To evaluate the influence of porosity and diameter of perforations, three scaled models comprising outer cylinder of 315 mm diameter and inner impermeable cylinder of 110 mm in diameter are fabricated with uniform annular space. Steel frames are used for clamping the inner cylinder and the outer cylinder in the wave flume; model is suspended with a clear gap of about 50 mm above the seafloor, ensuring a cantilever action. Strain gauges are placed along the inner cylinder to determine the forces. Regular waves of height ranging from 5 to 25 cm for time periods of 1–2 s are generated for the tests.

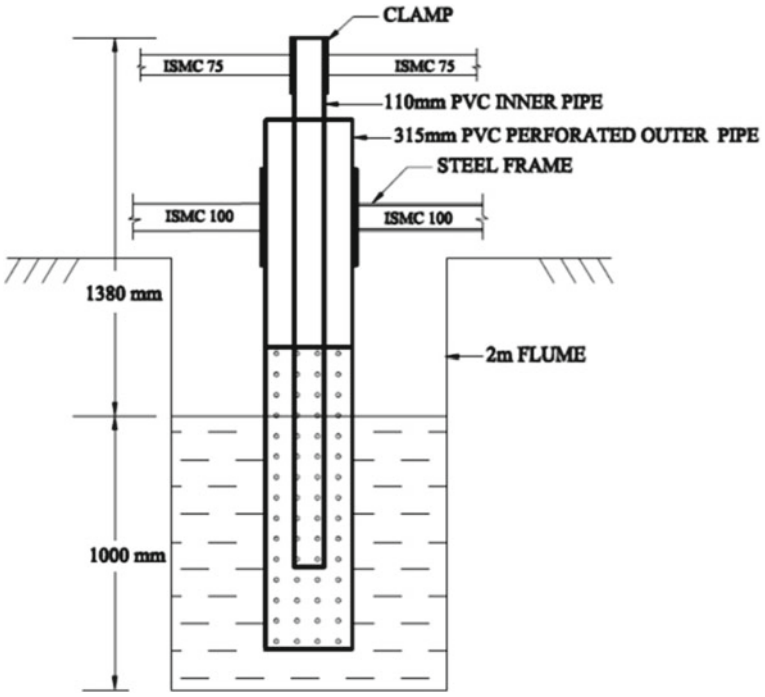

Fig. 5.2 Experimental setup to study response on perforated cylinder

Details of the inner and outer cylinders used for the study are given in Table 5.3. Diameter of perforations and length of perforations are varied to achieve different porosity ratios. Perforation ratios are in compliance with the Indian Standard Code of Practice IS 4985:2000. Figure 5.3 shows the inner and outer cylinders with different perforations; details of strain gauges affixed on the inner cylinder can also be seen.

Inner cylinder is fixed at one end, and the other end is set free to enable the cylinder to behave similar to that of cantilever beam. Known bending stresses are created by applying point load at a constant distance of 50 mm from the free end. Bending strain in the inner cylinder, with and without perforated outer cylinders, is measured during the passage of regular waves. Regular waves with wave heights 5–25 cm in the intervals of 5 cm and wave periods of 1–2 s in the intervals of 0.2 s are considered in the study. Bending strains are post-processed to determine hydrodynamic forces on the inner cylinder; their variations along its length are also studied. Maximum values of hydrodynamic forces computed on the inner cylinder encompassed by outer cylinders with different porosity are measured; a typical

Table 5.3 Geometric details of cylinders considered for the study

Description	Inner cylinder	Outer cylinder		
		A	B	C
Diameter (mm)	110	315	315	315
Thickness (mm)	4.4	8.7	8.7	8.7
Perforation diameter (mm)	–	10	15	20
Length of the cylinder (mm)	1,900	1,930	1,930	1,930
Length of perforations (mm)	–	1,450	1,050	1,050
No. of perforations along length	–	41	26	24
No. of perforations along circumference	–	28	24	24
Porosity (%)	–	6.3	10.6	16

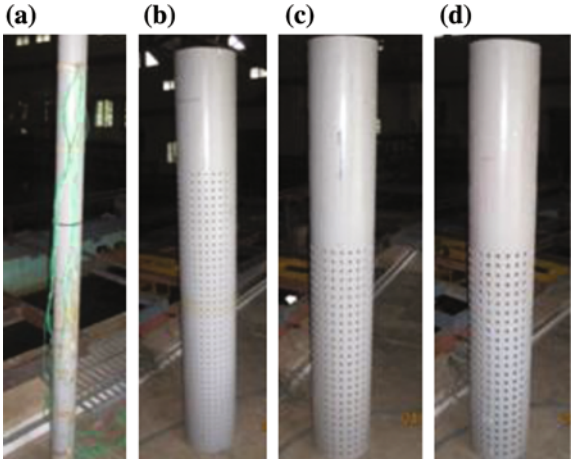

Fig. 5.3 Perforated cylinders considered for the study: **a** inner cylinder; **b** outer cylinder (A); **c** outer cylinder (B); and **d** outer cylinder (C)

Table 5.4 Hydrodynamic forces for 25 cm wave height (N)

Wave period (s)	Inner cylinder	Outer cylinder		
		A	B	C
1.2	24.77	5.80	9.07	12.53
1.4	20.17	5.26	7.69	9.67
1.6	17.19	4.05	6.05	8.83
1.8	16.84	4.00	7.42	9.51
2.0	15.29	4.93	6.22	9.19

value for 25 cm wave height is given in Table 5.4. It can be seen that force reduction decreases with increase in porosity as the inner cylinder shall be exposed to more hydrodynamic load due to increased porosity. Further, force on the inner cylinder decreases significantly for short-period waves compared to long-period waves.

Figures 5.4 and 5.5 show the force variation in inner cylinder, encompassed with outer cylinders with different porosities; the plots are drawn for different wave heights varying from 5 to 25 cm, respectively. Wave periods are selected appropriately with respect to the cylinder diameter so that the model remains in Morison regime. It is seen from the figures that force variation in the inner cylinder is nonlinear; decrease in wave force is not proportional to increase in time period and wave height as well.

The model investigated is built to a scale of 1:140, and the force reduction corresponding to the prototype cylinders with different porosities is shown in Table 5.5.

Based on the experiments conducted, it is seen that hydrodynamic forces on the inner cylinder decrease with the decrease in porosity. This reduction in the forces is significant for short-period waves when compared to long-period waves; variation

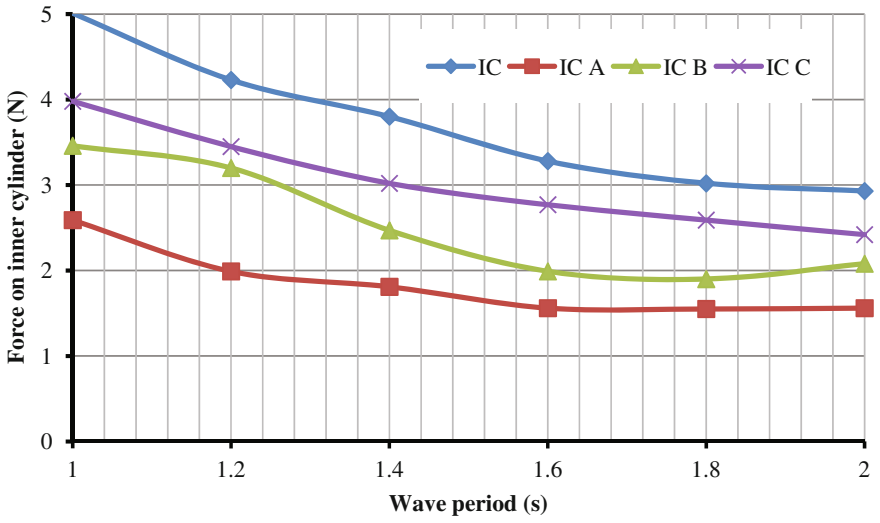

Fig. 5.4 Force variation in cylinders (WH = 5 cm)

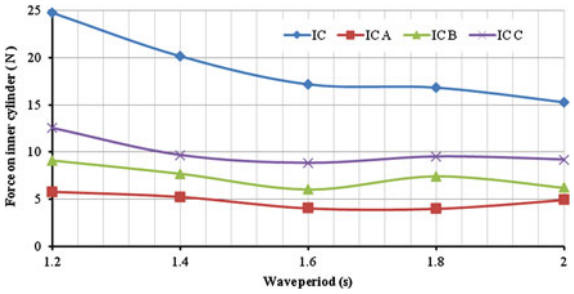

Fig. 5.5 Force variation in cylinders (WH = 25 cm)

Table 5.5 Force reduction in inner cylinder

S. No.	Description	Model (1:140)	Prototype
1	Water depth (m)	1.0	140
2	Diameter (inner cylinder)	0.11 m	15.4 m
3	Force reduction (H = 25 cm; T = 1.2 s)		
	With outer cylinder A	18.97 N (76.59 %)	52.05 MN
	With outer cylinder B	15.70 N (63.38 %)	43.08 MN
	With outer cylinder C	12.24 N (59.63 %)	33.58 MN
4	Force reduction (H = 5 cm; T = 2 s)		
	With outer cylinder A	1.37 N (35.54 %)	4.62 MN
	With outer cylinder B	0.85 N (29.02 %)	2.86 MN
	With outer cylinder C	0.51 N (17.41 %)	1.72 MN

is nonlinear and is not proportional to either the increase in wave height or wave period. The size of perforations and porosity influences hydrodynamic forces on cylindrical members significantly. It is also seen that the maximum force reduction is about 76 % and minimum is about 17 %. Presented study highlights the advantages of deploying perforated cylinders as outer cover on the impermeable inner cylinders. This has direct application of force reduction on the inner cylinders; though the application is not desired for new design, but recommended as an alternative method of retrofitting of offshore structures. The derived conclusions, based on the experiments conducted, emphasize the known concept of force reduction on inner cylinders; the study quantifies the values for different porosities and size of perforations, which can be seen as an original contribution to the design of offshore structures with perforated members.

5.10 Experimental Investigations on Perforated TLP Model

The pilot study of the present project is focused on detailed experimental investigations carried out on impermeable inner cylinder encompassed by a larger outer cylinder with perforations along its length. By varying the porosity and diameter of perforations, their influence on the hydrodynamic response of the cylindrical member is examined. As an extended concept of the study, offshore TLPs with perforated members are experimentally investigated. Offshore TLPs are hybrid structures whose heave motion is highly damped, posing operational advantages; however, large surge, sway, and yaw motions cause inconvenience to people on board though the platform remains stable for operational sea state. In order to reduce the wave impact on pontoons and cylindrical members of TLPs, perforated cylinders shall be used as an outer cover to the members at highly stressed regions. It is one of the practical techniques to retrofit offshore coastal and offshore structures and also to improve their structural safety. In this present experimental study, a 1:150 scale model of a prototype TLP is fabricated with and without perforated outer column. Dynamic response in various active degrees of freedom and tether tension variations are studied under the regular waves of different time period and wave heights. Details of the model are given in Table 5.6. Figure 5.6 shows the views of the TLP model considered for the study.

Table 5.6 Details of TLP model

Description	Notation	Units	Prototype TLP	Model (1:150)
Water depth	D	m	450	3
Material			Steel	Acrylic sheet
Unit weight of the material	ρ	kg/m^3	7,850	1,200
Side of the deck	S	m	70	0.47
Diameter of each leg	d	m	17	0.1
Draft	T	m	32	0.21
Total buoyancy	FB	kN	521,600	0.153
Self-weight of TLP + payload	W	kN	351,600	0.104

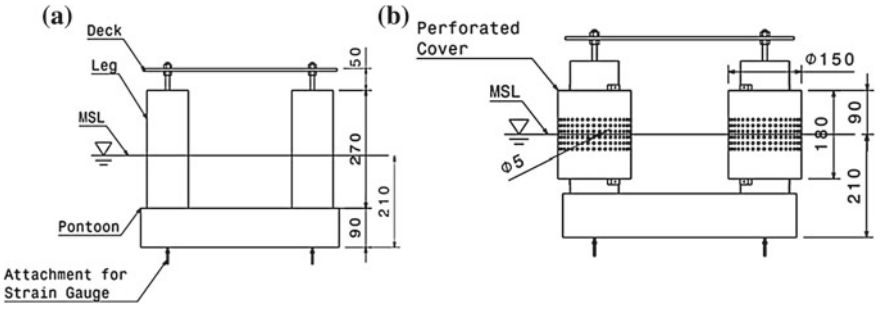

Fig. 5.6 Front view of TLP model: **a** without perforated cover; **b** with perforated cover

Table 5.7 Comparison of mass of acrylic and aluminum perforated covers

Part	Weight (kg)	Weight of cover (as percentage TLP) (%)
TLP without perforated cover	9.04	–
Perforated cover (acrylic)	2.48	27.4
Perforated cover (aluminum)	0.69	7.6

The outer perforated column is 150 mm in diameter with a height of 180 mm. The middle third portion of the outer column is perforated with holes of 5 mm diameter spaced at 12-mm intervals, resulting in a porosity of 13.5 %; outer column is connected to the inner column through a 10-mm thick ring to maintain the required annular space. A reasonable comparison is possible through the attempted study as the static characteristics such as mass and the center of gravity (KG) of the model remain nearly the same irrespective of the presence of the perforated cover. Table 5.7 shows the comparison of mass of acrylic and aluminum perforated covers. Figure 5.7 shows the experimental setup of the current study.

Free-vibration tests are carried out to determine the natural frequency and damping coefficient of the model. Figures 5.8 and 5.9 show the surge and heave acceleration of the free-vibration tests of the model with perforated cover (PC); Table 5.8 shows the results of the test. Establishing the natural frequency of the system will help to determine the range of the wave periods.

The model was subjected to waves in the head sea direction whose time periods are varied in the range of 0.8–2.4 s; wave heights are varied in the range of 5–9 cm. Figures 5.10, 5.11, and 5.12 show the response of TLP model in surge and heave degrees of freedom and tether tension variation, respectively.

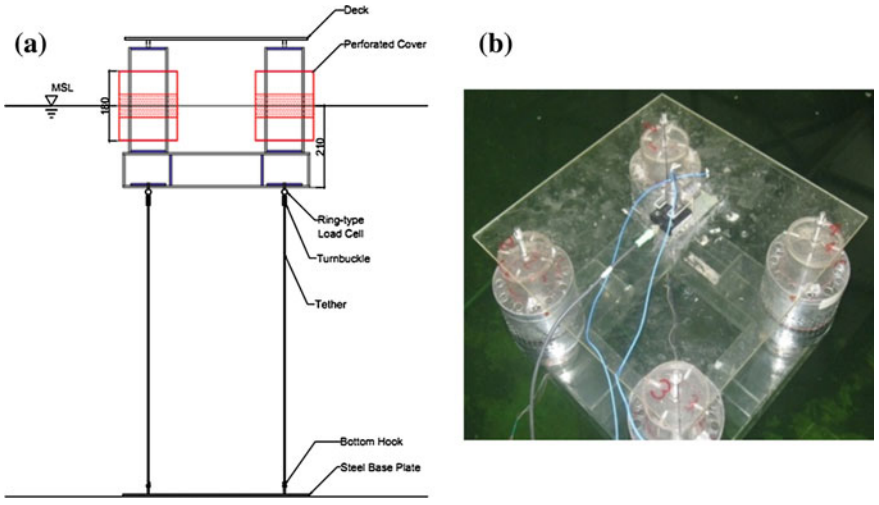

Fig. 5.7 Experimental setup: **a** components of the model; **b** instrumentation

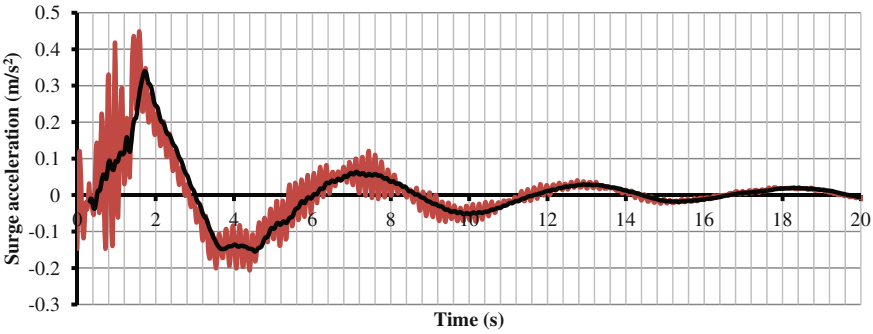

Fig. 5.8 Free surge acceleration with PC

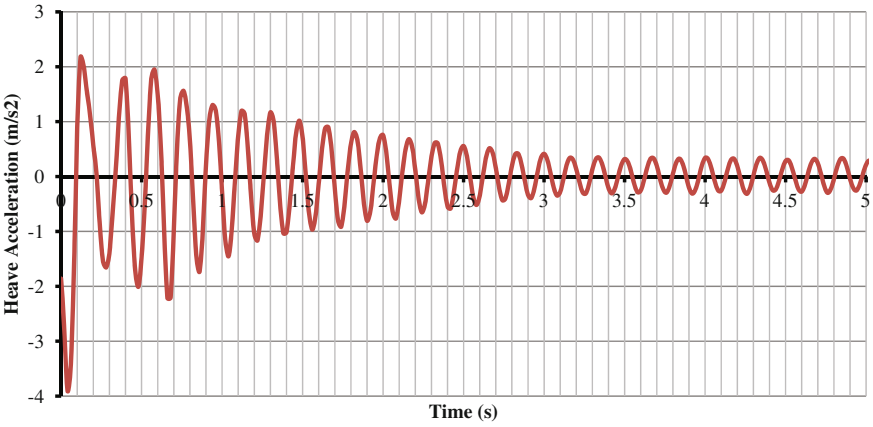

Fig. 5.9 Free heave acceleration with PC

Table 5.8 Results of free-vibration experiment

Description	TLP without PC	TLP with PC
Heave damped time period	0.17	0.18
Surge damped time period	4.68	5.61
Heave damping coefficient	0.014	0.02
Surge damping coefficient	0.148	0.251

It is seen that response of TLP is reduced in the presence of outer perforated cover. Tether tension variation also shows significant reduction in the presence of outer perforated cover. Hydrodynamic response on TLPs with outer perforated covers is also investigated for different wave approach angles. Table 5.9 shows the average

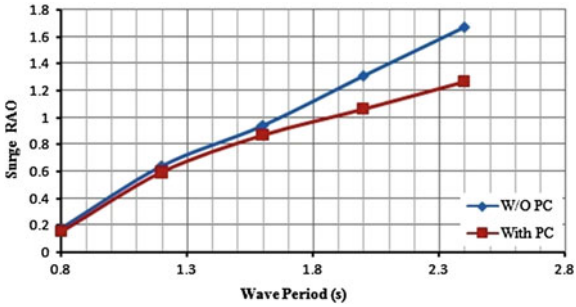

Fig. 5.10 Surge RAO for 7-cm wave

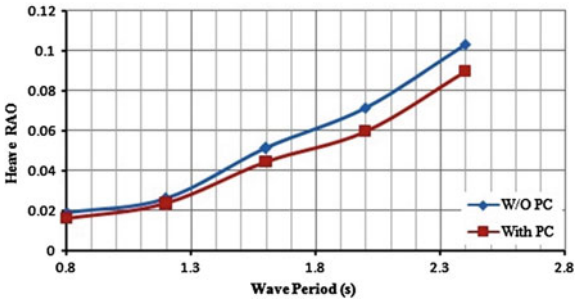

Fig. 5.11 Heave RAO for 7-cm wave

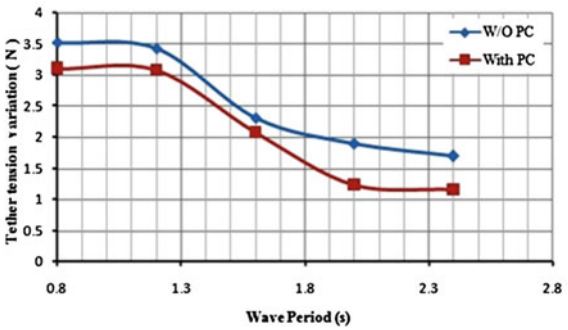

Fig. 5.12 Tether tension variation for 7-cm wave

Table 5.9 Average surge response reduction

Wave period (s)	Average response reduction (%)
0.80	13.35
1.20	7.07
1.60	6.78
2.00	18.01
2.40	24.84

reduction in surge response for different wave periods; the maximum response reduction seen is about 24 % due to the presence of outer perforated cylinders.

Presented study highlights the advantages of deploying perforated column members for TLP as outer cover on the impermeable inner cylinders. This has direct application of force reduction on the inner cylinders; though the application is not desired for new design, but recommended as an alternative method of retrofitting of offshore structures.

5.11 Numerical Studies on Perforated Cylinders

Numerical studies on perforated cylinders are carried out through simulation in STAR-CCM+ software. An attempt is made to simulate the hydrodynamic response of perforated cylinder with porosity 6.3 %, which is similar to that of perforated outer cylinder, designated as A in the experimental studies. Simulation through STAR-CCM+ software is chosen due to the numerical capabilities enabled in different modules to simulate viscous drag and turbulence effects that are caused by perforations. Details of the simulation, as attempted through several stages of the numerical modeling, are discussed in steps; various settings such as mesh and physics models used in the study and their significance are also presented.

5.11.1 Development of the Numerical Models

A model of the perforated cylinder is CATIA V5. Figure 5.13 shows the model of the perforated outer cylinder generated in the software. Table 5.10 shows the details of both inner and perforated outer cylinder, while Table 5.11 shows the details of the perforations. Using 'Pocket' tool, perforations are created along the circumference and length of the outer cylinder using 'Circular pattern' and 'Rectangular pattern' tools, respectively. Figures 5.14 and 5.15 show images of outer perforated cylinder and the assembly of inner with perforated outer cylinder, respectively.

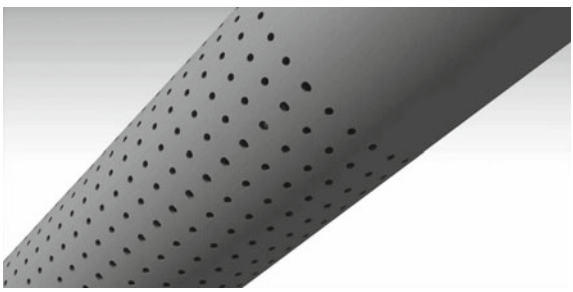

Fig. 5.13 Perforated outer cylinder

Table 5.10 Details of cylinders

Details of cylinders	Inner cylinder (mm)	Outer cylinder A (mm)
Diameter	110	315
Length	1,900	1,930
Thickness	4.4	8.7

Table 5.11 Details of perforations

Details of perforations	Outer cylinder A
Diameter of the perforation	10 mm
Length of perforation	1,450 mm
Number of perforations along the length	41
Number of perforations along the circumference	28
Porosity	6.3 %

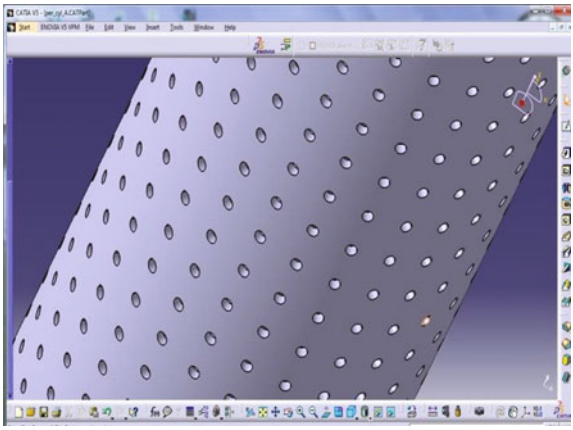

Fig. 5.14 Perforations along the circumference and length (Chandrasekaran et al. 2014)

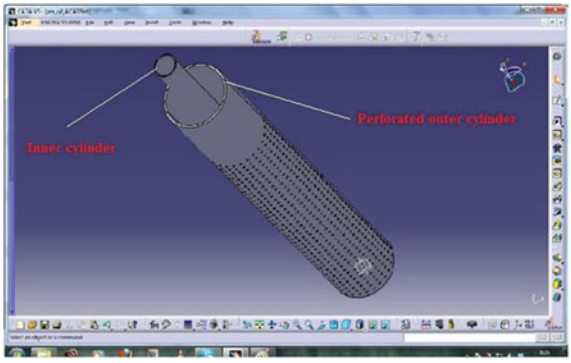

Fig. 5.15 Inner cylinder with perforated outer cylinder

Two different geometries, namely (i) inner cylinder and (ii) inner cylinder with perforated outer cylinder, are exported from CATIA V5, and new simulations are generated in STAR-CCM+ from the imported files. Figures 5.16 and 5.17 show the mesh generation of inner cylinder and inner cylinder with perforated outer cover, respectively; distribution of elements attained using the chosen volume control makes the mesh denser in the fluid region, as can be seen from the figures.

Subsequently, 'Generate volume mesh' tool is used to generate the mesh; 716,801 cells and 2,167,056 faces are generated for simulation of the inner cylinder, while 3,242,875 cells and 9,671,484 faces are generated for that of the inner cylinder with perforated outer cylinder, which is a fairly dense mesh. Several physics models are activated to simulate the wave forces on both the numerical models of inner cylinder and inner cylinder with perforated outer cylinder. A total of 16 physics models are used in the present simulation and activated. A new first-order wave is created under the 'Waves' child node of the 'VOF Waves' node in the list of chosen physics models. The 'Point on Water Level' is set to 0.54 m for the simulation of inner cylinder and 0.8825 m for the simulation of inner cylinder with

Fig. 5.16 Domain of inner cylinder generated with volumetric control (Chandrasekaran et al. 2014)

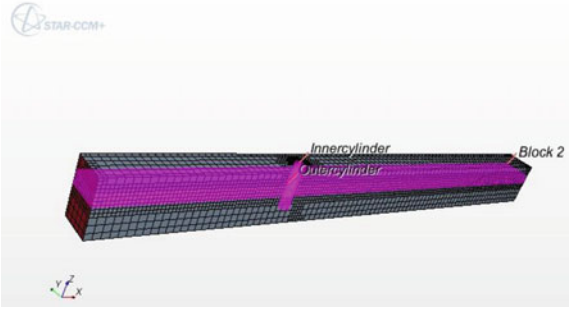

Fig. 5.17 Domain of inner cylinder with perforated outer cylinder generated with volumetric control (Chandrasekaran et al. 2014)

perforated outer cylinder; the chosen values also match the relevant values used in the experimental investigations. Wave amplitude is set to be 0.05 m. Specification type is set to 'Wave period' and numerical simulations are run for six waves for each model, for wave periods of 1.0–2 s with an interval of 0.2 s. The 'Volume Fraction' is set to composite, and the method of each of the phases, water and air, is set to 'Field Function.' Boundaries in the region are set to match various types of boundary conditions, namely (i) 'Inlet' boundary is set as a velocity inlet; (ii) 'Outlet' boundary is set as a pressure outlet; and (iii) 'Inner cylinder' and 'Outer perforated cylinder' are set as wall boundaries. The 'Velocity Specification' method in the velocity inlet is changed to 'Components', and the 'Velocity' and 'Volume Fraction' values are set identical to the experimental setup. Similarly, the 'Volume Fraction' and 'Pressure' settings of the pressure outlet are also set accordingly. The 'Time-Step' property of the 'Implicit Unsteady' solver is set to 0.01 s. Under the 'Stopping Criteria', the 'Maximum Inner Iterations' property is set to 10, and the 'Maximum Physical Time' is set to 10 s. The 'Initialize Solution' tool is selected to activate the required simulation. An iso-surface with an iso-value of 0.5 and a scalar set to 'Volume Fraction > Water' is used to visualize the free surface. Scalar is used to visualize both the inner cylinder and inner cylinder with perforated outer cylinder as shown in Figs. 5.18 and 5.19, respectively.

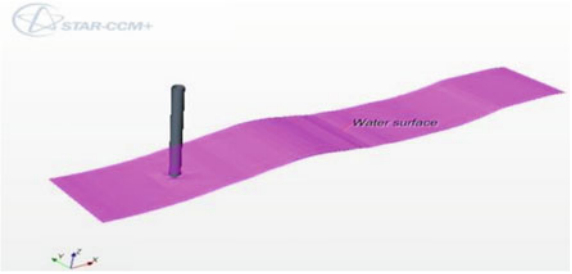

Fig. 5.18 Simulation of inner cylinder (Chandrasekaran et al. 2014)

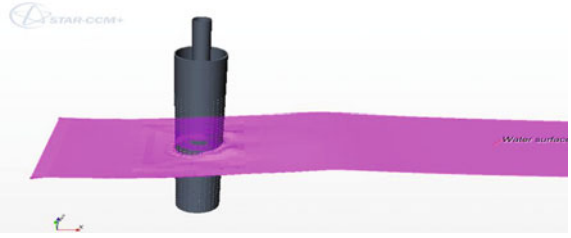

Fig. 5.19 Simulation of inner cylinder with perforated outer cylinder (Chandrasekaran et al. 2014)

Both the simulated models, namely inner cylinder and inner cylinder with perforated outer cylinder, are subjected to unidirectional waves of 10 cm wave height. Wave periods are varied from 1 to 2 s with 0.2 s interval; Reynolds-Averaged Navier–Stokes equation is solved, which is assumed to be converged when the residuals decrease by multiple orders before settling around 0.001. Figures 5.20 and 5.21 show the variation of forces on inner cylinder with and without perforated outer cover, respectively, for wave height of 10 cm and wave periods ranging from 1 to 2 s.

Forces on inner cylinder with and without perforated outer cylinder are obtained from the numerical simulation for 10 cm wave height and wave periods ranging from 1 to 2 s; obtained results are shown in Tables 5.12 and 5.13 for inner cylinder with and without perforated outer cylinder, respectively; comparison with the results obtained from the experimental investigations is also shown.

It can be seen from the tables that forces on inner cylinder without perforated outer cover, computed from both the numerical simulations and experimental results, are ranging from 1.99 to 13.63 % with an average error of 7.08 %. In case of

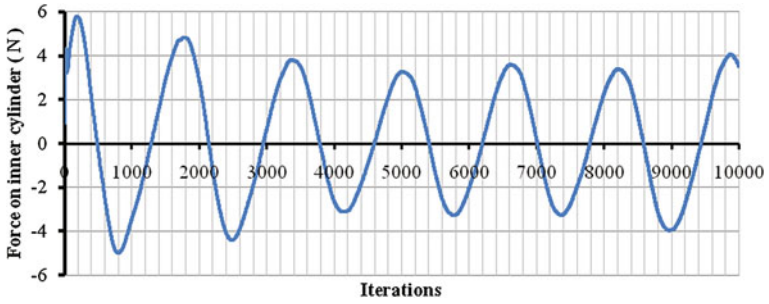

Fig. 5.20 Force on inner cylinder (WH = 10 cm; WP = 1.6 s) in numerical simulation

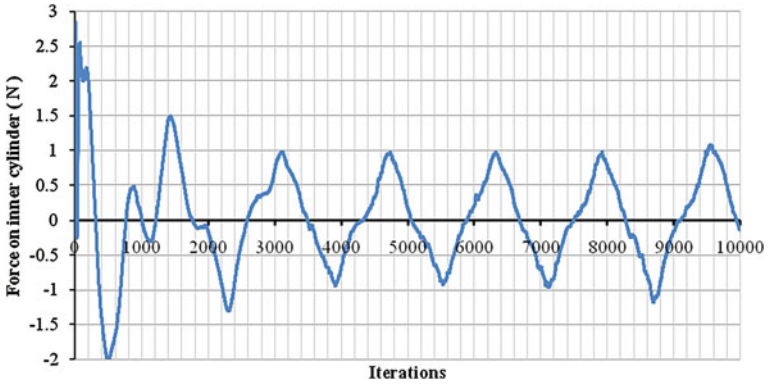

Fig. 5.21 Force on inner cylinder with perforated outer cylinder in numerical simulation (WH = 10 cm; WP = 1.6 s)

Table 5.12 Forces on inner cylinder (WH = 10 cm)

Wave period (s)	Numerical (N)	Experimental (N)	Error in %
1.0	11.06	10.11	8.59
1.2	10.2	8.81	13.63
1.4	8.45	7.69	8.99
1.6	6.84	6.65	2.78
1.8	6.52	6.39	1.99
2.0	6	5.61	6.50

Table 5.13 Forces on inner cylinder with perforated outer cylinder (WH = 10 cm)

Wave period (s)	Numerical (N)	Experimental (N)	Error in %
1.0	4.02	3.73	−7.81
1.2	3.65	3.28	−11.28
1.4	3.106	3.03	−2.51
1.6	2.75	2.85	3.51
1.8	2.51	2.77	9.39
2.0	2.32	2.59	10.42

forces computed on inner cylinder with perforated outer cylinder, errors between numerical simulations and experimental results range from 2.51 to 11.28 %, with an average of 7.5 %. Figure 5.22 shows the graphical comparison of the results obtained from numerical simulation and experimental investigations. It is also seen from the figure that both the results agree well within the acceptable error of tolerance for the chosen range of wave periods.

Based on the experimental investigations and numerical studies carried out, it is seen that the force estimates between both the studies are in good agreement, validating the numerical procedure adopted in the study. Few problems associated with the simulation are (i) high cell numbers and (ii) larger domain attempted to

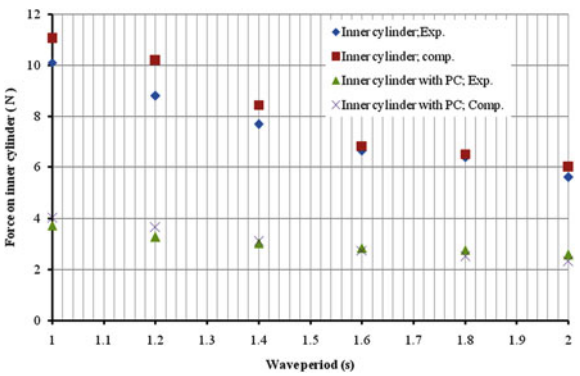

Fig. 5.22 Comparison of forces on inner cylinder with and without perforated outer cylinder

simulate the conditions as that of the wave flume resulted in not yielding the velocity profile variation at the desired points along the cylinder. An attempt shall be made to simulate the numerical model for a 2D plate with relatively smaller domain so as to trace the variation of velocity profile along the water depth; in addition, parametric studies such as (i) size of perforation, (ii) perforation ratio, and (iii) location of perforation will be examined to derive the velocity profile variation under the influence of the chosen parameters. When the train of waves hits the cylinder, the energy get dissipated due to back and forth movement causing a partial breaking of waves. Hence, this phenomenon acts as a good energy dissipation technique, which is an economical approach preferred by the design engineers. The reflection of the waves may also cause force on the outer porous cylinder. The horizontal velocity is a function of following parameters:

$$V = f(\rho, g, D, H, a, \sigma, d) \tag{5.2}$$

where ρ is the mass density of water, g is the acceleration due to gravity, D is the diameter of the cylinder, H is the wave height, σ is the frequency of wave, a is the area of perforation, and d is the water depth. The present study is done for the perforation ratio between 10 and 15 %. Hence, the above is transformed as given below:

$$V = f\left(\frac{H}{L} \text{ or } \frac{H}{d} \text{ or } \frac{d}{l} \text{ or } K_a, \frac{a}{D^2}, \sigma\sqrt{\frac{D}{g}}\right) \tag{5.3}$$

H/L parameter is generally used for the deep-water conditions. For clear understanding, the sea states are represented with H/L parameters. The sea states are grouped into three categories such as steep, medium, and low wave steepness. H/L ranging between 0.0051 and 0.0167 is categorized as waves with low steepness; H/L ranging between 0.0198 and 0.0445 is categorized as medium wave; and H/L ranging between 0.0491 and 0.1002 is categorized as steep waves. The cylinder is subjected to unidirectional waves of considered sea states. The horizontal velocity variation along the depth is derived. Figures 5.23, 5.24, and 5.25 show the horizontal velocity profile along the depth of cylinder for different sea states.

The zones of perforation are marked by a dotted line, and solid horizontal line indicates the mean sea level (MSL) of the cylinder. Velocity variations at few sections are plotted for discussion. For the all H/L considered, the profile of horizontal velocity along the water depth is highly nonlinear in the zone of perforation. It is also noted that there is a phase change in the velocity profile between the zones of perforation. As we know, the water particles try to take a shorter path during the flow; they try to escape through the nearby perforation, which leads to phase change in the perforation zones. The velocity variation along the depth of the cylinder with outer perforation cover is compared with the velocity profile without outer perforation cover; the plots show a significant deviation of the velocity vector with perforated cover. Hence, the study of water particle kinematics has become very

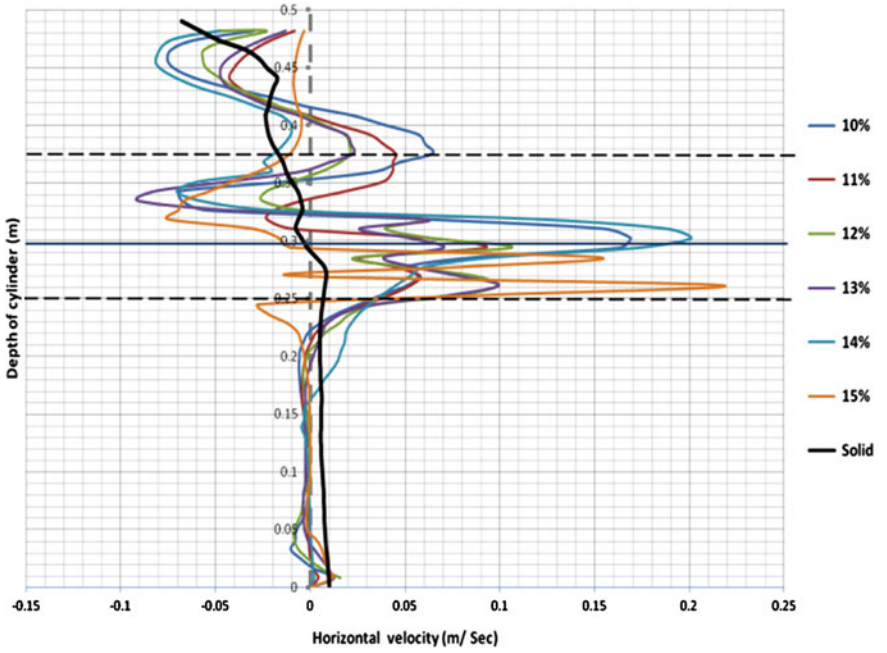

Fig. 5.23 Horizontal velocity variation for various percentages of perforation with wave steepness 0.0051

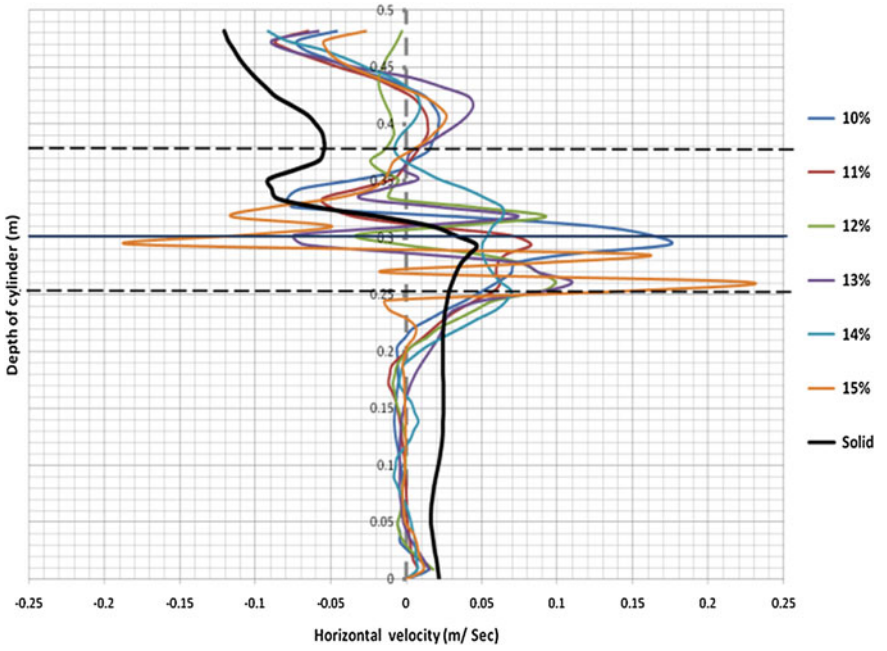

Fig. 5.24 Horizontal velocity variation for various percentages of perforation with wave steepness 0.0103

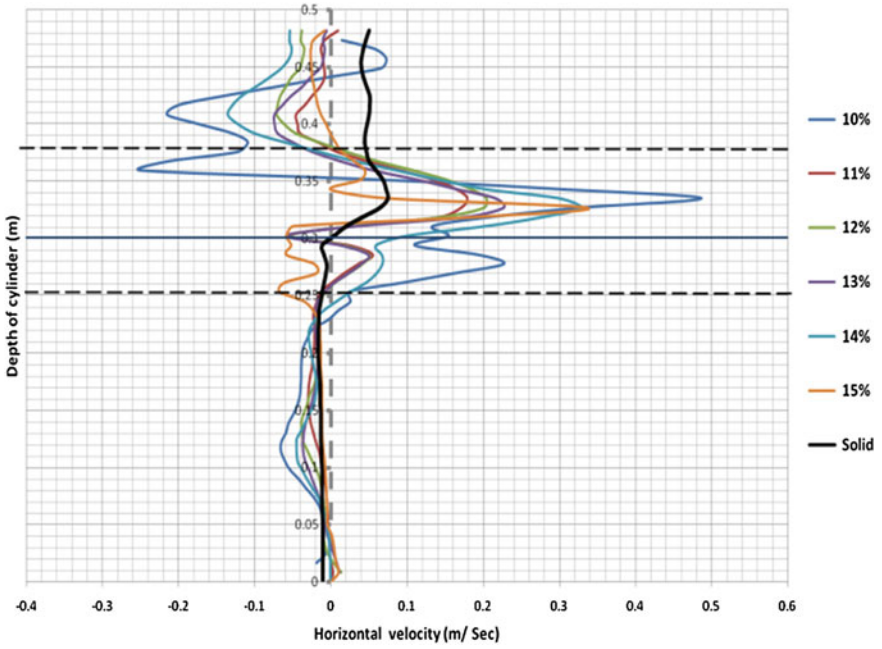

Fig. 5.25 Horizontal velocity variation for various percentages of perforation with wave steepness 0.0164

important with the perforation cover. The peak also changes its phase for different perforation ratio, which is clearly shown in the Fig. 5.26.

The variations of horizontal velocity at MSL for different perforation ratio for the considered sea states are non-proportional. This plot confirms that the range of perforation found optimum is between 11 and 12 % with the considered geometrical parameters. Figure 5.26 shows the variation of horizontal velocity along the depth of the cylinder with and without perforation for different chosen sections such as Sects. 1-1 and 2-2, as shown in Fig. 5.27.

The plot indicates that there is significant reduction of horizontal velocity along the wave advancing direction. From the plot, it is also seen that the horizontal velocity which is associated directly with horizontal force increases in the region of perforation as it is placed just beneath the free surface. It is seen that the horizontal components of hydrodynamic characteristics are significantly influenced by the presence of porous zone. Figures 5.28, 5.29, and 5.30 show that the reduction in the horizontal velocity reduces with the reduction of wave steepness.

It is seen from the figures that there is no significant variation in the velocity component between the sections for the waves with low steepness. It is also seen that in the zone of perforation, the velocity profile is highly nonlinear. There is significant reduction in the horizontal velocity along the wave advancing direction. Steeper waves show higher reduction in the velocity than the waves with mild wave

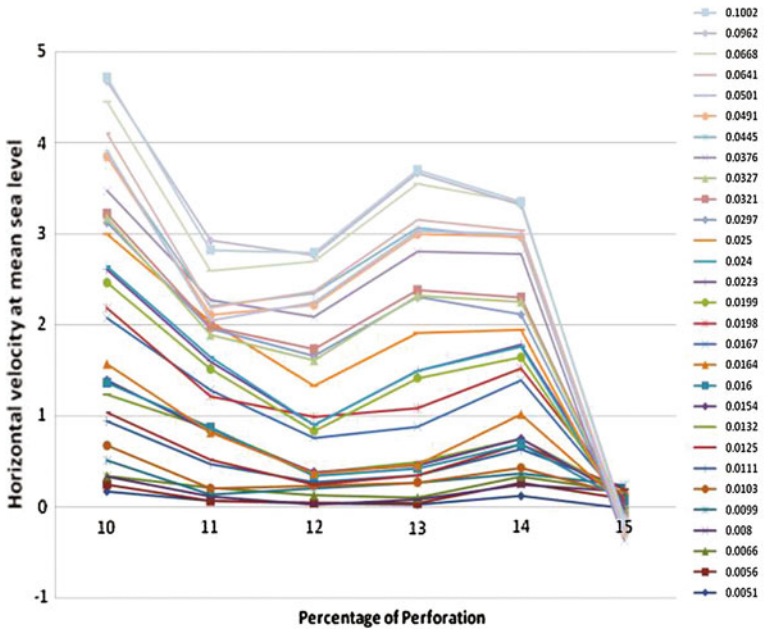

Fig. 5.26 Horizontal velocity at mean sea level for various wave steepness

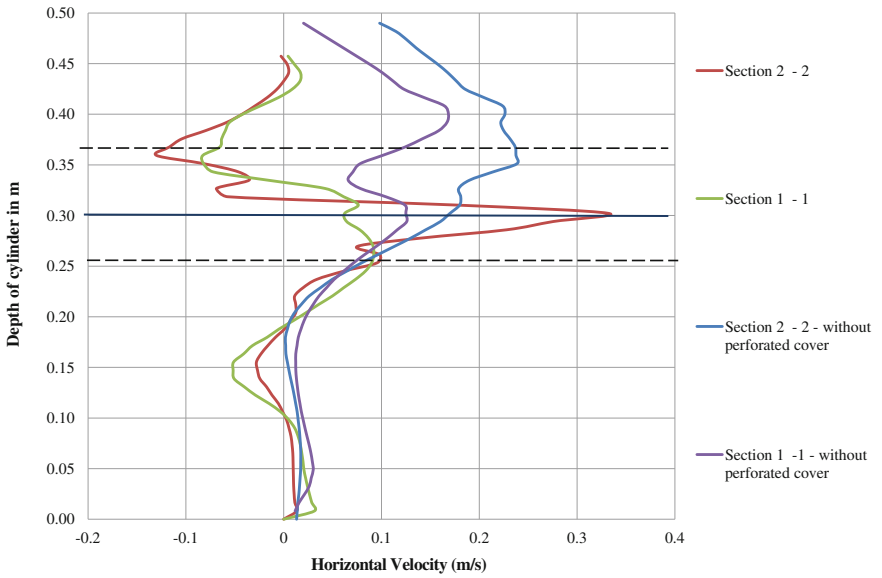

Fig. 5.27 Change in horizontal velocity between sections and perforation ratio 11 %, and *H*/*L* 0.0962

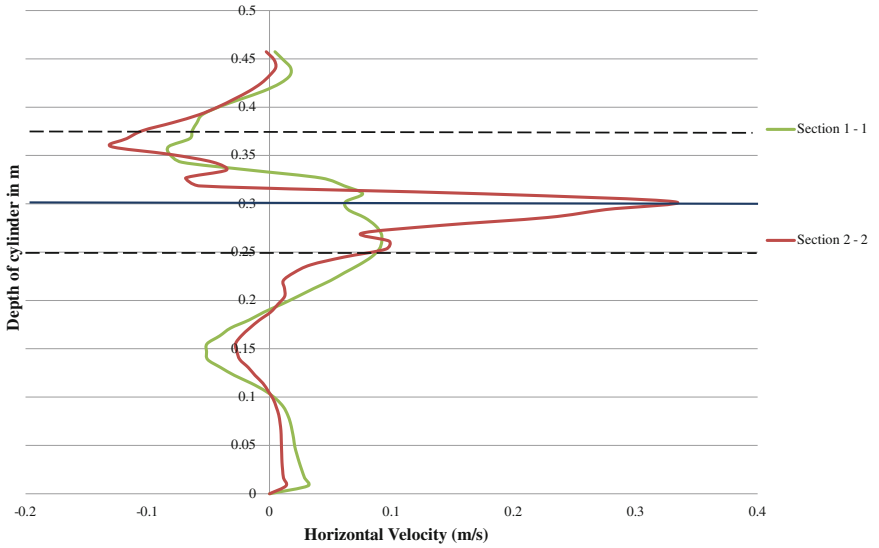

Fig. 5.28 Change in horizontal velocity between sections and steep wave

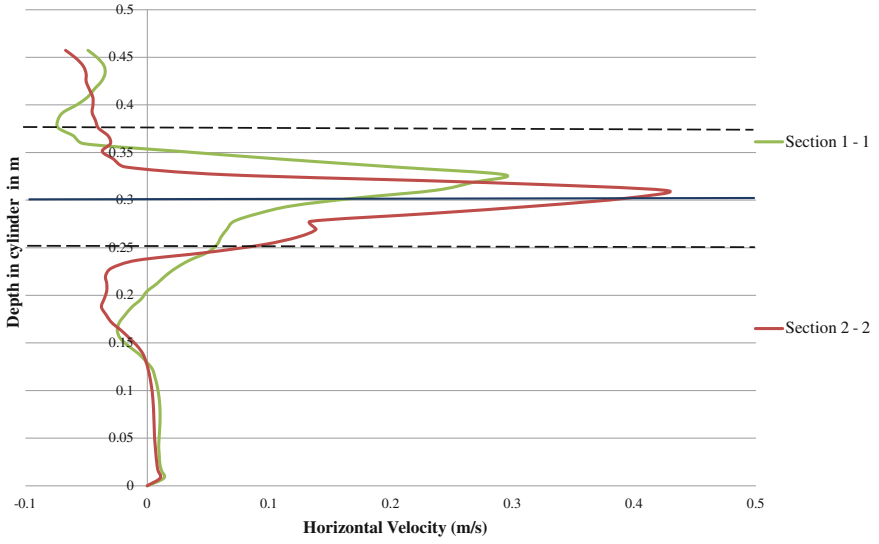

Fig. 5.29 Change in horizontal velocity between sections and medium steep wave

steepness. The design charts provided aids directly the design engineers to derive the horizontal velocity for different sea states and perforation ratio for the chosen geometric model. Based on the numerical studies conducted, the optimum percentage of perforation ratio for the chosen geometric model is recommended as 11–12 %.

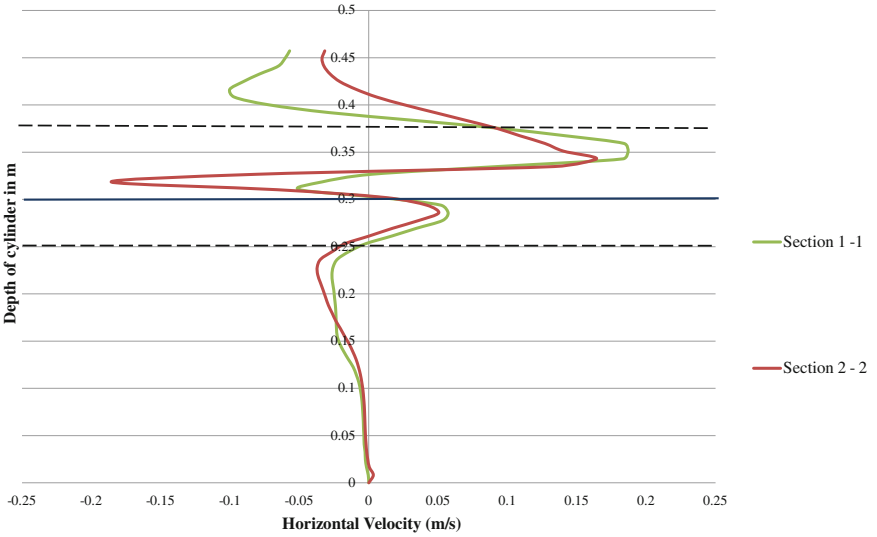

Fig. 5.30 Change in horizontal velocity between section and low-steep wave

Exercise

1. List and explain briefly the forces acting on the structure?
2. In the _____, there will be one-to-one relationship between the extent of wake region and restraint loads.
3. Variation in _____ causes downward flow along the length.
4. In _____, vertical cylinder will show vortices at the same frequency over its entire length, whereas in shear flow, frequency changes _____.
5. Horizontal cylinders will also be subjected to _____ _____.
6. Explain blockage factor?
7. _____ in porosity reduces wave exciting forces.
8. _____ in the porous body changes the response behavior of TLP significantly.
9. Perforated cylindrical structures reduce _____ and _____ considerably.
10. Introduction of perforated member acts as a _____, which is an economical approach. Profile of horizontal velocity along the water depth is highly _____ in the zone of perforation.

Answers

1. Forces acting on the structures in fluid medium shall be classified as drag (acting in-line with the direction of flow) and lift (transverse to the direction of flow). Further, drag force can be classified as higher and smaller frequency components. These components will be functions of the geometry of the structure and flow conditions. Lift forces contain oscillatory components with multiple frequencies. On the downstream side, flow will return to its unaltered condition. This is due to fluid viscosity and damping. The region of altered flow directly behind the structure is called *wake region*.
2. Wake regions.
3. Stagnation pressure.
4. Uniform flow; continuously.
5. Flow-induced vibrations.
6. Closely spaced members, connected in different orientations, cause distortion in the fluid field around them. For closely spaced members, the structure becomes dense. For dense structures, flow field slows down as it travels through the structure. This causes blockage effect and complicates the actual velocity field around the structure. Load on the structure increases due to this blockage.
7. Increase.
8. Drag force.
9. Wave–structure interaction and scouring problems.
10. Good energy dissipation technique; Nonlinear.

Chapter 6
Introduction to Stochastic Dynamics

Abstract This chapter deals with introduction to stochastic dynamics and its application to offshore structures. This chapter introduces the basics of reliability approach to the ultimate load design, levels of reliability, methods of reliability, reliability estimates, and limitation. The limitations and advantages of stochastic models are also explained. A quick preview about FOSM and advanced FOSM is also given in this chapter. Introduction to fatigue and fracture assessment is also provided.

Keywords Stochastic dynamics · Ultimate load · Reliability · FOSM · Advanced FOSM · Offshore structures

6.1 Introduction

In most of the cases, offshore structures are exposed to the environmental loads that can be modeled as a piecewise stationary process. A stationary process is one for which the statistical properties such as mean value and standard deviation are same for all points in time (or) position. Hence, the following equation holds good:

$$m_x = E[X(t)] = \text{constant} \tag{6.1}$$

For the condition $m_x = m_{x(t)}$ to be satisfied, autocorrelation function is given by:

$$R_X(\tau) = E[X(t)X(t+\tau)] \text{ to remain function of } \tau \text{ only} \tag{6.2}$$

To check whether the following are independent of time:

$$\hat{m}_x(t) = \frac{1}{N}\sum_{j=1}^{N} x_j(t) \tag{6.3}$$

S. Chandrasekaran, *Dynamic Analysis and Design of Offshore Structures*,
Ocean Engineering & Oceanography 5, DOI 10.1007/978-81-322-2277-4_6

$$\hat{R}_x(t, t+\tau) = \frac{1}{N}\sum_{j=1}^{N} x_j(t)x_j(t+\tau) \tag{6.4}$$

If they remain independent of time, the process is said to be a stationary process. Stationary process is defined by satisfying the condition given in Eq. (6.1):

The auto-covariance function should be as follows:

$$C_X(\tau) = E[(X(t) - m_x)(X(t+\tau) - m_x)] = \text{function of } \tau \text{ only} \tag{6.5}$$

For a stationary process, transfer between the load and the response can be modeled as linear, time-invariant, while the system can be characterized by a transfer function. Hence, the relationship between variance spectrum of the response (called response spectrum) and variance spectrum of load (called load spectrum) is determined by a transfer function.

Let $F(t)$ denote a stochastic load process. Assuming that $F(t)$ acts as a linear, time-invariant system, which has an impulse response function $h_{FX(t)}$, for each realization $f(t)$ of $F(t)$, we get the corresponding realization $x(t)$ of the response $X(t)$. Hence,

$$\begin{aligned} x(t) &= \int_{-\infty}^{\infty} h_{FX(s)} f(t-s)\mathrm{d}s \\ &= \int_{0}^{\infty} h_{FX(s)} f(t-s)\mathrm{d}s \end{aligned} \tag{6.6}$$

$$\text{because} \quad h_{FX(s)} = 0 \text{ for } s < 0$$

Equation (6.6) establishes the connection between the realization of the load process and the corresponding realization of the response process. This connection can also be described as below:

$$X(t) = \int_{0}^{\infty} h_{FX(s)} F(t-s)\mathrm{d}s \tag{6.7}$$

The above equation interprets that *there exists a relation between all the corresponding pairs of realization of F(t) and X(t)*. It is important to note that the impulse response function or the transfer function, which determines the connection between the load and the response, is completely defined by the properties of the linear system. This remains independent of any given load. In the term of $h_{FX(t)}$, index FX is to be understood only as the visual indicator for the connection between $F(t)$ and $X(t)$. For example, if $Y(t)$ is the response of the load process $G(t)$, acting on the same linear system, then $h_{GY(t)} = h_{FX(t)}$.

6.1.1 Mean Value of the Response Process

Assuming that $f_1(t), \ldots, f_N(t)$ is the sequence of realization of $F(t)$, let $x_1(t), \ldots, x_N(t)$, which denotes the corresponding response realization, then

$$\frac{1}{N}\sum_{j=1}^{N} x_j(t) = \frac{1}{N}\sum_{j=1}^{N} \int_0^{\infty} h_{FX(s)} f_j(t-s)\mathrm{d}s \tag{6.8}$$

$$= \int_0^{\infty} h_{FX(s)} \left\{ \frac{1}{N}\sum_{j=1}^{N} \int_0^{\infty} f_j(t-s)\mathrm{d}s \right\} \tag{6.9}$$

This leads to the following relationship:

$$E[X(t)] = \lim_{N\to\infty} \frac{1}{N}\sum_{j=1}^{N} x_j(t) = \int_0^{\infty} h_{FX(s)} \left\{ \lim_{N\to\infty} \frac{1}{N}\sum_{j=1}^{N} f_j(t-s) \right\} \mathrm{d}s \tag{6.10}$$

$$= \int_0^{\infty} h_{FX(s)} E[F(t-s)]\,\mathrm{d}s \tag{6.11}$$

If $F(t)$ is a stationary process, then $m_F = E[F(t)]$ is a constant. Then,

$$E[X(t)] = m_F \int_0^{\infty} h_{FX(s)}\mathrm{d}s \tag{6.12}$$

It can be seen that the above equation is independent of time. Hence,

$$m_X = E[X(t)] = \text{constant} \tag{6.13}$$

Let $H_{FX}(\omega)$ be the transfer function that corresponds to the impulse response function of $h_{FX(t)}$. Then,

$$\begin{aligned} H_{FX}(0) &= \int_0^{\infty} h_{FX(s)}\mathrm{d}s \\ E[X(t)] &= m_F H_{FX}(0) = m_X \end{aligned} \tag{6.14}$$

For the system, whose equation of motion is given by:

$$m\ddot{u} + c\dot{u} + ku = P_0 \cos(\omega t) \tag{6.15}$$

The transfer function for the linear system, described by the above equation of motion, is given by $H_{FX}(\omega)$. For the steady-state response of the system under the given excitation load, the dynamic amplification factor D is given by:

$$D = \frac{1}{\sqrt{(1-\beta^2)^2 + (2\xi\beta)^2}} \tag{6.16}$$

For a weakly damped system, we also know that the maximum amplification factor is given by:

$$D_{\max} = \frac{1}{2\xi} \tag{6.17}$$

For $\xi = 2\ \%$, $D_{\max} = 25$, which implies that, even small oscillating forces may lead to large responses. For the analysis of structural response to various forcing frequencies, it is therefore better to introduce a complex-valued function as given below:

$$\begin{aligned} H(\omega) &= |H(\omega)|\mathrm{e}^{-i\varphi} \\ u(t) &= |H(\omega)|P_0 \cos(\omega t - \varphi) \end{aligned} \tag{6.18}$$

In the above equation, $H(\omega)$ gives the amplitude amplification and ϕ gives the phase shift. For example, if $H(\omega) = 0.001$, for a particular frequency ω, then a force amplitude of 100 N will give rise to the displacement of 0.1 m at this frequency. The generalized expression for the steady-state response of the oscillating system is given by:

$$\begin{aligned} &u_p(t) = \rho \cos(\omega t - \varphi) \\ &\frac{\rho}{x_{\text{static}}} = \frac{\rho}{\left(P_0/K\right)} = D \\ &\text{Hence,} \\ &u_p(t) = \frac{P_0}{K} \frac{1}{\sqrt{(1-\beta^2)^2 + (2\xi\beta)^2}} \cos(\omega t - \varphi) \end{aligned} \tag{6.19}$$

Comparing Eqs. (6.18) and (6.19), we get

$$H(\omega) = \frac{1}{K} \frac{1}{\sqrt{(1-\beta^2)^2 + (2\xi\beta)^2}} \tag{6.20}$$

where $H(\omega)$ is called the transfer function or frequency response function, which maps the response behavior of the linear system to the external forcing function. It is seen that this function is proportional to the dynamic amplification factor. It contains all relevant information about the dynamic amplification. Incorporating also the information related to the phase shift, transfer function is modified as:

$$H(\omega) = \frac{1}{K} \frac{1}{\sqrt{(1-\beta^2)^2 + (2\xi\beta)^2}} \mathrm{e}^{-i\varphi} \tag{6.21}$$

The reason, why it is easier to use $\mathrm{e}^{-i\phi}$, in comparison to $\sin\phi$ or $\cos\phi$ is that

$\frac{\mathrm{d}}{\mathrm{d}t}(\mathrm{e}^{i\varphi}) = i\frac{\mathrm{d}\varphi}{\mathrm{d}t}(\mathrm{e}^{i\varphi})$, where $\mathrm{e}^{i\varphi}$ factor does not change

$\mathrm{e}^{i\varphi_1}\mathrm{e}^{i\varphi_2} = \mathrm{e}^{i(\varphi_1+\varphi_2)} = \mathrm{e}^{i\varphi_3}$, where the product of two factors are of the same kind.

The above two properties give many advantages in the derivations. Further, $H_{FX(0)} = (1/k)$ and $m_X = (m_F/K)$. This means that the *mean value of the response is equal to the product of the mean value of the load and the system response to a static load of unit size*; hence, the following equation holds good:

$$m_X = H_{FX(0)} m_F \tag{6.22}$$

It is seen from the above equation that, for the excitation force with zero mean value, response also has zero mean value.

6.2 Auto-Covariance of the Response Process

It is seen from the above section that for $m_F = 0$, m_X is also zero. Hence, for $F(t)$ to be a stationary process, it is convenient to assume $F'(t) = F(t) - m_F$, which also has zero mean value. Let $X'(t)$ be the response to the load process, $F'(t)$. Then,

$$\begin{aligned} X'(t) &= \int_0^\infty h_{FX(s)}\, F'(t-s)\, \mathrm{d}s \\ &= \int_0^\infty h_{FX(s)} F(t-s)\mathrm{d}s - \int_0^\infty h_{FX(s)}\, m_F\, \mathrm{d}s \\ &= X(t) - m_X \end{aligned} \tag{6.23}$$

For $X'(t)$ to have a zero mean value, $F(t)$ and $F'(t)$ have the same auto-covariance. Then, the following relation holds good:

$$x_j(t)x_j(t+\tau) = \int_0^\infty h_{FX(s_1)} f_j(t-s_1)\,\mathrm{d}s_1 \cdot \int_0^\infty h_{FX(s_2)} f_j(t+\tau-s_2)\mathrm{d}s_2$$
$$= \int_0^\infty \int_0^\infty h_{FX(s_1)} h_{FX(s_2)} f_j(t-s_1) f_j(t+\tau-s_2)\mathrm{d}s_1\mathrm{d}s_2 \tag{6.24}$$

It is also known that:

$$E[X(t)X(t+\tau)] = \lim_{N\to\infty} \frac{1}{N}\sum_{j=1}^{N} x_j(t)x_j(t+\tau) \tag{6.25}$$

Hence, Eq. (6.24) can be rewritten as:

$$= \int_0^\infty \int_0^\infty h_{FX(s_1)} h_{FX(s_2)} \lim_{N\to\infty} \frac{1}{N}\sum_{j=1}^{N} f_j(t-s_1) f_j(t+\tau-s_2)\mathrm{d}s_1\mathrm{d}s_2$$
$$= \int_0^\infty \int_0^\infty h_{FX(s_1)} h_{FX(s_2)} E[F(t-s_1)F(t+\tau-s_2)]\mathrm{d}s_1\mathrm{d}s_2 \tag{6.26}$$
$$= \int_0^\infty \int_0^\infty h_{FX(s_1)} h_{FX(s_2)} C_F(\tau+s_1-s_2)\mathrm{d}s_1\mathrm{d}s_2$$

Since $F(t)$ is assumed to be stationary, $E[X(t)\,X(t+\tau)]$ will also be independent of time. The auto-covariance $C_X(\tau)$ will be as same as the auto-correlation $R_X(\tau)$, as the process is a zero mean process. Then, the following relation holds good:

$$C_X(\tau) = \int_0^\infty \int_0^\infty h_{FX(s_1)} h_{FX(s_2)} C_F(\tau+s_1+s_2)\mathrm{d}s_1\mathrm{d}s_2. \tag{6.27}$$

6.3 Response Spectrum

Let $S_X(\omega)$ be the variance spectrum of the response of the process *X(t)* and $S_F(\omega)$ be the variance spectrum of the load process $F(t)$, then variance spectrum of *X(t)* will be defined by the Fourier transform of the auto-covariance of the response, which is given by

$$
\begin{aligned}
S_X(\omega) &= \frac{1}{2\pi}\int_{-\infty}^{\infty} C_X(\tau)\mathrm{e}^{-i\omega\tau}\mathrm{d}\tau \\
S_X(\omega) &= \int_0^{\infty} h_{FX(s_1)}\int_0^{\infty} h_{FX(s_2)}\frac{1}{2\pi}\int_{-\infty}^{\infty} C_F(\tau+s_1-s_2)\mathrm{e}^{-i\omega\tau}\mathrm{d}\tau\mathrm{d}s_2\mathrm{d}s_1 \\
&\text{Put } \tau+s_1-s_2=\theta, \quad \mathrm{d}\theta=\mathrm{d}\tau, \quad \text{then} \\
S_X(\omega) &= \int_0^{\infty} h_{FX(s_1)}\int_0^{\infty} h_{FX(s_2)}\frac{1}{2\pi}\int_{-\infty}^{\infty} C_F(\theta)\mathrm{e}^{-i\omega\theta}\mathrm{d}\theta\mathrm{e}^{i\omega(s_1-s_2)}\mathrm{d}s_2\mathrm{d}s_1
\end{aligned}
\tag{6.28}
$$

$S_X(\omega) = H_{FX}(-\omega)H_{FX}(\omega)S_F(\omega)$ because $\mathrm{e}^{(-ix)^*} = \mathrm{e}^{ix}$ and $h_{FX(t)}$ is a real function.

Imposing the above condition, we get:

$$
\begin{aligned}
H_{FX}(-\omega) &= \int_0^{\infty} h_{FX}(t)\mathrm{e}^{i\omega t}\mathrm{d}t = \int_0^{\infty} h_{FX}(t)\mathrm{e}^{-i\omega t^*}\mathrm{d}t \\
&\int_0^{\infty} h_{FX}(t)\mathrm{e}^{-i\omega t^*}\mathrm{d}t = H_{FX}(\omega)^* \\
S_X(\omega) &= |H_{FX}(\omega)|^2 S_F(\omega)
\end{aligned}
\tag{6.29}
$$

The above equation gives the relationship between the response spectrum $S_X(\omega)$ and the load spectrum $S_F(\omega)$. Please note that Eq. (6.29) does not contain information about the phase shift between the load and the response; only amplitude amplification is known. From the response spectrum, one can compute several other statistical quantities that are important for assessing the response. For example, standard deviation of the response is obtained as follows:

$$
\begin{aligned}
m_X &= H_{FX}(0)m_F \\
\sigma_X^2 &= \int_{-\infty}^{\infty} |H_{FX}(\omega)|^2 S_F(\omega)\mathrm{d}\omega
\end{aligned}
\tag{6.30}
$$

For *X(t)* be the response of a linear system with transfer function $H_{FX}(\omega)$ to a stationary load process *F(t)*, RHS of the Eq. (6.30) for standard deviation is to be computed numerically. For very less damping, $|H_{FX}(\omega)|^2$ becomes narrow around the resonance frequency, ω_r. This implies that the main contribution to the integral Eq. (6.30) comes from a small interval around ω_r, which is evident from the Fig. 6.1.

If $S_F(\omega)$ varies much slower than that of $|H_{FX}(\omega)|^2$, then it is often possible to replace $S_F(\omega)$ in Eq. (6.30) by $S_0 = S_F(\omega_r)$. Hence, Eq. (6.30) can be rewritten as

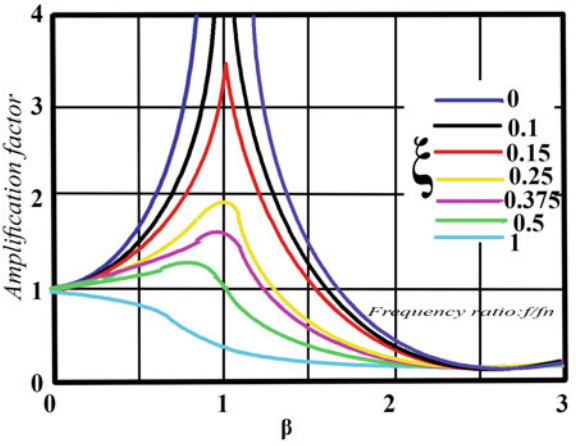

Fig. 6.1 Amplitude amplification for various damping ratios

$$\sigma_X^2 = S_0 \int_{-\infty}^{\infty} |H_{FX}(\omega)|^2 \mathrm{d}\omega \tag{6.31}$$

This procedure of replacing the input spectrum by a constant (S_0) is called *white noise approximation*. A typical feature of the response spectrum of a weakly damped system is that it is narrow-banded. This follows the fact that the response spectrum, to a large extent, is determined by the value of $|H_{FX}(\omega)|^2$. With the *white noise approximation*, variance is given by Eq. (6.31).

6.4 Stochastic Process

Dynamic analyses can be carried out in two ways depending on the description of loads, namely (i) deterministic analysis, which requires the complete knowledge of load time history and (ii) stochastic analysis where statistical concepts are used to specify the loads. For example, when waves or wind loads are described in terms of statistical quantities, then the response should also be described and analyzed in terms of same kind of quantities.

6.4.1 Example of Stochastic Modeling

Sea surface elevation, $X(t)$, is a good example of a random variable. A stochastic process is an abstract notion in a similar manner as that of a random variable. The values of the variables that can be observed physically are the outcomes, which are usually referred as realizations. A sea surface time history that has a high randomness can be easily overcome by assuming the time history to be a realization

of ergodic stationary process. The assumption implies that the statistical information about the process is in fact contained in a single realization of the process. For example, cumulative distribution function (CDF) $F_{X(t)}(x)$ assumes the values lesser than or equal to x, as given below:

$$F_{X(t)}(x) = \lim_{T\to\infty} \frac{T[x(t) \le x]}{T}$$

where T denotes the record length and $T[x(t) \le x]$ denotes the total amount of time during T where $[x(t) \le x]$. The quantity $X(t)$ is called as a stochastic process if $X(t)$ is a random variable for each value of t in an interval (a, b).

6.4.2 Example of a Stochastic Process

Assume X as a random variable, which is normally distributed with a mean value m and standard deviation σ (>0). Its probability density function is given by:

$$f_X(x) = \frac{1}{\sqrt{2\pi}\sigma} \exp\left\{ -\frac{1}{2}\left[\frac{x-m}{\sigma}\right]^2 \right\}$$

If $g(t)$ is known, which is a real function defined for $(-\infty < t < \infty)$, then

$$g(t) = \cos(\omega t)$$

where ω is a positive constant. Hence, $X(t) = Xg(t)$ is also a stochastic process defined for the same interval $(-\infty < t < \infty)$. Realization of the process is then given as a product of $g(t)$ with an outcome x of the random variable X. In that case, the following equation holds good:

$$x(t) = xg(t)$$

Hence, if $g(t) = \cos(\omega t)$; its realization could be harmonic function of the same period, but with a different amplitude. Hence, the mean value is given by:

$$\begin{aligned} m_X(t) &= E[X\, g(t)] = E[X]g(t) = mg(t) \\ \sigma_{X(t)} &= \sqrt{E[X\, g(t)^2 - m\, g(t)^2]} \\ &= \sqrt{E[X^2]g(t)^2 - m^2 g(t)^2} \\ &= \sqrt{E[X^2 - m^2|g(t)|]} \\ &= \sigma|g(t)| \end{aligned}$$

For each value of t, $g(t)$ is a constant; Hence $X(t) = Xg(t)$ is also normally distributed if $g(t) \neq 0$

The probability density function of $X(t)$ becomes:

$$f_{X(t)}(x) = \frac{1}{\sqrt{2\pi}\sigma|g(t)|}\exp\left\{-\frac{1}{2}\left(\frac{x - m\,g(t)}{\sigma|g(t)|}\right)^2\right\}.$$

6.5 Return Period

Let Z be a random variable. Then,

$$p = \text{Prob}[Z > z] = 1 - F_Z(z) \tag{6.32}$$

Assuming that we can make series of observations of Z, mean number of observations to the first observed or measured value of X exceeds z is called the *return period* for exceedance of z, which is denoted by $\bar{R}(z)$.

$$\bar{R}(z) = \frac{1}{p} = \frac{1}{1 - F_Z(z)} \tag{6.33}$$

This equation can be described as an average of $(1/p)$ trails conducted before an event of probability p occurs. $\bar{R}(z)$ refers to the number of observations, and these are assumed to be statistically independent. If return period needs to be explained in terms of time, one needs to know the time interval between the observations. If the observation interval is Δt, then the return period, in terms of time, is given by:

$$R(z) = \Delta t\,\bar{R}(z) \tag{6.34}$$

The observation interval must be chosen sufficiently long such that individual observations become approximately independent. For example, a design load with a probability of 10^{-2} being exceeded during 1 year is often used in offshore structures. If we let $F(t)$ denote the relevant load process considered for the design and ξ denote the corresponding load level, then

$$\text{Prob}(Z > \xi) = 0.01, \text{ where } Z = \max\left(F(t)\right); 0 \leq t) \leq 1 \text{ year}.$$

Return period of exceedance of ξ then becomes as follows:

$$\bar{R}(z) = \frac{1}{\text{Prob}(Z > \xi)} = \frac{1}{0.01} = 100 \text{ years} \tag{6.35}$$

Reference period, in this case, is 1 year, and therefore, return period of exceedance is 100 years. It is important to note that the time-varying loads, caused by waves, cannot be considered stationary over an extended period. This means that the quantities such as yearly maxima must be computed using long-term statistics. Return periods are also computed based on the risk associated. This is a common practice in case of earthquake loads and seismic design of structures. For example, design basis earthquake (DBE) has a risk level of 10 % at occurrence of 50 years and that of maximum credible earthquake (MCE) is 2 %. Based on the risk associated, return period is computed as below:

$$R = 1 - \left[1 - \frac{1}{T}\right]^{n}$$

$$\text{For DBE, } 0.1 = 1 - \left[1 - \frac{1}{T}\right]^{50} \text{ yields return period } (T) \text{ as 475 years} \tag{6.36}$$

$$\text{For MCE, } 0.02 = 1 - \left[1 - \frac{1}{T}\right]^{50} \text{ yields a retrun period of 2,500 years.}$$

6.6 Safety and Reliability

Safety is a measure used to indicate the reliability. But this demands a traditional way of analysis. Reliability offers probabilistic meaning to this traditional concept. Extension of reliability analysis also includes the consequences of failure. Safety assessment and risk characterization are vital for offshore plants. Since risk is the realization of hazard and hazard scenario is unavoidable in any process industry, the most important aspect of reliability is to account for all uncertainties that make the structure vulnerable to failure under a pre-defined limit state. Accuracy of the reliability studies depends on how accurately these uncertainties are accounted for in the analysis. Many assumptions are made during the reliability analyses, which influence the accuracy of the reliability studies. Furthermore, it is also important to note that analytical formulation of the limit state surface and integration of the probability density function within the domain of interest is also very complex.

6.7 Reliability Framework

In the general sense, offshore platform should perform its intended function for a specified period of time under specific conditions. In the mathematical sense or narrow sense, reliability is estimating the probability of the structure for not attaining the limit state of collapse within the specified conditions, for the specified period of time.

$$\text{Reliability} = 1 - P_f \tag{6.37}$$

which implies the fact that it is $(R - S)$, where R is the resistance of the structure and S is the load effects. For the resistance greater than the load effects, the structure is always in the safe domain. If the load effects and resistance are expressed by their respective PDF as $f_s(S)$ and $f_s(R)$, respectively, then probability of failure is given by:

$$P_f = \text{Prob}\ (R \leq S) \tag{6.38}$$

$$\begin{aligned} &= \int_0^\infty f_R(s) - f_s(s)\mathrm{d}s \\ &= f_m(0) \end{aligned} \tag{6.39}$$

where M is called margin of safety, which is given by $(R - S)$. If the probability density function $\{f_m(m)\}$ and CDF $F_m(m)$ are known, then probability of failure P_f can be computed analytically or numerically as given below:

(a) *R and S are normally distributed*

If R and S are normally distributed, then

$$p_f = \varphi(-\beta) \tag{6.40}$$

where the reliability index is given by:

$$\beta = \frac{\mu_R - \mu_S}{\sqrt{\sigma_R^2 - \sigma_S^2}} \tag{6.41}$$

(b) *R and S are log-normally distributed*

In such cases, reliability index is given by:

$$\beta = \beta_{LN} = \frac{\ln\left[\frac{\mu_R}{\mu_S}\sqrt{\frac{(1+V_S^2)}{(1+V_R^2)}}\right]}{\sqrt{\ln(1+V_R^2)(1+V_S^2)}} \tag{6.42}$$

$$\beta_{LN} \approx \frac{\left(\frac{\mu_R}{\mu_S}\right)}{\sqrt{V_R^2 + V_S^2}} \tag{6.43}$$

6.8 Ultimate Limit State and Reliability Approach

For an implicit failure probability in the design under random load effects, the following equations hold good:

$$\mu_S = B_S S_C \tag{6.44}$$

(a) For $BS \leq 1.0$, $VS = 0.15$–0.30 and $\mu_R = B_R R_C$

where B_S reflects the ratio of the mean load if the period of variation is annual and then it should refer to the annual value of probability of failure. S_c is the characteristic value with 100 years return period. For (R, S) be log-normal, the following equation holds good:

$$\beta_{LN} = \frac{\ln \frac{\mu_R}{\mu_S}}{\sqrt{V_R^2 + V_S^2}} \tag{6.45}$$

For ($V_R V_S$) be the partial safety factor of 1.5, $B_S = 0.8$, $B_R = 1.0$, $V_R = 0.15$, the above equation reduces to the following form:

$$= \frac{\ln \frac{1.1}{0.8}}{\sqrt{0.10^2 + 0.20^2}} = 13.5 \tag{6.46}$$

Ultimate limit state can affect the design since the method is based on the maximum load effect. It is also affected by the strength of the material, which is determined traditionally. Reliability framework is based on establishing a limit state function $g(x)$ for a single R and S, where the limit state function $g(x)$ is subjected to large uncertainties. The preferable design format is then given by:

$$\frac{R_c}{V_R} \geq V_{s1} S_{1c} + V_{s2} S_{2c} \tag{6.47}$$

where subscript stands for the characteristic value, R is the resistance, S is the load effect, γ_R is the resistance factor, $V_{S1} V_{S2}$ are the load factors. Resistance refers to a characteristic strength of 5 % of the fractal materials' strength, while load effect refers to the annual probability of exceedance of 10^{-2}. Design criterion is now given by g (R_d, S_{1d}, S_{2d}) > 0.

$$\begin{aligned} R_d &= \frac{R_c}{V_R} \\ S_{1d} &= V_{S1} S_{1C} \\ S_{2d} &= S_{2c} V_{2c} \end{aligned} \tag{6.48}$$

For multiple values of (R and S), the structure is subjected to different load combinations for which the bending failure criteria can be formulated as:

$$g(R_1, R_2, R_3, S_{1j}, S_{2j}) := 1 - \left[\frac{S_{ij}}{R_1} + \frac{S_{2j}}{\left(1 - \frac{S_{1j}}{R_2}\right)R_3}\right] \tag{6.49}$$

The above equation can also be set as:

$$= 1 - \left[\frac{X_1}{X_1} + \frac{X_3}{\left(1 - \frac{X_1}{R_4}\right)}\right] \tag{6.50}$$

where S_{1j}, S_{2j}, etc., are load effects for different combination and R is the resistance (the count j stands for load type). The above equation is based on the Perry-Robertson approach in which R_1, R_2 be the axial force and R_3 be the Euler load. In the partial design values of (R and S), they are represented by their respective characteristic values. But in the reliability study, they are considered random variables.

6.9 Short-term Reliability of Single Load Effect

If the resistance (R) is constant overtime and the load effect is of the single load (S), then the characteristics value of the load effect can be obtained from the distribution of the individual maximum of the largest value in a given time period. The reliability problem can be arrived based on the extreme value of statistics to characterize $S_{\max}$.

Fracture probability in the short time period is given by:

$$\begin{aligned} P_f(t) &= \text{Prob}(g(R, \max_{0 \le t \le T} S(Q(t)) \le 0 \\ &= \text{Prob}(g(R, S_{\max}(T) \le 0 \end{aligned} \tag{6.51}$$

where $g(\cdot)$ is the limit state function, R is the structural resistance, and S in the load effect resulting from the load process $Q(t)$.

6.9.1 Up-Crossing Approach

The alternate approach is the up-crossing rate approach. This is time-dependent reliability, while the main interest lies in the time (t_f) to the first failure.

For a simple problem, following equation holds good:

$$M(t) = g(R, S(t)) = R - S(t) \tag{6.52}$$

t_f is the first time when $M(t) = 0$ that is when t_f is the time of first excursion of $M(t)$ from positive to negative value assuming $M(t)$ is a continuous process.

Probability of failure is the period [0, T] and is equivalent to the probability that $t_f < T$

$$\begin{aligned} P_f &= 1 - \text{Prob}\left(t_f > T\right) \\ &= 1 - \text{Prob}\left(N(t) = 0 \vdots M(0) > 0\right)\text{Prob}(M(0) > 0) \end{aligned} \tag{6.53}$$

where $N(t)$ is the number of up-crossing in (0, t) or number of crossing from safe to failure design. $M(t) = R - S(t)$ is in the safe domain at zero time. If $M(0) > 0$ signifies the safety margin. In general, calculation of P_f is a complex task and approximate solution can be achieved by assuming $N(t)$ as a Poisson process that is uncertainty of level R by $s(t)$ is independent with the mean rate of $v_s^+(R) = v_m^-(0)$ per unit time:

$$\text{Prob}(N(T) = 0) = \frac{\left(v_s^+(R)T\right)^0}{0!}\mathrm{e}^{-v_s^{+(R)T}} = \mathrm{e}^{-v_s^{+(R)T}} \tag{6.54}$$

Also $\text{Prob}(M(T) > 0) = 1 - P_f(0)$, which means that the probability of number of failure at $t = 0$; hence $P_f(o) = 0$ then $P_f(t)$ is given by

$$P_f(T) \cong 1 - \mathrm{e}^{-v_s^{+(R)T}} \cong v_s^+(R)T = v_m^-(o)T \tag{6.55}$$

As a special case, when $s(t)$ is a Gaussian process, then

$$\begin{aligned} v_s^+(R) &= v_0^+ \exp\left(-\frac{(R - \mu_s)^2}{2\sigma_s^2}\right) \\ v_0^+ &= v_s^+(0) \end{aligned} \tag{6.56}$$

For the given value of random variable $X = (X_1, \ldots, X_n)^{\mathrm{T}}$ that represents those uncertainties, the conditioned failure probability is determined by down-crossing of 0 by $M(t; X)$ for $t \geq 0$.

$$\begin{aligned} P_f(x) &= \text{Prob}\left(\min_{0 \leq t \leq T} M\left(t \vdots x\right) \leq 0\right) \\ &= 1 - \exp\left[-v_m^-(0; x)T\right] \end{aligned} \tag{6.57}$$

where $v_m^-(0; x)$ is the zero down-crossing rate which depends on the parameter of vector x. The total failure probability considering the uncertainty in X can be calculated by unconditional probability, as given below:

$$P_f = \int_x P_f(x) f_x(x) \mathrm{d}x \tag{6.58}$$

The integral represents expected value of $P_f(x)$. Hence, P_f can be calculated as a random value, as shown below:

$$P_f \cong \frac{1}{N} \sum_{i=1}^{N} P_f(x_i). \tag{6.59}$$

6.10 Long-term Reliability of Single Load Effect

For a non-stationary process $M(t;\ x)$ which could be for a long-term, failure probability is given by:

$$P_f(x) = 1 - \exp\left\{ - \int_0^T v_m^-(0;t;x) \mathrm{d}t \right\} \tag{6.60}$$

where $v_m^-(0;t;x)$ is the mean down-crossing rate which depends as the sea state and changes with time. For the given set of properties of the sea states, let W be the captured value, which is given by

$$W = \left(H_s, T_p, u_c, u_w, \vec{\text{wave}}\ , \vec{\text{wind}}, \vec{\text{current}} \right)$$

where H_s is the significant wave height, T_p spectral peak period, u_c current velocity, u_w mean wave speed, and $\vec{\text{wave}}\ , \vec{\text{wind}}, \vec{\text{current}}$ are wave, wind, current direction. Pre-requisite of the long-term failure probability is to impose an ergodicity assumption on the environmental process $W = W(t)$, then

$$P_f(x) = 1 - \exp\left\{ -T \int_w v_m^-(0;w;x) f_x(w) \mathrm{d}w \right\} \tag{6.61}$$

where $v_m^-(0;w;x)$ derives mean zero down-crossing rate of M for the sea state $W = w$:

$$f_w(w) = \text{PDF of } W \tag{6.62}$$

The full long-term failure probability occurring for both environment variability and parameter uncertainty is given by:

$$P_f = \int_x P_f(x) f_x(x) \mathrm{d}x. \tag{6.63}$$

6.11 Levels of Reliability

Reliability studies are considered in different levels in the literature. Level I is focusing on the probability aspects of the problem. Suitable characteristic values of the random variables are introduced in the safety analysis. Main objective of this level of study is to minimize the deviation of the design values from that of the target value. For example, load-resistance factor design (LRFD) is of level I of reliability. Level II has two values for each parameter to be defined in the analysis, namely mean and standard deviation. Level III is a complete analysis of the problem addressing the multi-dimensional probability density function of random variables, which is extended over the safety domain. Reliability is expressed in terms of suitable safety indices. In level IV, engineering economics is also applied in the reliability study. This level of reliability study is usually applied to structures of strategic importance. The study includes cost-benefit analysis, rehabilitation, consequence of failure, and return on capital investment.

Reliability methods offer many advantages: (i) they account for the uncertainties; (ii) they are rational methods to estimate safety; and (iii) they offer decision-making support for non-economic and better balanced design. Optimal distribution of material among various components of structure can be benefitted through a constant update mechanism, on the basis of which FEED function of engineering judgment are circumscribed. Reliability studies expand the knowledge of uncertainties in the response of the structure. There are few obstacles in implementing the reliability studies to the offshore plants in operation. They are classified as inertial, cultural, and philosophical. Different types of variables used in reliability study are, namely (i) elementary variables (static variables) like material properties, (ii) geometry of the platform, (iii) boundary conditions, and (iv) issues related to the location and behavior dependent data.

Failure modes such as limit stress and limit displacement depend upon the system variables, which are in turn dependent on location behavior and failure modes. There are different steps of reliability, namely elementary level, component level, system level, and detailed field investigation. The first step is handled by stochastic modeling, while the second step can be handled by probabilistic study of failure of components. In case of system-level studies, probabilistic studies on the failure of the whole system can be investigated. One of the serious limitations of reliability study is that it requires a large amount of data on the failure scenario. Other parameters that influence the accuracy of the results of the reliability studies are as follows:

1. Separation of two variables, namely safety domain and failure domain.
2. Nature of variables, namely external or internal and whether they are independent or not.
3. Effect of time indicating the static content or the cyclic (dynamic) content.
4. Form of the performance function, which is dependent on the physical model of the system.

6.12 Reliability Methods

The main interest is to develop a reliability method in relation to modeling the materials and structures. The primary advantage of the reliability method in structures is to calculate the reliability estimates by nominal or conditional probability; reliability index; serviceability of failure to stochastic date description. Three fields of application are particularly targeted; they are as follows:

1. Exceptionally highly innovative structures for which experience accumulated in last few certainties are inadequate. Reliability methods were first used for designing offshore platform.
2. Design of ordinary-type structures with codes whose current evolutions offer possibility of calibration of partial coefficients using reliability methods.
3. Monitoring of structures during the life span so that repair strategies can be optimized through reliability.

6.12.1 Advantages of Reliability Methods (ASC-83)

The advantages of reliability methods are as listed below

- Offer a realistic procession of uncertainties and the methods for evaluating the safety factors that are often too arbitrary.
- Offer decision-making support for more economic and better balanced design.
- Analyze failure modes and measure the reliability provided by application and regulations.
- Allow the optimal distribution of material and arrange various components of the structure.
- Benefit from the experience acquired in design by updating on the basis of feedback from the experience.
- Expand the knowledge of uncertainty in response to the structure.

There are some obstacles in the implementation of these advantages. They are as follows:

- These methods demand new approach and call to our thinking and working pattern.
- Because it is more of a probabilistic approach and lesser statistical approach, it demands more mathematical concepts rather than engineering skills.
- They explicitly underscore the acceptance of risk, and using safety coefficients, they demand the judgment and decision.
- One should have minimum statistical knowledge of elementary properties of variables, and we need to use these in modeling.

6.13 Stochastic Models

The stochastic modeling essentially helps to establish variability by best-suited probability density function. They can be done by two approaches, namely naturalist's approach and physicist's approach. Reliability is also an observation of the sample that estimates μ, SD, and variance. This often gives ad hoc estimates or estimates by interval. These estimates are themselves a random variable, since based on this best judgment, PDF has to be determined. Alternatively, as per the physicist's approach, this seeks to understand the variability of the material's behavior on a microscopic scale. Results of reliability calculation depend on the quantity of data. But these data are always insufficient due to limitations that arise from the size of test samples, infinite domain, and distribution trails. Reliability analysis also requires failure scenario, which separates the situation that the designer decides as acceptable from those of the other. Complexities of reliability are mainly due to the nature of the random variables, effect of time, mechanical models and the form of performance function chosen for the analysis.

6.13.1 First-Order Second-Moment Method (FOSM)

In this case, first-order Taylor series approximation of the limit stat function is used for the analysis. Only second moments of the random variables are used to estimate the probability of failure. Limit state function is defined as:

$$M = R - S \tag{6.64}$$

where R and S are statistically independent and assumed to be normally distributed. Hence, following relationship holds good:

$$\mu_m = \mu_R - \mu S \tag{6.65}$$

$$\sigma_m = \sigma R_2 + \sigma S_2 \tag{6.66}$$

Probability of failure is given by:

$$\begin{aligned} P_f &= P(M<0) \\ &= P[(R-S)<0] \end{aligned} \tag{6.67}$$

If M is the normal variant, then

$$P_f = \phi\left(\frac{-\mu_m}{\sigma m}\right) \tag{6.68}$$

$$\beta = \text{reliability index} = \frac{\mu_m}{\sigma_m} \tag{6.69}$$

where ϕ is the case CDF of standard normal variable. Probability of failure is given by:

$$P_f = 1-\phi\left(\frac{\mu_R - \mu_S}{\sigma_R^2 + \sigma_S^2}\right) \tag{6.70}$$

If R and S are log-normal, then following relationship holds good:

$$P_f = 1 - \emptyset\left[\frac{\ln\left[\frac{\mu_R}{\mu_S}\sqrt{\frac{(1+V_S^2)}{(1+V_R^2)}}\right]}{\sqrt{\ln(1+V_R^2)(1+V_S^2)}}\right] \tag{6.71}$$

Advantages and disadvantages of FOSM method are summarized in Table 6.1.

6.13.2 Advanced FOSM

As seen above, dependency of the reliability index on the chosen form of the limit function is one of the major drawbacks of FOSM. Further, the reliability index computed on the assumption that the random variables are statistically independent and normally distributed poses an additional complexity to FOSM. This makes its application limited to problems validating the above assumptions. In a more generic

Table 6.1 Merits and demerits of FOSM of reliability

Advantages	Disadvantages
It is easy to use	Results can cause serious errors. The tool used for the distribution function cannot be approximated by normal distribution
It does not require knowledge of distribution of random variables	Values of β depend on the specific form of the limit state function. This is an invariance problem

form, advanced FOSM gives reliability index; Hasofer Lind method is one of the advanced FOSMs, which is discussed below.

The key point of the method is to estimate a *design point*, which is the minimum distance of failure from the origin. The minimum distance is the safety index (β_{HL}). The method actually transforms the random variable into a reduced form, which can be given as:

$$X_i = \frac{x_i - x_i}{\sigma_{xi}} \{\text{for } i = 1, 2, \ldots, n\} \tag{6.72}$$

This reduced variable will have a zero mean and unit standard deviation, which is a special process of distribution. Hence, the performance function $G(x) = 0$ is converted into $G(x') = 0$ to enable the mapping between the required domains. Reliability index β_{HL} is given by:

$$\beta_{HL} = \sqrt{x_d x_d^{\mathrm{T}}} \tag{6.73}$$

where x_d is the minimum distance of the design point from the origin, which is also referred as a check point.

Following cases are specific:

Case 1: Limit state function is linear

$$\text{Let us consider } M = R - S \tag{6.74}$$

The reduced values are computed for the domain mapping, as discussed below:

$$R = \frac{R - \mu_R}{\sigma_R} \tag{6.75}$$

$$S = \frac{S - \mu_S}{\sigma_S} \tag{6.76}$$

$$M = (\sigma_R + \mu_R) - (\sigma_S + \mu_S) \tag{6.77}$$

As the limit state function moves closer to the origin, failure region is mapped. Reliability index is given by:

$$\beta = \frac{\mu_R - \mu_S}{\sqrt{\sigma_R^2 + R\sigma_R^2}} \tag{6.78}$$

Case 2: Limit state function is nonlinear

In such cases, computing the minimum distance for calculating the reliability index actually becomes an optimization problem.

$$\beta_{HL} = D = \sqrt{(x)t(x)} \tag{6.79}$$

The above function is to be minimized subject to the condition that $G(x) = 0$ for many random variables (x_1, x_2,…, x_n), which originates from the safe state of the domain; $G(x) < 0$ indicates failure. Hence $G(x) > 0$ denotes the minimum distance from the origin to a point on the limit state function, which is called design point. The problem is now reduced to determining the coordinates of the design point, geometrically or analytically. By this definition, reliability index becomes invariant as the minimum distance remains constant regardless of the shape of the limit state function. Using the Lagrange multipliers, one can find the minimum distance as given below:

$$\beta_{HL} = \frac{-\sum_{i=1}^{n} x'_{\mathrm{d}i} \frac{\partial G}{\partial' x_{di}}}{\sqrt{\sum_{i=1}^{n} \left(\frac{\partial G}{\partial X_{\mathrm{d}i}}\right)^2}} \tag{6.80}$$

where $\frac{\partial G}{\partial X_{\mathrm{d}i}}$ is the partial derivative, evaluated at the design point with coordinates (x_{di}, x_{d2}, …).

6.14 Fatigue and Fracture

Fatigue design of marine structures requires a description of long-term variation of local stress caused by wave action, variable buoyancy, slamming, and vortex shedding. Main contribution to fatigue damage is caused by the frequency of load occurring that are of the order of 10–20 % of that of extreme load effects in the service life. Fatigue failures are catastrophic as they come without warning and cause significant damage. Physical process of fatigue consists of initiation of crack, stable crack growth, and unstable crack growth until rupture. Once the crack is initiated, it will tend to grow in a direction orthogonal to the direction of the oscillatory tensile stresses. Fatigue is a challenging failure mode to deal with because the initiation process of fatigue is unpredictable; difficulties exist in mapping the studies carried out in the lab scale to real structures. Fatigue failure is controlled by the following: (i) design, material, and structural detailing to address the probability of crack initiation; (ii) regular inspection during construction and operation; and (iii) following repair procedures as advised by the design loads. In case of design, the limiting conditions are already defined in advance, which are

referred as limit states. This will include the case of failure at some defined extreme loads, which will include fatigue life requirements. Commonly checked limit state for marine structures are strength under extreme loading, fatigue life, fracture, and deflection. It is a common practice to present the results of strength, fatigue, and fracture as unity check.

Let $U = \frac{\text{actual or factored load}}{\text{Acceptable load}}$ which is used for strength check.

For fatigue, the unity check is $U = \sqrt[m]{\text{Design life damage}}$ where $m = -\text{slope}^{-1}$ of S–N curve.

6.15 Fatigue Assessment

When the steel member is subjected to large fluctuating tensile stress, small cracks develop; these cracks grow in size and further progress, which make the structure to break. For machinery design where the stress fluctuation is similar throughout the design life, cyclic stresses are kept below the endurance limit. But for structures, this method is not permissible as the mixture of large-amplitude and small-amplitude stresses occur due to environmental loads. Hence, it becomes necessary to design the structures for intended fatigue life. Common design approach is nothing but the usage of S–N curve. These curves are based on experiments conducted on different types of structures. Fatigue failure can be detected by the occurrence of visible cracks, thickness of the crack, and complete loss of load-carrying capacity.

6.15.1 SN Approach

Test on the steel specimen subjected to fluctuating loading showed that the number of cycles to failure (N) is inversely proportional to the stress range that is maximum and minimum stress, let it will be S, which is the power of m:

$$N \propto \frac{1}{s^m}$$

$$N = ASm^{-1}$$

If measures are taken to prevent corrosion, then for constant amplitude of stress cycling there is a cutoff stress below which no fatigue occurs. This is found to be 2×10^8 cycles. For variable amplitude stress cycling, which is the most general case with the marine structures, the cutoff value of stress decreases as the fatigue crack grows. The slope of S–N curve changes beyond 10^7 cycles from m to $m + 2$. This effect is significant if one is looking for the higher order of fatigue lives. Hence, for preliminary analysis, S–N curve can be taken as linear, which often simplifies the

analysis. Over the range where m is constant, the S–N curves are plotted as straight line on log–log scale, whose slope is $(-1/m)$. Since S–N curves are experimentally plotted, for welded specimen, $m = 3$. Local stress concentration effect is caused by the shape of welds, and the specimen reduces the value of constant A. Increase in thickness reduces the fatigue life and hence A. Fatigue life decreases in freely corroding condition. Tubular joints have been subjected to a separate study, and a number of cycles are used for T-joints. One of the most proffered curve is UK T-Curve, which is given in Fig. 6.2.

S–N curve may be typically be formulated as

$$\begin{aligned} N &= ASm^{-1} \\ N &= ASm^{-1} \quad \text{for } s > s'; \\ N &= \infty \quad \text{for } s \le s'; \\ &\text{or} \\ N &= A_1 S^{-m_1} \quad \text{for } s > s'; \\ N &= A_2 S^{-m_2} \quad \text{for } s \le s'; \end{aligned} \tag{6.81}$$

where the point of intersection between the two equations will be (N', S') with

$$N' = A_1 \left(S'\right)^{-m_1} = A_2 \left(S'\right)^{-m_2}$$

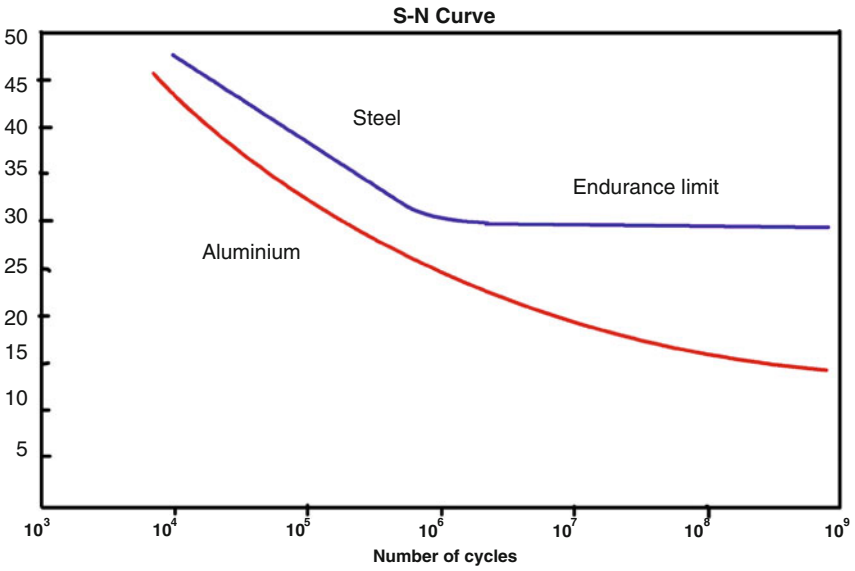

Fig. 6.2 Typical S–N curve

Alternatively S–N curve defined by $A = A_c$ is used to design the checks:

$$\log_{10} A_c = \mu - 2S$$

where μ is the mean value of parameter of $\log_{10}N$ and S is the standard deviation of parameter of $\log_{10}N$.

Consider typical $\mu \approx 12$; S $\approx$ 0.2; hence, $\frac{A_c}{\mu_A} \approx 0.4$. It is noted that $A = A_{\text{ref}}\left(\frac{t_{\text{ref}}}{t}\right)^{m/4}$ where A_{ref} is the reference parameter in the S–N curve, t and t_{ref} are the plate thickness and the reference plate thickness, which are measured in mm.

S–N curves are traditionally determined by constant amplitude testing with large stress method:

$$R = \frac{\sigma_{\min}}{\sigma_{\max}} > 0.5 \tag{6.82}$$

Simplifying that stress, we can obtain the crack opening mode. Factors affecting S–N curve are relaxation of residual stresses, external loading with partly compression, and crack closure effects, which would make the actual crack growth lesser than the implied load by the stress ranges used in the existing S–N curve.

6.16 Miner's Rule

For variable amplitude environmental loading, the S–N curve provides information on constant amplitude loading, which is supplemented by Miner's rule. This allows the number of drift amplitude cycle and concept of fatigue damage based on this rule. Fatigue damage for a joint, under n cycles of constant amplitude loading when it could be taken as $N = AS^{-m}$ cycles, is given by n/N. If the joint is subjected to variable amplitude loading, the load on the cycles can be divided into groups of approximately equal stress ranges. If there are g such groups with almost equal stress range in a given variable amplitude loading, then let s_g be the stress range in each group and n_g be the number of cycles in each group. Fatigue damage for each group will be

$$D_g = \frac{n_g}{N_g} \quad \text{where} \quad N_g = AS_g^{-m} \tag{6.83}$$

Miner's rule states that the failure under variable amplitude loading which will occur when

$$\sum_{g=1}^{G} D_g = 1 \tag{6.84}$$

Fatigue analysis will often refer to the values of n_g and S_g as the fatigue spectrum.

6.17 Fatigue Loading and Fatigue Analysis

Local stresses for fatigue design need to be determined for the temporal and spatial variation.

Figure 6.3 shows the spatial definition of notch, hot spot in the plane surface. Figure 6.4 shows the hot spot. For welded structures, the main parameter that represents the variation in time is called the stress range. This approach is based on the fact that tensile residual stresses are always present and that all stress cycles effectively derive the crack. The spatial stress variation can be accounted for by using nominal hot spot stress approach. Fatigue loading is a dynamic load such as wind, wave, and machine operation on marine structures. The primary source of the fatigue loading is the wave loads. Global analysis of the fatigue loading causes undesirable effects on the members. Local stress analysis is carried out to determine the hot spot stresses.

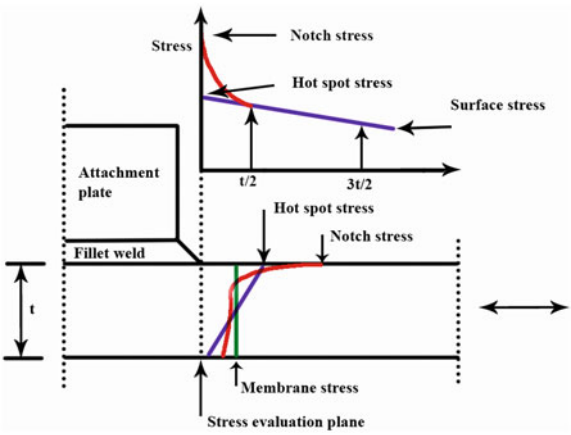

Fig. 6.3 Spatial definition of notch, hot spot and surface in a plane surface

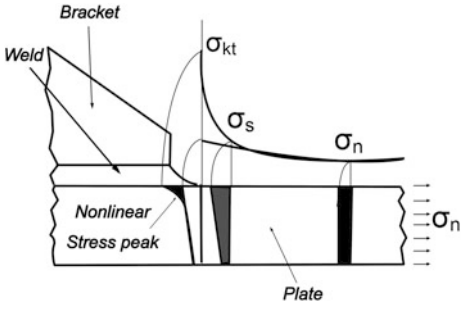

Fig. 6.4 Hot spot stresses

6.18 Time Domain Fatigue Analysis

Time domain fatigue analysis results in time series of stress. For narrowband Gaussian response, the cycles are well defined. For more general stress time histories, cycle counting methods have to be applied to all types of response time series. Time domain methods use only the information provided by the series of peaks (local maximum) and valleys (local minima). According to different methods of constructing the effective stress ranges from these identified peaks and valleys, various cycle counting methods are used. The procedures are described by ASTM-1985. This includes peak counting, range counting, level-crossing counting, and rain flow counting. Among these, rain flow counting is the best for fatigue damage estimates.

6.18.1 Rain Flow Counting

This method was first proposed by Matsuishi and Endo (1968). Let us consider a stress time series of peaks and valleys with the time axis vertically downwards. Lines connecting peaks and valley from a series of pagoda roofs are constructed. Each rain flow begins at the beginning of the time series at the inside every peak and valley. Rain flow initiating at a peak (or a valley) drop down until it reaches peak more positive (or a valley, more negative) than the peak (or the valley) from where it started. Rain flow also stops when it meets the rain flow roof assume. Rain flow must terminate at the end of the time series. Horizontal length of each rain flow is counted as half-cycle with that stress range.

6.18.1.1 Methodology

1. Reduce the time history to a sequence of (tensile) peaks and (compressive) troughs.
2. Imagine that the time history is a pagoda.
3. Turn the sheet clockwise 90°, so the starting time is at the top.
4. Each tensile peak is imagined as a source of water that 'drips' down the pagoda.
5. Count the number of half-cycles by looking for terminations in the flow occurring when:

- it reaches the end of the time history;
- it merges with a flow that started at an earlier tensile peak; or
- it encounters a trough of greater magnitude.

6. Repeat Step 5 for compressive troughs.
7. Assign a magnitude to each half-cycle equal to the stress difference between its start and termination.

8. Pair up half-cycles of identical magnitude (but opposite sense) to count the number of complete cycles. Typically, there are some residual half-cycles.

From Fig. 6.5, it is observed that rain flow starts at a valley point 1 drops down to 2 and 3 and so on. The cycle ends at 10, which is found to be a peak. These are 9 half-cycles that could be extracted. The rain flow initiates at valley point 1 and drops down to 2 and ends at 4 because the following valley has smaller value than initiating at point 1. Since the half-cycle 1–2–4 is identified, the same rule is applied to half-cycle 5–6. The second rain flow starts at 2 and ends at 3 because the success peak at 4 is larger than 2 similarly half-cycle 4–5–7 and 8–9 are extracted half-cycle 7–8–9 is found because time series end at 10. Half-cycles 3–2′, 6–5′, and 9–8′ are determined because of rain flow starts at 3, 6, and 9 peaks meets the rain flow at roofs above. When all half-cycle are exhausted, the horizontal length of each cycle is used as an effective stress range to calculate the fatigue damage based on the linear damage accumulation law (Table 6.2).

$$D_{RC} \leq D_{RFC} \leq D_{LCC} (= D_{NB}) \leq D_{PC} \tag{6.85}$$

D_{RC} be the fatigue damage estimated by range counting
D_{RFC} be the rain flow counting
D_{LCC} be the level-crossing counting
D_{PC} be the peak counting
D_{NB} be the narrowband approximation

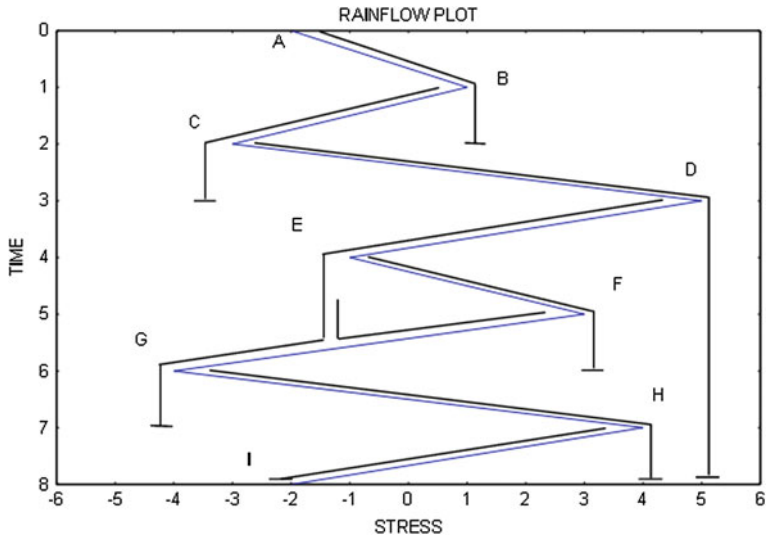

Fig. 6.5 Example of rain flow counting

Table 6.2 Rain flow counting

Rain flow cycles by path		
Path	Cycles	Stress range
A–B	0.5	3
B–C	0.5	4
C–D	0.5	8
D–G	0.5	9
E–F	1.0	4
G–H	0.5	8
H–I	0.5	6
Rain flow, total cycles		
Stress range	Total cycles	Path
10	0	–
9	0.5	D–G
8	1.0	C–D, G–H
7	0	–
6	0.5	H–I
5	0	–
4	1.5	B–C, E–F
3	0.5	A–B
2	0	–
1	0	–

6.19 Deterministic Fatigue Analysis

The deterministic fatigue analysis method applies Miner's rule. The loading of the structure is represented by loading cases $g = 1$ to G, each with a defined number of cycles (n_g) and time T. The structure is analyzed to determine the stress S_g for each group and hence the total damage D_t in time T. If the value of T is chosen as a year, then the fatigue life is $1/D_{\text{year}}$. When fatigue damage is high, majority of damage occurs on the low cycle end of the curve, where M is typically 3. But when the structure is subjected to dynamic loading and the band of periods near the natural period, then the small change in an assumed period of the applied load changes the result significantly. Marine structures which are subjected to wind and wave loading act as period-dependent filters. As a result, the number of cycles of stress response may differ from the number of loading cycles. This difficulty can be handled in spectral analysis. Deterministic fatigue analysis is often performed using semiempirical relationship. When structures are subjected to waves, only 1 wave analysis is used to describe the lifetime stress history of the structure. For long-term exceedance to be Weibull function:

$$n(\text{stress} > \sigma) = n_o \exp\left\{ \left(\frac{\sigma}{\sigma_o}\right)^h \ln\, n_o \right\} \tag{6.86}$$

where n is the number of stress cycles exceeding stress in n_o cycles, σ_o is stress that is exceeded once in n_o cycles, and h is the parameters (0.5–1.5) that depend on load and response characteristics of the structures. For long-term exceedance to be log-linear,

$$n(\text{Wave height} > H) = n_o \exp\left\{ -\left(\frac{H}{H_0}\right) \ln\, n_o \right\} \tag{6.87}$$

where H_o is the wave height exceeded once in the number of cycles known. H is the wave height exceeded n times in the number of cycles. The long-term exceedance can be considered with single-slope S–N curve to estimate the fatigue damage in n_L cycles.

For Weibull distribution:

$$D_L = \frac{n_L \sigma_o^m}{A} \left[\frac{\Gamma\left(1 + \frac{m}{h}\right)}{(\ln n_o)^{m/h}} \right] \tag{6.88}$$

For log-linear wave, height exceedance is given by:

$$D_L = \frac{n_L \left(a H_o^b\right)^m}{A} \left[\frac{\Gamma(1 + bm)}{(\ln n_o)^{bm}} \right]$$

Γ is a gamma function defined as

$$\Gamma(g) = \int_0^\infty x^{g-1} \mathrm{e}^{-x} \mathrm{d}x \tag{6.89}$$

This is a standard function and the values are available in standard tables.

6.20 Spectral Fatigue Analysis

Spectral fatigue analysis is applicable to structures that are executed by dynamic loading which has statistically stationary properties for a large number of stress cycles, for example, wind turbulence and wave load. The spectral method uses the shape of the stress spectrum to determine the number of stress cycles of various sizes. The stress spectrum can be narrowbanded or broadbanded.

6.20.1 Narrowband Spectrum

To perform fatigue calculation, we should compute zeroth and second moment of the spectrum about the line $f = 0$. It is common to assume Rayleigh distribution of the stress range in a given stress spectrum. m_0 and m_2 can be computed using numerical integration technique, that is, by trapezoidal rule. m_0 is the area under the spectrum which will correspond to variance of the signal and represented as the spectrum. For the spectrum with the Hz frequency axis, the square root of the ratio of second moment (m_2) to the area (m_o) is the mean zero-crossing period of the signal.

$$T_Z = \sqrt{\frac{m_o}{m_2}} \tag{6.90}$$

The number of stress cycles (n) in time (T) in seconds is given by

$$n = \frac{T}{T_z} \tag{6.91}$$

Rayleigh distribution assumes the plot of the shear range σ_r as:

$$p(\sigma_r) = \frac{\sigma_r}{4m_0}\exp\left(-\frac{\sigma_r^2}{8m_o}\right) \tag{6.92}$$

In T seconds, the number of stress cycles (δ_n) in the band ($\delta\sigma_r$) cantered as σ_r is given by

$$\delta_n = n * p * (\sigma_r)(\delta\sigma_r)$$

Fatigue damage associated with that band of stress cycle

$$\delta_D = \frac{\delta_n}{N} = \frac{\delta_n}{A\sigma_r^{-m}} = \frac{n\left(\frac{\sigma_r}{4m_0}\right)\exp\left[-\left(\frac{\sigma_r}{8m_o}^2\right)\right]\delta\sigma_r}{A\sigma_r^{-m}} \tag{6.93}$$

Fatigue damage of all σ cycles band is found by integration, which is given by

$$\begin{aligned} D &= \int_0^\infty \frac{n\left(\frac{\sigma_r}{4m_0}\right)\exp\left[-\left(\frac{\sigma_r}{8m_o}^2\right)\right]\delta\sigma_r}{A\sigma_r^{-m}} \\ D &= \frac{n}{4Am_0}\int_0^\infty \sigma_r^{(1+m)}\exp\left(-\frac{\sigma_r^2}{8m_o}\right)\delta\sigma_r \end{aligned} \tag{6.94}$$

The integral has a standard solution of S–N curve, which is a gamma function:

$$\int_0^\infty x^a \exp\left(-bx^2\right)\mathrm{d}x = \frac{\Gamma\left(\frac{a+1}{c}\right)}{C\left(B^{\left(\frac{a+1}{c}\right)}\right)} \tag{6.95}$$

where $\Gamma(g) = \int_0^\infty x^{(g-1)}\mathrm{e}^x\mathrm{d}x$.

6.20.2 Broadband Spectrum

There are many methods available to explain how to count the stress range cycles in stationary broadband time history. Rain flow counts in largest cycles are extracted first. The smaller cycles are considered superimposed on the larger cycle. This is considered the most reliable method for fatigue σ range counting. Each crest is matched with the following trays. Now, the above definition is of use for frequency-domain calculation because the definition of cycles was set up in terms which were not amenable with statistical analysis. The spectral fatigue damage analysis of structures subjected to random loading assumes that the signal is stationary, Gaussian, and random. Results are generally produced for mean period of zero crossing per unit time.

$$T_Z = \sqrt{\frac{m_0}{m_2}} \tag{6.96}$$

For mean time between the peaks or crests per unit:

$$T_c = \sqrt{\frac{m_2}{m_4}} \tag{6.97}$$

where m_n is the nth moment of the PSD function.

$$m_n = \int_0^\infty f^n S_{\sigma\sigma}(f)\mathrm{d}f \tag{6.98}$$

$S_{\sigma\sigma}(f)$ is one-sided stress spectrum, f is the frequency in Hz.
m_n values are obtained by numerical integration.

An irregularity factor, β is defined as $\beta = \frac{T_c}{T_z}$

β is an important factor in fatigue analysis because difficulty of prediction of σ cycle distribution from a σ spectrum is largely determined by whether its value lies between 0 and 1. As it approaches 1, the signal becomes narrowband, and probability density of the peak is given by

$$p(\sigma_p) = \frac{\sigma_p}{m_o} \exp\left(-\frac{\sigma_p^2}{2m_o}\right) \tag{6.99}$$

Cycle counting in this case is relatively easy. As β approaches zero, signal becomes more like with noise. In this case, signal is said to be completely wideband. Probability density function peaks become Gaussian:

$$p(\sigma_p) = \frac{1}{\sqrt{2\pi m_0}} \exp\left(-\frac{\sigma_p^2}{2m_o}\right) \tag{6.100}$$

In reality, the response is neither narrow nor completely wideband. It is in between, so one can apply correction factors to the solution. Several researchers attempted to correct the narrowband fatigue damage calculation for the effects of a broad bandwidth. They are developed by generating sample time histories from stress spectra using inverse Fourier transform, and then, a conventional rain flow cycle count can be obtained.

6.20.2.1 Wirsching's Correction Factor

$$D_{\mathrm{RF}} = \lambda D_{\mathrm{NB}}(M, \in)$$

D_{RF} = rain flow-counting damage; D_{NB} = damage calculated using NB formula.

$$\lambda(M, \in) = a(m) + [1 - a(m)](1 - \in)^{c(m)}$$
$$a(m) = 0.926 - 0.333 \text{ m}$$
$$c(m) = 1.587 - 2.323 \text{ m}$$
$$\varepsilon = \sqrt{1 - \beta^2}$$

6.20.2.2 KAM and Doves—Alternative Approach

This expression uses equivalent σ range parameter called σ_{efr}. The idea is to conceive total linearity cumulative fatigue damage caused by constant amplitude σ range using rain flow cycles extracted from the stress cycle.

$$\sigma_{\text{efr}} = \left[\int_0^{\infty} \sigma_r^m p(\sigma_r) \mathrm{d}\sigma_r\right]$$

$$\sigma_{\text{efr}} = 2\sqrt{2m_0}\left[\lambda(m,\varepsilon)\Gamma\left(\frac{m}{2}+1\right)\right]^{1/m}$$

6.20.2.3 Chaudhary and Dover Approach

Based on the study of peak distribution in different sea-state spectra, following equation is proposed by Chaudhary and Dover (1985):

$$\sigma_{\text{efr}} = 2\sqrt{2m_0}\left[\frac{\varepsilon^{m+2}}{2\sqrt{\pi}}\Gamma\left(\frac{m+1}{2}\right) + \frac{\beta}{2}\Gamma\left(\frac{m+2}{2}\right) + \text{err}(\beta)\frac{\beta}{2}\Gamma\left(\frac{m+2}{2}\right)\right]^{1/m} \tag{6.101}$$

where err $(\beta) = 0.3012(\beta) + 0.4916(\beta)^2 + 0.918(\beta)^3 - 2.3534(\beta)^4 - 3.3307(\beta)^5 + 15.654(\beta)^6 - 10.7846(\beta)^7$ for $0.13 < \beta < 0.96$.

6.20.2.4 Hancock's Equation

Hancock and Gall (1985) proposed equations to include β and ε into narrowband equation:

$$\begin{aligned}\sigma_{\text{efr}} &= \sqrt[2]{2m_0}\left[\beta\Gamma\left(\frac{m}{2}+1\right)\right]^{1/m} \\ \sigma_{\text{efr}} &= \beta\sqrt[2]{2m_0}\left(2-\varepsilon^2\right)\left[\Gamma\left(\frac{m}{2-\varepsilon^2}+1\right)\right]^{1/m}\end{aligned} \tag{6.102}$$

The above factors are used to amend the traditional narrowband approach. An alternate approach is to avoid narrowband assumption and to develop fatigue life prediction in terms of rain flow ranges.

Probability density function of rain flow ranges $P_{\text{RF}}(\sigma_r)$ is given as:

$$\begin{aligned}P_{\text{RF}}(\sigma_r) &= \frac{\left(D_1/Q\right)e^{-2/Q} + \left(D_2 Z/R^2\right)e^{-z^2/2R^2} + D_3 Z e^{-z^2/2}}{2m_o^{1/2}} \\ \beta &= \frac{T_c}{T_Z} = \sqrt{\frac{m_2^2}{m_0 m_4}}\end{aligned} \tag{6.103}$$

$$x = \frac{T_c}{T_Z} = \frac{m_1}{m_0}\sqrt{\frac{m_2}{m_4}}; Z = \frac{\sigma_r}{2\sqrt{m_0}}$$

$$D_1 = \frac{2\left(x_m - \beta^2\right)}{1+\beta^2}$$

$$D_2 = \frac{1-\beta-D_1+D_1^2}{1-R}$$

$$D_3 = 1 - D_1 - D_2$$

$$R = \frac{\beta - x_m - D_1^2}{1-\beta-D_1+D_1^2}$$

$$Q = \frac{1.25(\beta - D_3 - RD_2)}{D_1}$$

$m_n = \int_0^\infty f^n S_{\sigma\sigma}(f)\mathrm{d}f$ which is given as nth moment used in above equation.

$$\sigma_{\text{efr}} = \int_0^\infty \sigma^m \beta(\sigma_r)\mathrm{d}\sigma_r \tag{6.104}$$

Now instead of $\beta(\sigma_r)$, substitute $P_{RF}(\sigma_r)$ in the above equation to obtain the effective stress range.

For $n = T/T_c$ damage can be estimated by:

$$D = \left(\frac{T}{T_c}\right)\left(\frac{1}{A}\right)\int_0^\infty \sigma_r^m P_{RF}(\sigma_r)\mathrm{d}\sigma_r \tag{6.105}$$

6.20.2.5 Summary of Broadbanded Fatigue Damage Calculation

A general solution for fatigue damage can be obtained for wideband case using the rain flow range probability density function. There is one stress range for each peak stress in the response so that the number of the stress range in time T is $\mathrm{T}/\mathrm{T_C}$. The equation for damage in time T is given by

$$D = \left(\frac{T}{T_c}\right)\left(\frac{1}{A}\right)\int_0^\infty \sigma_r^m P_{RF}(\sigma_r)\mathrm{d}\sigma_r \tag{6.106}$$

6.21 Stress Concentration Factor (SCF)

Fatigue damage estimates are highly dependent on the stress cycle range, which need to be considered in the S–N curve.

$$N = AS^{-m}$$

But in marine structures, stress concentration effects in the joints should be augmented for using them in the fatigue damage estimates. For plated construction, the procedure is quite simple to determine the applied stress with an additional stress concentration factor by equations or graphs. But when the crack growth is expected from a sharp notch or corner, which is not a part of the geometry, stresses may show infinite enhancement that makes the S–N curve approach unsatisfactory. For example, tubular joints show stress changes rapidly in the vicinity of the joint which has no reference stress in the S–N curve approach. This problem is generally solved by extrapolating the stress from 2 points away from the weld. Approximate stress concentration factor, as per the designer's choice, can be used. In a tubular joint, fatigue is dominated by the stress perpendicular to weld, so the other stress components need to be considered in the damage estimates.

6.22 Crack Propagation

Application of fracture mechanics to the fatigue of the steel structures uses Paris and Erdogan (1983) law. The law states that the crack growth (δ_a) in δN cycles in the applied stress range of (σ_r) is given by

$$\begin{aligned} \delta_a &= C\left[y\sigma_r\sqrt{\pi a}\right]^m \delta N \\ \delta a &= C[\delta K]^m \delta N \end{aligned} \tag{6.107}$$

where y is the crack and geometry-dependent factor. For a through thickness crack that occurs at the center of a very wide plate, $y = 1$; a is the crack length, which increases with the increase in the applied stress cycles; C and m are material-dependent constants. For example, typical mean values for C and m for BS 4,360 grade 50D steel is $C = 5.2 \times 10^{-12}$ to 7.1×10^{-12} meters $/\text{MPa}\sqrt{(\text{meters})^{\text{m}}}$ where $m = 3$.

Unit of C is complex, which makes the conversion difficult. Hence, the following table can be used (Table 6.3).

Fatigue crack propagation based on fracture mechanics is normally worked out in a tabular form (Table 6.4):

Each row of the table calculates the crack growth in every δN cycle, which is chosen so that δa is reasonably small when compared with the value of crack length (a); this makes the crack length independent of the increment of the crack growth.

Table 6.3 C conversion table

To convert	From to	Multiply C by
Crack size	m to mm	$10^{3(1-m/2)}$
Stress	MPa to kPa	10^{-3m}
Stress	MPa to Pa	10^{-6m}

Table 6.4 Fatigue crack propagation

a	σ_r	y	Δk	δN	δa
1	2	3	4	5	6

6.22.1 Step-by-Step Procedure to Compute the Fatigue Crack Propagation

Step 1 An initial value of the crack length (a) is known at the beginning of the calculation

Step 2 Stress range σ_r may vary for the wave to wave case; hence, it is advisable to use σ_{efr}

$$\sigma_{\text{efr}} = m\sqrt{\frac{1}{N}\sum_{i=1}^{N}\sigma_{r_i}^{m}}$$

It is important to note that *growing crack leads to the reduction of stiffness and causes redistribution of stresses away from the crack. This would require computation of the effective stress for different crack length*. But for simplification, this need not be done.

Step 3 y is calculated at each stage of the crack growth.

Step 4 $\Delta k = y\sigma_r\sqrt{\pi a}$

Step 5 δN is selected to give small changes in the crack length. Depending on the rate of crack growth, this value may be selected corresponding to the number of cycles in 1 year or 1 month, etc.

Step 6 $\delta a = C(y\sigma_r\sqrt{\pi a})^m$.

Step 7 Crack length (a) is increased from a to ($a + \delta a$).

Step 8 Use the effective stress, same as in Step 2.

Step 9 y is calculated now for the new crack length.

Step 10 Thus, all the values in the above table will be filled up in the sequential manner.

Calculation is repeated for as many crack growth increments as that are required to reach a critical crack size. Computation is terminated until the defect may be then large enough to result in failure due to large stress values.

Exercise

1. Explain stationary process?
2. Explain impulse response function or the transfer function?
3. $H(\omega)$ is called the transfer function or _____ function.
4. Write down the equation which gives the relationship between the response spectrum $S_X(\omega)$ and the load spectrum?
5. The procedure of replacing the input spectrum by a constant (S_0) is called _____.
6. Explain the two approaches in dynamic analysis?
7. Explain return period?
8. Safety is a measure used to indicate the _____.
9. Reliability offers _____ meaning to this traditional concept.
10. Explain the levels of reliability?
11. List the advantages of reliability methods?
12. The stochastic modeling essentially helps to establish variability by best-suited _____.
13. Differentiate merits and demerits of FOSM of reliability?
14. The reliability index computed on the assumption that the random variables are _____ and _____an additional complexity to FOSM.
15. _____ of marine structures requires a description of long-term variation of local stress caused by wave action, variable buoyancy, slamming and vortex shedding.

Answers

1. A stationary process is one for which the statistical properties such as mean value and standard deviation are same for all points in time (or) position. Hence, the following equation holds good. For a stationary process, transfer between the load and the response can be modeled as linear, time-invariant, while the system can be characterized by a transfer function. Hence, the relationship between variance spectrum of the response (called response spectrum) and variance spectrum of load (called load spectrum) is determined by a transfer function.
2. Impulse response function or the transfer function, which determines the connection between the load and the response, is completely defined by the properties of the linear system. This remains independent of any given load.

3. Frequency response.

$$H_{FX}(-\omega) = \int_0^\infty h_{FX}(t)\mathrm{e}^{i\omega t}\,\mathrm{d}t = \int_0^\infty h_{FX}(t)\mathrm{e}^{-i\omega t*}\mathrm{d}t$$

$$\int_0^\infty h_{FX}(t)\mathrm{e}^{-i\omega t*}\mathrm{d}t = H_{FX}(\omega)^*$$

$$H_{FX}(-\omega) = \int_0^\infty h_{FX}(t)\mathrm{e}^{i\omega t}\,\mathrm{d}t = \int_0^\infty h_{FX}(t)\mathrm{e}^{-i\omega t*}\mathrm{d}t$$

4. $$\int_0^\infty h_{FX}(t)\mathrm{e}^{-i\omega t*}\mathrm{d}t = H_{FX}(\omega)^*$$

$$S_X(\omega) = |H_{FX}(\omega)|^2 S_F(\omega)$$

5. White noise approximation.
6. Dynamic analyses can be carried out in two ways depending on the description of loads, namely (i) deterministic analysis, which requires the complete knowledge of load time history and (ii) stochastic analysis where statistical concepts are used to specify the loads. For example, when waves or wind loads are described in terms of statistical quantities, then the response should also be described and analyzed in terms of same kind of quantities.
7. Return period of exceedance of ξ then becomes as follows:

$$\bar{R}(z) = \frac{1}{\mathrm{Prob}(Z > \xi)} = \frac{1}{0.01} = 100 \text{ years}$$

Reference period, in this case, is 1 year, and therefore, return period of exceedance is 100 years. It is important to note that the time-varying loads, caused by waves, cannot be considered stationary over an extended period. This means that the quantities such as yearly maxima must be computed using long-term statistics. Return periods are also computed based on the risk associated. This is a common practice in case of earthquake loads and seismic design of structures.

8. Reliability.
9. Probabilistic.
10. Reliability studies are considered in different levels in the literature. Level I is focusing on the probability aspects of the problem. Suitable characteristic values of the random variables are introduced in the safety analysis. Main objective of this level of study is to minimize the deviation of the design values from that of the target value. For example, LRFD is of level I of reliability. Level II has two values for each parameter to be defined in the analysis, namely mean and standard deviation. Level III is a complete analysis of the problem

addressing the multi-dimensional probability density function of random variables, which is extended over the safety domain. Reliability is expressed in terms of suitable safety indices. In level IV, engineering economics is also applied in the reliability study. This level of reliability study is usually applied to structures of strategic importance. The study includes cost-benefit analysis, rehabilitation, consequence of failure, and return on capital investment.

11. The advantages of reliability methods are as listed below

- Offer a realistic procession of uncertainties and the methods for evaluating the safety factors that are often too arbitrary.
- Offer decision-making support for more economic and better balanced design.
- Analyze failure modes and measure the reliability provided by application and regulations.
- Allow the optimal distribution of material and arrange various components of the structure.
- Benefit from the experience acquired in design by updating on the basis of feedback from the experience.
- Expand the knowledge of uncertainty in response to the structure.

12. Probability density function.
13.

Advantages	Disadvantages
It is easy to use	Results can cause serious errors. The tool used for the distribution function cannot be approximated by normal distribution
It does not require knowledge of distribution of random variables	Values of β depend on the specific form of the limit state function. This is an invariance problem

14. Statistically independent and normally distributed poses.
15. Fatigue design.

Chapter 7
Applications in Preliminary Analysis and Design

Abstract This chapter deals with a few application problems in the design and development on new offshore structures based on the dynamic analyses. Studies presented in this chapter are based on the recent research conducted by the author, which are presented as a part of intuitive studies to the readers.

Keywords Design · Offshore structures · Preliminary design · Triceratops · Buoyant leg structure · Ball joints · Response isolation · Structural forms · Wave directionality · Springing · Ringing · Tension leg platforms

7.1 Free Vibration Response of Offshore Triceratops

Offshore triceratops is relatively a new type of compliant structure suitable for deepwater oil exploration. The structural form of the platform enables to counteract the encountered environmental loads efficiently. Triceratops consists of three or more buoyant leg structures (BLSs) to achieve the required buoyancy, to support the deck structure, to restrain system, and to serve storage requirements. The deck and BLSs are connected by ball joints that transfer translational motion but restrain rotations from BLS to deck and vice versa. Free-decay studies are conducted on 1:150 scaled model, in free-floating and tethered conditions experimentally, analytically and numerically; natural periods in heave and pitch/roll degrees of freedom are discussed for installation and decommissioning purposes. Experimental and analytical free-decay tests are conducted on the installed structure in surge and heave degrees of freedom; experimental, analytical, and numerical results are in good comparison. Based on the studies carried out, it is seen that the free-floating natural periods of both single BLS and tethered triceratops are away from the bandwidth of encountered wave periods, making the proposed platform safe and suitable for the chosen sea state and ultra-deep waters.

S. Chandrasekaran, *Dynamic Analysis and Design of Offshore Structures*,
Ocean Engineering & Oceanography 5, DOI 10.1007/978-81-322-2277-4_7

7.2 New Structural Form

There exist many offshore structures for deep waters such as compliant towers, tension leg platforms (TLPs), spars, semi-submersibles, and FPSOs. Recent developments focus on the optimization of structural form of compliant structures with respect to their cost, reduction in structural response, and enhancing their payload capacities. Operational features including the stability of tethered buoyant platforms are addressed by performing stochastic stability analysis (Muhuri and Gupta 1983). Buchner et al. (1999) discussed the complexities in model tests carried out on the new state-of-the-art deepwater offshore basin of Maritime Research Institute Netherlands (MARIN). Jayalekshmi et al. (2010) investigated the effect of tether-riser dynamics on the response characteristics of deepwater TLPs in water depths 900 and 1,800 m under random waves in time domain; statistical values of responses are found to increase with increase in water depth and significant increase is observed when risers are included in the analysis. Comparative studies carried out on TLPs with two different geometries that show the triangular TLPs are cost effective (Chandrasekaran and Jain 2002). It is also shown that triangular TLPs exhibit lesser response in the surge and heave degrees of freedom than that of the four-legged (square) TLPs. Chandrasekaran et al. (2007) presented the response behavior of triangular TLP under regular waves using Stokes nonlinear wave theory, and results show that the response in surge and pitch degrees of freedom obtained using Stokes' theory is lesser than that obtained using the Airy's wave theory.

Offshore triceratops is relatively a new concept with respect to the structural form that is attempted for ultra-deep waters (Charles et al. 2005); the chosen structural form enables reduction of response when compared with conventional deepwater offshore structures such as TLPs, imparting economic, and structural advantages in the design. Triceratops consists of BLS, deck structure, ball joint, and foundation system, which is usually with tethers. BLS is a positively buoyant, floating, deep-draft structure intended for use in ultra-deep waters (Rodert and Cuneyt 1995). It is simple cylindrical structure that is used to provide required buoyancy to support deck structure, buoyant leg, and tethering system. BLS unit appears to resemble a spar due to its deep draft, but the restraining system resembles the behavior of a TLP; restraining system provides less rotational stiffness, and hence the pitch and roll responses are more than TLP but lesser than spar (Shaver et al. 2001). Capanoglu et al. (2002) showed a good comparison of the results of model tests with that of the analytical studies of a BLS. Chandrasekaran et al. (2010, 2011) carried out analytical and experimental studies on offshore triceratops under unidirectional regular waves; the influence of ball joint on the response of the deck in pitch and heave degrees of freedom are focused. Limitations of the experimental investigations on triceratops for ultra-deep waters are also discussed in detail. In the present study, natural period of free-floating and tethered (600 m) triceratops is examined to analyze few critical features: (i) installation; (ii) operational; and (iii) decommissioning feasibility. Foundation system is chosen as

Table 7.1 Mass properties of free-floating and tethered offshore triceratops

Details	Free-floating		Tethered	
	Prototype (ton)	Model (kg)	Prototype (ton)	Model (kg)
Payload	4,059	1.2	4,059	1.2
Ball joint	1,013	0.3	1,013	0.3
Leg weight	18,225	5.4	18,225	5.4
Ballast	21,032	6.23	21,032	6.23
Additional ballast	8,635	2.56	–	–
Pretension	–	–	8,635	2.56
Total	52,982	15.7	52,982	15.7
Displacement	52,982	15.7	52,982	15.7

tethered system since flexible behavior is economical for ultra-deep waters. Ball joint is placed between the BLS and deck to reduce the rotational response of the deck when the BLS is exposed to wave, current, and impact loads; in addition, it reduces rotational response of BLS units when the deck is exposed to aerodynamic loads. In the present study, triceratops consists of three BLS units whose geometric form and mass distribution are derived from Norwegian TLP at 600 m water depth; vertical center of gravity (VCG) to draft ratio is maintained as 0.5, as desired for deep-draft compliant structures. Free-decay oscillation studies are performed experimentally, analytically, and numerically on 1:150 scaled free-floating and tethered models; mass properties and structural details of both the models are given in Tables 7.1 and 7.2, respectively, while Fig. 7.1 shows the elevation of the scaled model considered for the study.

7.3 Model Details

BLS units are fabricated with acrylic cylinders of 100 mm diameter. Two-tier deck systems are fabricated with 1.5-mm thick aluminum sheets and placed at two different elevations to maintain the required VCG. Three tethers are connected to respective the BLS units using steel wire ropes of 0.3 mm diameter. Ball joints are made of Perspex material and placed between BLS units and the deck. Mild steel rods are used for the permanent ballast in each of the BLS unit so as to match the mass properties close to that of the prototype. Accelerometer and inclinometers are placed on the BLS units, while the deck is placed with the instruments to measure heave and pitch responses. Figure 7.2 shows the model commissioned in the wave flume.

Table 7.2 Details of prototype and model of free-floating and tethered triceratops

Details	Free-floating		Tethered	
	Prototype (m)	Model (mm)	Prototype (m)	Model (mm)
Water depth	600	4,000	600	4,000
Draft	97.5	645.5[a]	97.5	650
Each buoyant leg structure				
Outer diameter	15	100.0	15	100.0
c/c distance	70	467.0	70	467.0
Cylinder height	120.0	800.0	120.0	800.0
VCG	−51.36	−337.8	−58.87	−392.5
r_x, r_y	31.81	212.1	33.31	222.05
r_z	4.98	33.2	5.02	33.49
Deck				
r_{Dx}, r_{Dy}	24.9	165.9	24.9	165.9
r_{Dz}	24.6	164.5	24.6	164.5
VCG	46.35	309.0	46.35	309.0
VCG of the whole structure	−55.39	−236.07[a]	−49.23	−328.22
Tether[b]			*t*	kg
Pretension			8,652	2.56
			kN/m	N/mm
AE/*l*			84,000	3.73

l length of the tether; A_w water plane area
[a] Corrected to flume density
[b] Bare tether

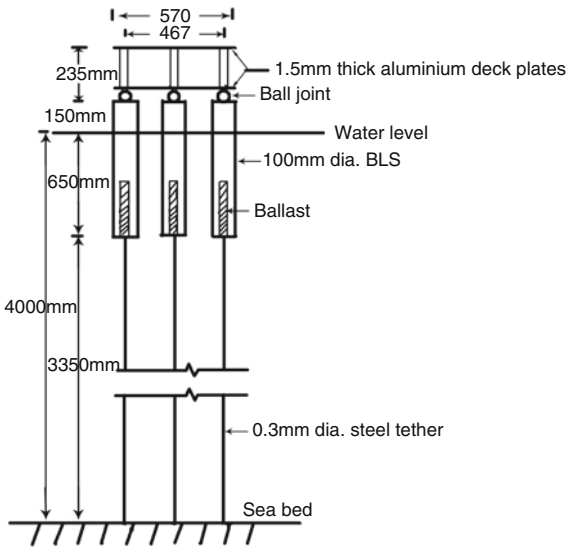

Fig. 7.1 Details of the scaled model

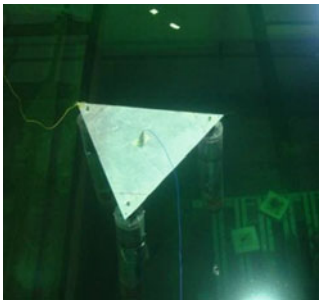

Fig. 7.2 Model installed in the wave flume

7.4 Experimental Studies

7.4.1 Free-floating Studies

This study is significant for installation and decommissioning purposes of the newly proposed triceratops. Though buoyancy of triceratops is more than the total mass of the structure, additional ballast is required to achieve the required buoyancy during installation. Free-floating heave and pitch periods are studied to avoid resonance during installation. As installation can be planned with each BLS unit separately or with the complete structure on the basis of the capacity of the lifting equipment available, free-floating studies are carried out on both the single BLS unit and on the complete structure as well. As the displacement of single BLS unit is lesser than the complete triceratops, lifting equipment of larger capacity is not required for installation, which would result in significant saving of installation cost.

7.4.2 Free-decay Studies on Tethered Triceratops

On removal of additional ballast at the free-float state, tethers are pre-tensioned. The structure is now tested for free oscillations in surge and heave degrees of freedom.

7.5 Analytical Studies

The analytical studies are performed in ANSYS AQWA software. The free-floating model is analyzed at 4 m water depth, while the tethered model of prototype is analyzed at 600 m water depth. Since BLS units are Morison elements, the line elements are modeled with segments, and the deck is modeled as quadratic plate elements; inbuilt ball joint is used in the analysis. Since BLS units do not have rigid

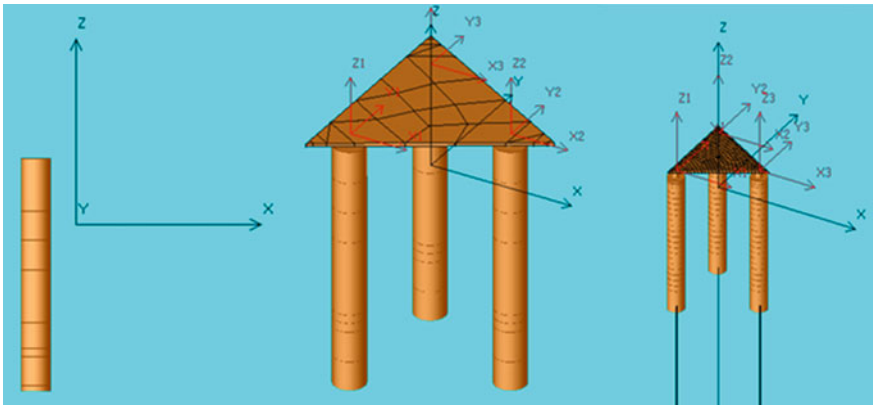

Fig. 7.3 Analytical model of single BLS, free-floating triceratops, and tethered triceratops

body motion, each BLS unit is considered a separate structure (3 structures) and connected to deck structure (4th structure) with ball joints. The flume water density is also considered in the analysis. Prototype of tethered triceratops is modeled at 600 m water depth; tethers are modeled as steel wire ropes. Free-floating analytical models of single BLS, triceratops, and tethered triceratops are shown in Fig. 7.3. Free-decay test is carried out analytically by subjecting the structure to zero wave amplitude and necessary initial conditions in the respective degree of freedom. Equation of motion for the free-decay test is as follows:

$$[M + M_{\mathrm{a}}]\ddot{X} + [C]\dot{X} + [K]X = 0 \tag{7.1}$$

where M is mass matrix; M_{a} is the added mass matrix, $[C]$ is the damping matrix, $[K]$ is the stiffness matrix at any instantaneous position and $\{\ddot{X}, \dot{X}, X\}$ are acceleration, velocity, and displacement, respectively. Stiffness matrix of the structure, in free-floating condition is given by:

$$\begin{bmatrix} 0 & 0 & 0 & 0 & 0 & 0 \\ 0 & 0 & 0 & 0 & 0 & 0 \\ 0 & 0 & \rho g A_w & \rho g A_p & -\rho g A_p & 0 \\ 0 & 0 & \rho g A_p & \Delta g GM_{\mathrm{La}} & -\rho g A_p & -\Delta g GM_{\mathrm{La}} \\ 0 & 0 & -\rho g A_p & -\rho g A_p & \Delta g GM_{\mathrm{Lo}} & -\Delta g GM_{\mathrm{Lo}} \\ 0 & 0 & 0 & 0 & 0 & 0 \end{bmatrix} \tag{7.2}$$

where $[K]$ is stiffness matrix, ρ is density of seawater, g is acceleration due to gravity, A_w is water plane area, A_p is projected area in respective degree of freedom, Δ is displacement, GM_{La} and GM_{Lo} are the lateral and longitudinal meta-centric heights, respectively; stiffness matrix coefficients include changes in tether stiffness, hydrostatic stiffness, and hydrodynamic stiffness.

7.6 Empirical Prediction

Heave natural period of single BLS and triceratops is predicted empirically. Added mass of the cylindrical BLS units is found by using semi-sphere volume whose radius is taken as same as that of the cylinder. Tethered surge natural period is also found empirically from the following equation (Faltinsen 1990).

$$T = 2\pi\sqrt{\frac{(M + M_a)}{\left(\frac{p}{l}\right)}} \tag{7.3}$$

where p is pretension and l is the length of the tether. Table 7.3 shows the comparison of the results of model tests and empirical prediction.

Based on the studies carried out, it has been found that the installation of triceratops can be done with each BLS unit separately or as a complete structure; free-floating periods are not matching with the wave periods in both the cases and hence no resonance during installation. Should the transportation be economical, installation cost can be minimized by installing each BLS unit separately. As the natural periods of tethered triceratops are also not matching with that of the wave periods, structural performance will be better during operational conditions. Permanent ballast in BLS units results in significant reduction in the pretension in tethers in comparison with that of TLPs. Hence offshore triceratops does not require high-strength tethers as required for TLPs. Since it has vertical restraining system, heave response is lesser than that of spar, making offshore triceratops more economical for ultra-deep waters.

Table 7.3 Natural periods of the structure

DOF	Experimental	Analytical	Numerical
Single BLS			
Heave	1.6	1.6	1.59
Roll	1.59	1.38	
Pitch	1.59	1.38	
Free-floating triceratops			
Heave	1.66	1.65	1.65
Roll	8.04	8.57	
Pitch	8.04	8.57	
Tethered triceratops			
Surge	11.92	13.6	11.9
Heave	0.48	0.4	

7.7 Wave Directionality Effects on Offshore Triceratops

The primary objective of the current study is to investigate the nonlinear dynamic response characteristics of offshore triceratops under regular waves for different wave approach angles. In the present study, 1:150 scaled model of offshore triceratops is investigated under regular waves by varying the wave period. Geometric characteristics of the platform and mass distribution are derived from Norwegian TLP (Minoo and Joel 1991) at a water depth of 600 m for equivalent buoyancy as that of the TLP. Buoyancy of pontoons of TLP is distributed to each BLS unit by increasing its draft; this is required to ascertain symmetric response in all BLS units for the considered wave approach angles. Mass distribution and geometric properties are given in Tables 7.4 and 7.5, respectively. BLS units are fabricated with acrylic material, and PVC ball joints are placed between the deck and the BLS units. Deck consists of two aluminum plates of 570 mm width and 1.5 mm thickness that are placed at two levels so as to obtain the representative value of center of gravity of the deck. In order to ensure equal payload distribution on each BLS unit, triangular geometry of the deck plate is chosen for the study; center of gravity of the BLS units and the deck is maintained on the same vertical axis. Components of the triceratops are shown in Fig. 7.4. Figure 7.5 shows the 1:150 scaled model considered for the study. The model is free-floated by ballasting each BLS unit; ballast mass is kept equivalent to the amount of pretension in each tether. Experimental studies are carried out in the wave flume of 4 m width, at a water depth of 4 m. Details of prototype and scaled wave data are given in the Tables 7.4 and 7.5. Dynamic response of the platform is measured for three different wave approach angles with reference to the axis of symmetry of the structure; details of instrumentation are shown in Fig. 7.6. Two accelerometers (surge/sway of BLS, heave of deck) and two inclinometers (pitch/roll of BLS and deck) are used to measure the acceleration and pitch responses. Surge, heave, and pitch RAOs (response amplitude operators) of the model are scaled up to the prototype and plotted for BLS units and the deck under the regular wave loads; three wave approach angles namely 0°, 90°, and 180° are considered in the present study.

7.8 Discussions of Experimental Studies

Free oscillation tests are conducted on free-floating and tethered models of the structure to determine their natural periods of vibration. These tests are conducted in two stages: (i) each BLS is freely floated by ballasting, while free oscillation tests are conducted on single BLS in heave and pitch degrees of freedom; and (ii) deck is connected to BLS units through ball joints for a desired draft of 650 mm, and subsequently free oscillation tests are conducted on the whole platform. Tethers are then connected to the model, and the platform is de-ballasted to enable the desired pre-tension in tethers. Free-floating natural periods and theirs scaled-up values of

Table 7.4 Details of model and prototype of free-floating and tethered triceratops

Description	Free-floating		Tethered	
	Prototype (m)	Model (mm)	Prototype (m)	Model (mm)
Water depth	600	4,000	600	4,000
Draft	97.5	645.5[a]	97.5	650
Each buoyant leg structure				
Outer diameter	15	100.0	15	100.0
c/c distance	70	467.0	70	467.0
Length	120.0	800.0	120.0	800.0
VCG from MSL	−51.36	−337.8	−58.87	−392.5
VCB from MSL	−48.75	−322.8	−48.75	−325.0
	(m^2)	(mm^2)	(m^2)	(mm^2)
Water plane area	176.71	7,854.0	176.71	7,854.0
	t-m^2	kg-mm^2	*t*-m^2	kg-mm^2
I_{xx}, I_{yy}	16,550,362	217,947.2	14,892,025	196,109
I_{zz}	146,775.3	1,932.8	81,067.6	1,067.6
	(m)	(mm)	(m)	(mm)
r_x, r_y	31.81	212.1	33.31	222.05
r_z	4.98	33.2	5.02	33.49
Deck	m^2	mm^2	m^2	mm^2
Deck area	6,330.86	281,372	6,330.86	281,372
I_{Dxx}, I_{Dyy}	1,256,831	16,550.9	1,256,831	16,550.9
I_{Dzz}	1,236,483	16,282.9	1,236,483	16,282.9
r_{Dx}, r_{Dy}	24.9	165.9	24.9	165.9
r_{Dz}	24.6	164.5	24.6	164.5
VCG	−46.35	−309.0	−46.35	−309.0
VCG of the whole structure	−55.39	−236.07[a]	−49.23	−328.22
Tether			*t*	kg
Pretension			8,652	2.56
			kN/m	N/mm
AE/*l*			84,000	3.73
Area of tether			0.211 m^2	0.07[b] mm^2
			(m)	(mm)
Length of the tether			502.5	3,350.0
			kN/m^2	N/mm^2
Modulus of elasticity			2×10^8	2×10^5

[a] Corrected to flume density
[b] Bare tether

the prototype are given in Table 7.3. It is seen that natural periods of the platform are away from the bandwidth of the operation wave periods; this is advantageous during installation, operation, and decommissioning as well.

Table 7.5 Natural period of the structure(s)

1:150 model			
Degree of freedom	Free-floating triceratops	Free-floating BLS	Tethered
Surge	–	–	11.92
Heave	1.66	1.60	0.48
Pitch	8.04	1.59	–
Prototype			
Surge			145.98
Heave	20.33	19.59	5.88
Pitch	98.47	19.47	

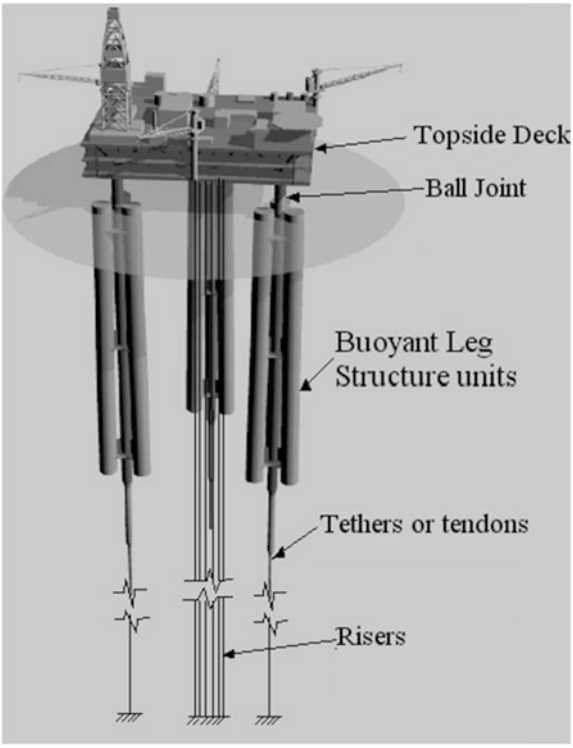

Fig. 7.4 Components of triceratops

Surge/sway and heave RAOs are shown in Figs. 7.7 and 7.8, respectively. It is seen from Fig. 7.7 that the variations in surge/sway responses are not significant for different wave approach angles; however, it shows maximum variation for 180° wave approach angle. Figure 7.8 shows significant influence of wave directionality

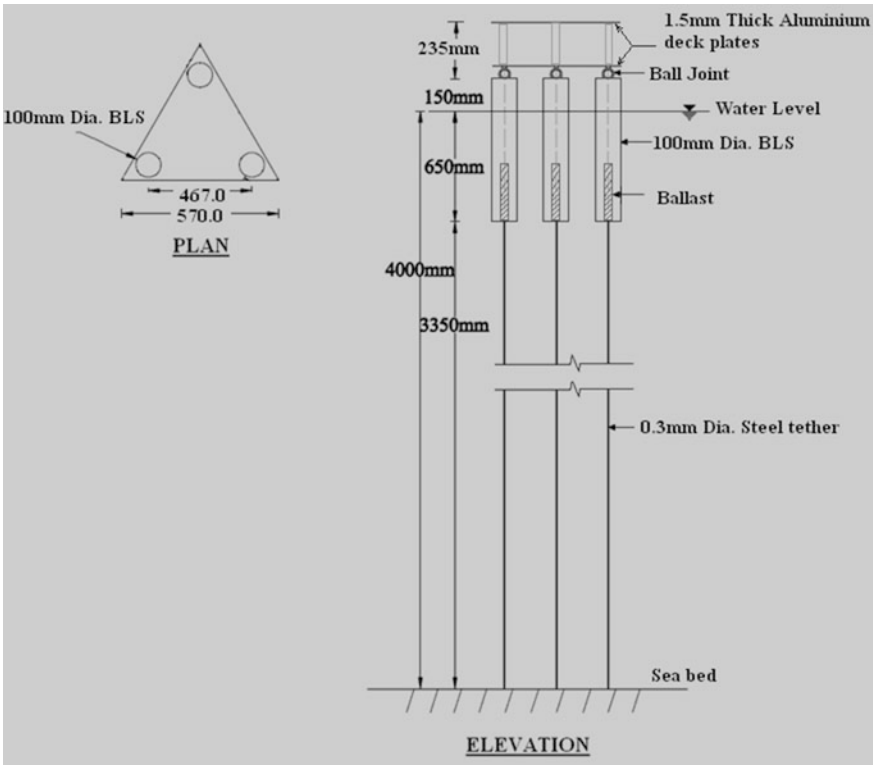

Fig. 7.5 Plan and elevation of the scaled model

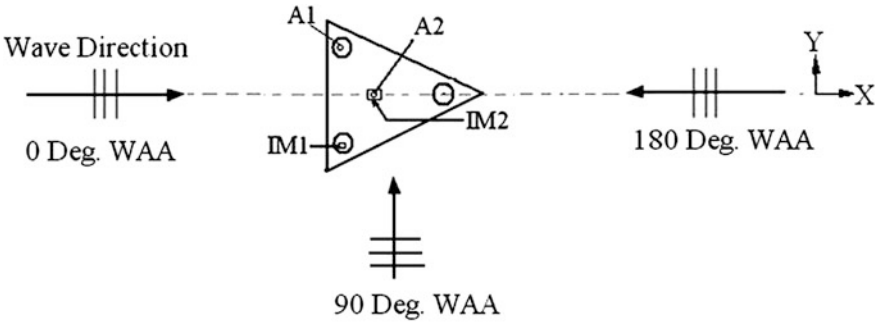

A1 — Accelerometer 1 (Surge/Sway of BLS)
IM1 — Inclinometer1 (Pitch/Roll of BLS)
A2 — Accelerometer 2 (Surge/Sway of Deck)
IM2 — Inclinometer2 (Pitch/Roll of Deck)

Fig. 7.6 Instrumentation for different wave approach angles

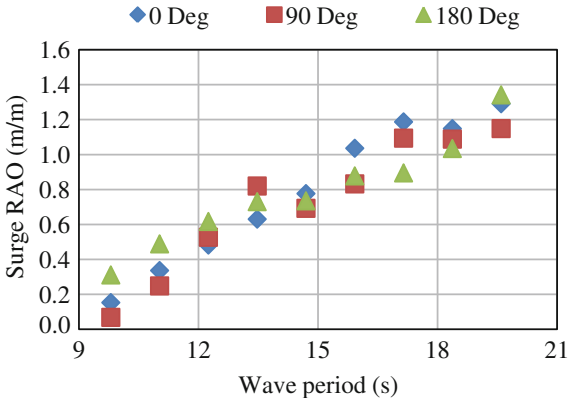

Fig. 7.7 Surge/sway RAOs of triceratops

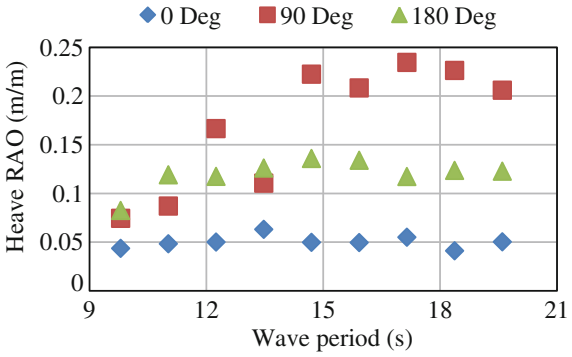

Fig. 7.8 Heave RAOs of triceratops

on heave RAO; variation is minimum at 0° and maximum at 90°. Variations in heave response for different wave approach angles shall be attributed to the phase lag of BLS legs when compared with that of the approaching waves. Pitch RAOs of BLS and deck are shown in Figs. 7.9 and 7.10. It is seen from the figures that there are no significant variations in the pitch response of both the deck and BLS units for different wave approach angles; compliancy offered by the ball joints shall be seen as a major contributing factor to this behavior. Pitch in the deck is observed mainly due to the transfer of heave from BLS to deck. Pitch/roll response of BLS is similar in all wave approach angles, indicating circular mass distribution in the BLS.

Experimental investigations are carried out on the scaled model of offshore triceratops to ascertain the influence of wave directionality on its response behavior. Experimental results show that the wave directionality does not influence surge/sway response of the platform significantly. Comparison of surge/sway RAO with that of heave shows that the structure is restrained in heave degree of freedom,

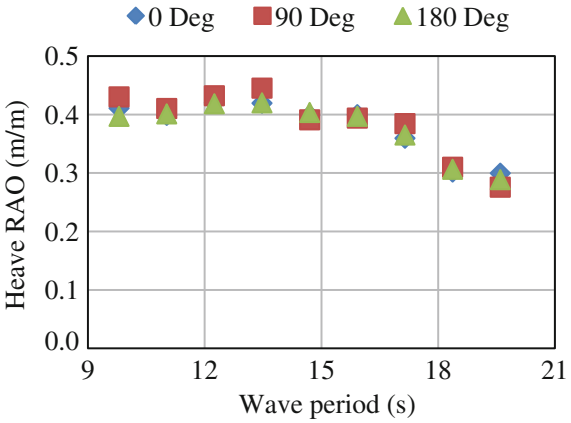

Fig. 7.9 Pitch/Roll RAOs of BLS

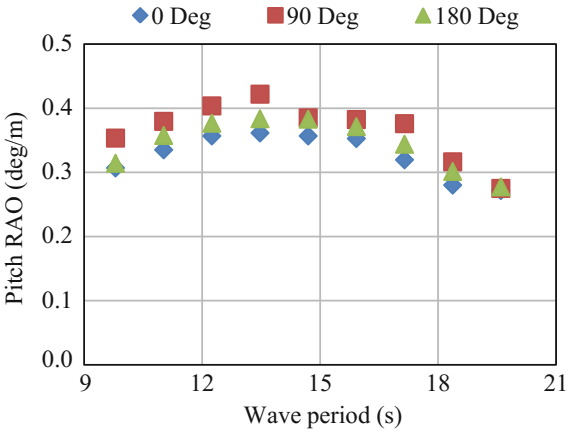

Fig. 7.10 Pitch/Roll RAO's of deck

which is expected for a compliant platform. Wave directionality does not influence pitch response of both the deck and BLS units; compliancy offered by the ball joints shall be seen as a major contributing factor to this behavior. For the chosen deck of triangular geometry, reduced rotational response under different wave approach angles reinforces the suitability of triceratops for irregular sea states; insensitivity of pitch/roll response for different wave approach angles indicates circular mass distribution in the BLS. Presented studies validate the suitability of offshore triceratops for ultra-deep water; however, more detailed analytical investigations are preferable to strengthen the present experimental observations.

7.9 Springing and Ringing Responses of Tension Leg Platforms

Certain class of offshore structures exhibits highly intense nonlinear behavior called springing and ringing. Dynamic response of compliant structures like TLPs under impact and non-impact waves responsible for ringing and springing phenomenon is of large interest to marine engineers. This section describes the mathematical formulation of impact and non-impact waves and discusses the method of analysis of TLPs of triangular geometry under these wave effects. Responses of square and equivalent triangular TLPs are compared. Heave response in square TLPs shows bursts, but there are no rapid buildups; gradual decays are seen in most cases looking like a beat phenomenon, while such results are not predominantly noticed in case of equivalent triangular TLPs. Ringing caused by impact waves in pitch degree of freedom and springing caused by non-impact waves in heave degree of freedom in both the platform geometries are undesirable, as they pose serious threat to the platform stability. Analytical studies conducted show that equivalent triangular TLPs positioned at different water depths are less sensitive to these undesirable responses, thus making it as a safe alternative for deepwater oil explorations. The study presented can be seen as a prima facie to understand the geometric design and form development of offshore structures for deepwater oil exploration.

7.9.1 Springing and Ringing

Springing and ringing shown by a certain class of compliant offshore structures namely TLPs and gravity-based structures (GBSs) gained research focus since they were first observed in a model test of the Hutton TLP in the North Sea in 1980s (Mercier 1982). Springing is caused in the vertical/bending modes by second-order wave effects at the sum frequencies; this behavior is common in both mild and severe sea states. Ringing is attributed to strong transient response observed in these modes under severe loading conditions triggered presumably by passage of a high, steep wave. This transient response further decays to steady state at a logarithmic rate depending on the system damping. Figure 7.11 shows a schematic view of

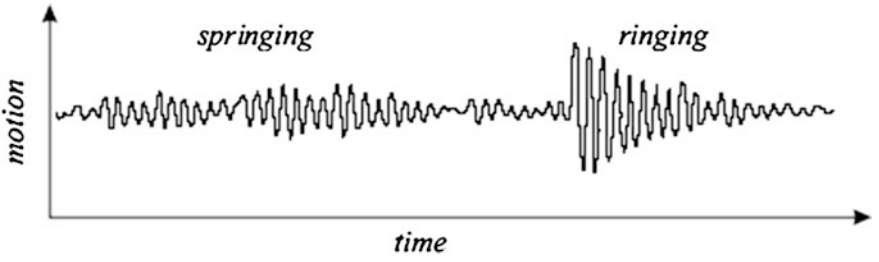

Fig. 7.11 Schematics of springing and ringing

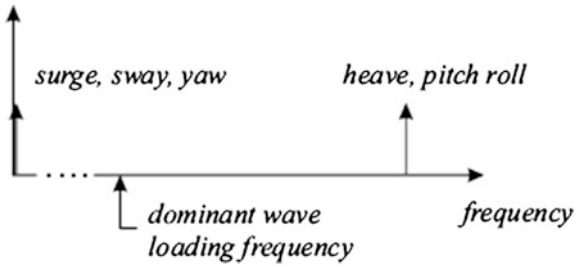

Fig. 7.12 Frequency range of TLPs relative to dominant wave frequency

springing and ringing. TLPs are generally designed to keep their natural frequencies in heave, pitch, and roll degrees of freedom, several times above the dominant wave frequency, whereas structural frequencies in surge, sway, and yaw degrees of freedom are designed to be lower than the dominant wave frequency as shown in Fig. 7.12. Though TLPs are designed with this kind of shift in their structural frequencies, springing and ringing still become important when the range of structural frequency is several times higher than the dominant wave frequencies. As a result, ringing can not only cause total breakdown of these platforms even in moderate storms but can also hamper daily operations and lead to fatigue failure (Winterstein 1998; Ude et al. 1994; Marthinsen et al. 1992). Studies on ringing and springing response had a primary focus on large volume structures that are dominated by wave diffraction inertial-type loading and minimally affected by drag forces (Natvig 1994; Jefferys and Rainey 1994; Faltinsen et al. 1995); these studies discussed the response of TLPs and GBS with slender cylinders. Kim and Zou (1995) and Kjeldsen and Myrhaug (1979) observed that waves causing ringing response are highly asymmetric. Gurley and Kareem (1998) showed that viscous loads are also capable of inducing ringing response of members with large wavelength-to-diameter ratios, where instantaneous moment acting on the cylinder is a quadratic function of wave elevation. The precursors of ringing and springing phenomenon are given as (i) the generation of high-frequency force necessitating the presence of steep, near-vertical wave fronts; and (ii) resonant buildup due to subsequent loading within the range of the time period of TLP. This could be realized by setting the dominant wave frequency as several times as the natural frequency of the structure. Also frequency at which ringing occurs is well above the incident wave frequency and is close to the natural frequency of the structure.

7.10 Evolution of Platform Geometry

Natvig and Vogel (1995) reported several advantages of TLPs with triangular geometry namely: (i) no tether tension measurements required on day-to-day operation; (ii) increased tolerances for the position of foundation; and (iii) increased

draft and heel tolerances, making it more advantageous than four-legged square TLPs. Triangular TLPs that are statically determinate can have foundations placed with larger tolerances without affecting tether behavior. With the near-equal load sharing of all tethers of triangular TLP despite weather directions, the maximum load level in one group reduces, thus resulting in decreased cross-sectional material of tethers, which is an important area for cost savings in TLPs while they show lesser response under regular and random waves as well (Chandrasekaran and Jain 2002a, b). Stability analysis performed on triangular TLPs under impact loading and influence of wave approach angle showed that they are more stable in the first mode of vibration in comparison with square TLPs, while impulse loading acting on their corner column affects their performance behavior significantly (Chandrasekaran et al. 2006, 2007a, b). The aspects of platform geometry that affect tether loading and tether system thus become the focus on design of future TLPs.

7.11 Mathematical Development

A *ringing* event involves the excitation of transient structural deflections at/close to the natural frequency of the platform arising at third harmonic of the incident wave field, whereas *springing* effect involves excitation of motion in vertical degree of freedom, for example, in heave in TLPs due to nonlinear forces arising at the second harmonic of the incident waves (see, e.g., Peter et al. 2006). The shape of the impact wave generating ringing is hence crucial and is experimentally observed that these waves are steep and asymmetric with respect to both horizontal and vertical axes; Kim et al. (1997) recommended to use laboratory-generated ringing waves in case of non-availability of any analytical wave models. Therefore, the generation of impact wave time histories from currently available wave theories and random wave elevation spectrums suffers from potential difficulties such as the following: (i) shape of experimentally observed ringing waves being different from analytical ones; (ii) absence of a systematic method to categorize such steep, irregular, and asymmetric waves; and (iii) insufficiency of these theories to generate extreme waves that could cause impact forces. These limitations restrict the use of existing theories for generation of impact waves that are associated with the onset of ringing (see for example, Son 2006). Thus, the necessity of steep waves conforming to experimentally generated waves calls for implementation of a higher-order nonlinear wave kinematic theory and nonlinear fluid model. On the other hand, this could lead to complicated mathematical formulations that will become computationally inefficient when solved numerically. Because of these reasons, several researchers (Ronalds and Stocker 2002, 2003; Ronalds 2003) successfully simulated ringing and springing waves using Airy's wave theory and used dynamic Morison equation for force evaluation. Also in the current study, water particle kinematics for ringing and springing waves is obtained using Airy's wave theory from a randomly generated sea surface elevation using Pierson Moskowitz (PM) spectrum. The original PM spectrum, a function of wind velocity, is modified as a

function of modal frequency and later modified again as a function of significant wave height and modal frequency (Michel 1999). For ringing to be present in the considered sea state, dominant wave frequency should be several times higher than surge natural frequency. Therefore, modal frequency used in the PM spectrum is chosen to be about five times of the surge frequency. The modified one parameter formula given by Eq. (7.4) is employed in the present study. Figure 7.13a shows the PM spectrum.

$$S_{\eta\eta}(\omega) = \frac{8.1 \times 10^{-3} g^2}{\omega^5} \exp\left[-1.25\left(\frac{\omega_m}{\omega}\right)^4\right] \tag{7.4}$$

where g is acceleration due to gravity, ω_m is the modal frequency, and $S_{\eta\eta}$ is the power spectral density of wave height. Wave elevation, $\eta(t)$, realized as a discrete sum of many sinusoidal functions with different angular frequencies, and random phase angles is given by:

$$\eta(t) = \sum_{i=1}^{n} \sqrt{2S_{\eta\eta}(\omega_i)\Delta\omega_i} \cdot \cos(\omega_i t - \varphi_i) \tag{7.5}$$

where ω_i are discrete sampling frequencies ($\Delta\omega_i = \omega_i - \omega_{i-1}$), n is the number of data points, and ϕ_i are random phase angles. Range of random phase angles are set to decide the generated wave to be an impact or a non-impact wave. Impact waves shall have wave profile with a peak at a particular time (t_0) that will be distinctly higher than other wave heights; wave heights that become comparable at all time periods and lie within the prescribed limits are termed as non-impact waves. For generating a non-impact wave profile, phase angles ϕ_i are chosen as random numbers within the range [0, 2π]. For an impact wave at an arbitrary time t_0, ϕ_i is chosen in the range [0, 0.01] at time $t = t_0$; Eq. (7.5) is subsequently modified as given below:

$$\eta(t) = \sum_{i=1}^{n} \sqrt{2S_{\eta\eta}(\omega_i)\Delta\omega_i} \cdot \cos(\omega_i(t - t_0) - \varphi_i) \tag{7.6}$$

A sample impact and non-impact wave thus generated using the above equations is shown in Fig. 7.13b, c, respectively.

7.12 Analytical Model of TLP

Equivalent geometrical configuration of triangular TLP is evolved on the basis of equation of equilibrium applied in the static sea conditions. For TLPs of square and triangular geometry, the respective equations are given as follows:

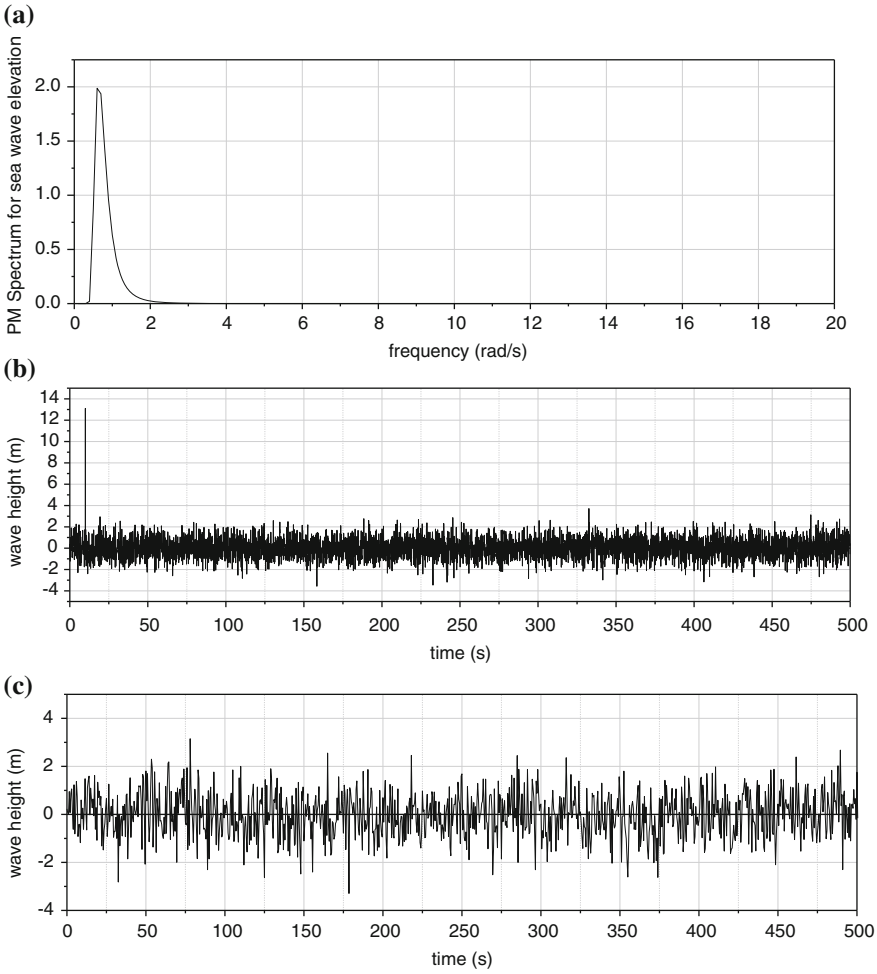

Fig. 7.13 **a** PM spectrum for wave height elevation. **b** Impact wave profile with impact wave at t = 10 s. **c** Non-impact wave profile

$$F_B = 4(T_0)_{\text{square}} + W \tag{7.7}$$

$$F_B = 3(T_0)_{\text{square}} + W \tag{7.8}$$

where F_B is the buoyant force, T_0 is the initial pre-tension in each tether, and W is the total weight of the platform. Equivalent triangular TLP is arrived by considering two cases namely: (i) buoyant force and initial pre-tension per tether are considered equal for both the geometries resulting in reduced total pretension in triangular TLP; and (ii) total initial pre-tension, weight, and buoyancy are kept the same for both geometries thereby increasing the initial pretension per tether in the triangular

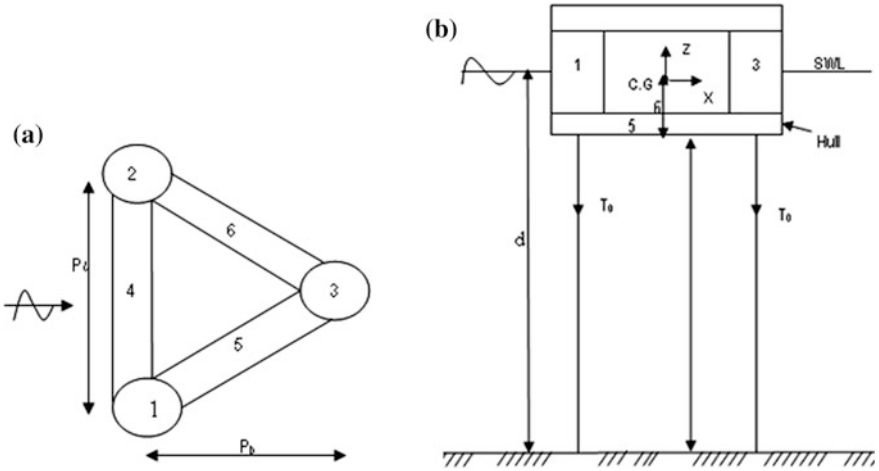

Fig. 7.14 **a** Plan and **b** elevation of example TLP

TLP. The platform considered in the study is a rigid body having six degrees of freedom. Figure 7.14 shows the plan and elevation of the triangular TLP having plan dimension as P_l used in the study.

Unidirectional waves with incident angle normal to one of the pontoons are considered. Maximum absolute response in pitch degree of freedom is obtained when the waves are normally impinged; other degrees of freedom namely sway, roll, and yaw that are activated by a non-normal wave show minimal effects. Four square TLPs at different water depths, reported in the literature (Chandrasekaran and Jain 2002a), are considered for the analysis, and their geometric properties are given in Table 7.6, whereas Table 7.7 shows time periods of equivalent triangular TLPs with initial pre-tension same as that of these square ones. Hydrodynamic coefficients of drag (C_d) and inertia (C_m) used in Morison equation are asserted to be independent of the wave frequencies. C_d is taken as unity, while C_m is assumed to vary along the water depth (Chandrasekaran et al. 2004) and is interpolated for the entire water depth using a second-degree polynomial as given below:

$$C_m(y) = p_1 \cdot y^2 + p_2 \cdot y + p_3 \tag{7.9}$$

where y is the water depth measured from sea bed; p_1, p_2, and p_3 are coefficients used for interpolation and given in Table 7.8. Tethers are modeled as elastic cables with axial AE/*l* when taut, and zero when they slack.

Table 7.6 Geometric properties of square TLPs considered

Property	TLP_1	TLP_2	TLP_3	TLP_4
Weight (kN)	351,600.00	330,000.00	330,000.00	370,000.00
F_B (kN)	521,600.00	465,500.00	520,000.00	625,500.00
T_0 (kN)	170,000.00	135,500.00	190,000.00	255,500.00
Tether length, ℓ(m)	568.00	269.00	568.00	1,166.00
Water depth (m)	600.00	300.00	600.00	1,200.00
CG (m)	28.44	27.47	28.50	30.31
AE/ℓ (kN/m)	84,000.00	34,000.00	82,000.00	45,080.00
Plan dim (m)	70.00	75.66	78.50	83.50
D and D_c (m)	17.00	16.39	17.00	18.80
r_x (m)	35.10	35.10	35.10	35.10
r_y (m)	35.10	35.10	35.10	35.10
r_z (m)	35.10	42.40	42.40	42.40

Table 7.7 Natural wave periods and frequencies of equivalent triangular TLPs with T_0 per tether same

Case	Natural time period (s)			Natural frequency (Hz)		
	Surge	Heave	Pitch	Surge	Heave	Pitch
TLP_1	98.00	1.92	2.110	0.0102	0.5208	0.4739
TLP_2	87.20	1.96	2.155	0.0115	0.5102	0.4640
TLP_3	97.00	1.92	2.060	0.0103	0.5208	0.4854
TLP_4	132.0	3.11	3.120	0.0076	0.3215	0.3205

Table 7.8 Values of coefficients for interpolation of C_m

Description	p_1	p_2	p_3
TLP_1	7.780×10^{-7}	-9.667×10^{-4}	1.8
TLP_2	3.111×10^{-6}	-1.933×10^{-3}	1.8
TLP_3	7.778×10^{-7}	-9.667×10^{-4}	1.8
TLP_4	1.944×10^{-7}	-4.833×10^{-4}	1.8

7.13 Hydrodynamic Forces on TLP

Modified Morison's equation accounting for the relative motion between the platform and waves is used to estimate hydrodynamic force per unit length $f(t)$ on the members of TLP and is given by:

$$f(t) = \frac{\pi D_C^2}{4}\rho C_m \ddot{u} + \frac{1}{2}\rho C_d D_c(\dot{u} - \dot{x})|\dot{u} - \dot{x}| \pm \frac{\pi D_C^2}{4}(C_m - 1)\rho\ddot{x} \qquad (7.10)$$

where $\dot{x}, \ddot{x}$ are the horizontal structural velocity and acceleration, $\dot{u}$, $\ddot{u}$ are the horizontal water particle velocity and acceleration, ρ is mass density of sea water, C_d and C_m are hydrodynamic drag and inertia coefficients, and D_c is diameter of

pontoons, respectively. As there is no significant variation in water depth for the pontoons at the bottom, constant C_d (as 1.0) and C_m (as 2.0) values are used for them. The last term in Eq. (7.10) is the added mass term and is taken as positive when the water surface is below mean sea level. The hydrodynamic force vector $F(t)$ is given by:

$$\{F(t)\} = \{F_1 \quad F_2 \quad F_3 \quad F_4 \quad F_5 \quad F_6\}^T \tag{7.11}$$

where F_1, F_2, and F_3 are total forces in surge, sway, and heave degrees of freedom and F_4, F_5, and F_6 are moments of these forces about X, Y and Z axes, respectively.

7.14 Dynamics of Triangular TLP

Equation of motion describing the dynamic equilibrium between the inertia, damping, restoring, and exciting forces can be assembled as follows:

$$[M]\{\ddot{x}\} + [C]\{\dot{x}\} + [K]\{x\} = \{F(t)\} \tag{7.12}$$

where $[M]$ is the mass matrix, $[C]$ is the damping matrix, $[K]$ is the stiffness matrix, and $\{F(t)\}$ is the force vector as defined by Eq. (7.11).

7.14.1 Mass Matrix

The structural mass is assumed to be lumped at each degree of freedom. Hence, it is diagonal in nature and constant. The added mass M_a due to the water surrounding the structural members is also been considered up to MSL. The presence of off-diagonal terms in mass matrix indicates contribution of added mass due to the hydrodynamic loading in the activated degrees of freedom due to unidirectional wave load.

$$[M] = \begin{bmatrix} M_1 + M_{a11} & 0 & 0 & 0 & 0 & 0 \\ 0 & M_2 & 0 & 0 & 0 & 0 \\ 0 & 0 & M_3 + M_{a33} & 0 & 0 & 0 \\ 0 & 0 & 0 & M_4 & 0 & 0 \\ M_{a51} & 0 & M_{a53} & 0 & M_5 & 0 \\ 0 & 0 & 0 & 0 & 0 & M_6 \end{bmatrix} \tag{7.13}$$

where $M_{11} = M_{22} = M_{33}$ = total mass of the structure, M_4 is mass moment of inertia about the x axis $= Mr_x^2$, M_5 is mass moment of inertia about the y axis $= Mr_y^2$, M_6 is mass moment of inertia about the z axis $= Mr_z^2$, and r_x, r_y, and r_z are radius of gyration about the x, y, and z axes, respectively. M_{a11}, M_{a33} are added mass terms in

surge and heave degrees of freedom, M_{a51}, M_{a53} are added mass moment of inertia due to the additional mass in surge and heave degrees of freedom, respectively. The presence of off-diagonal terms indicates contribution of added mass due to hydrodynamic loading. The contribution of added mass up to MSL has already been considered along with the force vector. The added mass terms are given by:

$$M_{a11} = 0.25\pi\rho D^2[C_m - 1]x_{\text{surge}} \tag{7.14}$$

$$M_{a33} = 0.25\pi\rho D^2[C_m - 1]x_{\text{heave}} \tag{7.15}$$

7.14.2 Stiffness Matrix

The coefficients K_{ij} of the stiffness matrix of triangular TLP are derived from the first principles, as presented in the literature (Chandrasekaran and Jain 2002a), and the same has been used in the current study.

$$[K] = \begin{bmatrix} K_{11} & 0 & 0 & 0 & 0 & 0 \\ 0 & K_{22} & 0 & 0 & 0 & 0 \\ K_{31} & K_{32} & K_{33} & K_{34} & K_{35} & K_{36} \\ 0 & K_{42} & 0 & K_{44} & 0 & 0 \\ K_{51} & 0 & 0 & 0 & K_{55} & 0 \\ 0 & 0 & 0 & 0 & 0 & K_{66} \end{bmatrix} \tag{7.16}$$

The coefficients of the stiffness matrix have nonlinear terms due to cosine, sine, square root, and square terms of the structural displacements. Furthermore, tether tension changes due to TLP motion making $[K]$ response dependent. Off-diagonal terms reflect the coupling effect between various degrees of freedom. Change in tether tension updates $[K]$ at every time step and also changes buoyancy of TLP. It is interesting to note that coefficients of $[K]$ continuously vary at every time step and are replaced by new values based on the structural response of TLP.

7.14.3 Damping Matrix

Damping matrix $[C]$ is assumed to be proportional to initial values of $[M]$ and $[K]$ and is given by:

$$[C] = a_0[M] + a_1[K] \tag{7.17}$$

where a_0 and a_1 are, respectively, the stiffness and mass proportional damping constants. Damping matrix given by the above equation is orthogonal as it permits modes to be uncoupled by eigenvectors associated with the undamped Eigen

problem. Damping constants a_0 and a_1 are determined by choosing the fractions of critical damping (ξ_1 and ξ_2) at two different frequencies (ω_1 and ω_2) and solving simultaneous equations for a_0 and a_1.

$$a_0 = 2(\xi_2\omega_2 - \xi_1\omega_1)/\left(\omega_2^2 - \omega_1^2\right) \tag{7.18}$$

$$a_1 = 2\omega_1\omega_2(\xi_1\omega_2 - \xi_2\omega_1)/\left(\omega_2^2 - \omega_1^2\right) \tag{7.19}$$

Damping attributable to $a_0[K]$ increases with increasing frequency, whereas damping attributable to $a_1[M]$ increases with decreasing frequency. In the current study, value of these coefficients are obtained using the above equations by taking damping ratio $\zeta = 0.05$ in surge and yaw degrees of freedom. Free vibration analysis is performed to find out natural frequencies of the platform corresponding to these degrees of freedom and found that damping ratios maintain reasonable values for all the other modes which are contributing significantly to the response. Initial pretension in all tethers is assumed to be equal and total pretension changes with the motion of platform. The equation of motion is solved in time domain by employing Newmark's integration scheme by taking $\alpha = 0.25$ and $\beta = 0.5$. The solution procedure incorporates the changes namely: (i) stiffness coefficients varying with tether tension; (ii) added mass varying with sea surface fluctuations; and (iii) evaluation of wave forces at instantaneous position of the displaced platform considering the fluid structure interaction. Behavior under wave loading becomes nonlinear, and components of the equation of motion at each step components are updated. Ten terms in the power series are found to be sufficient to give convergence in the iterative scheme. The time step Δt has been taken as 0.1 s, which is a relatively small value in comparison with the natural period (T_n) and hence yields accurate values for the response.

7.15 Ringing Response

Ringing is usually a phenomenon attributed to response of compliant structures such as TLPs under impact waves. Figures 7.15, 7.16 and 7.17 show heave, pitch, and surge responses of all four cases of TLPs under impact waves, namely (i) square TLPs; (ii) equivalent triangular TLPs with T_0 per tether same as that of square; and (iii) equivalent triangular TLPs with total T_0 same as that square, respectively. It can be seen that the response is primarily triggered in pitch degree of freedom for a wide range of time period similar to the response of a bell vibrating for a longer time when struck by a large impact force. This is noticed in both the geometries of TLPs, which shall be attributed to a ringing response. Though a similar response is noticed under the influence of non-impact waves also, it can be seen that the intensity of pitch response caused by the latter is less compared with that caused by impact waves. By comparing the ringing response in pitch degree of

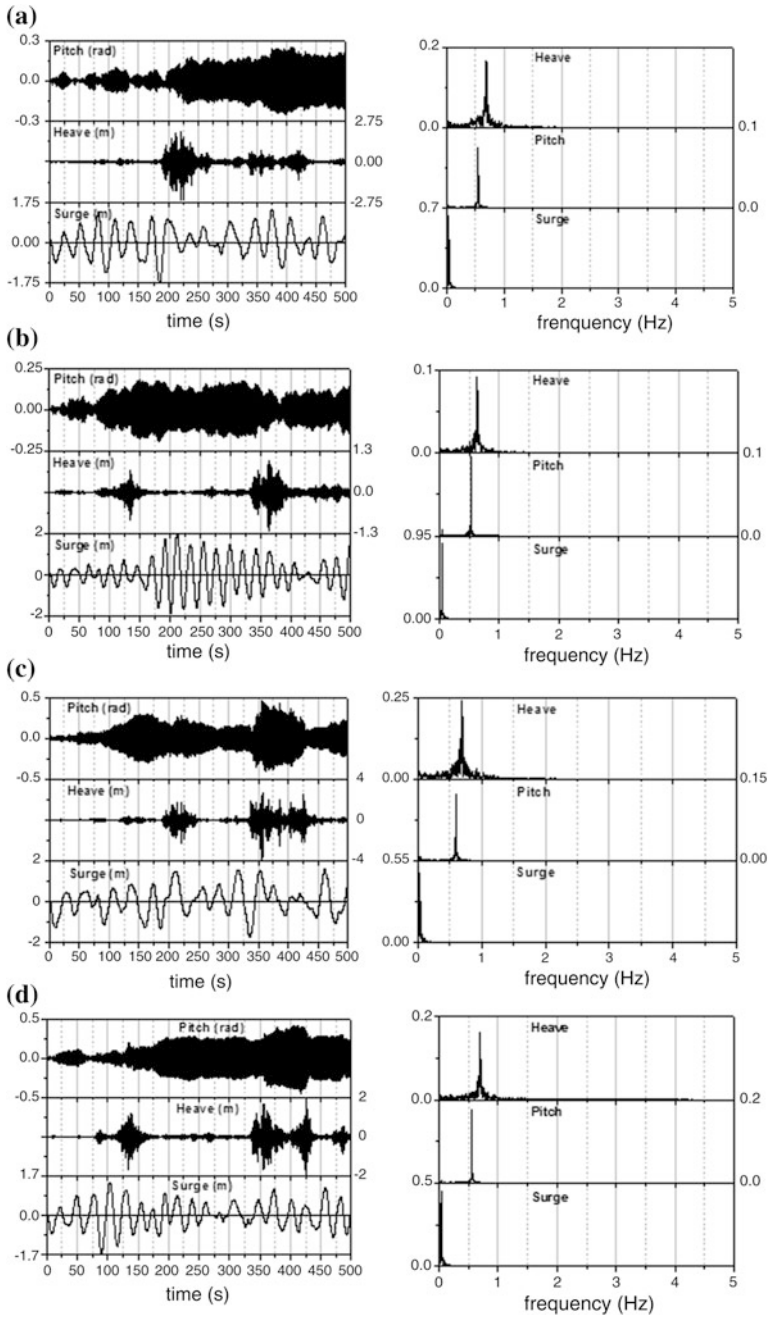

Fig. 7.15 Response of square TLPs to impact waves. **a** Response of TLP_1. **b** Response of TLP_2. **c** Response of TLP_3. **d** Response of TLP_4

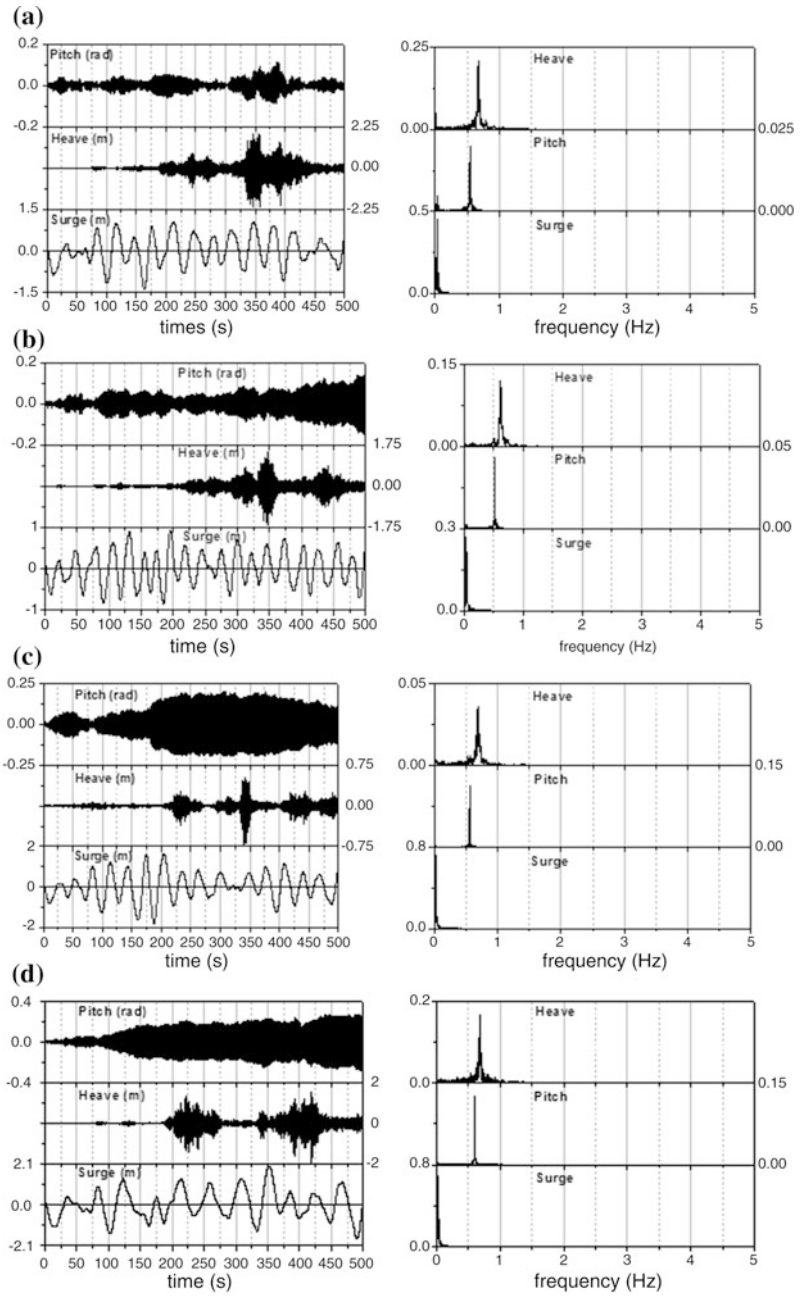

Fig. 7.16 Response of equivalent triangular TLPs to impact waves (T_0 per tether same). **a** Response of TLP_1. **b** Response of TLP_2. **c** Response of TLP_3. **d** Response of TLP_4

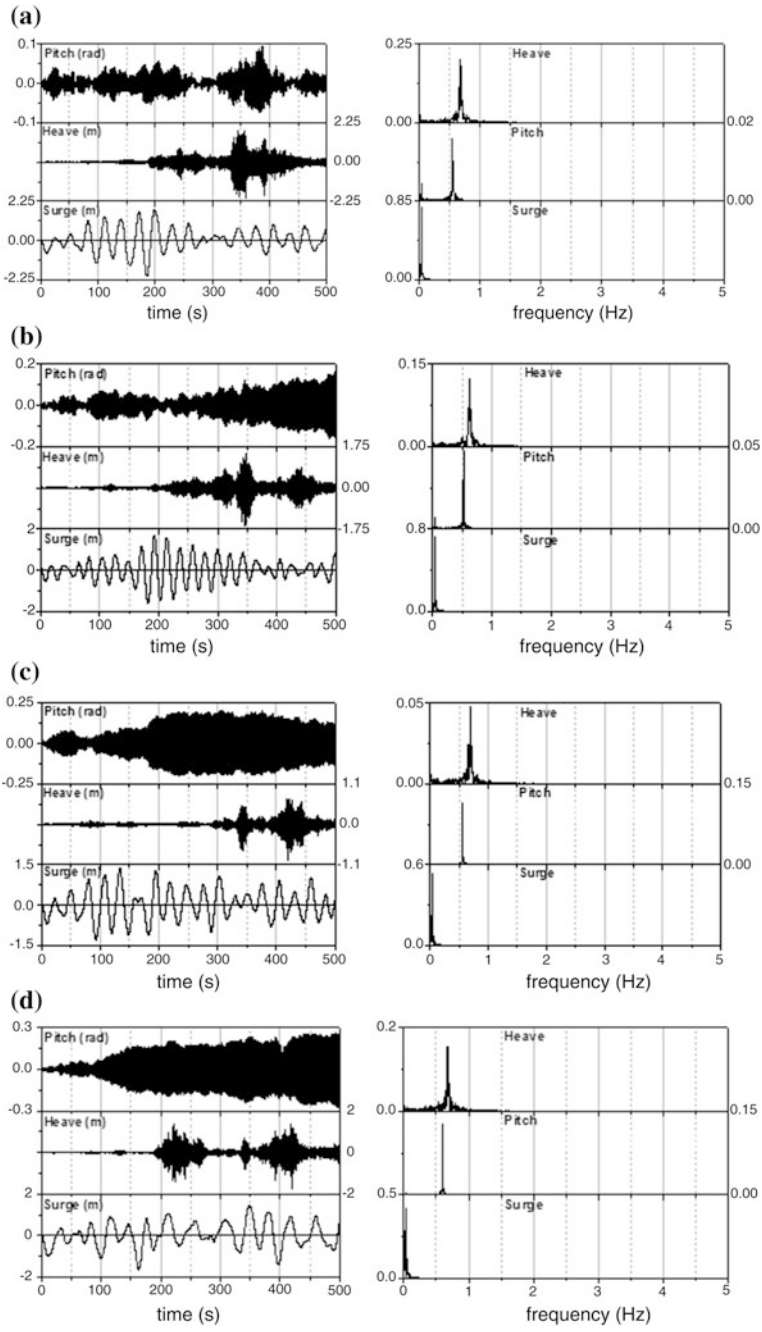

Fig. 7.17 Response of equivalent triangular TLPs to impact waves (total T_0 same). **a** Response of TLP_1. **b** Response of TLP_2. **c** Response of TLP_3. **d** Response of TLP_4

freedom of TLP_1 and TLP_3 at the same water depth but with different tether tension, it can be seen that increased tether tension enhances pitch response due to impact waves in both the geometries; however, pitch response of triangular TLPs of both cases (i and ii) is lesser than the square ones. Further comparison of pitch response of TLP_2, TLP_3, and TLP_4 under impact waves shows increase in water depth from 300 to 600 m increases the response by about 50 %, and further increase to 1,200 m enhances the response by 100 %. This behavior is seen in both the geometries, but it is interesting to note that increase in water depth does not enhance the ringing response in pitch degree of freedom in triangular TLP (with T_0 per tether same case) as much as the square ones (see for example, pitch response of TLP_3 and TLP_4 of triangular TLP with same T_0 per tether case). It is also important to note that the influence of increase in water depth on pitch response of triangular TLPs with total T_0 same as that of square is even lesser. By considering TLPs as most suitable for deepwater situation, it can be seen that ringing response in pitch degree of freedom in triangular TLPs (T_0 per tether same case) under impact waves is lesser that of the square ones, and it is further reduced for triangular TLP with total T_0 same as square (see for example, TLP_4). While attributing pitch response to impact waves, which is clearly a ringing phenomenon, as undesirable, triangular TLPs showing lesser response in this front make them a focus for futuristic design of TLPs in deep water.

7.16 Springing Response

The response behavior of TLPs with different geometry shows a near resonating case of heave response under non-impact waves. This phenomenon is usually known as springing. Figures 7.18, 7.19 and 7.20 show heave, pitch, and surge responses of all four cases of TLP under non-impact waves, namely (i) square TLPs; (ii) equivalent triangular TLPs with T_0 per tether same as that of square; and (iii) equivalent triangular TLPs with total T_0 same as that square, respectively. It can be seen that heave response is triggered at a frequency near to that of its natural frequency causing springing response. The broad band in frequency response commonly noticeable in both the geometries indicates more energy concentration near the natural frequency of heave degree of freedom. By comparing springing response in heave degree of freedom of TLP_1 and TLP_3 at same water depth but with different tether tension, it is seen that heave response under non-impact waves decreases with increase in tether tension for same water depth in both the geometries; however, heave response of triangular TLPs of both the equivalence cases is lesser than the square ones. Further, increase in water depth from 300 to 600 m increases the heave response by about 45 %, and further increase in water depth to 1,200 m increases it to about 100 %. Though this behavior is common to both the geometries, increase in water depth does not enhance heave response in both equivalent cases of triangular TLPs (see for example, TLP_2, TLP_3 and TLP_4). It is quite interesting to note that the response in case of triangular TLPs with total T_0 same as that of square is even lesser. It can be seen that springing response in heave degree of freedom of triangular TLPs (of both

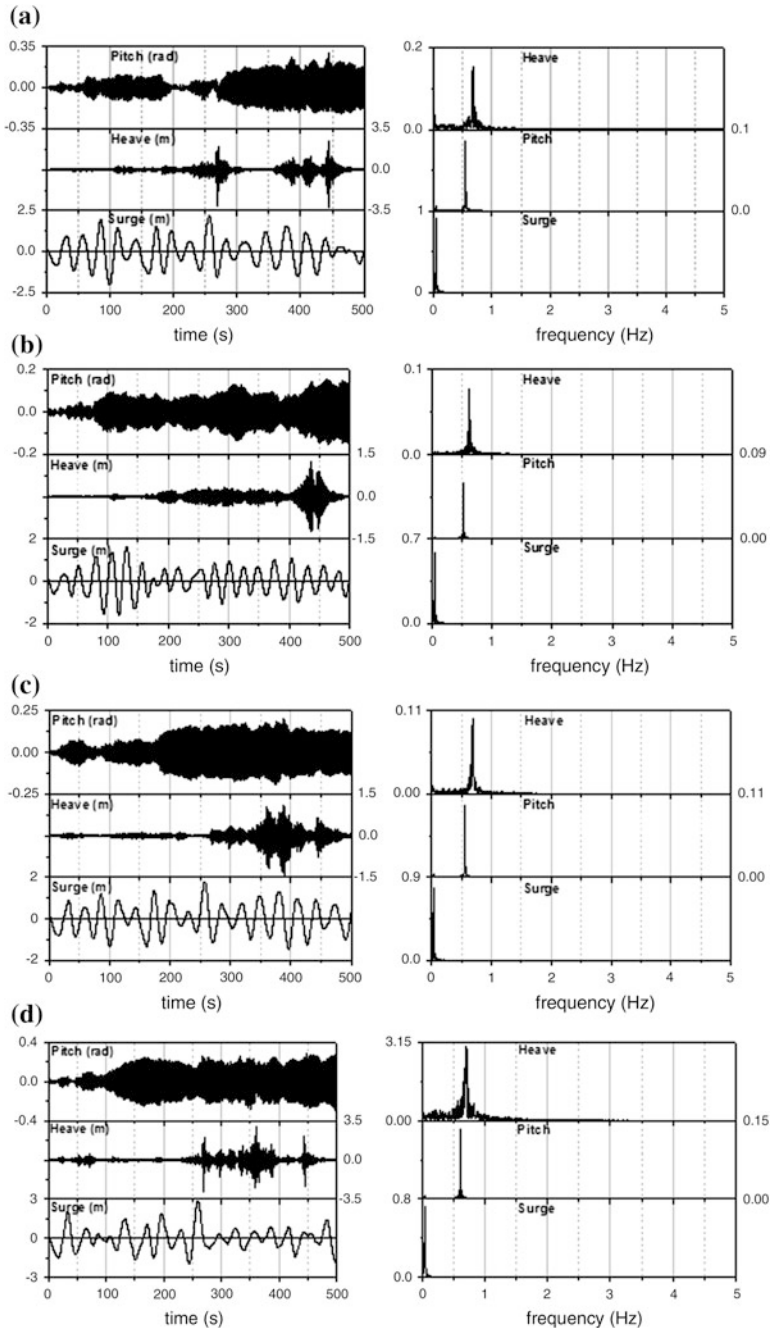

Fig. 7.18 Response of square TLPs to non-impact waves. **a** Response of TLP_1. **b** Response of TLP_2. **c** Response of TLP_3. **d** Response of TLP_4

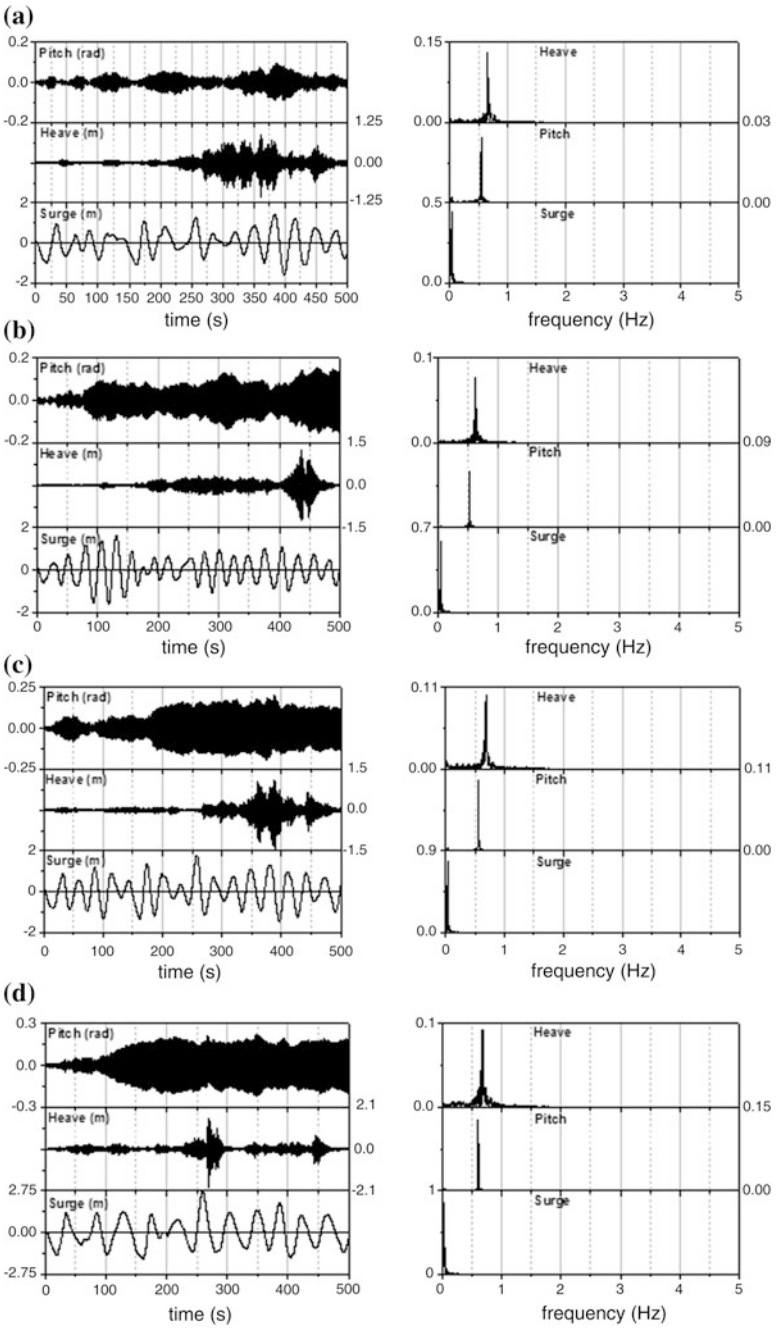

Fig. 7.19 Response of equivalent triangular TLPs to non-impact wave. **a** Response of TLP_1. **b** Response of TLP_2. **c** Response of TLP_3. **d** Response of TLP_4

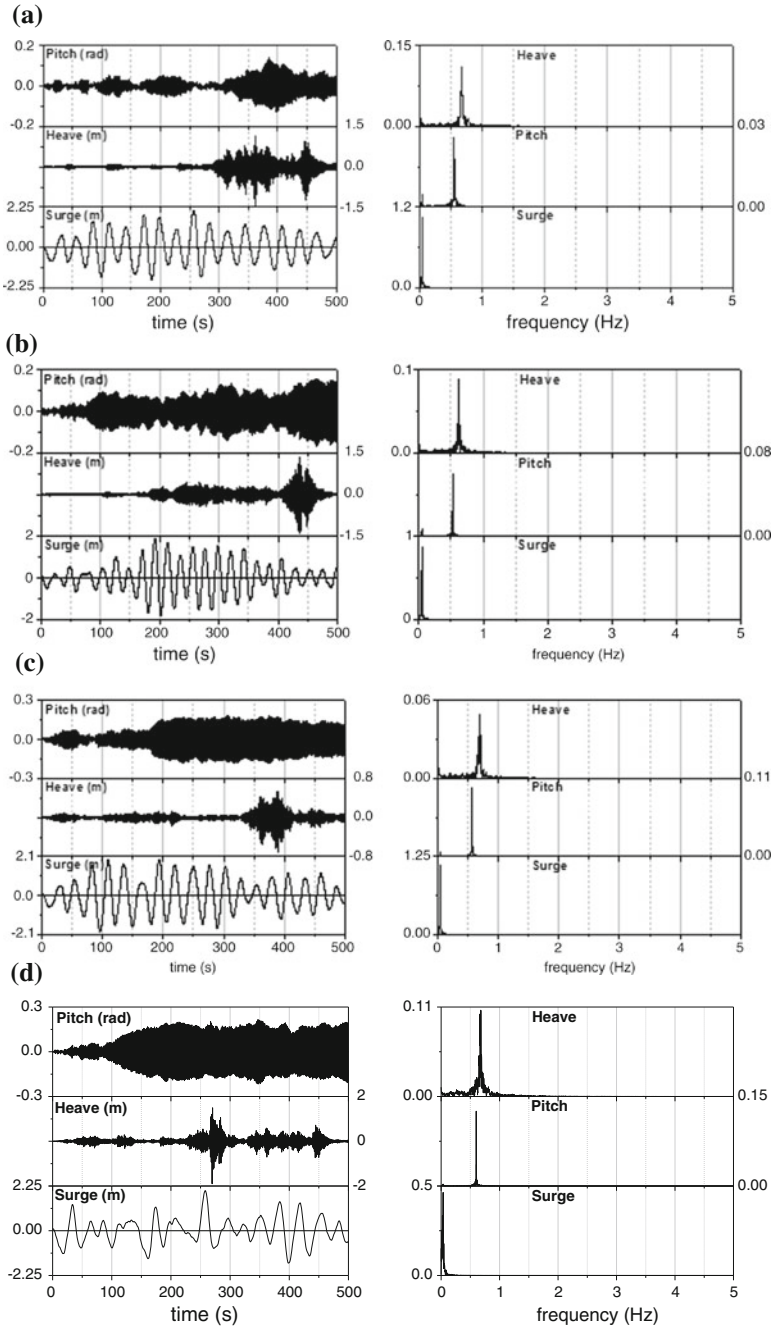

Fig. 7.20 Response of equivalent triangular TLPs to non-impact waves (total T_0 same). **a** Response of TLP_1. **b** Response of TLP_2. **c** Response of TLP_3. **d** Response of TLP_4

equivalence case) under non-impact waves is lesser than that of square ones (see for example, TLP_4). Further, almost heave response in all square TLPs shows bursts, but there are no rapid buildups and gradual decays in most cases, looking like a beat phenomenon. This is possibly due to the superimposition of waves of nearly same frequency, while such results are not predominantly noticed in case of equivalent triangular TLPs. This type of response makes square TLPs more prone also to fatigue failure due to repeated buildup and decay of tether forces. Heave response under non-impact waves, which is clearly a springing response, poses a threat to the platform stability since they occur closer to the natural frequency of heave degree of freedom causing a near resonating case. Triangular TLPs showing lesser response in comparison with square in this front make them more attractive for deepwater conditions. The response in surge degree of freedom does not show any such undesirable phenomenon under the influence of impact and non-impact waves as well probably because of its high degree of compliancy.

7.17 Significance of Springing and Ringing Response

As such, ringing and springing response, occurring at the natural frequency of one of the stiff degree of freedom, say heave, can endanger the stability of the platform. In addition, ringing can not only cause total breakdown of these platforms even in moderate storms but also can hamper daily operations and lead to fatigue failure. The variations in dynamic response with respect to water depth and tether tension are presented by showing their influence on springing and ringing response. While some of these observations are already noticed in case of square TLPs, the amount of change in the response has been quantified in this study apart from presenting their influence on platform geometry. Note that the choice of equivalent triangular TLPs as an example highlights the vulnerability of heave motion characteristics of the stiff system.

Some of the specific conclusions that can be drawn from the study are as follows: (i) impact waves cause ringing response in pitch degree of freedom in both the geometries; (ii) increased tether tension enhances pitch response in both the geometries under impact waves, but this enhancement is less in triangular TLP (with same T_0 case) compared with square; (iii) increase in water depth enhances pitch response due to impact waves for both geometries of TLPs, but this increase is less in triangular TLPs compared with square ones; (iv) pitch response in triangular TLPs (T_0 per tether same case) under impact waves is much reduced as compared to square, and it is further reduced for triangular TLP with total T_0 same as square; (v) the broad band in frequency response of heave degree of freedom under non-impact waves, occurring near to its natural frequency of TLPs of both geometries, is attributed to springing; (vi) heave response under non-impact waves decreases with increase in tether tension for same water depth in both the geometries, but it is further less in case of triangular TLPs; and (vii) beat phenomenon noticed in heave response of square TLPs under non-impact waves is not seen in triangular TLPs.

Exercise

1. Triceratops consists of _____ to achieve the required buoyancy, to support the deck structure, to restrain system and to serve storage requirements.
2. BLS is a _____, _____, _____ _____ intended for use in ultra-deep waters.
3. _____ is placed between the BLS and deck to reduce the rotational response of the deck when the BLS is exposed to wave, current and impact loads.
4. _____ is carried out analytically by subjecting the structure to zero wave amplitude and necessary initial conditions in the respective degree of freedom.
5. Write the Equation of motion for the free-decay test?
6. _____ in BLS units results in significant reduction in the pretension in tethers in comparison with that of TLPs.
7. Offshore structures exhibit highly intense nonlinear behavior called _____ and _____.
8. Explain Springing and Ringing response of TLP's?
9. _____ of compliant structures like TLPs under impact and non-impact waves responsible for ringing and springing phenomenon is of large interest to Marine Engineers.
10. A _____ event involves the excitation of transient structural deflections at/close to the natural frequency of the platform arising at third harmonic of the incident wave field.

Answers

1. Three or more BLSs.
2. Positively buoyant, floating, deep-draft structure.
3. Ball joint.
4. Free-decay test.
5. Equation of motion for the free-decay test is as follows

$$[M + M_a]\ddot{X} + [C]\dot{X} + [K]X = 0$$

where M is mass matrix; M_a is the added mass matrix, $[C]$ is the damping matrix, $[K]$ is the stiffness matrix at any instantaneous position and $\{\ddot{X}, \dot{X}, X\}$ are acceleration, velocity and displacement, respectively.
6. Permanent ballast.
7. Springing and Ringing.

8. Springing is caused in the vertical/bending modes by second-order wave effects at the sum frequencies; this behavior is common in both mild and severe sea states. Ringing is attributed to strong transient response observed in these modes under severe loading conditions triggered presumably by passage of a high, steep wave. This transient response further decays to steady state at a logarithmic rate depending on the system damping.
9. Dynamic response.
10. Ringing.

References

Adams AJ, Baltrop NDP (1991) Dynamics of fixed Mar Struct. Butterworth-Helneman Ltd., London

Adrezin R, Bar-Avi P, Benaroya H (1996) Dynamic response of compliant offshore structures-review. J Aerosp Eng 9(4):114–131

Anagnostopoulos SA (1982) Dynamic response of offshore structures to extreme waves including fluid-structure interaction. Eng Struct 4:179–185

API-RP2A (1989) Recommended practice for planning, designing and constructing fixed offshore platforms, 18th edn. American Petroleum Institute, Washington, DC

ASTM (2005) Rainflow counting method. ASTM E 1049–1085

Bai Y (2001) Pipelines and risers. Elsevier Ocean Eng book series, vol. 3. Elsevier, Amsterdam

Bar-Avi P (1999) Nonlinear dynamic response of a tension leg platform. J Offshore Mech Arct Eng 121:219–226

Basim Mekha B, Johnson C, Philip Jose, Roesset M (1996) Implication of tendon modeling on nonlinear response of TLP. J Struct Eng 122(2):142–149

Bathe KJ, Wilson EL (1987) Numerical methods in finite element analysis. Prentice Hall, New Delhi

Bea RG, Xu T, Stear J, Ramas R (1999) Wave forces on decks of offshore platforms. J Waterw Port Coast Ocean Eng 125(3):136–144

Bearman PE, Russell MP (1996) Viscous damping of TLP hulls. In: Managed program on uncertainties and loads on offshore structures (ULOS), Project Report, Imperial College

Bhattacharyya SK, Sreekumar S, Idichandy VG (2003) Coupled dynamics of Sea Star mini tension leg platform. Ocean Eng 30:709–737

Boaghe OM, Billings SA, Stansby PK (1998) Spectral analysis for non-linear wave forces. J Appl Ocean Res 20:199–212

Booton M, Joglekar N, Deb M (1987) The effect of tether damage on tension leg platform dynamics. J Offshore Mech Arct Eng 109:186–192

Bringham EO (1974) The fast fourier transform. Prentice Hall, Englewood Cliffs

Buchner B, Bunnik T (2007) Extreme wave effects on deepwater floating structures. In: Proceedings of offshore technology conference OTC 18493, Houstan, Texas, April 30–May 3

Buchner B, Wichers JEW, de Wilde JJ (1999) Features of the state-of-the-art deepwater offshore basin. In: Proceedings of offshore technology conference OTC 10841, Houstan, Texas, May 3–6

Burrows R, Tickell RG, Hames D, Najafian G (1992) Morison wave forces co-efficient for application to random seas. J Appl Ocean Res 19:183–199

Chaudhury G, Dover W (1995) Fatigue analysis of offshore platforms subjected to sea wave loading. Int J Fatigue 7(1):13–19

CAP 437 (2010) Offshore helicopters landing areas: guidance on standards, 6th edn. Civil Aviation Authority, UK

Capanoglu CC, Shaver CB, Hirayama H, Sao K (2002) Comparison of model test results and analytical motion analyses for buoyant leg structure. In: Proceedings of 12th international offshore and polar engineering conference, Kitakushu, Japan, May 26–31, pp 46–53

S. Chandrasekaran, *Dynamic Analysis and Design of Offshore Structures*,
Ocean Engineering & Oceanography 5, DOI 10.1007/978-81-322-2277-4

Caughey TK (1960) Classical normal modes in damped linear dynamic systems. J App Mech (ASME) 27:269–271
Chakarabarti SK, Hanna SY (1990) Added mass and damping of a TLP column model. In: Proceedings of offshore technology conference, No. 4643, pp 533–545
Chakrabarti SK (1984) Steady drift force on vertical cylinder—viscous vs potential. Appl Ocean Res 6(2):73–82
Chakrabarti SK (2002) The theory and practice of hydrodynamics and vibration. World Scientific, Singapore
Chakrabarti SK (1987) Hydrodynamics of offshore structures: computational mechanics. WIT Press, Southampton
Chakrabarti SK (1990) Non-linear method in offshore engineering. Elsevier Science Publisher, The Netherlands
Chakrabarti SK (1994) Offshore structure modeling. World Scientific, Singapore
Chandrasekaran S (2013a) Dynamic of ocean structures. Web-based course on National program on Technology Enhanced Learning, IIT Madras. Available at nptel.ac.in/courses/114106036
Chandrasekaran SS (2013b) Ocean structures and materials. Web-based course on National program on Technology Enhanced Learning, IIT Madras. Available at: nptel.ac.in/courses/114106035
Chandrasekaran S (2013c) Advanced Mar Struct. Web-based course on National program on Technology Enhanced Learning, IIT Madras. Available at nptel.ac.in/courses/114106037
Chandrasekaran S, Jain AK (2002a) Dynamic behavior of square and triangular offshore tension leg platforms under regular wave loads. Ocean Eng 29(3):279–313
Chandrasekaran S, Jain AK (2002b) Triangular configuration tension leg platform behavior under random sea wave loads. Ocean Eng 29(15):1895–1928
Chandrasekaran S, Jain AK (2004). Aerodynamic behavior of offshore triangular tension leg platforms. In: Proceedings of ISOPE, Toulon, France, pp 564–569
Chandrasekaran S, Pannerselvam R (2009) Offshore structures: materials, analysis, design and construction. In: Proceedings of short course on offshore structures and materials, IITM, Chennai, December 14–18, p 156
Chandrasekaran S, Gaurav (2008) Offshore triangular tension leg platform earthquake motion analysis under distinctly high sea waves. J Ships Offshore Struct 3(3):173–184
Chandrasekaran S, Bhaskar K, Muhammed H (2010). Experimental study on dynamic response behavior of multi-legged articulated tower. Proceedins of 29th international conference on ocean, offshore and arctic engineering, OMAE 2010, June 6–11, Shanghai, China
Chandrasekaran S, Bhaskar K, Lino H, Brijit R (2010). Dynamic response behavior of multi-legged articulated tower with and without TMD. In: Proceedings of International Conference on Mar Technol MARTEC–2010, December 11–12, Dhaka, Bangladesh, pp 131–136
Chandrasekaran S, Chandak NR, Gupta A. (2006) Stability analysis of TLP tethers. Ocean Eng 33(3):471–482
Chandrasekaran S, Jain AK, Chandak NR (2004) Influence of hydrodynamic coefficients in the response behavior of triangular TLPs in regular waves. Ocean Eng 31:2319–2342
Chandrasekaran S, Jain AK, Chandak NR (2006) Seismic analysis of offshore triangular tension leg platforms. Int J Struct Stab Dyn 6(1):97–120
Chandrasekaran S, Jain AK, Chandak NR (2007) Response behavior of triangular tension leg platforms under regular waves using stokes nonlinear wave theory. J Waterw Port Coast Ocean Eng (ASCE) 133(3):230–237
Chandrasekaran S, Jain AK, Gupta A (2007) Influence of wave approach angle on TLP's response. Ocean Eng 8-9(34):1322–1327
Chandrasekaran S, Jain AK, Gupta A, Srivastava A (2007) Response behavior of triangular tension leg platforms under impact loading. Ocean Eng 34:45–53
Chandrasekaran S, Seeram M, Jain AK, Gaurav M (2010) Dynamic response of offshore triceratops under environmental loads. In: Proceedings of international conference on Mar Technol MARTEC, December 11–12, Dhaka, Bangladesh, pp 61–66

Chandrasekaran S, Sharma A, Srivastava S (2007) Offshore triangular TLP behavior using dynamic Morison equation. J Struct Eng 34(4):291–296

Chandrasekaran S, Sundaravadivelu R, Pannerselvam R, Madhuri S (2011) Experimental investigations of offshore triceratops under regular waves. In: Proceedings of 30th international conference on ocean, offshore and arctic engineering, OMAE, 19–24 June 2011, Rotterdam, The Netherlands

Chandrasekaran S, Sundaravadivelu R, Pannerselvam R, Madhuri S, Shyamala Varthini D (2011) Experimental investigations of offshore triceratops under regular waves. In: Proceedings of 30th international conference on ocean, offshore and arctic engineering, OMAE, June 19–24, Rotterdam, The Netherlands, 49826

Chandrsaekaran S, Bhattacharyya SK (2011) Analysis and design of offshore structures. HRD Center for Offshore and Plant Engineering (HOPE), Changwon National University, Republic of Korea, p 285

Charles WN, Robert CW, Capanoglu C (2005) Triceratops: an effective platform for developing oil and gas fields in deep and ultra deep water. In: Proceedings of 15th international offshore and polar engineering conference, June 19–24, Seoul, Korea, pp 133–139

Chen X, Ding Y, Zhang J, Liagre P, Neidzwecki J, Teigen P (2006) Coupled dynamic analysis of a mini TLP: comparison with measurements. Ocean Eng 33:93–117

Choi Han S, Lou, Jack YK (1991) Nonlinear behavior of an articulated offshore loading platform. Appl Ocean Res 13(2):63–74

Chopra AK (2003) Dynamics of structures: theory and applications to earthquake engineering, 2nd edn. Person Education, Singapore

Clauss GF, Birk L (1996) Hydrodynamic shape optimization of large offshore structures. J Appl Ocean Res 18:157–171

Clauss GT et al (1992) Offshore structures: conceptual design and hydromechanics, vol 1. Springer, London

Copple RW, Capanoglu CC (1995) A buoyant leg structure for the development of marginal fields in deep water. In: Proceedings of fifth international offshore and polar engineering conference, June 16–11,The Hague, The Netherlands, p 163

Dawson TH (1983) Offshore structural engineering. Prentice-Hall, Englewood Cliffs

de Boom William C, Pinkster Jo A, Tan PSG (1984) Motion and tether force prediction of a TLP. J Waterw Port Coast Ocean Eng 110(4):472–486

Demirbilek Z (1990) Design formulae for offset, set down and tether loads of a tension leg platform (TLP). Ocean Eng 17(5):517–523

Devon R, Jablokow K (2010) Teaching FEED. In: Proceedings of mid-atlantic ASEE conference, October 15–16, Villanova University, Pennsylvania, USA

DNV (1982) Rules for the design, construction and inspection of offshore structures. Det Norske Veritas, Oslo

DOE-OG (1985) Offshore installation: guidance on design and construction. Department of Energy, London

Ertas A, Eskwaro-Osire S (1991) Effect of damping and wave parameters on offshore structure under random excitation. Nonlinear Dyn 2:119–136

Ertas A, Lee JH (1989) Stochastic response of tension leg platform to wave and current forces. J Energy Resour Technol 111:221–230

Faltinsen OM (1990) Sea loads on ships and offshore structures. Cambridge University Press, New York

Faltinsen OM, Newman JN, Vinje T (1995) Nonlinear wave loads on a slender vertical cylinder. J Fluid Mech 289:179–198

Gadagi MM, Benaroya H (2006) Dynamic response of an axially loaded tendon of a tension leg platform. J Sound Vib 293:38–58

Gaurav, Sharma A (2008) Influence of varying inertia coefficient and wave directionality on TLP geometry. In: Proceedings of ISOPE, November 2008, Bangkok, Thailand, pp 255–261

Gerwick BC Jr (1986) Construction of offshore structures. Wiley, New York

Graff WJ (1981) Introduction to offshore structures. Gulf Publishing Co., Houston
Graff WJ (1981) Introduction to offshore structures: design, fabrication and installation. Gulf Publishing Co., Tokyo
Guo B, Song S, Chacko J, Ghalamber A (2005) Offshore pipelines. Gulf Professional Publishing, MA
Gurley Kurtis R, Ahsan Kareem (1998) Simulation of ringing in offshore systems under viscous loads. J Eng Mech ASCE 124(5):582–586
Gusto MSC (2010) The exploration market. Inside 15:4–7
Halkyard JE, Davies RL, Glanville RS (1991) The tension buoyant tower: a design for deep water. 23rd annual offshore technology conference, OTC 6700, May 69,Houston, Texas, pp 41–55
Hancock JW, Gall DS (1985) Fatigue under narrow and broad band stationary loading. Final report of cohesive program of R&D in fatigue of offshore structures, Marine Tech. Directorate Ltd., Texas, USA
Haritos N (1985) Modeling the response of tension leg platforms to the effects of wind using simulated traces. Math Comput Simul 27:231–240
Harvy JF (1985) Theory and design of pressure vessels. Van Nostrand Reinhold Co, New York
Helvacioglu IH, Incecik A (2004) Dynamics of double articulated towers, integrity of offshore structures, vol 4. Elsevier, London
Hitchings GA, Bradshaw H, Labiosa TD (1976) Planning and execution of offshore site investigations for North Sea gravity platform. In: Proceedings of offshore technology conference, Paper No. 2430
Hoeg K (1976) Foundation engineering for fixed offshore structures. In: Proceedings of first international conference behaviour of offshore structures, vol 1, pp 39–69
Hove K, Foss I (1974) Quality assurance for offshore concrete gravity structures. In: Proceedings of Offshore Technology Conference, Paper No. 2113
HSE (2010) Offshore helideck design guidelines: health & safety executive. John Burt Associates Ltd, UK
Hsu HT (1981) Applied offshore structural engineering. Gulf Publishing Co., Houston
Humphries JA, Walker DH (1987) Vortex excited response of large scale cylinders in shear flow. In: Proceedings of Sixth OMAE, vol 2, Houston, TX, pp 139–143
Islam N, Ahmad S (2003) Nonlinear seismic response of articulated offshore tower. Def Sci J 53 (1):105–113
Issacson M, Det St Q (1982) Non-linear wave effects on fixed and floating bodies. J Fluid Mech 120:267–281
Iwasaki H (1981) Preliminary design study of tension leg platform. MIT University
Jayalekshmi R, Sundaravadivelu R, Idichandy VG (2010) Dynamic analysis of deep water tension leg platforms under random waves. J Offshore Mech Arct Eng 132(4):041605
Jefferys ER, Patel MH (1982) Dynamic analysis models of tension leg platforms. J Energy Resour Technol 104:217–223
Jefferys ER, Rainey RCT (1994) Slender body models of TLP and GBS 'ringing'. BOSS, McGraw-Hill Inc, New York
Joseph A, Idichandy VG, Bhattacharyya SK (2004) Experimental and numerical study of coupled dynamic response of a mini tension leg platform. J Offshore Mech Arct Eng 126(4):318–330
Kam JCP, Dover WD (1988) Fast fatigue assessment procedure under random time history. Proc Inst Civil Eng Part 2 85:689–700
Kam JCP, Dover WD (1989) Advanced tool for fast assessment of fatigue under offshore random wave stress history. Proc Inst Civil Eng Part 2 87:539–556
Kawanishi T, Katoh W, Furuta H (1987) Tension leg platform earthquake motion analysis. Oceans 19:543–547
Kawanishi T, Ohashi S, Takamura H, Koboyashi H (1993) Earthquake response of tension leg platform under unbalanced initial tension. In: Proceedings of ISOPE, Singapore, pp 319–325
Ker W-K, Lee C-P (2002) Interaction of waves and a porous tension leg platform. J Waterw Port Coast Ocean Eng 128(2):88–95

Kim C-H, Zou J (1995) A universal linear system model for kinematics and forces affected by nonlinear irregular waves. Int J Offshore Polar Eng 5(3):166–170
Kim C-H, Kim MH, Liu YH, Zhao CT (1994) Time domain simulation of nonlinear response of a coupled TLP system. Int J Offshore Polar Eng 4(4):281–291
Kim C-H, Lee C-H, Goo J-S (2007) A dynamic response analysis of tension leg platforms including hydrodynamic interaction in regular waves. Ocean Eng 34:1680–1689
Kim C-H, Zhao CT, Zou J, Xu Y (1997) Springing and ringing due to laboratory-generated asymmetric waves. Int J Offshore Polar Eng 7(1):30–35
Kjeldsen SP, Myrhaug D (1979) Wave-wave interactions and wave-current interactions in deep water. In: Proceedings of 5th POAC Conference, Trondheirn, Norway, vol. III, p 179
Klaus-Jurgen B, Wilson EL (1987) Numerical methods in finite element analysis, 2nd edn. Pearson Education, Singapore
Kobayashi M, Shimada K, Fujihira T (1987) Study on dynamic responses of a TLP in waves. J Offshore Mech Arct Eng 109:61–66
Kurian et al (2008) Parametric study of TLPs subjected to random waves. In: Proceeding of international conference on construction and building technology, Kuala Lumpur, Malaysia, pp 1–9
Kurian VJ, Idichandy VG, Ganapathy C (1993) Hydro dynamic response of tension leg platforms: a model. Exp Mech 33(3):212–217
Leffler William WL, Pattarozzi R, Sterling G (2011) Deep-water petroleum: exploration and production. Pennwell Corp., Oklahama, p 350
Li Y, Liu Y, Teng B (2006) Porous effect parameter of thin permeable plates. Coast Eng 48 (4):309–336
Love AEH (1994) Mathematical theory of elasticity. Dover Publications, New York
Low YM (2009) Frequency domain analysis of a tension leg platform with statistical linearization of the tendon restoring forces. Mar Struct 22:480–503
Malenica S, Molin B (1995) Third-harmonic diffraction by a vertical cylinder. J Fluid Mech 302:203–229
Marthinsen T, Winterstein SR, Ude TC (1992) TLP fatigue due to second-order springing. Probabilistic methods and structural and geotechnical reliability. In: Proceedings of specialty conference, pp 455–458
Mather A (2000) Offshore engineering: an introduction, 2nd edn. Witherby & Co Ltd., London
Matsuishi M, Endo T (1968) Fatigue of metals subjected to varying stresses. Jpn Soc Mech Eng 3:37–40
McCamy RC, Fuchs RA (1954). Wave force on piles: a diffraction theory. Technical Memorandum, No. 69, Beach Erosion Board, US. Army Corps of Engineers, Washington, DC
Mercier JA (1982) Evolution of tension leg platform technology. In: Proceedings of 3rd international conference on the behaviour of offshore structures, MIT
Mercier RS (1997) Mars tension leg platform: use of scale model testing in the global design. In: Proceedings of offshore technology conference, OTC 8354-MS, May 5–8, Houston, Texas
Michel WH (1999) Sea spectrum revisited. Mar Technol 36(4):211–227
Moe G, Verley RLP (1980) Hydrodynamic damping of offshore structures in wave and currents. Offshore technology conference, 12th Annual OTC, Houston, Texas, pp 37–44
Morison JR, O'Brien MP, Johanson JW, Shaaf SA (1950) The forces exerted by surface waves on pile. Trans AMIE 189:149–154
Muhuri PK, Gupta AS (1983) Stochastic stability of tethered buoyant platforms. Ocean Eng 10 (6):471–479
Munkejord T (1996) The Heidrun TLP and concept development for deep water. In: Proceedings of ISOPE, May, Los Angeles, USA, pp 1–11
Naess A, Moan T (2013) Stochastic dynamics of marine structures. Cambridge University Press, New York
Nagamani K, Ganapathy C (2000) Dynamic response of three leg articulated tower. Ocean Eng 27:1455–1471

Natvig BJ (1996) TLP installation without motion compensation. In: Proceedings of ISOPE, Los Angeles, CA, USA, 1, pp 228–231
Natvig BJ (1994) A proposed ringing analysis model or higher order tether response. In: Proceedings 4th international offshore and polar engineering conference, ISOPE, Golden, CO, pp 40–51
Natvig BJ, Vogel H (1995)TLP design philosophy—past, present, future. In: Proceedings of international conference offshore and polar engineers, The Hague, pp 64–69
Neelamani S, Muni Reddy MG (2002) Wave forces on a vertical cylinder defenced by a perforated vertical and inclined barriers. Indian J Mar Sci 31(3):179–187
Neelamani S, Uday Bhaskar N, Vijayalakshmi K (2002) Wave forces on a seawater intake caisson. Ocean Eng 29(10):1247–1263
Neville AM (1997) Properties of concrete, 4th edn. Wiley, New York
Niedzwecki JM, Van de Lindt JW, Gage JH, Teigen PS (2000) Design estimates of surface wave interaction with compliant deepwater platforms. Ocean Eng 27:867–888
Nobuyoshi Y (1976) Experimental and theoretical study of a tension leg platform in deep water. In: Proceedings of offshore technology conference, OTC 2690-MS, May 3 6, Houston, Texas
Nordgren RP (1987) Analysis of high frequency vibration of tension leg platforms. J Offshore Mech Arct Eng 109:119–125
NPD (1985) Regulation for structural design of load-bearing structures intended for exploitation of petroleum resources. Norwegian Petroleum Directorate, Oslo
OCS (1980) Requirements for verifying the structural integrity of OCS platforms. United States Geologic Survey, National Centre, Reston
Paik JK, Thayamballi AK (2007) Ship-shaped offshore installations: design, building and operations. Cambridge University Press, New York
Paik I, Roesset JM (1996) Use of quadratic transfer functions to predict response of tension leg platforms. J Eng Mech 122(9):882–889
Patel MH (1989) Dynamics of offshore structures. Butterworth, London
Patel M, Witz JA (1991) Compliant offshore structures. Butterworth-Heinemann Ltd., Oxford
Perryman SR, Horton EE, Halkyard JE (1995) Tension buoyant tower for small fields in deep waters. Offshore technology conference, OTC 7805, May 1–4, Houston, Texas, pp 13–22
Pilotto BM, Ronalds, BF, Stocker R (2002) Dynamic response of shallow water mono-pod platforms. In: Proceedings of international conference on offshore mechanics and arctic engineering, Oslo, Norway, 1, pp 113–120
Pilotto BM, Ronalds BF, Stocker R (2003) Nonlinear dynamic analysis with deterministic and random seas. Oceans Conf Rec (IEEE) 5:2908–2915
Pilotto BM, Ronalds BF (2003) Dynamic behavior of minimum platforms under random loads. In: Proceedings of international conference on offshore mechanics and arctic engineering, Cancum, Mexico, 1, pp 441–449
Popovics JS, Zemajtis J, Shkilnik I (2008) Study on static and dynamic modulus of elasticity of concrete. American Concrete Institute, CRC Report
Reddy DV, Arockiasamy M (1991) Offshore Structures, vol I. Kriger Publishing Co., Malabar
Rijken OR, Niedzwecki JM (1991) A knowledge base approach to the design of tension leg platform. Center for Offshore Technology, Offshore Technology Research Center, Texas, pp 24–100
Roark RJ, Yooung WC (1989) Formula for stress and strain, 6th edn. McGraw Hill Inc, New York
Robert WC, Capanoglu CC (1995) Buoyant leg structure for the development of marginal fields in deep water. In: Proceedings of International Offshore and Polar Engineering Conference, June 11–16, The Hague, The Netherlands, p 163
Ney R, Andrade RFM, Batista RC (1992) Dynamic response analysis of small-scale model tension leg platform. Mar Struct 5:491–513
Sadehi K (1989) Design and analysis of marine structure. Khaje Nasir Toosi University of Technology, Tehran

Sadehi K (2001) Coasts, ports and offshore structures engineering. Power and Water University of Technology, Tehran
Sadehi K (2007) Offshore and petroleum platforms for cyprus oil/gas fields. J Soc Appl Sci 2(4):1–16
Sankarbabu K, Sannasiraj SA, Sundar V (2007) Interaction of regular waves with a group of dual porous circular cylinders. Appl Ocean Res 29(4):180–190
Sarpkaya T, Isaacson M (1981) Mechanics of wave forces on offshore structures. Van Nostrand Reinhold, New York
Seeram M (2013) Nonlinear dynamic behaviour of offshore triceratops. PhD thesis, Indian Institute of Technology Madras, p 145
Shaver CB, Capanoglu CC, Serrahn CS (2001) Buoyant leg structure preliminary design, constructed cost and model test results. In: Proceedings 11th international offshore and polar engineering conference, Stavanger, Norway, June 17–22, pp 432–439
Shinozula M (1983) Basic analysis of structural safety. J Struct Div ASCE 109(3):721–740
Soding H, Blok JJ, Chen HH, Hagiwara K, Issacson M, Jankowski J, Jefferys ER, Mathisen J, Rask I, Richer JP, Romeling JU, Varsta P (1990) Environmental forces on offshore structures: a state-of-art review. Mar Struct 3:59–81
Son S (2006) Design of ocean platforms against ringing response. MS thesis, Mechanical Engineering Department, Texas Tech University, Lubbock, TX, USA
Song H, Tao L (2007) Short-crested wave interaction with a concentric porous cylindrical structure. Appl Ocean Res 29(4):199–209
Stansberg CT, Ormberg H, Oritsland O (2002) Challenges in deep water experiments: hybrid approach. J Offshore Mech Arct Eng 124:90–96
Stoke's GG (1880) On the theory of oscillatory waves. Math Phys Pap 1:225–228
Subramanaim KV, Popovics JS, Shah SP (2000) Determining elastic properties of concrete using vibration resonance frequencies of standard test cylinders. Cem Concr Aggreg (ASTM) 22(2):81–89
Tabeshpour MR, Golafshani AA, Seif MS (2006) Comprehensive study on the results of tension leg platform responses in random sea. J Zhejiang Univ Sci 7(8):1305–1317
Tromans P, Swan C, Masterton S (2006) Nonlinear potential flow forcing: the ringing of concrete gravity based structures. Research Report No. 468, Ocean Wave Engineering Ltd, Health & Safety Executive Publication, Norwich, UK
Ude TC, Winterstein SR, Marthinsen T (1994) Volterra models for ocean structures: extreme and fatigue reliability. J Eng Mech ASCE 120(6):1369–1385
Vannucci P (1996) Simplified optimal design of tension leg platform TLP. Struct Optim 12:265–268
Venkataramana K, Toyoda S, Kawano K (1993) Dynamics of TLPs under current and earthquake forces. In: Proceedings of ISOPE, Singapore, pp 341–344
Vickery PJ (1990) Wind and wave loads on a tension leg platform: theory and experiment. Wind Eng Ind Aerodyn 36:905–914
Vickery PJ (1995) Wind induced response of tension leg platform: theory and experiments. Struct Eng 121(4):651–663
Vijayalakshmi K, Neelamani S, Sundaravadivelu R, Murali K (2007) Wave run up on a concentric twin perforated circular cylinder. Ocean Eng 34(2):327–336
Vijayalakshmi K, Sundaravadivelu R, Murali K, Neelamani S (2008) Hydrodynamics of a concentric twin perforated circular cylinder system. J Waterw Port Coast Ocean Eng 134(3):166–177
Wang K-H, Ren X (1994) Wave interaction with a concentric porous cylinder system. Ocean Eng 21(4):343–360
White NC, Copple WR, Capanoglu C (2005) Triceratops: an effective platform for developing oil and gas fields in deep and ultra-deep water. In: Proceedings of 15th international offshore and polar engineering conference, June 19–24, Seoul, Korea, pp 133–139

William AN, Li W (1998) Wave interaction with a semi-porous cylindrical breakwater mounted on a storage tank. Ocean Eng 25(2–3):195–219
William AN, Li W, Wang K-H (2000) Water wave interaction with a floating porous cylinder. Ocean Eng 27(1):1–28
Williams AN, Li W (2000) Water wave interaction with an array of bottom-mounted surface-piercing porous cylinders. Ocean Eng 27(8):841–866
Wilson James F (1984) Dynamics of offshore structures. Wiley Inter Science Publications, New York
Winterstein SR (1988) Nonlinear vibration models for extremes and fatigue. J Eng Mech ASCE 114(10):1772–1790
Wirsching P, Ortiz PK (2006) Random vibrations: theory and practice. Dover, NewYork
Wirsching PH, Light MC (1980) Fatigue under wide band random loading. J Struct Div ASCE 106:1593–1607
Witz JA, Patel MH, Harrison JH (1986) On the hydrodynamics of semisubmersibles with articulated members. Proc Roy Soc London Ser A Math Phys Sci 403:81–109
Yan F, Zhang D, Sun L, Dai Y (2009) Stress verification of a TLP under extreme wave environment. J Mar Sci Appl 8:132–136
Yoneya T, Yoshida K (1982) The dynamics of tension leg platforms in waves. J Energy Resour Technol 104:20–28
Yoshida K, Ozaki M, Oka N (1984) Structural response analysis of tension leg platforms. J Energy Resour 106:10–17
Young AG, Kraft LM, Focht JA (1975) Geotechnical considerations in foundation design of offshore gravity structures. In: Proceedings of offshore technology conference, Paper No. 2371
Zeng et al (2007) Parametric studies of tension leg platform with large amplitude motions. In: Proceedings 17th international offshore and polar engineering conference, Lisbon, Portugal, pp 202–209
Zhao F, Bao W, Kinoshita T, Itakura H (2009) Interaction of waves and a porous cylinder with an inner horizontal porous plate. Appl Ocean Res 32(2):252–259
Zhong Z, Wang KH (2006) Solitary wave interaction with a concentric porous cylinder system. Ocean Eng 33(7):927–949

Index

S. Chandrasekaran, *Dynamic Analysis and Design of Offshore Structures*,
Ocean Engineering & Oceanography 5, DOI 10.1007/978-81-322-2277-4